COMPRESSIVE AND FREE VIBRATION RESPONSE OF FIBER REINFORCED RUBBERIZED RECYCLED CONCRETE COLUMNS

By

Md. Shahjalal

MASTER OF SCIENCE IN CIVIL ENGINEERING (STRUCTURAL)

Department of Civil Engineering

BANGLADESH UNIVERSITY OF ENGINEERING AND TECHNOLOGY

April, 2022

COMPRESSIVE AND FREE VIBRATION RESPONSE OF FIBER REINFORCED RUBBERIZED RECYCLED CONCRETE COLUMNS

by

Md. Shahjalal

Submitted to the Department of Civil Engineering

Bangladesh University of Engineering and Technology (BUET), Dhaka

in partial fulfillment of the requirements for the degree

of

MASTER OF SCIENCE IN CIVIL ENGINEERING (STRUCTURAL)

Department of Civil Engineering

BANGLADESH UNIVERSITY OF ENGINEERING AND TECHNOLOGY

April, 2022

The thesis titled – **Compressive and free vibration response of fiber reinforced rubberized recycled concrete columns** submitted by Md. Shahjalal, Student No: 1018042332, Session: October 2018, has been accepted as satisfactory in partial fulfillment of the requirement for the degree of **Master of Science in Civil Engineering (Structural)** on 6th April, 2022.

BOARD OF EXAMINERS

Dr. Raquib Ahsan Professor (Supervisor) Department of Civil Engineering, BUET	**Chairman**
Dr. Md. Delwar Hossain Professor and Head Department of Civil Engineering, BUET	**Member** **(Ex-Officio)**
Dr. S.M. Faisal Mahmood Assistant Professor Department of Civil Engineering, BUET	**Member**
Dr. Md. Jahidul Islam Associate Professor Department of Civil Engineering, MIST	**Member** **(External)**

DEDICATION

Dedicated to my loving parents

DECLARATION

I hereby declare that this thesis is my original work and it has been written by me in its entirety. I have duly acknowledged all the sources of information that have been used in this thesis.

This thesis has not been submitted for any degree in any university previously.

Md. Shahjalal

ACKNOWLEDGEMENTS

First and foremost, I would like to thank Allah (SWT) with the blessings of Whom all the good deeds are fulfilled.

I would like to take this opportunity to express my sincere gratitude to my thesis supervisor Professor Dr. Raquib Ahsan, Department of Civil Engineering, Bangladesh University of Engineering and Technology (BUET) for his logical guidance, quick response, and continuous moral support throughout this thesis. His valuable suggestions and enthusiastic supervision were of immense help throughout my research work. Working under him was an extremely knowledgeable experience for me.

I would like to express my deep appreciation to my undergraduate co-supervisor Kamrul Islam for his unconditional help, inspiration, and guidance. It would not be possible to complete the thesis without his assistance. Besides, I express my profound gratitude to Major Joarder Md Sarwar Mujib (Retd), Associate Professor, Department of Civil Engineering, Military Institute of Science and Technology (MIST), for arranging all the funding. Besides, a special thanks to Gazi Algaj Hossain, Lecturer, MIST, for his unconditional help.

I also pay my deepest homage to the lab technicians who helped directly or indirectly in performing the work in connection with this thesis, especially Concrete Lab and SM Lab of BUET and MIST.

Last but not the least, I would like to thank my parents and my wife for their consistent assistance, encouragement, and motivation.

ABSTRACT

The production of sustainable green concrete is getting popularity in concrete industries. The increasing amount of waste tires and construction and demolition (C&D) wastes mounting up in the landfills create a concern for environmental sustainability. The construction industries are nowadays thinking of ways to reduce and reuse these waste materials. The use of recycled coarse aggregate (RCA) produced from the demolition of old concrete infrastructures and waste tires of vehicles in the concrete mixture can play a vital role in providing an economical solution. Thus, this study investigates the compressive behavior of steel-reinforced concrete columns that are made of RCA and waste tire-derived crumb rubber (CR) along with polypropylene (PP) fiber. A total of twenty-six short columns (kL/r = 11) having a size of 150 × 150 × 950 mm were cast and tested under uniaxial loading up to failure. Besides, from those twenty-six columns, nine columns were used for free vibration testing before applying compressive force. Different mechanical properties of rubberized recycled concrete (R^2C) and fiber-reinforced rubberized recycled concrete (FR^3C) were also evaluated by compressive strength test, tensile strength test, flexural test, ultrasonic pulse velocity test, surface resistivity test, and hardened density test.

Test parameters included longitudinal reinforcement ratio (1.4% and 2.0%), tie spacing (75 mm and 150 mm), and content of CR (0%, 5%,10%, and 15%). However, the RCA and PP percentages were fixed at 30% and 0.5%, respectively. The axial capacity, failure mode, influence of longitudinal and transverse reinforcement, effect of RCA, CR, and PP fiber, strain and deflection characteristics, dilation ratio, curvature, toughness, and ductility were examined. The free vibrational responses of columns are presented in terms of damping ratio, time period as well as frequency. Besides, an extensive regression analysis has been carried out based on the experimental data and a number of equations have been proposed for predicting different mechanical properties by considering the effect of CR and fiber. Furthermore, a cost analysis was conducted to examine the cost-effectiveness of these new types of concrete.

The axial capacity of columns decreased with increasing CR content by up to 39.6% and 35.5% for R^2C columns and FR^3C columns, respectively. However, the FR^3C columns exhibited higher axial capacity compared to the recycled aggregate concrete (RAC) column and R^2C columns. The ductility increased with increasing the CR percentage and the addition of fiber content. Approximately 167% and 70% higher ductility was achieved in 75 mm and 150 mm tie spaced columns by using 0.5% fiber content in the R^2C mixture with 15% CR content. The toughness value of R^2C columns was initially decreased for 0%, 5%, and 10% CR content but then increased for 15% CR content. However, all FR^3C columns exhibited a higher toughness value compared to the conventional column. From the free vibration test, it was found that the damping ratio of all RAC, R^2C, and FR^3C columns were higher than that of the conventional column. Up to 131% and 301% damping ratio was increased for R^2C columns and FR^3C columns depending on the percentage of CR content. The cost analysis showed that both the R^2C and FR^3C mixtures saved more energy costs and decreased fuel consumption. Considering all the parameters, it is recommended to use up to 5% CR content with 30% RCA and 0.5% fiber content. Finally, this study will help to develop sustainable and resilient fiber-reinforced recycled rubberized concrete for the application in structural members.

TABLE OF CONTENTS

LIST OF FIGURES

LIST OF TABLES

NOTATION

A_c	Concrete Area
A_g	Gross Area of Column
A_p	Peak Amplitude in Frequency Domain
A_s	Area of Steel Bar
Al_2O_3	Aluminium Oxide
As	Arsenic
C	Air-Conditioning Thermal Efficiency Coefficient
C	Carbon
CaO	Calcium Oxide
Cd	Cadmium
CO_2	Carbon dioxide
Cu	Copper
Cr	Chromium
CS_2	Carbon Disulfide
C_5	Damping Coefficient Corresponding to ζ_5
C_{10}	Damping Coefficient Corresponding to ζ_{10}
D	Degree-days
d_{actual}	Actual Steel Bar Dia
$d_{nominal}$	Nominal Steel Bar Dia
E	Annual Energy
E	Modulus of Elasticity of Concrete
E_{CR}	Modulus of Elasticity of Rubberized Recycled Concrete
$E_{CR.F}$	Modulus of Elasticity of Fiber Reinforced Rubberized Recycled Concrete
E_s	Modulus of Elasticity of Steel Bar
f_a	Frequencies Associated with Half-Power Points on One Side of Peak Amplitude
f_b	Frequencies Associated with Half-Power Points on Another Side of Peak Amplitude
f_c'	Compressive Strength of Concrete

$f_c'_{CR}$	Compressive Strength of Rubberized Recycled Concrete
$f_c'_{CR.F}$	Compressive Strength of Fiber Reinforced Rubberized Recycled Concrete
Fe	Iron
Fe_2O_3	Ferric Oxide
f_n	Natural Frequency
f_t	Tensile Strength of Concrete
$f_{t,CR}$	Tensile Strength of Rubberized Recycled Concrete
$f_{t,CR.F}$	Tensile Strength of Fiber Reinforced Rubberized Recycled Concrete
f_r	Flexural Strength of Concrete
$f_{r,CR}$	Flexural Strength of Rubberized Recycled Concrete
$f_{r,CR.F}$	Flexural Strength of Fiber Reinforced Rubberized Recycled Concrete
f_u	Ultimate Strength of Steel Bar
f_y	Yield Strength of Steel Bar
HCl	Hydrochloric Acid
h_b	Beam Depth
I	Iodine
I	Moment of Inertia of area
k	Stiffness
K_2O	Potassium Oxide
L	Length
m	Mass of the Column
M_{CO_2}	CO_2 Emission
m_{fA}	Fuel Consumption
MgO	Magnesium Oxide
M_{SO_2}	SO_2 Emission
Na_2O	Sodium Oxide
Ni	Nickel
NaOH	Sodium Hydroxide
O	Oxygen
P_{ACI}	Peak Axial Load by ACI Equation
Pb	Lead

$P_{C\text{-}peak}$	Axial Load Carried by Concrete
P_{CSA}	Peak Axial Load by CSA Equation
P_{exp}	Experimental Peak Axial Load
$P_{F\text{-}Crack}$	First Cracking Load
P_{peak}	Peak Axial Load
P_{pro}	Peak Axial Load by Proposed Equation
$P_{S\text{-}peak}$	Axial Load Carried by Steel reinforcement
P_0	Nominal Peak Axial Load
$P_{\Delta u}$	Axial Load Corresponding to Ultimate Deflection
R	Thermal Resistance
R^2	Coefficient of Determination
S	Sulfur
Si	Silicon
SiO_2	Silicon dioxide
SO_3	Sulfur trioxide
T_d	Damping Time-Period
T_n	Natural Time-Period
V	Ultrasonic Pulse Velocity
w_c	Density of Concrete
Zn	Zinc
Δ_{Peak}	Deflection Corresponding to Peak Axial Load
Δ_u	Ultimate Deflection
Δ_y	Yield Deflection
$\Delta_{0.85}$	Deformation Corresponding to 85% of Peak Axial Load on Descending Part
$\varepsilon_{S\text{-}peak}$	Axial Strain on Longitudinal Reinforcement Corresponding to Peak Load
ε_a	Axial Strain of Column
ε_l	Lateral Strain of Column
ε_v	Volumetric Strain
ε_y	Yield Strain of Steel Bar
ρ	Longitudinal Reinforcement Ratio
ρ_t	Transverse Reinforcement Ratio

λ	Thermal Conductivity
η_s	Space Heating System Efficiency
ν	Poisson's Ratio
μ	Ductility
μ_k	Curvature Ductility
φ_y	Yield Curvature
φ_u	Ultimate Curvature
α_1	Strength Reduction Factor
ζ	Damping Ratio
ζ_5	Damping Ratio Considering 5 Cycles
ζ_{10}	Damping Ratio Considering 10 Cycles
$\zeta_{5-log.Dec}$	Logarithmic Decrement Damping Ratio Considering 5 Cycles
$\zeta_{10-log.Dec}$	Logarithmic Decrement Damping Ratio Considering 10 Cycles
$\zeta_{half-power}$	Half-Power Bandwidth Damping Ratio
$\ddot{x}$	Max Acceleration
$\ddot{x}_0$	Initial Amplitude of Acceleration
$\ddot{x}_n$	Amplitude of Acceleration after n Cycles
ω_d	Damping Frequency
ω_n	Angular Frequency

LIST OF ABBREVIATIONS

AAPE	Average Absolute Percentage Error
ANN	Artificial Neural Network
BAC	Brick Aggregate Concrete
BF	Basalt Fiber
C&D	Construction and Demolition
COV	Coefficient of Variation
CR	Crumb Rubber
DICT	Digital Image Correlation Technique
DIF	Dynamic Increase Factor
EA	Expansive Agent
EC	Energy Cost
ECCO	Environmental Council of Concrete Organizations
EDS	Energy dispersive spectroscopy
ET	Energy Tariff of Electricity
FHWA	Federal Highways Administration
FR^2C	Fiber-Reinforced Recycled Concrete
FR^3C	Fiber-Reinforced Rubberized Recycled Concrete
FRP	Fiber-Reinforced Polymer
GFRP	Glass Fiber Reinforced Polymer
ITZ	Interfacial Transition Zone
LCA	Life Cycle Assessment
LFC	Lightweight Foam Concrete
LFRC	Lightweight Foam Rubberized Concrete
LHV	Lower Heating Value
LOI	Loss on Ignition
MAE	Mean Absolute Error
ML	Machine Learning
MoE	Modulus of Elasticity
NAC	Natural Aggregate Concrete

NCA	Natural Coarse Aggregate
NFA	Natural Fine Aggregate
NIOSH	National Institute for Occupational Safety and Health
NPV	Net Present Value
PCC	Portland Composite Cement
PF	Performance Factor
PP	Polypropylene
PWF	Present Worth Factor
RAC	Recycled Aggregate Concrete
RC	Reinforced Concrete
R^2C	Rubberized Recycled Concrete
RCA	Recycled Coarse Aggregate
RMSE	Root Mean Squared Error
RuC	Rubberized Concrete
SCA	Silane Coupling Agent
SEM	Scanning Electron Microscopy
SF	Silica Fume
SSD	Saturated Surface Dry
TSC	Two-Stage Concrete
UHP-FRC	Ultra-High-Performance Fiber-Reinforced Concrete
UPV	Ultrasonic Pulse Velocity
UTM	Universal Testing Machine

Chapter 1
INTRODUCTION

1.1 General

Sustainability is one of the primary concerns in this 21^{st} century. In this regard, concrete industries and scientific communities are devoting much effort to improving the sustainability of civil engineering structures. Each year, close to 13000 million natural aggregates are required for concrete construction on this planet [1]. With increasing these aggregates' demand, the rate of construction waste is also increasing parallelly. In Canada, concrete waste occupies the largest portion of all construction and demolition (C&D) waste [2], and this C&D waste is almost 27.5%, 29%, and 7.5 % of total municipal solid waste in British Columbia, Ontario, and Alberta, respectively [3]. In Europe and China, this C&D waste generation rate is near to 450 and 200 million tons each year [4, 5]. Even, in Bangladesh, the volume of demolished concrete is increasing due to the deterioration of old concrete structures and the replacement of many low-rise buildings with relatively high-rise buildings. For example, in 2016, Dhaka generated around 1.28 million tons of waste (0.149 million tons of construction and 1.139 million tons of demolitions) of which the three largest proportions were concrete (60%), brick/block (21%), and mortar (9%) [1]. Besides, according to the report of the U.S Tire Manufacturers Association [6], approximately 1.74 million tons of tires were generated only in the US in 2017, and among them, almost 0.65 million tons were disposed of in landfills. Thomas et al. [7] reported that every year almost 1000 million tires reach the end of their useful life and it will reach up to 1200 million by 2030. The disposal of these waste tires and the demolished concrete is becoming a major concern for scientific communities. However, these waste materials have great structural potential. The reuse of these waste materials can reduce the use of natural aggregate, side by side eliminating its related manufacturing processes, transportation exploration, and environmental costs as well as reduce the load on the landfill. The use of recycled coarse aggregate (RCA) is approved by the ACI Committee 555 [8] and also in the Canadian Standard [9]. Specifications are also included in the ASTM C33-18 [10] for regularizing the use of RCA in concrete.

1.2 Background

The use of RCA produced from the demolition of old concrete infrastructures and waste tires of vehicles in the concrete mixture can play a vital role in providing an economical solution to promote a sustainable construction practice. The RCA is capable of producing concrete with greater strength than concrete made of natural aggregate [11]. Besides, incorporating crumb rubber (CR) particles in concrete can increase toughness, ductility [12, 13], and energy dissipation capacity [14, 15]. The inclusion of RCA and CR in concrete reduces the strength but it can be improved significantly by incorporating fiber into the mixture [13, 16]. Furthermore, the fibers are capable of improving the ductility and toughness of concrete [13, 16]. The types of fibers being used by researchers so far may be categorized as natural, synthetic, glass, and steel fibers in a broad sense [17]. One of the synthetic fibers is PP fiber which is produced from the by-product of oil refining processes. The main advantage of PP fiber over steel fiber is that it does not suffer from corrosion as in the case with steel fiber, and thus polypropylene (PP) fiber reinforced concrete performs better in terms of durability [18]. Besides, the production and labor cost of PP fiber is relatively less [19], and low CO_2 emissions during the process of production [20].

Choi and Yun [21] worked with reinforced concrete columns containing both recycled coarse aggregate and recycled fine aggregate. It was observed that the axial capacity for recycled aggregate concrete (RAC) columns decreased by almost 10% compared to natural aggregate concrete (NAC) columns. Zhou et al. [22] showed that the RAC columns also possessed an elastic stage, crack stage, and fracture stage like NAC columns. Andrzej and Kliszczewicz [11] observed that RAC columns provided more ductile failure compared to NAC columns. Hassanli et al. [23] found that the confinement effect in rubberized concrete is higher than that of normal concrete due to the incompressible property of rubber. Besides, Son et al. [24] reported that the curvature ductility was increased up to 90% for rubberized concrete. Xue and Shinozuka [25] found that the average damping coefficient of rubberized concrete columns was 62% higher compared to conventional concrete columns.

Limited studies have been conducted on the combined effect of RCA, CR, and PP fiber in columns under uniaxial as well as dynamic loading conditions. Thus, this study investigates the combined effect of RCA, CR, and PP fiber on the compressive behavior and free vibration responses of reinforced-concrete columns subjected to pure axial loads and sufficiently stocky to ignore slenderness effects and evaluates the applicability of these newly developed rubberized recycled concrete (R^2C) and fiber-reinforced rubberized recycled concrete (FR^3C) columns by comparing them with the existing design standards developed for conventional reinforced concrete (RC) columns.

1.3 Objectives

The present study aims to investigate the effect of crumb rubber (CR) and polypropylene (PP) fiber on the compressive behavior and different dynamic properties of rubberized recycled concrete (R^2C) columns and fiber-reinforced rubberized recycled concrete (FR^3C) columns. Thus, the study is carried out with the following specific objectives:

1. To evaluate different fresh and hardened properties of R^2C and FR^3C mixtures.
2. To investigate the compressive behavior of various R^2C and FR^3C columns under uniaxial loading.
3. To determine different free vibration responses of R^2C and FR^3C columns through free vibration testing.
4. To examine the cost-effectiveness of R^2C and FR^3C mixtures.

1.4 Significance

The inclusion of RCA and CR particles in the reinforced concrete columns reduces axial capacity but improves ductility, energy absorption capacity, and lateral deformability. Besides, PP fiber can also increase the ductility and tensile capacity of concrete. However, all past studies investigated the individual effect of RCA, CR, and PP fiber on the compressive behavior of reinforced concrete (RC) columns, or their combined effects were limited to the concrete cylinders or small-scale prisms. Very few studies have been conducted with the combination of RCA, CR, and PP fiber in the RC columns. Besides, no appropriate methodology and design guidelines are found to be used for designing RC elements manufactured with this type of concrete. This research aims to investigate the effect of CR and PP fiber on the compressive behavior of R^2C and FR^3C columns by varying percentages of CR, steel longitudinal reinforcement ratio, and tie spacing. The failure modes of this new type of concrete are examined very carefully and explanations are provided for those failure mechanisms. The compressive behavior, influence of longitudinal and transverse reinforcement, effect of RCA, CR, and PP fiber, deflection characteristics, Poisson's ratio, curvature, toughness, and ductility have been examined. Besides, different dynamic properties have been evaluated through free vibration testing. The influence of CR and fiber on the natural frequency and damping ratio of concrete have been evaluated. An extensive regression analysis has been carried out based on the experimental result to predict different mechanical properties of FR^3C and R^2C. Finally, the test results are compared with different design formulas of conventional concrete, which are important to incorporate this new type of concrete in design guidelines. A cost analysis has been done to promote this new type of concrete as an eco-friendly and cost-effective concrete. Thus, this study creates a new horizon of opportunity to develop sustainable and resilient fiber-reinforced recycled rubberized concrete for the application in structural members and justify their applicability to the existing design code.

1.5 Scope

The present study is limited to investigating only the uniaxial behavior of R^2C and FR^3C columns under concentric compression loads. No eccentric load was applied. All the columns were scaled down to one-third of the original size of the columns due to the lower capacity of the universal testing machine (UTM). The RCA was used in all the columns for regularizing the use of C&D wastes and kept the replacement level constant at 30%. The effect of the percentage of PP fiber was ignored in this study. Production of high-strength concrete or self-compacting concrete was not either focused on in this study. Besides, the microscopy analysis was beyond the scope of this study.

1.6 Methodology

This research investigated the behavior of twenty-six one-third scale R^2C and FR^3C tied-square columns with 150 × 150 × 950 mm size subjected to monotonic concentric compression loads. From these twenty-six columns, nine columns were used for free vibration testing before conducting the compression test. The investigated parameters were longitudinal reinforcement ratio (1.4% and 2.0%), tie spacing (75 mm and 150 mm), and content of CR (0%, 5%, 10%, and 15%) with 0.5% PP fiber and 30% RCA replacement. The percentages were selected based on the previous studies. Choi and Yun [21] recommended using less than 30% RCA to produce more than 21 MPa concrete. Beyond that, the concrete strength was reduced. Thus, the RCA replacement level was fixed at 30% for conducting this research. Ismail and Hassan [12] found that using CR up to 10% provided a comparable strength with the control specimens and enhanced the deformation capacity, ductility, and toughness of concrete. Keeping these in mind, CR replacement levels were selected as 5% and 10% and for comparison purposes, a higher percentage (15%) was also selected. PP fiber provides various advantages over other fibers, such as reduced corrosion, greater durability, lower production, and labor costs, and lower CO_2 emissions during the manufacturing process [19,20]. However, Mohod [17] suggested limiting the use of PP fiber up to 0.5%.

To determine the compressive strength and modulus of elasticity of concrete, 108 concrete cylinders were cast having a diameter of 100 mm and a height of 200 mm. Besides, the concrete cylinders were used to determine the ultrasonic pulse velocity (UPV), hardened density, and surface resistivity of concrete. The tensile strength of concrete was determined by the direct tensile test of dog bone-shaped concrete specimens and the flexural strength was determined using 150 × 150 × 550 mm unreinforced concrete beams.

For the columns test, a displacement-controlled loading rate of 0.1 mm/min was applied gradually by a Universal Testing Machine (UTM). The columns were fixed at the top and bottom before starting the test. The applied load and its corresponding axial deformation were collected from the UTM. Moreover, to determine the midpoint lateral deflection four additional LVDTs were used at the mid-height of the column. Besides, three concrete strain gauges were glued on the surface of the concrete before testing at the mid-height of the column to determine the axial and transverse strain of concrete. Two steel strain gauges were mounted onto the internal reinforcement (one was with longitudinal reinforcement and one was with transverse reinforcement) before casting the concrete to determine the reinforcements strains. All data were collected at a regular interval by an automatic data logger system. Two high-resolution cameras were also used to capture the failure patterns of columns at different stages.

To investigate the free vibration responses of R^2C and FR^3C columns in comparison with the normal concrete columns, free vibration tests were carried out. Three accelerometers were used to collect the acceleration data. A hammer was employed to apply impact load to the mass. A displacement sensor was also mounted horizontally at the mid-point of the top head of the column, just opposite the hammer position. The free vibration data were recorded through a data acquisition system. Finally, different free vibrational responses were determined from the free vibration data.

1.7 Organization of the Thesis

The thesis work conducted for achieving the stated objectives is presented in seven chapters, which are briefly outlined in this section. Chapter 1 introduces the topic covering the general introduction to sustainable construction materials such as RCA and CR. Besides, the background of this study, objectives, significance, and scope of the study, a short brief of methodology, and the thesis outline have been summarized. Chapter 2 provides an extensive literature review on rubberized recycled concrete (R^2C) and fiber-reinforced rubberized recycled concrete (FR^3C). Different properties of R^2C and FR^3C along with their effect on reinforced concrete columns have been presented in this chapter. Chapter 3 describes the experimental procedure of this study. Physical properties of aggregates, mix design, specimens' preparation, and test setup are included here. Chapter 4 provides different fresh and hardened properties of R^2C and FR^3C. Besides, an extensive regression analysis has been carried out to predict different mechanical properties of R^2C and FR^3C considering the effect of CR and fiber. A cost analysis has been conducted to promote this new type of concrete as a cost-effective, sustainable, and eco-friendly concrete. Chapter 5 summarizes the uniaxial compressive behavior of the R^2C and FR^3C columns. The axial capacity, failure mode, influence of longitudinal and transverse reinforcement, effect of RCA, CR, and PP fiber, deflection characteristics, curvature, toughness, and ductility are presented in this chapter. Chapter 6 describes the free vibration responses of R^2C and FR^3C columns. The effect of CR and fiber on natural frequency, time period, and damping is briefly discussed in this chapter. Finally, Chapter 7 presents the conclusions, which can be drawn out from this study, and also discusses the research contribution, limitations of this study, and recommendations for future research.

Chapter 2
LITERATURE REVIEW

2.1 Introduction

As the world moves on with extreme urbanization, soon there will be insurmountable damages made to the non-renewable resources as well as to the environment. Concrete, as we know, is one of the biggest consumed products in the world [26]. Every year, throughout the world, almost thirteen million tons of natural aggregates are extracted for construction purposes [1]. The significant increase in aggregate demand has resulted in the depletion of natural resources and becoming a serious concern for environmentalists. On the other side, annually, a large amount of concrete waste is produced throughout the world during the demolition process. For instance, China alone generates 200 million tons of concrete waste each year [4]. Similarly, around 450 million tons of concrete waste is produced per year in European Union countries [5]. In Canada, concrete waste occupies the largest portion of all the construction and demolition (C&D) waste [2]. Using concrete waste as recycled coarse aggregates (RCA) has been a subject of interest for many researchers for a long [2, 8, 16, 27, 28]. Studies conducted in past had achieved remarkable results in the properties of concrete with the use of recycled aggregates [21, 29-32]. Later some studies reported a reduction in compressive strength and an increase in the water absorption capacity of concrete due to attached old mortar [28, 33, 34]. These findings and the cost involved in the processing of concrete waste demand the search for new aggregates replacement materials.

Over the last decade, the use of crumb rubber (CR) in concrete as aggregates replacement materials has gained popularity owing to its salient features such as low density and high ductility [12, 14, 35, 36]. These crumb rubbers are formed during the process of recycling scrap types and according to a report [6, 7], almost one billion tires annually reach to end throughout the world. These scrap tire wastes need special disposal treatments as they pose a serious fire threat. Past studies [21, 28, 30-34, 37-40] had reported the physical, mechanical, and thermal properties of crumb rubber used as an aggregate in normal concrete. These researchers suggested the use of crumb rubber as an aggregate replacement owing to its compatibility with concrete.

2.2 Recycled Coarse Aggregates, Crumb Rubber, and Fiber

This section presents the possible source and production process of recycled coarse aggregate (RCA), crumb rubber (CR), and fiber along with their advantages and disadvantages.

2.2.1 Recycled Coarse Aggregates

The source and production process of RCA and its merits and demerits over natural coarse aggregate (NCA) is discussed below.

Source and Production of Recycled Coarse Aggregates

The recycled coarse aggregates are produced from the demolition waste of concrete buildings and structures [2, 27]. These wastes after passing through different stages of crushing, shedding, grinding, and sorting are used in concrete as a replacement for aggregates [8]. During the recycling process, impurities are added to the aggregates. To make it environmentally friendly, Oikonomou [41] reported the maximum limit of possible harmful elements as presented in Table 2.1, for instance, zinc (Zn) and copper (Cu) need to be less than 400 and 200 (μg/l). In 2001, the ACI Committee 555 [8] approved the use of recycled coarse aggregates in concrete while the ASTM C33 [10] and CSA A23.1 [9] standards and specifications are also used by different countries which encourage to use of RCA. The schematic process of crushing and sorting the RCA from demolished structures is presented in Figure 2.1.

Table 2.1 Allowable limits of various harmful elements in RCA [41].

Element-Substance	Limit (μg/l)
Zinc (Zn)	400
Copper (Cu)	200
Lead (Pb)	100
Nickel (Ni)	100
Chromium (Cr)	100
Arsenic (As)	50
Cadmium (Cd)	5
Iodine (I)	2

(a) Demolished Building

(b) Removal of Contaminants & Dropped Inside Hopper

(c) Aggregates Passed Through Conveyor Belt

(d) Larger Particles Processed into Impact Crusher for Secondary Crushing

(e) Gathered into a Bucket Loader at the End of Crushing Stage for Marking

(f) RCA Used as Coarse Aggregate

Figure 2.1 Production of RCA (modified images from sources [2, 16, 42]).

Merits and Demerits of Using Recycled Coarse Aggregates

RCA is being used worldwide due to its environmentally friendly solution in opposite to the deterioration of limited resources in concrete construction. Besides, it can reduce loads on landfills by reusing this construction waste. In terms of physical properties of recycled aggregates, Hossain et al. [16] and Huda and Alam [2] found lower density in comparison to natural coarse aggregates (NCA) making it an ideal choice for lightweight as well as for energy-efficient structures. The reduction in compressive strength and an increase in water absorption with the addition of recycled aggregates was observed by past researchers [28, 31, 32, 43], and attached old mortar was mainly found responsible for variations in these results. However, some of the investigations had reported higher strength as compared to NCA [21, 29, 30]. The statistics presented by the Environmental Council of Concrete Organizations (ECCO) [33] had shown a 60% reduction in the cost with the use of RCA as compared to NCA concrete mixtures. Similarly, Verian et al. [34] reported a cost of \$2.26–\$2.93/ton in the concrete pavement with the addition of RCA. Also, had strongly encouraged the use of RCA in concrete to preserve the natural resources as well as the environment [30]. It was found that CO_2 emission was reduced up to 40% when NCA was replaced by RCA and arc furnace slag [44-46]. A study by Hossain et al. [47] also showed that the greenhouse gas footprints were reduced up to 65% when RCA derived from C&D waste was used in construction.

2.2.2 Crumb Rubber

Different types of rubber aggregates and their source and production process along with their merits and demerits over natural aggregate is described below.

Source and Production of Crumb Rubber

A huge amount of scrap tires is discarded throughout the world annually [7]. These scrap tires are shredded into pieces to make CR. The coarser particles which are used as a partial replacement of NCA are called chipped rubber aggregate. Secondly, the rubber particles which are typically sized between 4.75 and 0.425 mm and known as crumb rubber are used as a partial replacement for natural fine aggregate (NFA) [48]. The rubber aggregates passing through sieve No. 40 (0.425 mm) are classified as fine-grained rubber while fiber rubber aggregate is typically 8.5 - 21.5 mm long and in the form of strips ≤8 mm long [48-50]. The classifications of rubber aggregate are summarized in Table 2.2. The stage-wise processing of CR derived from scrap tires illustrated in Figure 2.2. The CR particles are generally composed of carbon and oxygen. The details of the chemical composition of rubber particles as reported by different researchers are presented in Table 2.3.

Table 2.2 Classifications of rubber aggregate.

Types of Rubber Aggregate				Reference
Shredded/Chipped Rubber (mm)	**Crumb Rubber (mm)**	**Ground/Powdered Rubber (mm)**	**Fiber Rubber Length (mm)**	
13–76	0.425–4.75	<0.425	-	Ganjian et al.[48]
13–76	0.5-5	0.15–19	8.5–21.5	Siddique and Cachim [54]
25–30	3-10	<1	-	Gerges et al. [55]
-	-	-	8.5-21.5	Baoshan et al. [49]
-	-	-	<8	Emiroglu et al. [50]

Figure 2.2 Stage-wise process of tire-shredding (modified images from sources [40, 51-53]).

Merits and Demerits of Using Crumb Rubber

Every year almost 1 billion tires reach to end of their service lives [7]. This huge amount of tires is generated as waste all over the world creating a great threat to the environment. The main advantage of using rubber in concrete is to produce sustainable and eco-friendly concrete that can also reduce the load on landfills as well as on the whole environment. It also reduces carbon dioxide emissions to the environment. The rubber particles derived from these waste tires have the potential for use as aggregate. The researchers had suggested the use of rubber as the replacement of NFA over NCA [15, 16, 31, 56, 64-66]. Past studies [12, 14, 35-38, 67, 68] had reported that CR not only provides an effective solution to excessive scrap management problems in the landfills but also is effective in producing concrete that possesses higher ductility, high energy dissipation capacity, enhanced resistance for cracking and spalling as well as improved freeze and thaw. The specific gravity of rubber is much lower than that of NFA [16, 56], thus reducing the self-weight of the structures. Presti [69] pointed out that a significant reduction in maintenance cost is achieved in rubberized concrete. Besides, Mhaya et al. [51] reported that the incorporation of CR in concrete mixes can reduce CO_2 emissions by 0.02%, 0.03%, 0.06%, and 0.09% for 5%, 10%, 20%, and 30% CR content, respectively. Despite these advantages the CR tends to decrease the compressive strength, modulus of elasticity (MoE), splitting tensile strength [56, 70-72], and increase water absorption and permeability [73, 74]. Such drawbacks of using CR have led the researchers to opt for pre-treated CR for a better performance of the rubberized concrete.

Table 2.3 Chemical composition of CR by different researchers.

Elements (Symbol)	**Weight (%)**											
	Untreated								**Treated**			
									20% NaOH	**10% NaOH**	**20% NaOH**	**NaOH**
	Meherier [56]	Gupta et al. [57]	Mhaya et al. [51]	Angelin et al. [58]	Tamanna et al. [31]	Chen et al. [60]	Copetti et al. [61]	Muñoz-Sánchez et al. [62]	Ahmed et al. [63]	Tamanna et al. [31]		Copetti et al. [61]
Carbon (C)	69.95	87.51	14	91.50	88.60	81.16-85.19	44.30	30-38	88.88	44.70	19.70	60.14
Oxygen (O)	20.93	9.23		3.30	9.40	1.72-2.07	6.54		8.65	29.60	57.2	5.36
Sodium (Na)	0.38			0.20					0.49			0.44
Magnesium (Mg)	0.23	0.14							0.06			0.08
Aluminium (Al)	0.71	0.08					0.95		-			
Silicon (Si)	1.53	0.20			0.20		1.32		0.09	22.70	22.90	0.21
Sulfur (S)	1.42	1.08		1.20		1.52-1.64	0.48	≤5	1.08			1.70
Potassium (K)	0.12								0.03			
Calcium (Ca)	0.22			0.10	0.70		0.39		0.26	3.00	0.20	0.26
Iron (Fe)	2.43						16.42		-			0.27
Copper (Cu)	0.15						3.58		-			
Zinc (Zn)	1.91	1.76		3.50	1.10		15.04		0.46	0.00	0.00	4.04
Hydrogen (H)				0.20		7.22-7.42						
Nitrogen (N)						0.31-0.47						
Acetone Extract			10									
Ketonic Extract								10-20				
Ash Content			24			3.84-7.44		3-7				
Rubber Hydrocarbon			52									
Polymers								40-55				
Natural Rubber								21-42				

2.2.3 Fibers

The types of fibers commonly used in concrete are natural, synthetic, glass, and steel fibers [17]. Among other fibers, steel fibers are most commonly used in the production of concrete as these are capable of reducing the shear reinforcement requirement in concrete structures [75]. One of the synthetic fibers is polypropylene (PP) fiber which is produced from the by-product of oil refining processes. The main advantage of PP fiber over steel fiber is that it does not suffer from corrosion as in the case with steel fiber, and thus PP fiber reinforced concrete performs better in terms of durability [18]. Besides, the production and labor cost of PP fiber is relatively less [19], and low CO_2 emissions during the process of production [20]. Besides, PP fibers perform better in decreasing segregation and increasing cohesiveness among the ingredients [31]. Due to its lower specific gravity, the requirement of PP fibers in the concrete is lower than that of steel fibers [76]. Over the last decade, the use of fibers in concrete had increased significantly. Past researchers [16, 77, 78] had reported improvement in ductility, energy absorption capacity, and the tensile and flexural strength of concrete with the addition of fibers. Although some of the investigations had observed a reduction in compressive strength and workability [16, 77, 78].

2.3 Properties of Concrete Containing RCA, CR, and Fiber

This section summarizes the different fresh and hardened properties of concrete containing RCA, CR, and Fiber. Besides, their microstructural characteristics and life cycle assessment have also been discussed.

2.3.1 Microstructure

The microscopic analysis and spectroscopic analysis of recycled aggregate concrete (RAC), rubberized concrete (RuC), and fiber-reinforced concrete are discussed below.

Scanning Electron Microscopy Images

Past researchers [42, 56, 61, 79] employed the scanning electron microscope (SEM) technique to understand the formation of the interfacial transition zone (ITZ) with the addition of CR, fiber, and RCA. Previous studies [42, 56, 61] reported irregular shapes and rough surfaces of

CR particles by using SEM images (Figure 2.3). This irregularity in shape could be the possible reason for entrapping air during the mixing process of rubberized recycled concrete (R^2C) [80]. In a recent study, Copetti et al. [61] reported a smoother surface texture of the crumb rubber particles after being treated with Sodium Hydroxide (NaOH). Similar findings were reported by Su [42] after treating with NaOH solution and silane coupling agent (SCA). A tight silicone coating was observed on the surface of CR particles after being treated with SCA. Also, the SEM micrographs showed loose attachment of NaOH crystals to the surface of CR particles with no evidence of surface roughness alternation. To observe the bonding characteristics between rubber particles and cement paste, Meherier [56] through SEM micrographs found failure occurring around the CR particles. The weaker ITZ between cement paste and CR particles could be the reason for this failure. Tamanna [31] studied the microstructure of CR particles treated with 10% and 20% of NaOH solution by using the SEM micrographs (Figure 2.4). The author observed a significant reduction in crack size and width in ITZ between CR and cement paste with a higher concentration of NaOH solution. Also, the improved ITZ contributed to gaining higher compressive strength than with untreated CR and with 10% treatment. Similar findings were reported by Ahmed et al. [63] for the CR 20% NaOH treated particles. Although Copetti et al. [61] reported no significant changes in the ITZ after the NaOH treatment but had observed the densification of ITZ with the addition of silica fume. This densification which happened due to the micro filling effect of silica fume had shown drastic improvement in the mechanical properties of R^2C.

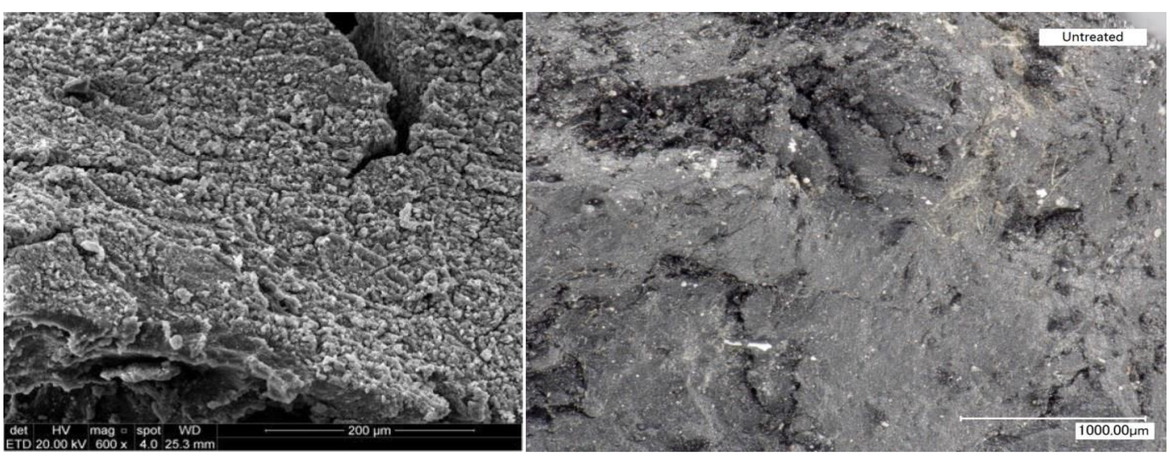

(a) (b)

Figure 2.3 Micrographs of untreated CR surface: (a) Copetti et al. [61], and (b) Su [42].

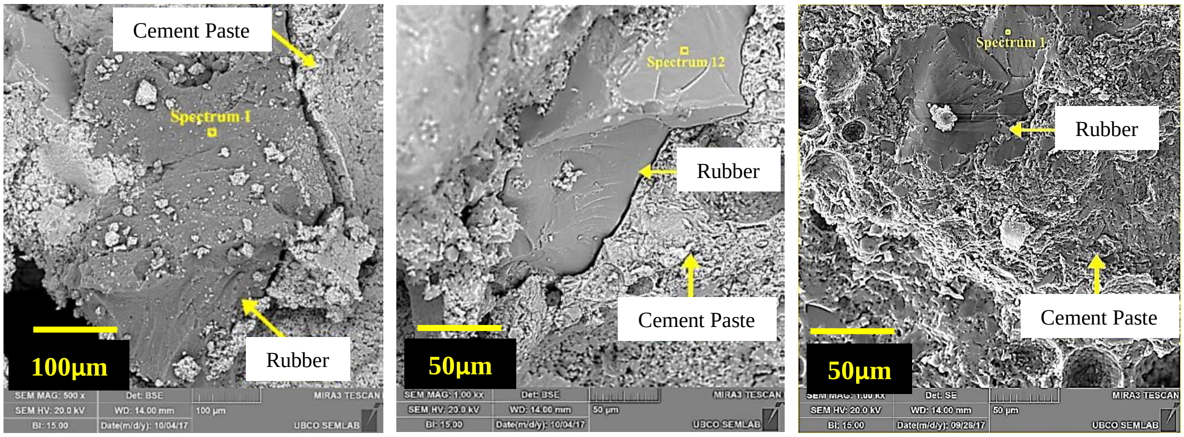

(a) **(b)** **(c)**

Figure 2.4 Concrete blended with 20% CR particles: (a) no pre-treatment, (b) treated with 10% NaOH, and (c) treated with 20% NaOH [31].

The interfaces of rubber-cement paste and recycled aggregate-cement paste were inspected by Su [42]. After studying different SEM micrographs, the author reported a smooth transition zone between RCA and cement paste as compared to rubber-cement paste (Figure 2.5). Also, cracks were noticed at the interface between rubber and cement paste indicating poor adhesion. In addition, Mohseni et al. [81] observed larger gaps at the interface of RCA and cement paste, primarily due to mortar attached to the surface of RCA. Comparing the control specimen with PP fiber reinforced concrete, Mohseni et al. [81] found that, before applying load on concrete, several microcracks were observed at the cement matrix of the control specimen due to the shrinkage of concrete (Figure 2.6 (a)) while a better restrain in crack propagation was observed in fiber reinforced concrete due to the strong bond between the fiber and cement paste (Figure 2.6 (b)). Besides, plenty of well-developed cement hydrated products were produced at the interface between the PP fiber and cement paste. No chemical reaction occurred between the fibers and cement paste during the hydration process which indicated that the both the cement paste and fibers were working effectively in the interfacial zone.

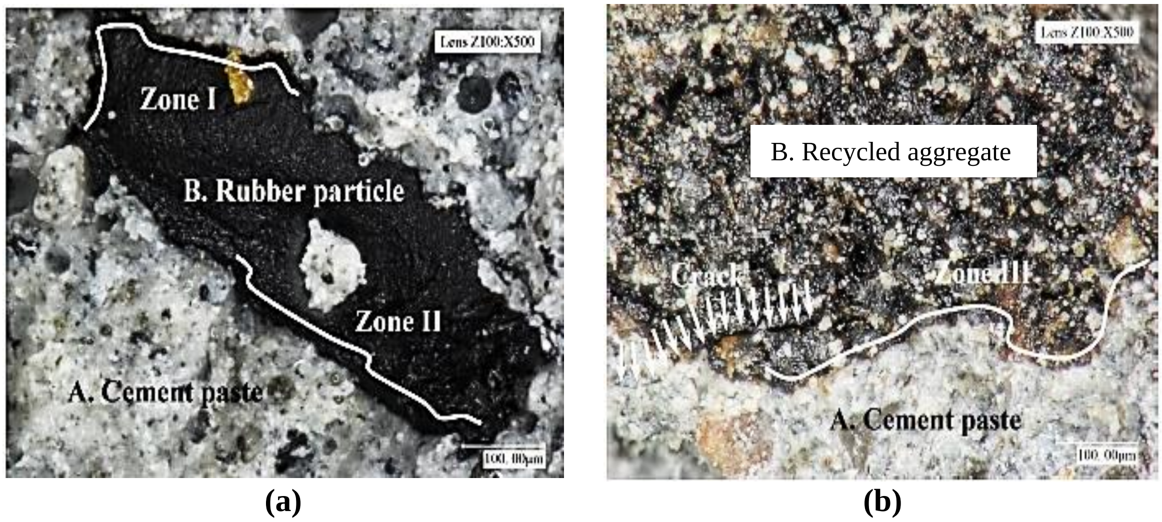

Figure 2.5 Concrete blended with CR particles: (a) interface of rubber-cement paste, and (b) interface of recycled aggregates-cement paste [42].

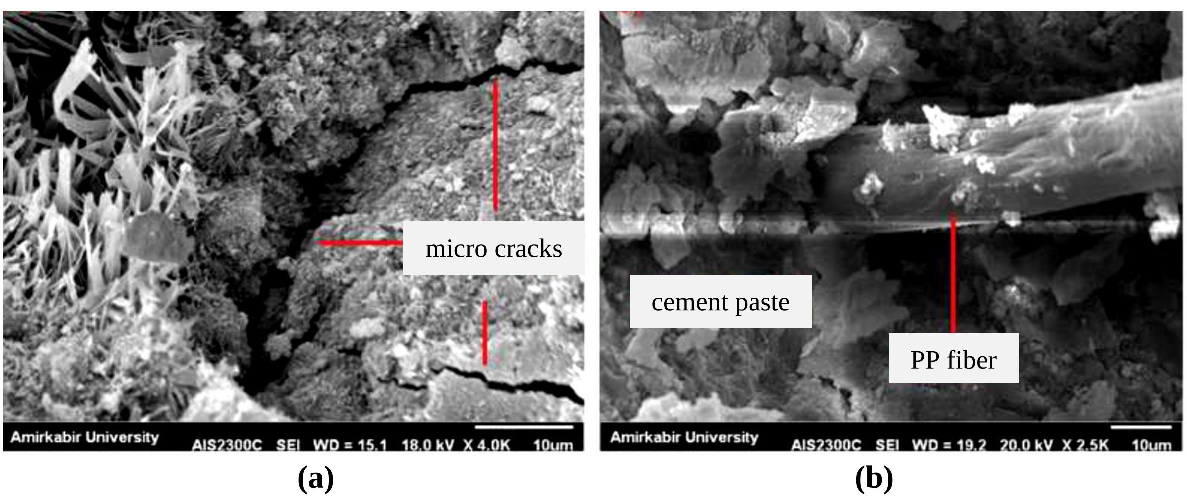

Figure 2.6 Micrographs of concrete: (a) control, and (b) specimen containing PP fiber [81].

Energy Dispersive Spectroscopy Technique

The energy dispersive spectroscopy (EDS) techniques are employed to get comprehensive information about the elements present in a material. By using this technique, Meherier [56] found that the CR particles contained Carbon (C) and Oxygen (O) elements, whereas Sulfur (S), Silicon (Si), Iron (Fe), and Zinc (Zn) were also present within a range of 1% to 3% by weight (Table 2.3). Meherier [56] and Richardson et al. [82] reported that hydrophobic elements such as Silicon (Si) and Zinc (Zn) are mainly responsible for increasing the initial and final setting time of R^2C which eventually makes crumb rubbers water-resistant. To improve the performance of CR particles, Tamanna et al. [31] treated with NaOH solutions and found complete removal of Zinc (Zn) from the particles (Figure 2.7). In addition, it was found that the reaction of CR particles and the cement paste produces oxidation elements such as oxygen (O) and silicon (Si). Most of the researchers [31, 56, 63] had suggested pre-treatment of CR with 20% NaOH solution for enhanced bonding between CR particles at ITZ.

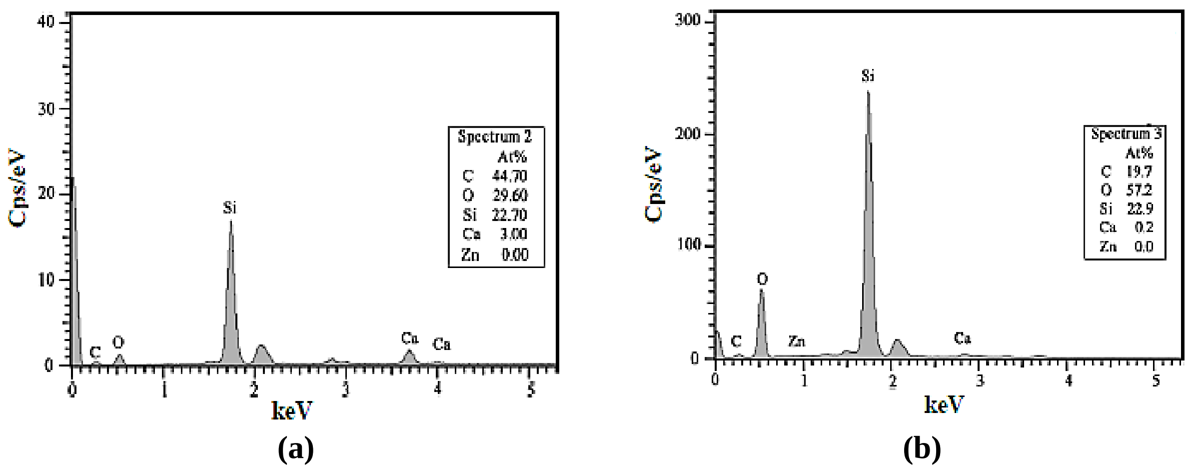

Figure 2.7 Energy dispersive spectroscopy analysis of treated CR particles in mortar mixture: (a) treated with 10% NaOH, and (b) treated with 20% NaOH [31].

2.3.2 Fresh Properties

The effect of RCA, CR, or fiber on different fresh concrete properties such as workability and air content is discussed below.

Workability

The decrease in the workability of concrete mixtures with the addition of RCA, CR, and fibers, has been reported by past researchers [16, 71-73, 83]. This drop is primarily due to different specific gravity of constituents present in the mixtures, for instance, fibers, crumb rubber, and recycled aggregates [31, 56, 73, 83]. Recently, Marie [84] observed a slump value of 75.3 mm for the control mixture and a decrease of 42% for R^2C mixtures blended with 20% of RCA and 20% of CR. However, Henry et al. [85] reported an increase in slump values (9.5 cm to 13 cm) for CR substitution of 25% to 50% with 100% RCA for concrete mixtures. After two years of

Henry et al. [85] findings, Guo et al. [86] observed a decrease in slump values (132 mm to 125 mm) with 100% RCA substitution and the addition of CR dropped these values further. Also, stable slump values were observed for the CR substitution range of 8% to 16% in concrete mixtures.

Chen et al. [87], Hossain et al. [16], and Shahjalal et al. [13] investigated the effect of polypropylene (PP) fiber along with CR and RCA in the concrete. Recently, Hossain et al. [16] observed that after the inclusion of PP fiber into the concrete mixture the slump value decreased and it decreased with increasing the percentage of PP fiber. For instance, approximately 41% reduction in slump values for the concrete mixtures blended with 10% of RCA, 5% of CR, and 1% of PP fibers. By increasing the PP fiber content to 2% the difference jumped to 65.5%. Similar findings were observed by Shahjalal et al. [13] while investigating the slump for FR^3C blended with 0.5% PP fiber. Most of the researchers [16, 31, 42, 66] had related reduction of slump values due to the high water absorption capacity of RCA and low density of fibers and CR. Apart from normal concrete, the decrease in the workability of rubberized recycled aggregates self-compacting concrete was also observed by Aslani et al. [39], especially with the change in RCA content. However, Chen et al. [87] suggested the use of RCA with a lower substitution ratio for achieving better workability results. Besides, the loss of workability due to RCA, CR, or fiber can be addressed by using saturated surface dry (SSD) aggregates, using water-reducing admixture, incorporating various supplementary cementitious materials such as fly ash, slag, silica fume, metakaolin, treated CR particles with NaOH solution [30, 31, 63, 86, 88, 89].

Air Content

Past studies [42, 56] had reported an increase in the air content value with the addition of CR in RAC mixtures. In a study, Tamanna [31] reported similar findings and inferred that adding CR in higher content could significantly increase the air content. Earlier, Henry et al. [85] observed no changes in air content values for mixtures blended with 100% RCA and CR added in 25% and 50% ratios. Later in 2017, Marie [84] noticed a surge in the air content value as the replacement ratio of RCA gets higher. Recently, Hossain et al. [16] attempted to investigate the effect of PP fiber on-air content. After adding PP fiber into the concrete mixture the air content value started to decrease. The authors found the highest values of air content for the

FR^{3}C mixtures blended with 1% PP fibers, 10% CR, and 30% RCA respectively. A difference of 62% was noticed in the air content values than with normal concrete. This difference was explained by Hossain et al. [16] due to the presence of adhered mortar in RCA particles becoming the source for entrapping air. Besides, the CR particles entrap air in the concrete mixture and increase the air content. Similar results were reported by Ahmed et al. [63] with 0.5% PP fibers.

2.3.3 Hardened Properties

The effect of RCA, CR, or fiber on different hardened properties of concrete such as compressive strength, modulus of elasticity, splitting tensile strength, flexural strength, impact resistance, toughness, ductility, density, etc. are discussed below

Compressive Strength

Most of the past researchers [70-72, 90-92] had recorded a reduction in compressive strength with the inclusion of CR and RCA. This reduction in strength was irrespective of the size, content, and treatment of CR. In a study, Henry et al. [85] found compressive strength relating inversely to the CR content when tested for samples with 100% RCA. Later, Feng et al. [93] also recorded a significant drop of 27.8%, 39.2%, and 47.2% in the strength of the concrete with 10%, 20%, and 30% of CR and 100% recycled aggregates. Next, Tamanna [31] investigates the strength of the R^{2}C samples in which CR was treated with 20% of NaOH and finally, the reduction was noticed. This reduction of compressive strength is primarily due to inadequate adhesion of CR with concrete, the low water absorption capacity of CR, and the porous nature of RCA [16, 31, 43, 71, 72, 84, 94]. Another factor found to influence the strength of R^{2}C mixtures was the particle size of CR as reported by Li et al. [95]. It was observed that as the size of the CR particles reduced the compressive strength dropped significantly and this was regardless of CR content. Similar results were reported by Ahmed et al. [63] but with different content of RCA. In addition, Aslani et al. [39] measure the strength of self-compacting R^{2}C incorporated with 20% CR but the results were not different from other researchers' findings. This reduction was explained by the researchers [96-98] due to the unbonded interface among recycled particles and cement paste that creates a weaker ITZ also due to the lower stiffness of rubber particles.

Nonetheless, some of the researchers, along with CR, and RCA tried using different fibers to improve the compressive strength and other hardened properties. Chen et al. [87] initially observed a decrease in the compressive strength for the samples with RCA (40%) and CR (10%) but after incorporating 4 kg/m^3 of basalt fibers a rising trend was observed. Similarly, Ahmed et al. [63] recorded compressive strength increased up to 31% compared to its counterpart sample with no fiber. The author used 0.1% of steel wire in FR^3C with RCA (100%) and CR (20%). Similarly, when PP fibers were added approximately 26.4 % rise in strength was noticed in FR^3C [15, 16]. According to Hossain et al. [16], the higher content of fibers was also found to enhance the strength while the optimum value of 0.5% for PP fibers for improving the properties was recorded by Shahjalal et al. [13]. However, Su [42] reported a decline in the compressive strength with 1 kg/m^3 of PP fibers in FR^3C. The author stated that when CR was limited to 20%, the compressive strength of most of the FR^3C samples exceeded the design target strength. The same trend was also noticed by Tamanna [31].

Alfayez [66] worked with preplaced aggregate concrete (PAC) also known as “two-stage concrete” (TSC), where coarse aggregates were firstly placed in a formwork, followed by injecting cementitious grout mixed with chemical admixtures to fill in the void along with RCA, CR, and fiber. It was noticed that the compressive strength of the FR^3C decreased with an increase in CR content and steel fibers. However, these findings were against the observation of Hossain et al. [16] as a reverse trend was noticed with a higher content of PP fibers. This phenomenon was explained by Alfayez [66] due to the obstruction posed by steel wires to fill the gaps between aggregates thus, leading to a porous microstructure. Nevertheless, if strength is of great concern then Guo et al. [86] suggested using 4% of CR in FR^3C. Xie et al. [99] thought of adding silica fume (SF) in FR^3C specimens by replacing cement with different substitutions. The addition of 10% SF along with 1% steel fibers and 5% CR enhanced the interface bond with filler effect and as a result higher compressive strength was achieved. Furthermore, Aslani and Klein [100] observed that 0.1% PP fiber and 0.75% of steel fiber can increase the compressive strength of lightweight self-compacting rubberized concrete by 22% and 47% respectively. From Tamanna's [31] and Ahmed et al.'s [63] studies, it was noticed that after the treatment of NaOH and with the addition of fibers (0.1% steel and 0.5% PP) a higher strength of 15%-59% (of control samples) can be achieved.

Modulus of Elasticity

The reduction in modulus of elasticity (MoE) values for RAC and R^2C concrete was recorded during the investigations by different researchers even though the increased content of RCA and CR brought no significant change in MoE results [31, 92, 101, 102]. Recently, Chen et al. [87] reported a nominal difference in MoE values for RAC in comparison with NAC. However, Gupta et al. [103] measured the reduction of 27% and 28% in MoE values for rubberized concrete (RuC) and R^2C samples respectively. Some of the researchers [101, 104, 105] found that CR particles were responsible for decreasing the MoE as the participation of rubber against external load was quite low in concrete. Tamanna [31] took a new direction and studied the effect of RCA and CR content on MoE in R^2C samples. The author reported improved results with 50% RCA compared to 100% RCA, especially with the combination of 10% CR which resulted in a 7.4% rise. Although, the addition of fibers was found to enhance the ductility, toughness, and tensile properties of the RuC but MoE properties remained unaffected [31, 94]. Steel fiber reinforced R^2C was studied by Xie et al. [99] and a decrease of 10% to 25% in MoE for rubber content range of 5% to 20% was observed. Also, a decrease in the stiffness of FR^3C was noticed with higher CR content. In another study, Jian-he et al. [106] reported a decrease of 43% in MoE value with the inclusion of steel fibers. Similar results were reported by Alfayez et al. [66] for pre-placed RAC. However, Tamanna [31] reported a 17% increase in the MoE value with the inclusion of 0.5% polypropylene fibers in FR^3C.

Stress-Strain Relationship

Chen et al. [87] observed that the addition of RCA and CR had significantly increased the ultimate strain of R^2C and RuC while the strength remained lower in comparison with NAC. Similar improvements were noticed by Feng et al. [93] and Su [42]. Accordingly, decreasing curves of stress and strain were observed with the higher content of RCA and CR in R^2C mixtures by Tamanna [31]. Earlier Feng et al. [93] had reported an optimal value of 20% CR content for strain and deflection. Other researchers [107, 108] also reported similar findings. During the investigation, Guo et al. [86] studied the FR^3C samples and observed a decrease in the slope of the stress-strain curve with an increase in CR content. However, the addition of basalt fiber (BF) in the proportion of 2 kg/m^3 and 4 kg/m^3 had resulted in improved ultimate stress and strain [87]. Recently, Alfayez [66] experienced an increased ductility of FR^3C with the addition of steel fibers and the effect was pronounced with higher CR content. Jian-he et al. [106] also reported similar results for FR^3C samples but with 100% RCA replacement.

Splitting Tensile Strength

Most of the results [13, 16, 31, 39] showed that the tensile capacity of the R^2C decreased as the CR content increased. Ahmed et al. [63] reported a drop of up to 38% tensile strength for samples replaced with RCA (0% to 100%) and added with CR in the ratio of 0% to 20%. Against these findings, Tamanna [31] reported that 50% of RCA and 10% of CR can increase 11% of tensile strength. Another mix showed improved strength with 100% RCA and 20% CR compared to the concrete containing either the RCA or CR. For further enhancement in the tensile strength, the researchers decided to add fibers along with RCA and CR. Most of the reports [13, 16, 31, 66, 87] concluded that steel and PP fibers contribute to increasing the tensile strength but if the RCA and CR content is increased for the same fiber ratio then the influence of fibers remains nominal. They reported an increment in tensile capacity because fibers have bridging characteristics hence allowing the tensile stresses to be distributed along the cracks formed during loading [109-111].

Flexural Strength

The significant influence of CR particle size on the flexural strength of R^2C has been reported by recent and past studies. Li et al. [95] reported an increase in flexural strength as the particle size of CR increased and this trend remained unaffected with higher CR content. However, Su [42] observed a decrease in the flexural strength with increased particle size. This reduction was up to 13%,11.3% and 10.9% for 3 mm, 0.5 mm and 0.3 mm (CR particles) respectively. The author found improved strength with smaller particle sizes due to the filler effect that increases the compactness of the concrete and consequently the likelihood of fracture reduces [42]. Feng et al. [93] reported that the inclusion of CR particles into the concrete mixture had resulted in a notable flexural strength reduction. However, the requirement of flexural strength for designing aircraft movement areas was still met by using CR content up to 20% which was greater than 4.5 MPa [93, 112]. The addition of fibers had significantly improved the flexural strength [16, 66, 87]. Hossain et al. [16] studied the effect of PP fibers on rubberized recycled concrete (R^2C) and reported an increase in flexural strength. This rise was found to strengthen further with higher fiber content. These results were expected as fibers possess an interlocking property that helps in creating a strong bridge between the aggregate and cement paste. Furthermore, the flexural strength of FR^3C was found to weaken with the inclusion of RCA and CR and the strength gets worse with higher replacement content [66, 87, 106, 113, 114].

Dynamic Behavior and Impact Resistance

The dynamic compressive strength of R^2C was found to improve by increasing CR particle size for instance 4.04 mm [95]. Li et al. [95] also notified that increasing the strain rate contributed to strengthening the dynamic compressive strength and this was found irrespective of CR particle size and content. However, with a higher CR replacement level, the dynamic compressive strength reduced but dynamic increase factor (DIF) values took the peak. This could be due to the inherent elasticity and relatively low strength of the rubber particles which weakens the bonds. To determine the impact resistance of fibers in R^2C, Shahjalal et al. [15] performed a repetitive drop-weight impact test on FR^3C and found an increase in energy absorption capacity. This capacity further increases by blending CR and PP fibers in higher proportions. The reported difference for 30% RCA, 10% CR along 1% or 2% PP fiber was 2.5x times that of normal concrete [15, 59]. Similarly, enhanced capacity was reported by Alfayez [66] where up to 40x times more impact resistance capacity was observed for steel fibers when used in the ratio of 1.5% in FR^3C. This rise in capacity is primarily due to the ability of steel fibers to restrain crack propagation under impact loading.

Toughness and Ductility

An enhanced energy absorption capability, ductility, and toughness were observed in previous studies in R^2C after the inclusion of CR content [93, 95]. However, excessive CR content would negatively affect the energy dissipation capacity of the R^2C [36, 101]. Xie et al. [99] noticed a 15% CR replacement as a cutoff point. Jian-he et al. [106] also found the same observation where with the increase of CR content, the compressive toughness initially increased and then started to decrease. Li et al. [95] investigated that the size of the CR particles had an influence on the toughness index of R^2C and reported that the toughness index was decreased for the greater particle size of CR. Hossain et al. [16] investigated the PP fiber-reinforced rubberized concrete containing RCA and reported a higher toughness value than the control samples. Moreover, the addition of fibers in higher quantity contributes further to increasing the toughness and ductility [16, 66]. This is primarily due to the higher energy absorption capacity of rubber improves the toughness ability which was further increased by adding fiber content [115-117]. Besides, a strong bond between aggregate and cement was built in the presence of fibers [16, 66]. Xie et al. [99] noticed an increase of 9% and 13.9% in the toughness of NAC and RAC when added with 1% of steel fibers. However, researchers suggest limiting the use of CR in FR^3C up to a certain level for better toughness value. For instance, Jian-he et al. [106] found optimal toughness with 8% of CR replacement in FR^3C while recently Hossain et al. [16] had reported 5% of CR ideal selection for increasing the toughness in FR^3C samples. Xie et al. [99] limited the CR content to 15% with 1% steel fibers.

Treatment Method

Most of the researchers [31, 118-124] had noticed a significant improvement in the performance of RAC, R^2C, and FR^3C with the appropriate treatment method. The contaminants and the attached mortar of RCA are mainly responsible for reducing the strength and increasing water absorption of RAC [30-32, 43]. The removal of unwanted contaminants and attached mortar on RCA can be done by crushing RCA with the appropriate type of crushers (i.e. impact crusher and cone crusher) [125]. Besides, washing the RCA for removing fine particles [8], and soaking in 0.1M of HCl solution for removing the old mortar [30] were also suggested. Some other common methods are pre-soaking into acids [119], coating with silane-based water repellent [120], and carbonation [121]. Although these methods had shown reasonable performance, the impact on the environment had concerned many researchers. Recently, Tang et al. [126] introduced a treatment agent based on lithium silicate. After being treated with this agent the reported compressive strength for self-compacted samples was 18.5% (50% RCA) and 16% (100% RCA) more than with untreated concrete. In addition, the tensile strength for RAC with 50% RCA was found close to normal concrete.

The researchers [31, 63, 118, 122, 124] improve the performance of CR by applying different pre-treatment methods. These treatments change the smooth textures of CR and develop a strong bond between CR and the cement matrix. Most commonly the rubber particles are treated with Sodium Hydroxide (NaOH) solution for a specified period making the surface of the CR uneven [31, 42, 56, 63, 122, 124, 127]. Meherier [56] reported that, due to the presence of zinc and silicon, the surface of the CR is hydrophobic that resulting in a weaker bond with the cement paste for which Mohammadi et al. [124] suggested the use of NaOH solution for making the rubber particles surface relatively rougher. Ahmed et al. [63] found that CR treated with 20% NaOH solution showed a reduction of 94% and 76% in the content of silicon and zinc. Some of the researchers [42, 127, 128] had applied coating with a silane coupling agent (SCA) while others simply washed the rubber particles with water [122, 129] (Table 2.4). Additives of cementitious materials like silica fume also showed good results [99, 130].

Table 2.4 Summary of treatment methods adopted by researchers.

Rubber Treatment Methods	References
Water washing	Najim and Hall [129], Youssf et al. [122]
10% and 20% concentrated NaOH solution	Ahmed et al. [63], Tamanna et al. [118], Tamanna [31]
10% NaOH solution for 120 min followed by water washing	Youssf et al. [122]
Saturated NaOH solution for 2 hours and 24 hours	Su [42], Su et al. [127]
Treatment with silica fume	Onuaguluchi and Panesar [130], Xie et al. [99]
Treatment with CS_2	Emam and Yehia [131]
Silane coupling agent	Su [42], Su et al. [127]
Coating of rubber particles with mortar	Najim and Hall [129]

Some of the researchers [42, 127] had noticed a decrease in the workability of R^2C with the use of CR treated with a silane coupling agent while the NaOH solution treatment had shown negligible effects. The researchers [42, 127] concluded that the reduction in workability by a silane coupling agent (SCA) is primarily due to increases in the stickiness of aggregate particles making concrete less flowable. In order to improve the hydrophilicity of the rubber surface, Tamanna [31] used 10% and 20% NaOH solutions for 30 minutes and reported a 26% increase in compressive strength with 20% NaOH treatment. Similarly, Emam and Yehia [131] reported an increase of 22% in compressive strength (7 days) with the use of carbon disulfide (CS_2) for treating CR. Also, Su [42] investigated the effect of surface treatment of rubber particles on the properties of rubberized recycled aggregate concrete (R^2C) with RCA being replaced by 50% and CR by 20%. Two different methods such as NaOH solution and SCA were used to treat the CR particles. The author revealed that soaking the rubber particles for 2 hours in NaOH solution decreased the compressive strength while soaking for 24 hours in

NaOH showed a modest increase in compressive strength. However, SCA treatment showed the highest increase in strength. Similar results can be noticed for the MoE and flexural strength. The treatment of SCA creates silicone coating on the surface of CR particles developing a strong bond in ITZ and leading to an increase in flexural strength [42]. Washing with water is another treatment found to increase the dynamic elastic modulus but no such change was observed on the static elastic modulus by Najim and Hall [129].

Temperature Effect

The performance of FR^3C under elevated temperatures was investigated by many researchers [86, 100, 132-134]. Most of these studies had reported a decline in the properties of FR^3C in comparison with normal conditions. For instance, Guo et al. [86] reported a significant drop in the compressive strength, stiffness, and MoE of FR^3C with an increase in temperature (25ºC to 600ºC). These specimens were prepared with 100% RCA, 4-16% CR along with 1% of steel fibers. Guo et al. [86] also reported a reduction in spalling of FR^3C samples which is most likely due to the presence of steel fiber, increasing the concrete resistance. Aslani and Klein [100] found that steel fibers performed better than PP fibers under 900ºC as 22% greater tensile strength was recorded. However, maximum MoE was obtained at 100ºC with the addition of 0.5% steel fibers but when exposed to 600ºC a drop of almost 50% was recorded.

In a recent study, Guo et al. [86] observed the formation of cracks on the surface of FR^3C under elevated temperatures. The fiber-reinforced recycled concrete blended with CR was found substantially reduce the formation of cracks under the temperature of 400ºC to 600ºC. Netinger et al. [133] stated that as rubber is melted at around 170ºC, therefore, water evaporates easily without creating pore pressure. Furthermore, the toughness trend remained unchanged under elevated temperatures. However, Guo et al. [86] stated that if toughness is of great concern then the addition of CR up to 4% would be an optimum choice. Although this CR content is not ideal for strength but would provide resistance to explosive spalling. In a separate study, Guo et al. [132] explored the fracture behaviors of FR^3C at different elevated temperatures (25^0C, 200^0C, 400^0C, and 600^0C). An inverse relation was observed between compressive strength and fracture energy of FR^3C at elevated temperature. Though the compressive strength of concrete decreased with increasing temperature, the energy dissipating capacity and fracture energy increased. From the experimental results, the increase of 1.80, 2.81, and 2.78 times in the fracture energy was observed after being exposed to 200^0C, 400^0C, and 600^0C, respectively. According to the author, this increase in fracture energy could be due to a tortuous pattern followed by cracks helping more dissipation of energy. In addition, the samples blended with 8% CR showed maximum fracture energy under elevated temperature.

Density

Studies investigating the properties of RAC, R^2C, and FR^3C had reported lower densities and these findings were not a surprise for researchers. As the specific gravity of RCA and CR are lower compared to NCA and NFA. In a study, Feng et al. [93] worked with R^2C concrete and reported a reduction of 3.7% in the hardened density of RAC (100% RCA) in comparison with NAC. Later the author incorporated CR in the ratio of 10%, 20%, and 30% and recorded a decrease of 6.2%, 8.1%, and 10.6% respectively. Similarly, Li et al. [95] reported a decrease in concrete density with higher CR content and also due to smaller CR particle sizes. Recently, Hossain et al. [16] verified previous researchers' results by observing a reduction in density with the addition of 10% CR. The authors also concluded that though the inclusion of fiber increased the density of FR^3C, it decreased with increasing the fiber content. However, this reduction cannot be classified as lightweight concrete.

Fatigue Life

Feng et al. [93] investigated the fatigue properties and damage characteristics of rubber-modified recycled aggregate concrete by replacing natural sand with CR content at 10%, 20%, and 30% (by volume) with 100% RCA. The double logarithmic fatigue equation curves (S-N curve) showed that the S-N curve for RAC was steeper than for NAC. With the increase of CR content up to 20%, the S–N curve became steeper which means that both the RCA and CR particles could enhance the bending fatigue life of the concrete. The fatigue strength of RAC (with 0% CR) increased by 3.39% compared to NAC (0% RCA & 0% CR), while the fatigue strength of rubber-modified recycled aggregate concrete containing 20% CR was increased by 6.56% compared to RAC and 9.95% compared to NAC. For a fixed N value, both the RCA and CR particles enhanced the fatigue strength of concrete up to a certain range. Finally, the authors recommended that the optimum CR percentage was 20% in terms of fatigue strength.

However, the concrete containing 30% CR also showed slightly better fatigue strength than that of normal concrete. Su [42] attempted to investigate the effect of rubber treatment on the fatigue properties of R^2C blended with RCA (50%) and CR (20%). In these samples, CR particles treated with NaOH solution and silane coupling agent (SCA) were used. It was found that the addition of rubber particles as well as SCA treatment improved fatigue life in comparison with untreated or NaOH treated rubber aggregate.

Code Prediction

Previous authors [16, 135, 136] compared the experimental measured mechanical properties of R^2C and FR^3C with available design equations for NAC. Recently, Hossain et al. [16] reported that the experimental results of splitting tensile strength and flexural strength for FR^3C were close to the code predicted results such as ACI 318 [137], ACI 209 [138], EC2 [139], and CSA A23.3 [140]. This reveals that the equations for normal concrete can also be used for determining the splitting tensile strength and flexural strength of FR^3C. In a separate study, Mutsuddy [136] made a comparison of experimental results of MoE with theoretical values of rubberized concrete and fiber-reinforced rubberized concrete samples and reported an overestimation by CSA A23.3 [140] equations. Similarly, Mendis et al. [135] found that the tensile strength values of rubberized concrete were less than 10% of the experimental results through the codes equation of AS 3600 [141], ACI 318 [137], ACI 363 [142], and fib2010 [143]. However, EC2 [139] was found to overestimate the strength by 15%. In addition, the code equations of AS 3600 [141], ACI 318 [137], and ACI 209 [138] were found to overestimate the modulus of rupture values by 20% while an undervalue of again 20% was reported with the use of ACI 363 [142], fib2010 [143] and EC2 [139] equations. For MoE, reasonable accuracy was recorded with AS3600 [141] and ACI 318 [137] equations but fib2010 [143] was found to overrate the value by 25%. As the equations in fib2010 [143] were developed without considering the effect of rubber aggregate therefore this overestimation occurred. Finally, the authors suggested that the existing design guidelines for normal concrete can be used to predict the splitting tensile strength and MoE of rubberized concrete with reasonable accuracy except for modulus of rupture.

Failure Pattern/ Crack Resistance

Comparing the failure mode of RAC and R^2C, Li et al. [95] observed that, the failure of RAC occurred rapidly providing a sharp cracking sound without warning whereas R^2C specimens failed slowly and exhibited more ductility because of the elastic properties of rubber and provided either a faintly cracking sound or not at all. Relatively wide cracks were observed in RAC concrete while a small number of fine cracks appeared on the surfaces of the R^2C specimens. Feng et al. [93] showed that under the bending test, the NAC and RAC showed a wide opening and deep penetration, while the crack resistance capability was improved significantly after adding CR contents (R^2C specimens) and the width and depth of the cracks were decreased with the increase of the CR contents The same behavior was also observed by other researchers [99, 132]. This may happen due to the anti-cracking performance of CR particles [144, 145]. Besides, Xie et al. [99] and Richardson et al. [82] described that due to the existence of two different materials at the interface (CR particles are organic with hydrophobic surfaces whereas cement paste is inorganic with ionic compounds), they cannot combine effectively because of the higher water absorbing phenomena of the cement paste compared to that of CR particles. In addition to that, the lower MoE of the CR particles can act as dampers and hence distribute the stress at the crack tips, resulting in a delay in the coalescence of the cracks described previously [116, 146].

In FR^3C specimens, it was observed that most of the concrete specimens containing CR and fiber content provided ductile failure mode compared to the brittle failure of reference concrete under compression [16, 31]. Besides, the FR^3C specimens remained intact at failure due to the confining effect of the PP fibers [31]. Hossain et al. [16] demonstrated that, under the splitting tensile strength test, the RAC specimens showed well-defined crack lines, whereas the FR^3C specimens followed an irregular and zigzag crack pattern. After inspecting the broken flexural specimens it was observed that the fibers were projecting outward and perpendicular to the cross-section helping to resist the crack propagation by their bridging phenomena. Jian-he et al. [106] found several major macro cracks in RAC specimens that crossed through the height of the concrete cylinders. However, in FR^3C specimens, only small multiple longitudinal cracks were observed on the surfaces of the specimens. The same behavior was also observed by Guo et al. [132]. Turatsinze et al. [116] reported that when the tip of the crack touched the

CR particles, it could resist the crack growth like a damper. The authors also claimed that incorporating steel fiber not only restrained crack propagation but also provided significant residual post-peak strength. However, Xie et al. [99] reported that the inclusion of silica fume in FR^3C helped to propagate the cracks through RCA and CR particles instead of passing them along with the interfaces. In the FR^3C specimens without silica fume, the internal crack propagation occurred along with the interface between the RCA and the cement paste bypassing the steel fiber and rubber because the strength of the RCA itself might be higher than the interface strength. Thus the fracture can easily occur at the interface and the failure surface was more distinct. However, silica fume can increase the interfacial bond strength and make a denser paste which promotes propagating the cracks through the RCA and rubber particles because of its higher strength.

2.3.4. Life Cycle Assessment

Life cycle assessment is a process that measures the effect on the environment through carbon emission and cost analysis during the period of the life cycle of the man-made products. The term global warming can also coincide with carbon dioxide emission or carbon footprint. Construction materials that will have lower environmental impacts are of prime importance among researchers for a long time. Therefore, when R^2C and FR^3C are sought to be accepted as attractive products worldwide, a thorough study of their effect on nature conservation is necessary which is often termed as a part of the life cycle assessment (LCA) process. A simplified illustration of the life cycle of the end life of tires and concrete elements and/or structures is shown in Figure 2.8.

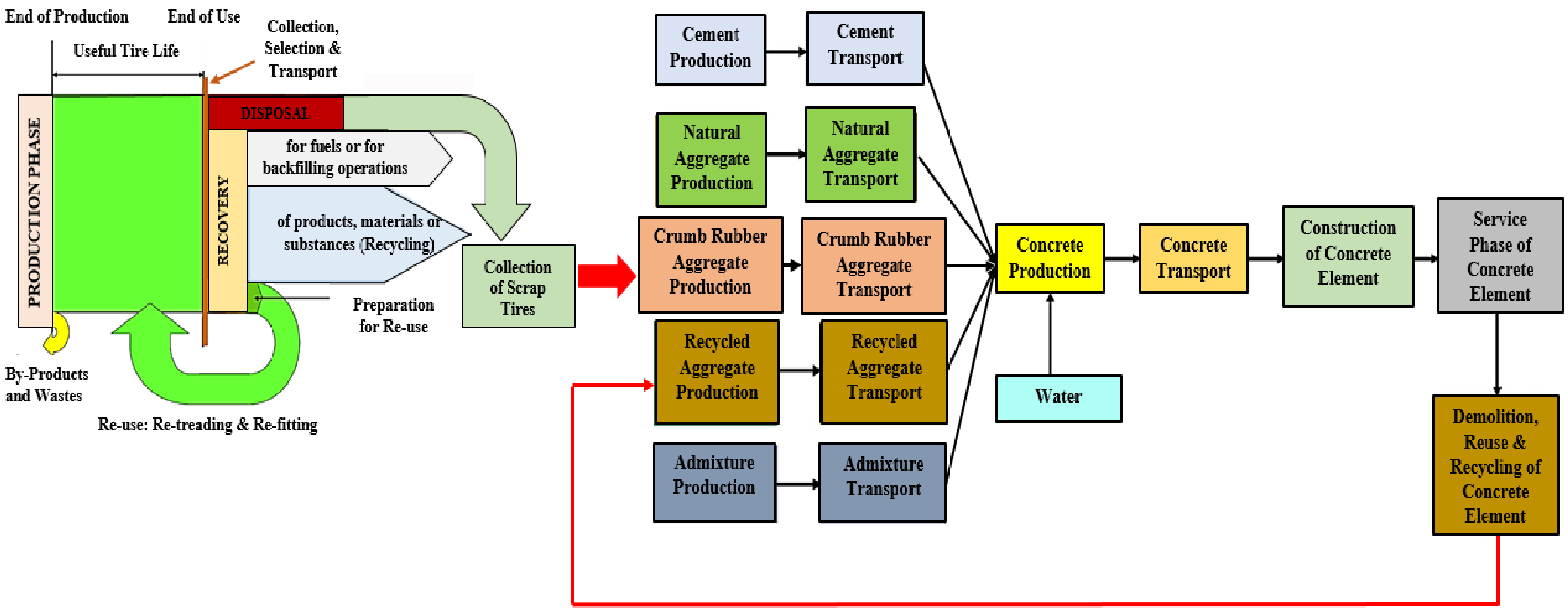

Figure 2.8 Life cycle of end of life of tires and concrete (modified from [69, 147]).

Cost Analysis

A review by Presti [69] pointed out that the Asphalt-Rubber is an attractive option for roads and pavement construction in terms of environmental concerns. The comparison between the cost incurred during maintenance and usage unraveled that an Asphalt-Rubber pavement was more cost-effective than conventional pavement. Besides, the author notified that after 10 years of construction, the difference in maintenance cost between the conventional bituminous pavement and Asphalt-Rubber pavement was quite significant, implying that the maintenance required by the conventional pavement is more. Mhaya et al. [51] demonstrated that replacing river sand with CR slightly increased the cost of modified concrete but was still less than that of the concrete cast with OPC. The Environmental Council of Concrete Organizations (ECCO) [33] reported that using RCA instead of NCA can save the cost up to 60%. Another study by Verian et al. [34] reported that using RCA can reduce the cost to $2.26–$2.93/ton in concrete pavement (without considering the savings of not using landfills). On the other hand, according to Martínez-Lage et al. [147] the concrete with 100% mixed RCA exhibited the highest cost considering the cost due to changes in mix proportion and the transport differences between natural and recycled aggregates. The authors identified that the transportation distance of RCA is a significant factor in affecting cost consumption. However, 20% replacement of RCA has a negligible difference in cost of production.

Carbon Emission

As mentioned before, the global warming potential is mainly quantified by the assessment of carbon emissions. Mhaya et al. [51] reported that CO_2 emission was reduced by 0.02%, 0.03%, 0.06%, and 0.09% when CR was used to replace the NFA by 5%, 10%, 20%, and 30%, respectively. Besides, when CR was used as a substitution for both NAC and NAF the emission level of CO_2 was reduced to 0.06%, 0.13%, 0.26%, and 0.41% for 5%, 10%, 20%, and 30% CR content, respectively. The authors concluded that CR can produce sustainable rubberized concrete having lower carbon emissions and reduced energy consumption compared to conventional concrete. On the other hand, according to Presti [69], the National Institute for Occupational Safety and Health (NIOSH) and Federal Highways Administration (FHWA), in their respective studies, had reported a negligible difference in emission exposures between

Asphalt-Rubber and conventional asphalt services. The authorities also mentioned that the effect of CR on the emission was insignificant compared to the other factors like fueling rate of the dryer, mix temperature and asphalt binder content. The study by Xie et al. [99] also addressed this particular environmental concern by calculating the total CO_2 emission by FR^3C. The general observation was that the CO_2 emission increased with an increase in the amount of CR. For instance, the CO_2 emission was 6.4%, 7.4%, 8.1%, 8.8% and 9.6% greater for samples with CR contents of 0%, 5% 10% 15% and 20%, respectively compared to that emitted by normal concrete. However, the authors reported that the addition of silica fume in the FR^3C mix reduced the CO_2 emission significantly. It was observed that, in the FR^3C sample with 20% CR content, as the amount of silica fume increased from 5% to 10%, the carbon emission was 270.1 kg/m^3 and 258.1 kg/m^3, respectively. As seen from experimental results, the CO_2 emission was reduced by more than 8% in FR^3C with 5% CR and 10% silica fume, compared to steel fiber reinforced natural aggregate concrete. The full NCA replacement by RCA showed a slight decrease in carbon emissions. Other authors also mentioned that CO_2 emission was reduced up to 40% when NCA was replaced by RCA and arc furnace slag [44-46]. Another study by Hossain et al. [47] showed that the greenhouse gas footprints were reduced up to 65% when RCA derived from C&D waste was used in construction.

Carbonation

The CO_2 emitted by constituents in R^2C and FR^3C can be estimated during the process of carbonation [148]. Carbonation is considered another aspect of LCA which quantifies the amount of CO_2 absorbed by the concrete in terms of carbonation depth [149]. The carbonation depth of a rubberized concrete was found to be greater than that of normal concrete and it increased with an increase in CR content [73]. The resistance to carbonation was found to reduce with an increase in CR content in a study by Gupta et al. [57], where the authors mentioned that the carbonation depth increased with an increase in exposure to CO_2. Such a behavior can be explained by the fact that the increment of void and reduction of density due to CR incorporation in the mix results in easier access to CO_2.

Energy Consumption and Carbon Footprint

During the CO_2 emission process, notable energy is consumed which leads to the importance of assessing the energy consumption in the LCA regime. Mhaya et al. [51] mentioned that concrete with CR replacing NFA and NAC required greater energy in the production stage. For instance, the replacement of NCA by CR caused an increase in energy consumption with the highest value of 1.5% for the specimen containing 30% CR. In the case of CR replacing both NCA and NFA almost 1.7% rise in energy consumption was reported for concrete with a 30% CR replacement level. The increase in energy consumption is due to the fact that the CR requires more electrical energy and fossil fuels during the concrete production phase than that is required by NFA. However, Li et al. [150] mentioned that the highest impact on the environment is due to the de-vulcanization stage in the process of production of CR as it includes large quantities of coal burning. The second highest load on the environment is due to the refining process primarily giving rise to electricity consumption. However, it is worth mentioning that the preparation of the CR by chopping, slicing, grinding and screening has the lowest environmental impact. Xiao et al. [151] studied the effect on carbon footprint due to the incorporation of RCA and reported that when RCA was used as a structural material, up to 2.175×10^5 kgCe carbon footprint was decreased. Also, the cumulative energy demand of the RCA structure was calculated to be 1.473×10^6 MJ which was about 12.8% lower than that of the NCA. Their study identified that the recycling process and transportation distance were chosen to play a vital role in reducing the embodied carbon and energy consumption which therefore makes the use of RCA more attractive. The study by Hossain et al. [47] found that by using RCA the energy consumption can be lowered up to 58%.

Eutrophication and Acidification

As stated by Kim and Chae [152], the substances emitted during the production of concrete do not have an impact on global warming only, but also on eutrophication and acidification. Both of these processes are responsible for air pollution as well as the deterioration of concrete. A paper by Piotrowska et al. [153] pointed out that the eutrophication and acidification of car tires are significant during production and mainly at the service stage. However, no effects on eutrophication and acidification were observed due to the recycling of the end-of-life tires

Martínez-Lage et al. [147] reported that the eutrophication potential increased as the mixed RCA replacement level increased. For instance, the eutrophication of concrete with 100% mixed RCA can be up to 12.5% higher than that of the reference concrete. It was also observed that the global warming potential increased as the replacement level of RCA increased in the concrete mix. The study by Moro et al. [154] also concluded that the eutrophication potential for the concrete sample having 100% RCA replacement was the highest whereas the conventional concrete was the lowest.

2.4 Compressive Behavior and Free Vibration Responses of Reinforced Concrete Columns Containing RCA, CR, and Fiber

The present section discusses various compressive behaviors and free vibration responses of different reinforced concrete columns containing RCA, CR, or fiber.

2.4.1 Compressive Behavior of Recycled Aggregate Concrete Columns

Choi and Yun [21] tested seventeen 400 × 400 mm square columns having different types, qualities, and quantities of recycled coarse and recycled fine aggregate subjected to monotonic concentric compression loads. It was found that the maximum load for columns with recycled coarse aggregate tends to decrease by almost 10% compared to the maximum load for columns with natural aggregate. This might be attributed to the lower compressive strength of the recycled concrete. But the recycled fine aggregate did not affect the axial strength of the columns. The ductility and cracking patterns of the recycled concrete column were almost similar to that of columns that are made with natural aggregates. Finally, it was recommended that the reinforced concrete columns constructed with recycled aggregate can be used as load-bearing structural elements in compression, but needed further investigation.

Zhou et al. [22] examined the compressive behavior of twenty-seven recycled aggregate concrete (RAC) columns including three natural aggregate concrete (NAC) columns under large eccentric (150 mm) loading having a slender proportion of 27 and a cross-section of 300 × 300 mm. The replacement level of NCA by RCA was up to 80%. It was observed that both the cracking load and ultimate load decreased with increasing the percentage of RCA. The bearing capacity of the column decreased by only 28.8% for the column containing 80% RCA. The authors also gave the same explanation as Choi and Yun [21] against this reduction.

However, an improvement was observed for the columns containing 50% RCA. This might happen due to the production of a good gradation of aggregates with the combining 1:1 mix-up of NCA and RCA. In resemblance to the columns of natural aggregate, recycled concrete columns also possessed an obvious elastic stage, crack stage, and fracture stage under eccentric load. It was suggested to use 50% RCA in the concrete structures.

Ajdukiewicz and Kliszczewicz [155] studied with compressive and flexural behavior of reinforced concrete members made with different amounts of recycled aggregate. No significant difference was observed in the behavior of all columns up to failure but RAC columns showed more ductile failure compared to normal concrete. It was concluded that though the differences in load-bearing capacity can be disregarded, the difference in deformability should be considered carefully.

Islam et al. [156] and Choudhury et al. [157] examined the dilation effects of the square and circular columns of different sizes containing brick, recycled brick, recycled stone, and natural stone chips. The columns were confined with fiber-reinforced polymer (FRP) to distribute the confining pressure uniformly and the stress-strain and post-peak failure processes were investigated with digital image correlation technique (DICT) measurements at the failure location. Both the brick aggregate concrete (BAC) and RAC columns exhibited greater dilation under axial compression loading compared to the NAC columns. The BAC and RAC columns showed a distinctly higher lateral strain compared to NAC columns due to the former's dilation property. The results showed that the circular columns could restrain the dilation-induced phenomena more effectively compared to square columns.

Breccolotti and Materazzi [158] performed a reliability analysis of reinforced concrete columns made with RAC. It was reported that, though RAC provides higher scattered compressive strength, they can be safely used in structural components even with a full replacement of NAC if they exhibit higher strength. However, it was suggested to adopt an appropriate adjustment in design procedure when dealing with RAC for structural use, such as a proper modification of the partial safety factor of concrete.

2.4.2 Compressive Behavior of Rubberized Concrete Columns

Hassanli et al. [23] worked with twenty-seven fiber-reinforced polymer (FRP) confined expansive rubberized concrete (RuC) columns with a size of 100 mm in diameter and 200 mm in height under axial compression where the FRP confining layer was pre-stressed by using an expansive agent (EA). The percentages of CR used in this study were 0, 20, and 40 of the volume replacement of sand, and the EA was used as a partial replacement of cement by 0%, 7.5%, and 15% of the weight. From the result, it was seen that the confining effect in rubberized concrete was higher than that of normal concrete due to the incompressible property of rubber with a Poisson ratio of about 0.5. However, the lateral stress provided by the FRP confinement and the expansive agent can increase the axial stiffness significantly. Besides, this phenomenon can also mitigate the typical strength reduction of rubberized concrete and also increase the interaction and interface friction between the rubber particles and cement paste by reducing the porosity.

Son et al. [24] tested twelve rubberized columns having a size of 200 mm wide × 300 mm deep × 1600 mm long to investigate the deformability and energy absorption capacity of RC columns. The variations considered in that study were concrete compressive strength (24 MPa and 28 MPa), the particle size of waste tire rubber (0.6 mm and 1 mm), and the percentage of rubber content (weight fraction of 0.5% and 1%). Results indicated that though the compressive strength, modulus of elasticity, and axial load carrying capacity were slightly lower than that of conventional concrete, the curvature ductility was increased up to 90%. Besides, rubberized concrete columns were capable of undergoing more than two times lateral deformation before buckling failure compared to the conventional concrete columns. The authors also concluded that this rubberized concrete is more suitable for seismic applications in structures due to its good energy dissipation capacity and ductility.

Eltayeb et al. [159] investigated the feasibility of using CR particles (8.5% of the total volume of concrete) with lightweight foam concrete as an infill material in double-skinned profiled composite walls. For this instance, five profiled steel-concrete composite walls with 100 × 550 × 600 mm (width × length × height) were tested under axial compressive loads. The DICT was used to determine the strains and deformations. Results showed that the concrete strength and modulus of elasticity of lightweight foam concrete (LFC) and lightweight foam rubberized concrete (LFRC) decreased by 19% and 20.1%, respectively. Due to this strength reduction, the axial capacity of the LFRC walls was reduced by 16.8% compared to LFC walls. However, the LFRC walls showed relatively fewer cracks than that of LFC walls due to the higher ductility of rubberized concrete.

2.4.3 Compressive Behavior of Fiber-Reinforced Concrete Columns

Raza et al. [160] investigated the structural behavior of fiber-reinforced (steel fiber and polypropylene fiber) concrete columns having both steel bars and GFRP (Glass Fiber Reinforced Polymer) bars as structural reinforcement. Six fiber-reinforced GFRP columns had been constructed with a diameter of 250 mm and height of 1150 mm and compared with six fiber-reinforced steel columns under both concentric and eccentric (30 mm and 60 mm) loading conditions. The experimental results revealed that the fiber-reinforced GFRP columns showed lower axial capacity (8.68%) than those of fiber-reinforced steel columns. However, the GFRP columns provided higher ductility (19.71%) compared to the steel columns. The lateral confining pressure and the ductility index were increased after decreasing the vertical spacing of spirals. On the other hand, the axial capacity decreased by 23.9% and 57.4% after applying the eccentricity of 30 mm and 60 mm for six fiber-reinforced steel columns having 38 mm spiral spacing. The same trend was also observed for 75 mm spiral spacing as well as GFRP columns. In addition, they noted that both GFRP columns and steel columns showed similar failure modes.

Chao et al. [161] tested two full-scale columns, one with normal strength concrete and the other with ultra-high-performance fiber-reinforced concrete (UHP-FRC) under simulated earthquake loads to evaluate their damage-resistance ability, deformation capacity, and failure mechanism. Experimental results showed that the use of UHP-FRC changed the failure mode of RC columns as it can improve the confinement and shear capacity, as well as can prevent concrete from crushing. Besides, the UHP-FRC column exhibited a higher peak strength, a greater deformation capacity, and limited damage even at large drift ratios compared to the normal-strength RC column. Finally, the authors concluded that the UHP-FRC will result in great post-earthquake functionality and considerable cost savings in repairs for structures.

2.4.4 Free Vibration Responses

Xue and Shinozuka [25] conducted a free vibration test of rubberized concrete columns with three different CR replacement levels such as 5%, 10%, and 15%. The CR was replaced with NCA. It was found that the average damping ratio of rubberized concrete columns was 62% higher compared to conventional concrete columns. The damping ratio of rubberized concrete columns varied from 5.9% to 8.3%. The following trend was also observed by other researchers [68, 162]. Moustafa and ElGawady [68] investigated the dynamic properties of rubberized concrete with the replacement of fine aggregate up to 30%. It was found that though the damping was found to increase with the increase of CR content, beyond 20%, the effect on damping was insignificant. Besides, the fracture energy was found to increase with the increase of CR content up to 20%. In terms of natural frequency, the frequency decreased with the addition of rubber. However, this reduction was not significantly affected by the rubber content. From another study of Moustafa et al. [163], it was observed that the fundamental period of the rubberized column containing 20% CR content was 7% higher than that of the RC column due to the lower stiffness of the rubberized column. Besides, the cumulative dissipated energy was increased by 16.5% in the rubberized column.

Zheng et al. [162] worked with two different types of rubber such as ground rubber and crushed rubber. It was found that the dynamic modulus elasticity of rubberized concrete was lower than that of plain concrete. However, the crushed rubber had more effects on both dynamic and static modulus of elasticity of rubberized concrete than ground rubber. The dynamic modulus of elasticity was approximately 50% higher than the static modulus of elasticity for rubberized concrete. The damping ratios of rubberized concrete beams with rubber contents of 15%, 30%, and 45% were found 1.86, 2.35, and 2.26 times higher than that of ordinary concrete beams. However, this damping ratio decreased when the rubber content was more than 30%. Another study by Pitilakis et al. [164] also suggested limiting the use of CR by up to 30%. For 30% rubber content, a significant modification in the dynamic properties had been noticed. A decrease of about 50% in the fundamental frequency and an average reduction of 40-60% in the structure’s response was observed which was comparatively much higher than 10% CR.

Youssf et al. [165] tested three circular RC columns having 240 mm diameter and 1500 mm shear span under incrementally increasing reversed cyclic loading. The results indicated that the use of CR content at 20% increased the hysteretic damping ratio and energy dissipation of the columns by 13% and 150% respectively but decreased the viscous damping ratio compared to a conventional concrete column. The viscous damping was decreased by 49% compared to conventional concrete. Besides, the rubberized column was able to sustain a lateral load and ultimate drift of about 98.6% and 91.5%, respectively, of those sustained by the conventional column. The authors suggested not to use rubber aggregate in concrete in large-scale structural applications.

Mo et al. [166] investigated the effects of polypropylene (PP) fiber and rubber powder on the damping capacity of concrete. It was found that the damping ratio was increased by about 60% when the mass ratio of PP fiber increased from 0.4% to 1.5%. This was due to the bridging action of PP fiber in concrete which was more obvious for a higher content of fiber. Besides, this bridging action led to absorbing more energy in the process of bonding, sliding, and pulling out between fiber and concrete matrix. With the addition of rubber powder, the damping capacity was also increased in fiber-reinforced rubberized concrete. The degradation rate of the bending dynamic stiffness of fiber-reinforced rubberized concrete beams slowed down with the increase of PP fiber content and accelerated with the addition of rubber powder.

2.5 Summary

Upon reviewing the existing literature, it is clear that very few studies have been conducted on the combination of RCA, CR, and PP fiber in reinforced concrete columns. The RCA is capable of producing concrete with the same or greater strength than the concrete made by NCA. Besides, the CR is helpful to improve the impact resistance, and shock absorption capacity as well as enhancing the dynamic properties of concrete such as damping ratio, natural time period, dynamic stiffness, and energy dissipation capacity. As concrete is a brittle material and weak in tension, its ductility, toughness, and tensile strength can be increased by incorporating PP fiber into concrete. So far, the flexural properties of concrete incorporating a combination of all these three have been assessed previously but the compressive behavior and free vibration test have been done in limited studies. The inadequacy of available test data makes it difficult to identify the compressive behavior of reinforced concrete made of RCA, CR, and PP fiber. Thus, this research will investigate the compressive behavior and different dynamic properties of reinforced concrete R^2C and FR^3C columns.

Chapter 3

EXPERIMENTAL DETAILS

3.1 Introduction

A detailed experimental investigation of the behavior of twenty-six one-third scale rubberized recycled concrete (R^2C) and fiber-reinforced rubberized recycled concrete (FR^3C) tied-square columns with 150 × 150 × 950 mm size subjected to monotonic concentric compression loads are presented in this chapter. The free vibration test of columns is also discussed. Besides, the test procedure for investigating different mechanical properties of R^2C and FR^3C is presented. The investigated parameters included longitudinal reinforcement ratio (1.4% and 2%), tie spacing (75 mm and 150 mm), and content of CR (5%, 10%, and 15%) with 0.5% PP fiber and 30% RCA replacement. A detailed description of the experimental program is presented below.

3.2 Materials

Nine different types of concrete mixtures were prepared for this study which were composed of Portland composite cement (PCC), natural fine aggregate (NFA), natural coarse aggregate (NCA), recycled coarse aggregate (RCA), crumb rubber (CR), and polypropylene (PP) fiber. The aggregates used in this study are shown in Figure 3.1. The RCA was obtained from an eight years old demolished building which was then crushed with a crusher machine at four different sizes such as 19 mm, 12.5 mm, 9.5 mm, and 4.75 mm. The particles less than 4.75 mm were removed through sieving. After that, the RCA was washed several times to dispel the impurities adhered to the surface of them. The physical properties of the RCA were determined using the same procedure followed for NCA. Many countries have specific guidelines for the use of recycled aggregate as a construction material. According to the Korean standard [167], the specific gravity of RCA should be more than 2.5, the water absorption rates should be less than 3% and the abrasion value should be less than 40%. The properties of RCA used in this study complied with these limits.

The CR was produced after shredding the waste tire with a shredder machine having a nominal maximum size of 4.75 mm. The maximum size of NCA and NFA was 19 mm and 4.75 mm, respectively. The gradation curves of NCA, RCA, NFA, and CR are presented in Figure 3.2. It is seen that the gradation curves of all the aggregates comply satisfactorily with the range specified by ASTM C33 [10]. The PP fiber having a length of 12 mm was collected from China and its specification provided by the company is presented in Table 3.3. Mild steel was used as longitudinal and transverse reinforcement. The stress-strain behavior of mild steel is presented in Figure 3.3. The properties of all materials were determined according to ASTM standards and summarized in Table 3.1 to Table 3.5.

(a) (b) (c)

Figure 3.1 Aggregates used in concrete: (a) RCA (b) CR (c) PP Fiber.

Table 3.1 Chemical and physical properties of Portland composite cement.

Component		**PCC (% Mass)**	**Standard**
Chemical Composition			
SiO_2		20.60	ASTM C114 -18 [168]
Al_2O_3		4.74	
Fe_2O_3		3.28	
CaO		64.82	
MgO		1.84	
SO_3		2.40	
Na_2O		0.21	
K_2O		0.38	
Loss on ignition (LOI)		1.73	
Physical Properties			**Standard**
Specific Gravity		2.95	ASTM C188-17 [169]
Blaine Fineness (m^2/kg)		367	ASTM C204-18 [170]
Normal Consistency (%)		27.6	ASTM C187 -16 [171]
Initial Setting Time (min)		140	ASTM C191-19 [172]
Final Setting Time (min)		195	
Mechanical Properties			**Standard**
Compressive Strength (MPa)	3 Days	20.3	ASTM C109-13 [173]
	7 Days	24.8	
	28 Days	37.3	

Table 3.2 Physical properties of aggregates.

Variables	NCA	RCA	NFA	CR	Standard
Nominal Maximum Size (mm)	19	19	4.75	4.75	ASTM C125-20 [174]
Apparent Specific Gravity	2.84	2.72	2.65	-	ASTM C127-15, ASTM C128-15 [175, 176]
Bulk Specific Gravity (SSD)	2.82	2.59	2.59	1.12	
Bulk Specific Gravity (OD)	2.81	2.51	2.55	-	
Absorption Capacity (%)	0.33	2.97	1.40	1.10	
% of Effective Absorption	99	99	99	99	
Fineness Modulus	6.73	6.73	2.48	3.12	ASTM C136-14 [177]
Loose Condition Unit Weight (kg/m^3)	1460	1380	1540	-	ASTM C29-17 [178]
Compact Condition Unit Weight (kg/m^3)	1580	1430	1620	-	
Loose Condition % of Voids	48	43	40	-	
Compact Condition % of Voids	44	41	37	-	
Abrasion Value (%)	17	32	-	-	ASTM C131-20 [179]
Elongation Index (%)	21	28	-	-	BS 812-105.2 [180]
Flakiness Index (%)	19	22	-	-	BS 812-105.1 [181]

Table 3.3 Specifications for polypropylene fiber.

Variables	Polypropylene fiber
No. of Denier	03
Specific gravity (g/cm^3)	0.91
Fiber Length (mm)	12
Tensile Strength (MPa)	480
Elastic Modulus (GPa)	7.0

Table 3.4 Mechanical properties of rebar (modulus of elasticity and yield strength).

SN	Bar Type	$d_{nominal}$ (mm)	Unit Weight (kg/m)	d_{actual} (mm)	A_s (mm^2)	E_s (GPa) Tested	E_s (GPa) Average	f_y (MPa) Tested	f_y (MPa) Average	f_y (MPa) Minimum (A615-60)	Standard
1	Steel 8mmØ	8	0.40	8.09	51	206	210	431	441	-	ASTM A615-20 [182]
2			0.43	8.36	55	215		448			
3			0.42	8.22	53	210		445			
4	Steel 10mmØ	10	0.62	10.02	79	209	213	447	451	420	
5			0.62	10.00	79	216		451			
6			0.62	10.01	79	214		455			
7	Steel 12mmØ	12	0.92	12.21	117	240	227	492	484	420	
8			0.93	12.29	119	234		476			
9			0.93	12.29	119	208		484			

Table 3.5 Mechanical properties of rebar (ultimate strength and strain).

SN	Bar Type	$d_{nominal}$ (mm)	f_u (MPa) Tested	f_u (MPa) Average	f_u/f_y	ε_y (mm/mm)	Elongation (%) Tested	Elongation (%) Minimum (A615-60)	Standard
1	Steel 8mmØ	8	562	553	1.25	0.00202	23	-	ASTM A615-20 [182]
2			539			0.00212	25		
3			557			0.00214	25		
4	Steel 10mmØ	10	551	543	1.20	0.00218	18	9	
5			545			0.00214	16		
6			532			0.00212	15		
7	Steel 12mmØ	12	556	558	1.15	0.00213	15	9	
8			565			0.00218	12		
9			555			0.00217	13		

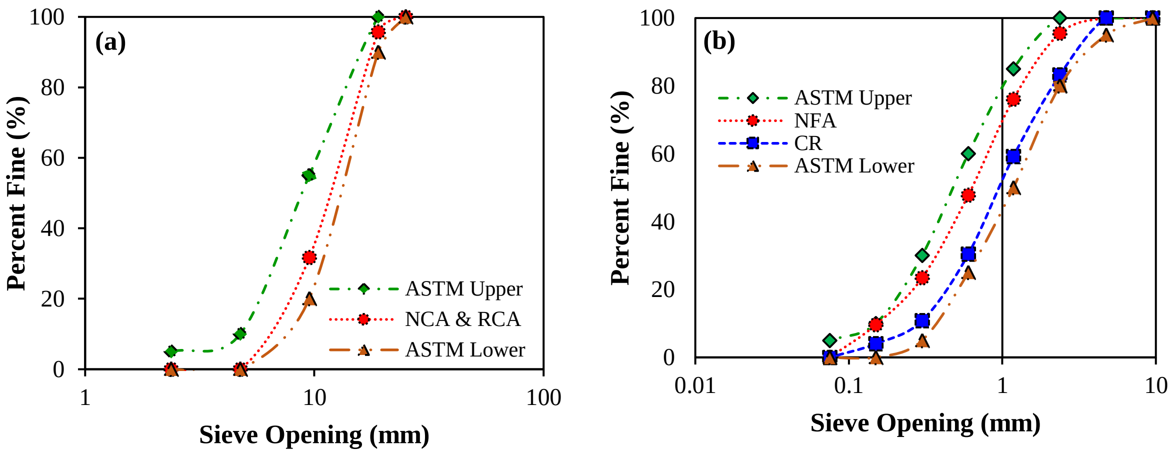

Figure 3.2 Gradation curve of (a) NCA and RCA; (b) NFA and CR.

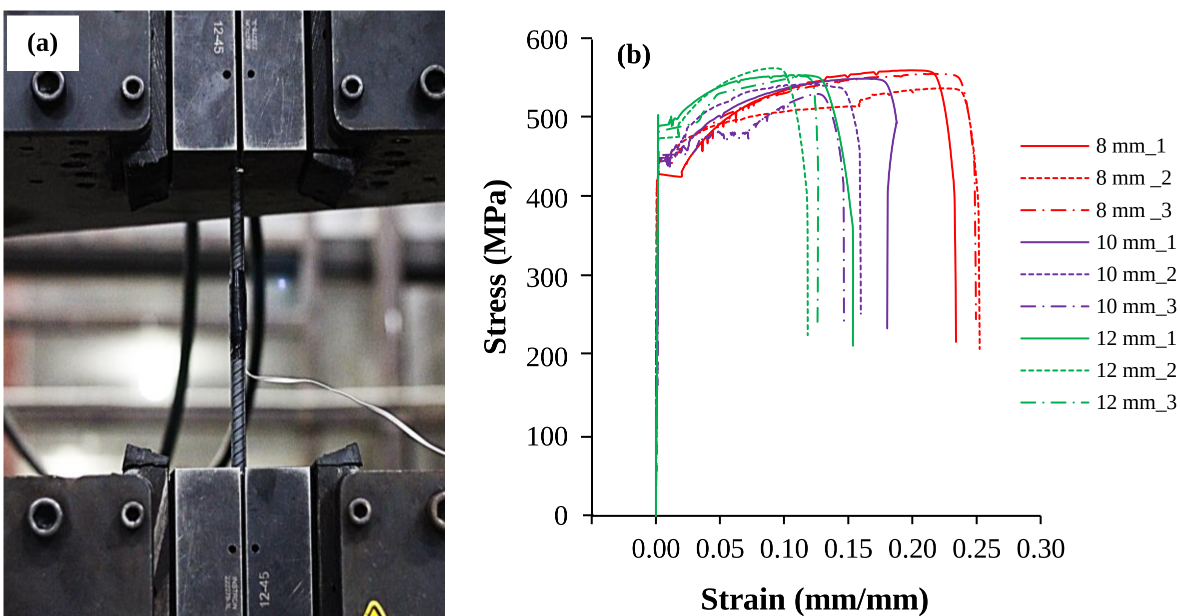

Figure 3.3 Tensile test of mild steel: a) Test set-up, b) Stress-strain relationship.

3.3 Concrete Mix Proportions

The percentages of NCA, RCA, NFA, CR, and PP fiber were varied during the mix design in this study. To investigate the effect of RCA, CR, and PP fiber on column compressive behavior, nine different concrete mixes were prepared with a design compressive strength of 30 MPa at 28 days. Some standards allow the complete replacement of NCA by RCA to make concrete with compressive strength up to 60 MPa [183, 184] and some standards allow to produce of only 10 MPa concrete by using 100% RCA [185]. Due to this uncertainty of recycled aggregate concrete (RAC) strength, Choi and Yun [21] suggested using RCA where the required concrete compressive strength is less than 27 MPa. It was recommended to use less than 30% RCA to produce concrete strength of more than 21 MPa to less than 27 MPa [21]. Besides, some previous researchers had pointed out that replacing the NCA with RCA by more than 30% by weight gradually decreased the mechanical properties of RAC [13, 21, 186-189]. Thus, the RCA replacement level was fixed at 30% of the weight of NCA for conducting this research.

The NFA was replaced with CR in 5%, 10%, and 15% proportions by volume. Meherier [56] and Ismail and Hassan [12] found that using CR up to 10% provided a comparable strength with the control specimens and enhanced the deformation capacity, ductility, and toughness of concrete. Keeping these observations in mind, CR replacement levels were selected as 5% and 10% and for comparison purposes, a higher percentage (15%) was also selected.

In addition, the PP fibers were added to the concrete mixture by 0.5% of the concrete volume as suggested by Mohod [190]. The PP fiber was selected instead of steel fiber because it does not suffer from corrosion like steel fiber, and thus PP fiber-reinforced concrete performs better in terms of durability [18]. As the surface of the columns is exposed to the environment, they may have the chance to be corroded. Besides, the production and labor cost of PP fiber is relatively less [19], and low CO_2 emissions during the process of production [20].

The coarse and fine aggregates were used in saturated surface dry (SSD) conditions. The mixed proportions of materials per cubic meter are presented in Table 3.6. Each mix design is designated with a unique name for ease of referencing within the text. For example, in the combination of $R_{30}C_{15}F_{0.5\_2.0\text{-}150}$ where R means RCA; 30 is % of RCA replacement; C is CR; 15 is % of CR replacement; F is polypropylene fiber; 0.5 is % of PP fiber; 2.0 is % of longitudinal reinforcement ratio and 150 is the tie spacing. No water-reducing admixture was used throughout the study.

Table 3.6 Mix proportion for 1 m^3 concrete.

Batch Code	RCA (%)	CR (%)	PP Fiber (%)	w/c	Water (kg)	Cement (kg)	Coarse Aggregate (kg)		Fine Aggregate (kg)		PP Fiber (kg)	Remarks
							NCA	RCA	NFA	CR		
$R_0C_0F_0$	0	0	0	0.45	205.0	456.0	979.6	-	731.4	-	-	NAC
$R_{30}C_0F_0$	30	0	0				685.7	293.9	731.4	-	-	RAC
$R_{30}C_5F_0$	30	5	0				685.7	293.9	694.8	15.9	-	R^2C
$R_{30}C_{10}F_0$	30	10	0				685.7	293.9	658.3	31.8	-	
$R_{30}C_{15}F_0$	30	15	0				685.7	293.9	621.7	47.7	-	
$R_{30}C_0F_{0.5}$	30	0	0.5				685.7	293.9	731.4	-	4.55	FR^2C
$R_{30}C_5F_{0.5}$	30	5	0.5				685.7	293.9	694.8	15.9	4.55	FR^3C
$R_{30}C_{10}F_{0.5}$	30	10	0.5				685.7	293.9	658.3	31.8	4.55	
$R_{30}C_{15}F_{0.5}$	30	15	0.5				685.7	293.9	621.7	47.7	4.55	

Note:
NAC = Natural Aggregate Concrete/Control, RAC = Recycled Aggregate Concrete, R^2C = Rubberized Recycled Concrete, FR^2C = Fiber-Reinforced Recycled Concrete, and FR^3C = Fiber-Reinforced Rubberized Recycled Concrete.

3.4 Specification and Fabrication of Specimens

The following section presents the specifications and fabrication procedures of different specimens for this study.

3.4.1 Specimens Specifications for Mechanical Properties Test

One hundred and eight (108) concrete cylinders having 100 mm diameter and 200 mm height were cast following the ASTM C31-19 [191] standard to determine the compressive strength and modulus of elasticity (MoE) of concrete. Hardened density, Ultrasonic Pulse Velocity (UPV), and surface resistivity data were collected from the concrete cylinders before the compressive strength test. To determine the direct tensile strength of concrete, dog bone-shaped specimens were prepared following Liu et al.[192]. Two smooth transitional zones were created between the end regions and the critical region of dog bone specimens to mitigate potential stress concentrations at those zones. The cross-section of the dog bone specimens is shown in Figure 3.4 (a). The flexural strength of concrete was determined using 150 × 150 × 550 mm size concrete prism beams. The specimen size was adopted from the Japan Concrete Institute Standard [193] for fiber-reinforced concrete which is shown in Figure 3.4 (b).

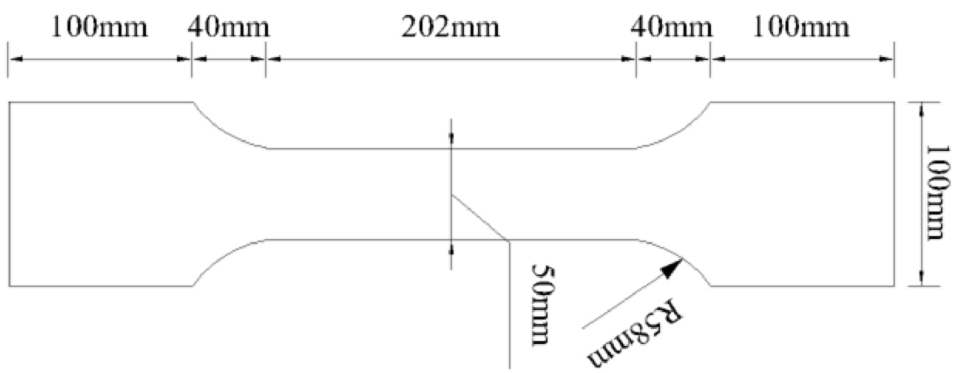

(a)

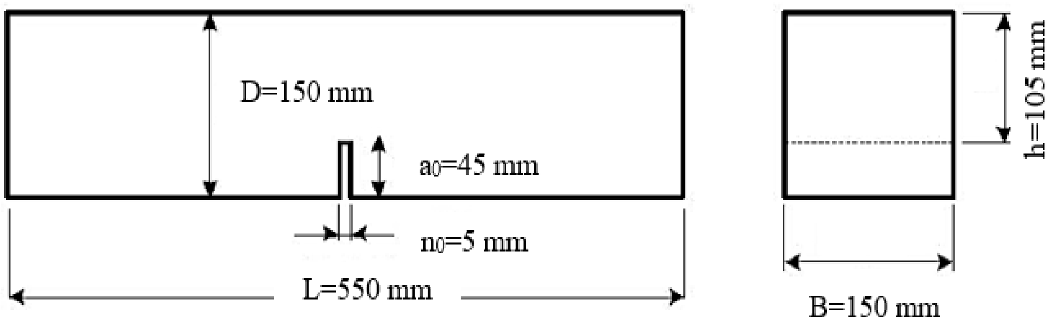

(b)

Figure 3.4 Dimensional details of specimens for (a) direct tension test of dog-bone-shaped specimens, and (b) flexural strength test of the concrete beam.

3.4.2 Column Specimens for Compression Test

Twenty-six square columns were fabricated according to ACI 318/318R [194] guidelines, each with a cross-section of 150 × 150 mm and a length of 950 mm. The columns were designed with haunched column heads of 250 × 250 ×100 mm. This modification of the design of the column ends was adopted from Manzur et al. [195] to eliminate any chance of premature failure due to excessive stress concentration at the column end regions and to ensure the crack propagation along the weak zone of the column. The columns had the minimum amount of longitudinal reinforcement (1%) and the maximum tie spacing mandated by ACI 318/318R [194]. Eighteen columns were reinforced with a 1.4% (four rebars of 10 mm diameter) longitudinal reinforcement ratio and four columns were reinforced with a 2.0% (four rebars of

12 mm diameter) longitudinal reinforcement ratio and the rest four were un-reinforced columns (plain concrete).

Two tie spacing were selected such as 75 mm and 150 mm center to center distance. According to ACI 318/318R [194], the vertical spacing of ties should not exceed 16 times of longitudinal bar diameters (to restrain rebar buckling), 48 times of tie diameters (to assure sufficient tie area to prevent the lateral displacement of the longitudinal rebars), or the least lateral dimension of the column (to develop the maximum strength of the concrete core). Thus, 150 mm tie spacing was selected for this study which corresponds to the requirement to develop the maximum strength of the concrete core. The other spacing (75 mm) was selected as the minimum practical spacing as well as the viewpoint of seismic provision which corresponds to half of the least lateral dimension of the column. A 25 mm spacing was provided at the end zones of columns to provide additional lateral support to eliminate any chance of disruption of concrete at those zones. For all columns, 8 mm diameter steel bars were used as transverse reinforcement.

Two electrical resistance steel strain gauges were mounted onto the internal reinforcement (one was with longitudinal reinforcement and one was with transverse reinforcement) before casting the concrete to determine the reinforcements strains. Besides, three concrete strain gauges were glued on the surface of the concrete before testing at the mid-height of the column to determine the axial and transverse strain. The detailed test matrix is listed in Table 3.7. The cross-section of the columns and reinforcement configurations are shown in Figure 3.5 and Figure 3.6.

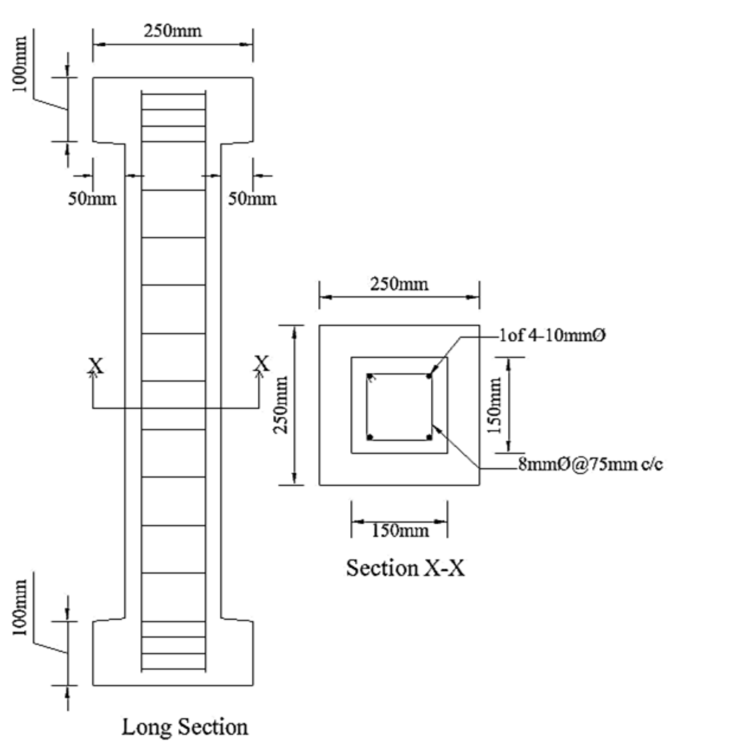

(a)

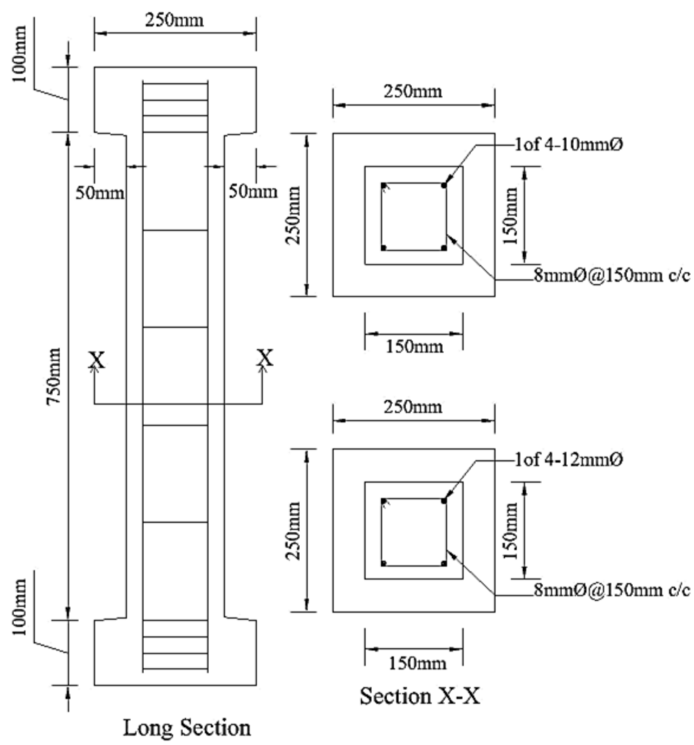

(b)

Figure 3.5 Longitudinal and transverse reinforcement configuration of columns: (a) 75 mm tie spacing and (b) 150 mm tie spacing.

Table 3.7 Test matrix for compression test of columns.

<table>
<tr><th rowspan="2">SN</th><th rowspan="2">Column Code</th><th colspan="2">Length × Width × Height (mm)</th><th colspan="2">Longitudinal Reinforcement</th><th colspan="3">Transverse Reinforcement</th></tr>
<tr><th>Top & Bottom Head</th><th>Main Body</th><th>Rebar</th><th>ρ (%)</th><th>Top & Bottom Head</th><th>Main Body</th><th>ρ_t (%)</th></tr>
<tr><td>1</td><td>$R_0C_0F_{0\_0-0}$</td><td rowspan="26">250 × 250 × 100</td><td rowspan="26">150 × 150 × 750</td><td rowspan="4">-</td><td rowspan="4">-</td><td rowspan="4">-</td><td rowspan="4">-</td><td rowspan="4">-</td></tr>
<tr><td>2</td><td>$R_{30}C_0F_{0.5\_0-0}$</td></tr>
<tr><td>3</td><td>$R_{30}C_{15}F_{0\_0-0}$</td></tr>
<tr><td>4</td><td>$R_{30}C_{15}F_{0.5\_0-0}$</td></tr>
<tr><td>5</td><td>$R_0C_0F_{0\_1.4-75}$</td><td rowspan="9">4-10mmφ</td><td rowspan="9">1.4</td><td rowspan="9">8mmφ@25 mm c/c</td><td rowspan="9">8mmφ@75 mm c/c</td><td rowspan="9">0.22</td></tr>
<tr><td>6</td><td>$R_{30}C_0F_{0\_1.4-75}$</td></tr>
<tr><td>7</td><td>$R_{30}C_5F_{0\_1.4-75}$</td></tr>
<tr><td>8</td><td>$R_{30}C_{10}F_{0\_1.4-75}$</td></tr>
<tr><td>9</td><td>$R_{30}C_{15}F_{0\_1.4-75}$</td></tr>
<tr><td>10</td><td>$R_{30}C_0F_{0.5\_1.4-75}$</td></tr>
<tr><td>11</td><td>$R_{30}C_5F_{0.5\_1.4-75}$</td></tr>
<tr><td>12</td><td>$R_{30}C_{10}F_{0.5\_1.4-75}$</td></tr>
<tr><td>13</td><td>$R_{30}C_{15}F_{0.5\_1.4-75}$</td></tr>
<tr><td>14</td><td>$R_0C_0F_{0\_1.4-150}$</td><td rowspan="9">4-10mmφ</td><td rowspan="9">1.4</td><td rowspan="9">8mmφ@25 mm c/c</td><td rowspan="9">8mmφ@150 mm c/c</td><td rowspan="9">0.22</td></tr>
<tr><td>15</td><td>$R_{30}C_0F_{0\_1.4-150}$</td></tr>
<tr><td>16</td><td>$R_{30}C_5F_{0\_1.4-150}$</td></tr>
<tr><td>17</td><td>$R_{30}C_{10}F_{0\_1.4-150}$</td></tr>
<tr><td>18</td><td>$R_{30}C_{15}F_{0\_1.4-150}$</td></tr>
<tr><td>19</td><td>$R_{30}C_0F_{0.5\_1.4-150}$</td></tr>
<tr><td>20</td><td>$R_{30}C_5F_{0.5\_1.4-150}$</td></tr>
<tr><td>21</td><td>$R_{30}C_{10}F_{0.5\_1.4-150}$</td></tr>
<tr><td>22</td><td>$R_{30}C_{15}F_{0.5\_1.4-150}$</td></tr>
<tr><td>23</td><td>$R_0C_0F_{0\_2.0-150}$</td><td rowspan="4">4-12mmφ</td><td rowspan="4">2.0</td><td rowspan="4">8mmφ@25 mm c/c</td><td rowspan="4">8mmφ@150 mm c/c</td><td rowspan="4">0.22</td></tr>
<tr><td>24</td><td>$R_{30}C_5F_{0.5\_2.0-150}$</td></tr>
<tr><td>25</td><td>$R_{30}C_{10}F_{0.5\_2.0-150}$</td></tr>
<tr><td>26</td><td>$R_{30}C_{15}F_{0.5\_2.0-150}$</td></tr>
</table>

Note:
For $R_{30}C_{15}F_{0.5\_2.0-150}$ combination, R is RCA; 30 is % of RCA replacement; C is crumb rubber; 15 is % of CR replacement; F is polypropylene fiber; 0.5 is % of PP fiber; 2.0 is % of longitudinal reinforcement ratio and 150 is tie spacing.

(a) Installation of Strain Gauge on Column Reinforcement

(b) Column Reinforcement Detailing

(c) All Columns After Installation of Strain Gauges

Figure 3.6 Preparation of columns before casting.

3.4.3 Column Specimens for Free Vibration Test

The columns having 150 mm tie spacing were used for the free vibration test before conducting the compression test. The effect of RCA, CR, and PP fiber on different free vibrational responses was evaluated. The detailed test matrix and the configuration of the reinforcement were shown in Table 3.8 and Figure 3.7.

Table 3.8 Test matrix for free vibration test of columns.

SN	Column Code	Length × Width × Height (mm)		Longitudinal Reinforcement		Transverse Reinforcement		
		Top & Bottom Head	Main Body	Rebar	ρ (%)	Top & Bottom Head	Main Body	ρ_t (%)
1	$R_0C_0F_{0\_1.4\text{-}150}$	250 × 250 × 100	150 × 150 × 750	4-10mmφ	1.4	8mmφ@25 mm c/c	8mmφ@150 mm c/c	0.22
2	$R_{30}C_0F_{0\_1.4\text{-}150}$							
3	$R_{30}C_5F_{0\_1.4\text{-}150}$							
4	$R_{30}C_{10}F_{0\_1.4\text{-}150}$							
5	$R_{30}C_{15}F_{0\_1.4\text{-}150}$							
6	$R_{30}C_0F_{0.5\_1.4\text{-}150}$							
7	$R_{30}C_5F_{0.5\_1.4\text{-}150}$							
8	$R_{30}C_{10}F_{0.5\_1.4\text{-}150}$							
9	$R_{30}C_{15}F_{0.5\_1.4\text{-}150}$							

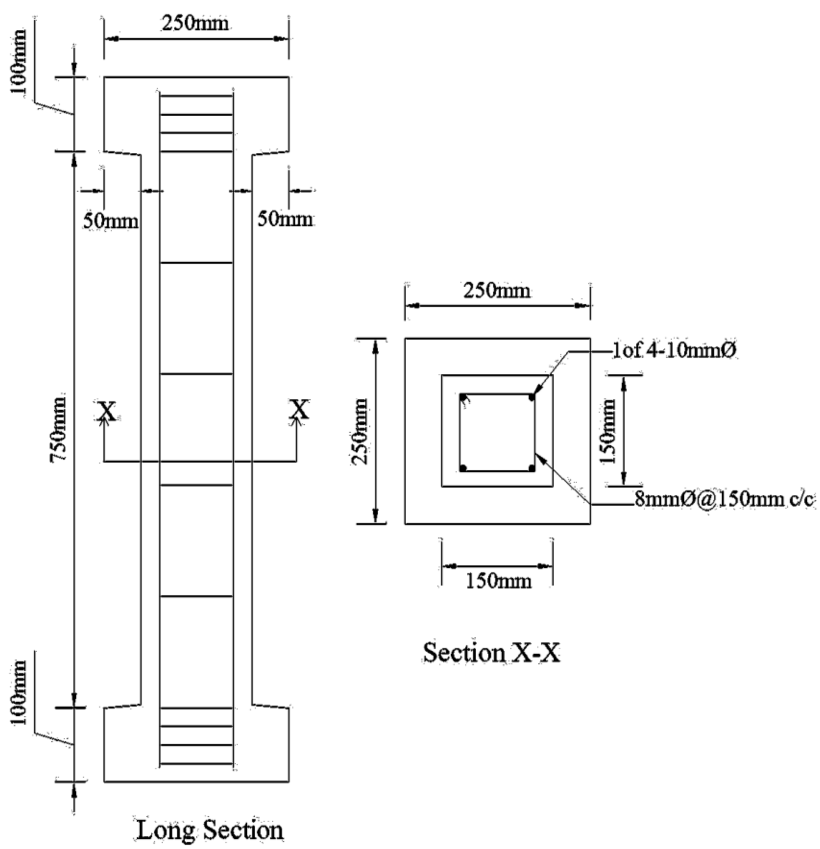

Figure 3.7 Longitudinal and transverse reinforcement configuration for free vibration testing columns.

3.4.4 Fabrication of Specimens

The mixing procedure of CR and PP fiber in the concrete mixture was adopted from Shahjalal et al. [13]. At first, the CR was mixed manually with NFA. Then, the PP fiber was thoroughly mixed with the designed cement content by hand to ensure uniform distribution. In addition, to ensure uniform distribution of fibers, molds were filled with fresh concrete from one end in a single layer. The concrete mixtures were prepared in the concrete laboratory using a concrete mixture machine and after mixing the fresh concrete was poured on a dry surface. At first, the designated amounts of NCA and RCA were inserted into the mixture machine. Then the combined ingredient of CR and NFA were added followed by the addition of the mixture of cement and PP fiber with the last ingredient being water. A vibrator was used during the casting of the specimens. The fabrication of the different specimens is shown in Figure 3.8. The columns and other specimens were moist cured under wet jute fibers layer for 28 days which is a common practice of curing different structural members in Bangladesh (Figure 3.9).

(a) Preparation of Columns Molds

(b) Casting of Columns Specimens

(c) Preparation of Dog Bone Molds

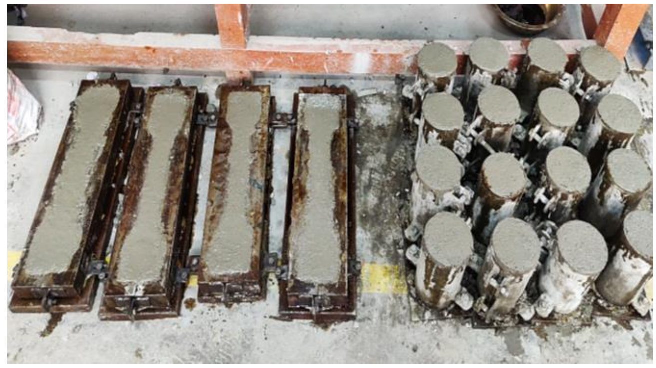

(d) Casting of Dog Bone Specimens and Cylinders

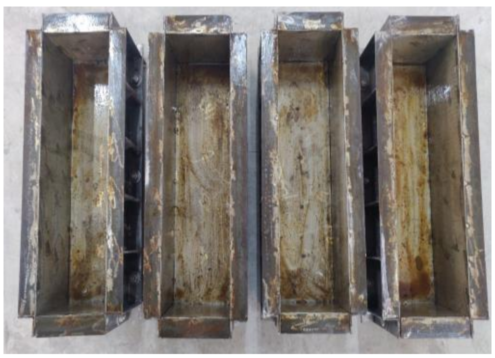

(e) Preparation of Beam Molds

(f) Casting of Beam Specimens

Figure 3.8 Fabrication of the specimens.

Figure 3.9 Curing of specimens.

3.5 Test Setup and Procedure

The following section describes the detailed setup and procedures of different tests of this study.

3.5.1 Test Setup for Mechanical Properties of Concrete

The fresh concrete was used to determine the slump value, air content, and fresh density of concrete. ASTM C143-15 [196] was used to determine the slump value whereas ASTM C231-17 [197] was used for determining the air content. The compressive strength was done as per ASTM C39-18 [198] using a compression machine of 2000 kN capacity. To determine the MoE of concrete, two concrete strain gauges were attached at the mid-height of each concrete cylinder (Figure 3.10). The longitudinal and transverse strains of concrete cylinders were collected by those strain gauges through a data logger using a loading rate of 0.3 kN/s which is displayed in Figure 3.11 (a). the test was conducted as per ASTM C469-14 [199]. Before the test, the top and the bottom surface of the concrete cylinder were leveled with a grinding machine to eliminate the eccentricity of loading. For the direct tensile strength test of concrete, a customized steel fixture was prepared to hold the specimens in UTM shown in Figure 3.11 (b). A displacement rate of 0.05 mm/min was used in the tensile test.

The ultrasonic pulse velocity (UPV) of concrete was determined following ASTM C597-16 [200] (Figure 3.11 (c)). To determine the surface resistivity of concrete against chloride ion penetration, the surface resistance value was determined. Before the test, the cylinder was cleaned up very carefully. Then, with the help of the surface resistivity meter, the value of surface resistance was recorded at the right angle around the cylinder. After that, the value was linked with the chloride ion penetrability chart that is guided in AASHTO TP 95 [201]. The test setup is presented in Figure 3.11 (d). The hardened density of concrete was determined according to ASTM C642-13 [202]. The flexural strength was determined using a three-point bending test on the notched beam and the setup was adopted from the Japan Concrete Institute Standard [193] for fiber-reinforced concrete (Figure 3.11 (e)). A constant loading rate of 0.075 mm/min was given using a UTM. All the test set up for determining different mechanical properties of concrete is summarized in Figure 3.11. The standards and duration of conducting different tests is summarized in Table 3.9.

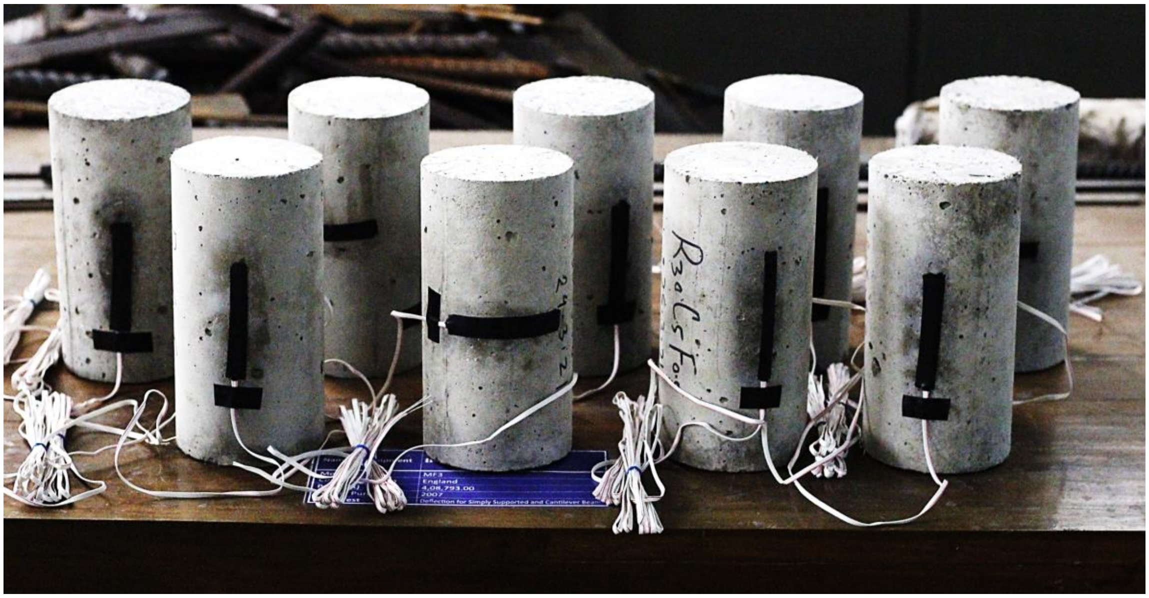

Installation of Strain Gauge on Concrete Cylinders

Figure 3.10 Installation of strain gauge.

(a) Compressive Strength Test of Concrete Cylinders

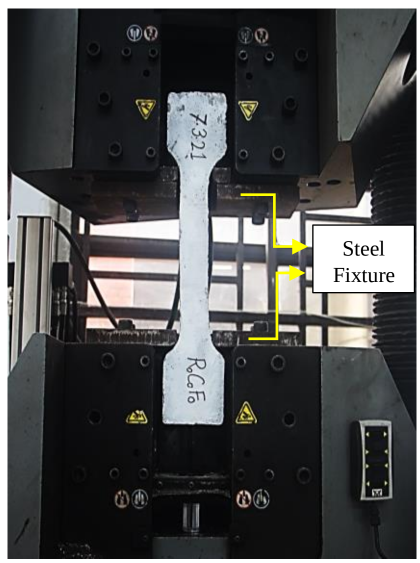

(b) Direct Tensile Test of Concrete

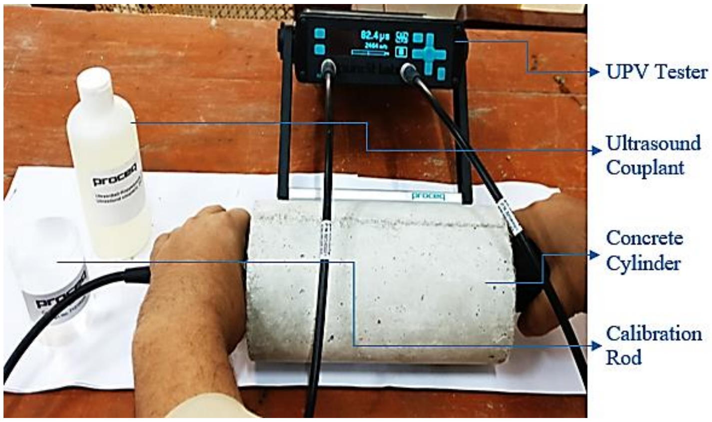

(c) UPV Test

(d) Surface Resistivity Test

(e) Flexural Strength Test

Figure 3.11 Test setup for determining different mechanical properties of concrete.

3.5.2 Compression Test of Reinforced Concrete Columns

All the columns were whitewashed and the surfaces were gridded with small square boxes to get an idea of the crack lengths which is shown in Figure 3.12 (a). Three concrete strain gauges were glued on the mid surface of the column before starting the test. Among them, two were mounted longitudinally and one was transversely Figure 3.12 (b). All the column specimens were tested under uniaxial loading up to failure by using a Universal Testing Machine (UTM) with a capacity of 1000 kN. A displacement-controlled loading rate of 0.1 mm/min was applied gradually until failure. The columns were fixed at the top and bottom before starting the test. The top and bottom ends of the columns were leveled evenly during the casting and testing process to ensure a uniform distribution of loading throughout the cross-section. Special care was taken to set the column specimens at the center of the machine so that no eccentricity was produced. The applied load and its corresponding axial compression were taken from UTM. Moreover, to determine the midpoint lateral deflection four additional LVDTs were used at the mid-height of the column. The longitudinal/axial and transverse strains of reinforcement and concrete columns were collected by steel and concrete strain gauge. All data were collected at a regular interval by an automatic data logger system. The formation of cracks and their corresponding loads were noted very carefully. A high-resolution camera was also used to capture the failure patterns of columns at different stages. The total arrangement of the instruments is presented in Figure 3.13.

(a) Whitewashed and Gridded the Columns' Surfaces

(b) Installation of Concrete Strain Gauge on Column Surface

Figure 3.12 Column preparation before testing.

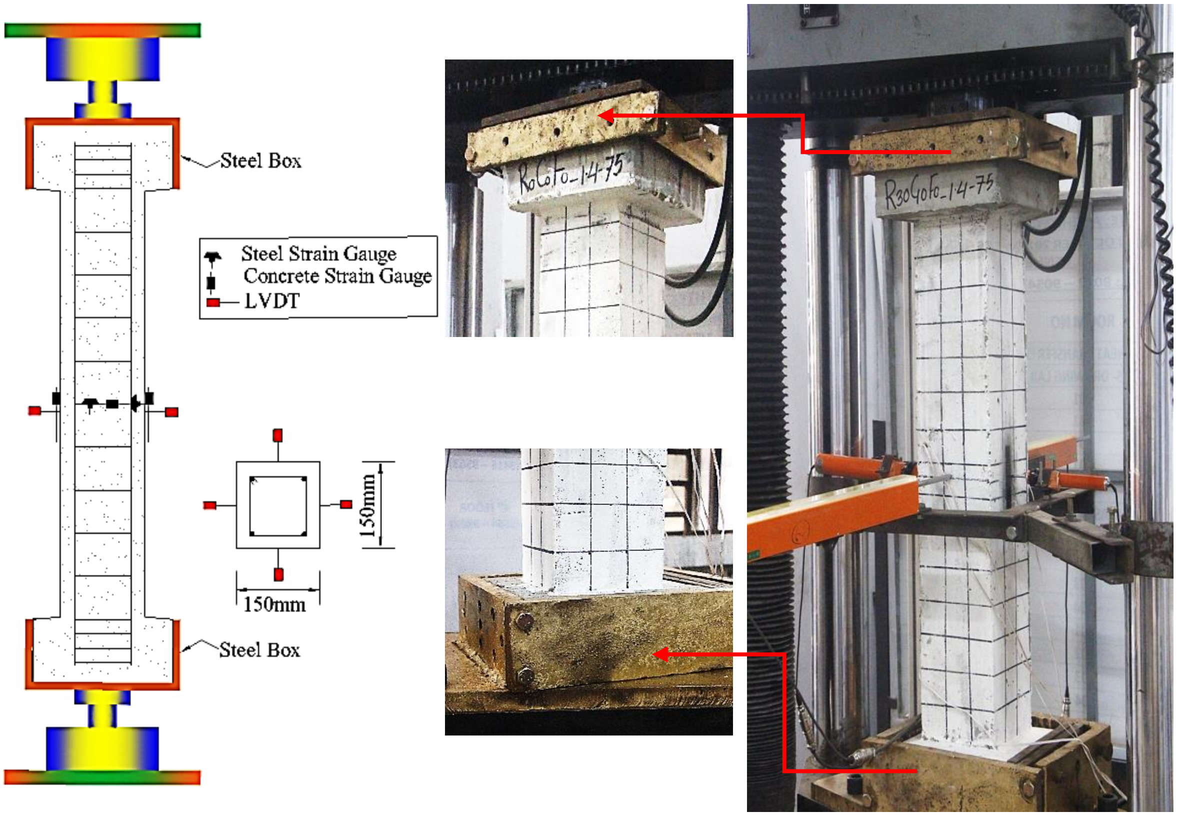

(a) Schematic diagram **(b)** Top and Bottom Fixing **(c)** LVDT setup

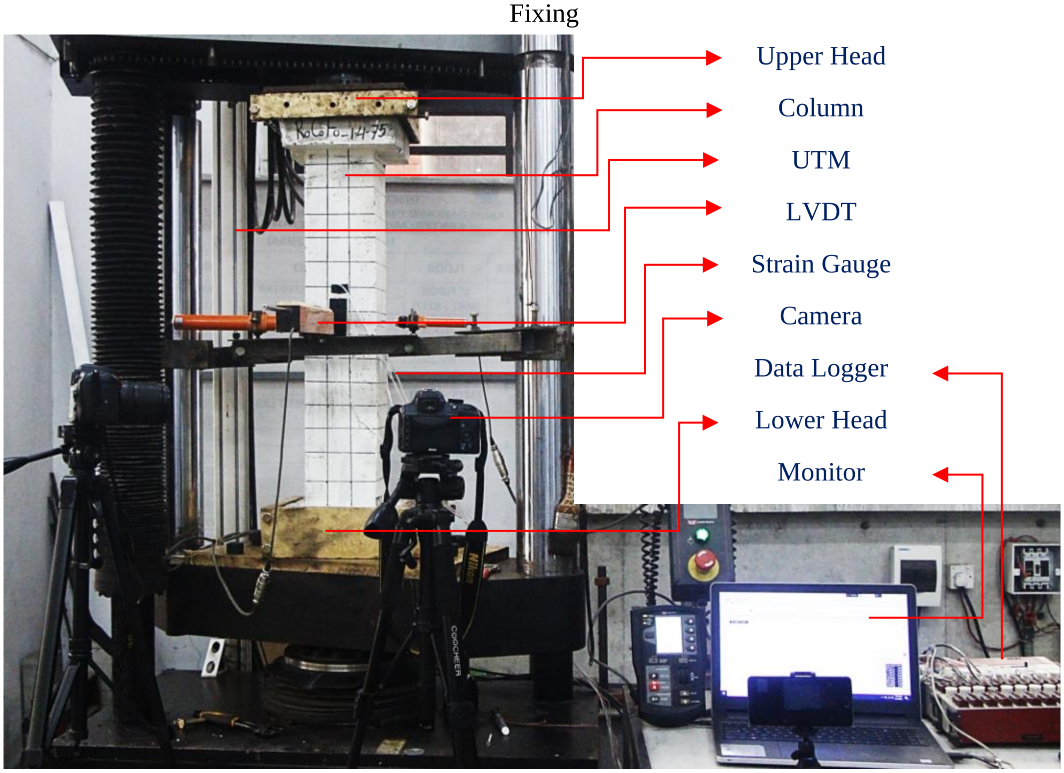

(d) Actual setup for columns

Figure 3.13 Test set-up for uniaxial compression test of columns.

3.5.3 Free Vibration Test of Reinforced Concrete Columns

To investigate the energy dissipation capability of the rubberized concrete and fiber-reinforced rubberized concrete free vibration test was carried out in this study for different combinations of concrete. As shown in Figure 3.14 (a), a 2.5 kg hammer was employed to apply impact load to the mid-point of the top head of the column. Three different impact energy was generated by changing the horizontal length of the hammer arm by 30 cm, 35 cm, and 40 cm. Thus three different impact energy was generated such as 1.54 N.m, 2.13 N.m, and 2.83 N.m, respectively. Three accelerometers were used to collect the acceleration data. Among them, two were glued on the midpoint of the top surface of the top head and another one was at the top surface of the bottom head as presented in Figure 3.14 (b). A displacement sensor was also placed horizontally at the same level as the hammer but on the opposite surface of the column. The free vibration data were recorded through a data acquisition system. The positions of the accelerometers and the displacement sensor are shown in Figure 3.14 (b). Each test was repeated three times and the average result was presented. The full test setup for the free vibration test is displayed in Figure 3.14 (c).

Table 3.9 Standards and duration of conducting different tests.

SL	Name of Test	Code/ Standard/Reference	Test Conducted on (Days)
1	Slump	ASTM C143-15 [196]	0
2	Air Content	ASTM C231-17 [197]	0
3	Compressive Strength	ASTM C39-18 [198]	7, 28, 56
4	Modulus of Elasticity	ASTM C469-14 [199]	56
5	Tensile Strength	Liu et al.[192]	56
6	Flexural Strength	Japan Concrete Institute Standard [193]	56
7	Ultrasonic Pulse Velocity	ASTM C597-16 [200]	7, 28, 56
8	Surface Resistivity	AASHTO TP 95 [201]	56
9	Hardened Density	ASTM C642-13 [202]	7, 28, 56
10	Compression Test of Columns	-	56
11	Free Vibration Test of Columns	-	56

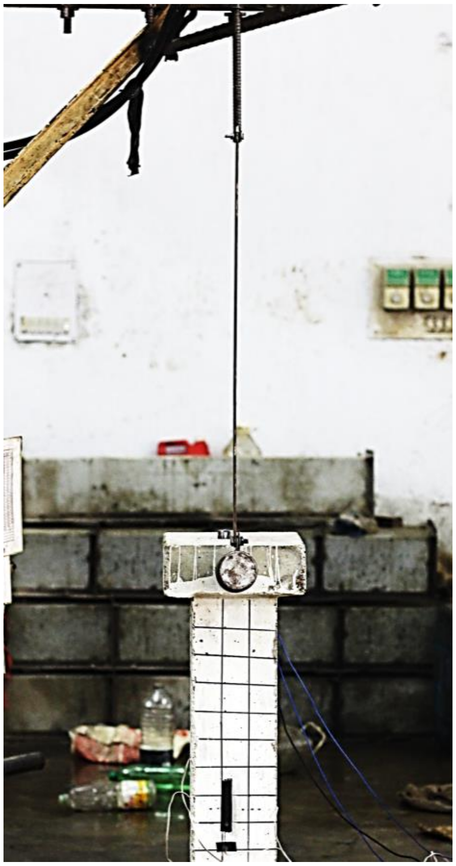

(a) Location of the Impact Hammer

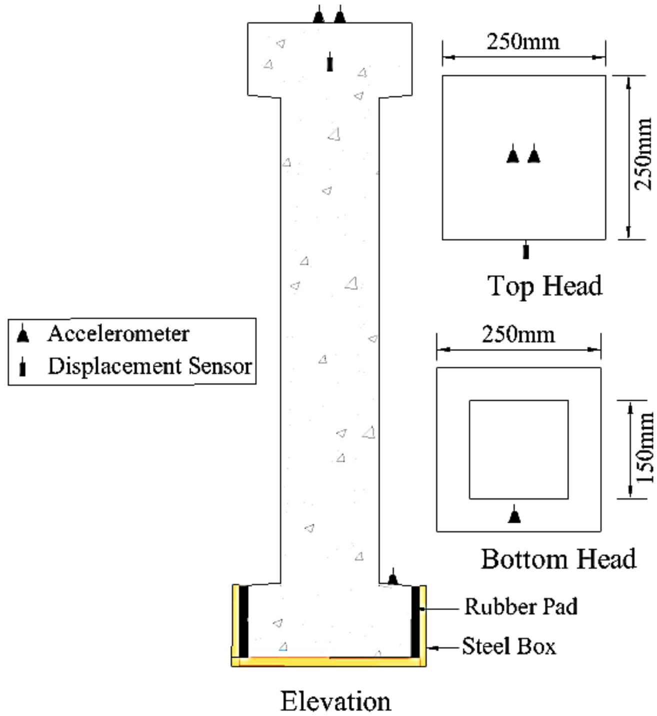

(b) Schematic Diagram of the Location of Accelerometer and Displacement Sensor

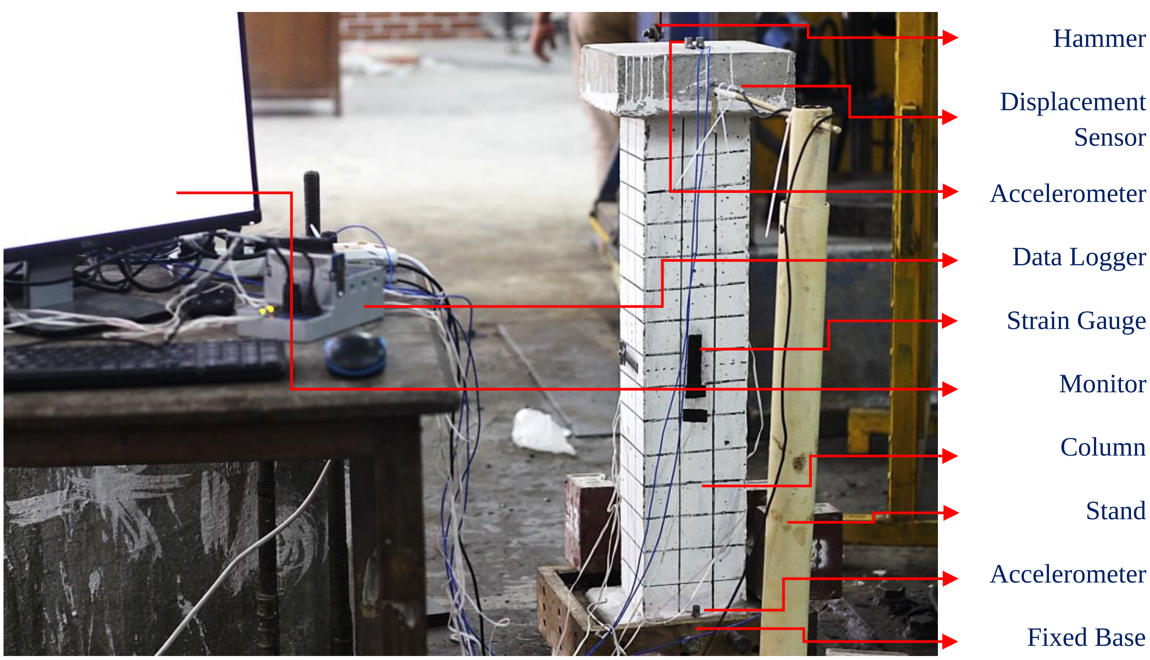

(c) Data Acquisition System

Figure 3.14 Test setup for free vibration test.

3.6 Summary

Using 9 concrete proportions a total of 108 concrete cylinders, 36 dog bone specimens, and 36 prism beams were cast to determine the different mechanical properties of concrete. Portland composite cement (PCC), natural fine aggregate (NFA), natural coarse aggregate (NCA), recycled coarse aggregate (RCA), crumb rubber (CR), and polypropylene (PP) fiber, mild steel rebar were used as materials. To determine the compressive behavior of reinforced concrete R^2C and FR^3C columns 26 columns were fabricated by varying the percentage of CR content at 0%, 5%, 10%, and 15%, tie spacing at 75 mm and 150 mm as well as longitudinal reinforcement ratio at 0%, 1.4%, and 2.0%. However, the RCA was fixed at 30% in all combinations. In FR^3C combinations, 0.5% PP was used additionally. From those 26 columns, 9 columns having the tie spacing of 150 mm were used for the free vibration test before conducting the compression test. All the tests had been performed as per standards at their specified ages.

Chapter 4
MECHANICAL PROPERTIES OF CONCRETE

4.1 Introduction

The present chapter describes the fresh and hardened properties of different rubberized recycled concrete (R^2C) and fiber-reinforced rubberized recycled concrete (FR^3C). The fresh properties contain slump value, air content, and fresh density whereas hardened properties are presented in terms of compressive strength, modulus of elasticity, tensile strength, flexural strength, hardened density, ultrasonic pulse velocity, and surface resistivity. Besides, an extensive regression analysis has been carried out and proposed different equations for predicting various mechanical properties considering the effect of crumb rubber (CR) and fiber. A cost analysis has been done for establishing R^2C and FR^3C as cost-effective and eco-friendly concrete.

4.2 Fresh Properties

The following section presents various fresh properties of different concrete mixtures.

4.2.1 Slump Value

The slump value of different concrete mixtures is presented in Figure 4.1. Overall, it is seen that all the rubberized recycled concrete (R^2C) mixtures and fiber-reinforced rubberized recycled concrete (FR^3C) mixtures exhibit a reduced slump compared to the control mix of 165 mm. This drop is primarily due to different specific gravity of constituents present in the mixtures, for instance, fibers, crumb rubber (CR), and recycled coarse aggregate (RCA). After the inclusion of 30% RCA, the slump is reduced to 150 mm as a result of the increased absorption capacity of RCA. The same trend is also observed when CR is introduced in the mix design. The slump value begins to decrease with an increase in amounts of CR in the mixture. As the surface of the CR particles is too rough, they create internal friction between the ingredients of the concrete which leads to a decrease in the slump value. The slump values of R^2C containing 0%, 5%, 10%, and 15% CR content are decreased by 9.1%, 21.2%, 45.5%, and 54.5%, respectively compared to the control mixture. Besides, from Figure 4.1, it is distinct that when an additional 0.5% PP fiber is added the workability of concrete reduces further. The slump values of FR^3C containing 0%, 5%, 10%, and 15% CR content are found to be decreased further by 43.3%, 42.3%, 33.3%, and 33.3%, respectively compared to R^2C combinations. As CR is a porous material, more water is required to overcome inter-particle friction which reduces the workability. Besides, this reduction in workability can also be greatly attributed to the increased density and the apparent dryness imparted by PP fiber. Moreover, fiber creates higher interlocking between aggregates which drastically reduces the workability. Batch-9 ($R_{30}C_{15}F_{0.5}$) exhibits the lowest slump which is 69.7% lower than that of the control mixture.

Slump value is used to quantify the degree of workability and the slump class. The correlation between the workability and slump value and the slump class is presented in Table 4.1. The slump value of all R^2C mixtures falls within the range of 60/80 - 120/150 which complies with the "High" degree of workability and slump class of S3. Thus, the workability will not significantly drop for CR content. On the contrary, the slump value of FR^3C mixtures complies with the "Medium" degree of workability and slump class of S2. However, though the slump value decreases with RCA, CR, and fiber, it still provides a medium degree of workability.

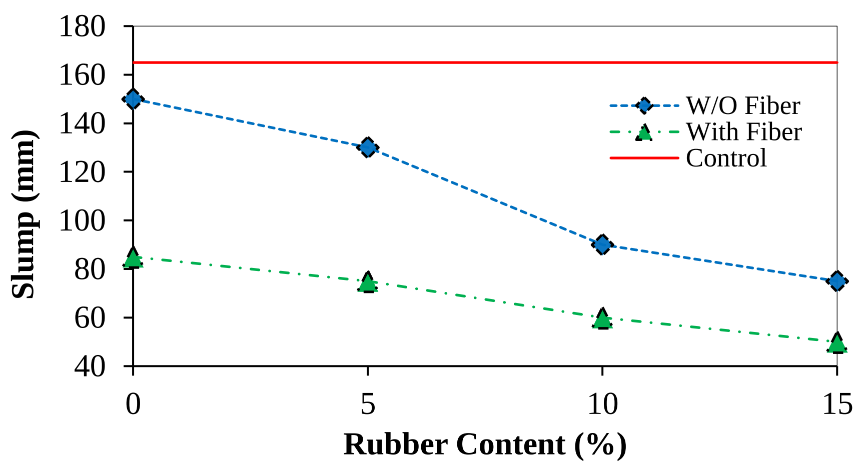

Figure 4.1 Slump value of different concrete mixtures.

Table 4.1 Degree of workability and class of slump

Bartos et al. [203]		EN 206-1 [204]	
Slump (mm)	**Degree of workability**	**Slump (mm)**	**Class**
0	No Slump, Zero Slump		
0 – 10	Very Low	10-40	S1
10 – 30	Low	50-90	S2
30 - 60/80	Medium	100-150	S3
60/80 - 120/150	High	160	S4
120/150 – collapsed	Very High		

4.2.2 Air Content

The air content of different concrete mixtures is summarized in Figure 4.2. Overall, it is seen that the air content of concrete mixtures with the addition of RCA, CR, and fibers, is increased. After replacing the NCA with 30% RCA, the air content of recycled aggregate concrete (RAC) is found to increase by 10.0% compared to natural aggregate concrete (NAC). The presence of adhered mortar in RCA particles becomes the source for entrapping air. Besides, the air content is also found to increase as the CR content increases. The CR particles are irregular in shape which could be one of the possible reasons for entrapping air during the mixing process. Besides, due to the lower specific gravity and porous nature of CR, it cannot mix properly with the other ingredients, thus providing a higher value of air content. The air content of R^2C is increased by 10.0%, 20.5%, 27.3%, and 34.1% for 0%, 5%, 10% and 15% CR content, respectively compared to the control mixture. However, from Figure 4.2 it is clear that adding PP fiber to concrete slightly decreases the air content value as it creates a strong interlocking between the aggregates. The air content values of FR^3C containing 0%, 5%, 10%, and 15% CR content are found to be decreased by 2.9%, 9.4%, 10.0%, and 11.9%, respectively compared to R^2C combinations but still higher than that of control mixture. This result is consistent with the previous study [16].

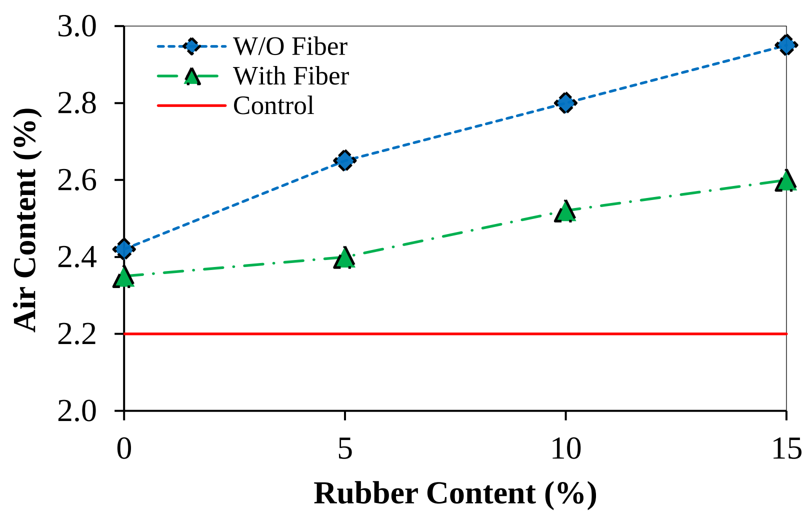

Figure 4.2 Air content of different concrete mixtures.

4.2.3 Fresh Density

Figure 4.3 demonstrates the fresh concrete densities of different concrete mixtures. In general, it is seen that the fresh density decreases after the inclusion of RCA CR, and fiber. Due to the reduced specific gravity and unit weight of RCA, CR, and PP fiber in comparison to NCA, NFA, and cement, the concrete density reduces. With increasing the percentage of CR content in the R^2C mixture the density reduces 2.5%, 6.3%, 7.1%, and 8.3% for 0%, 5%, 10%, and 15% CR content, respectively compared to the control mixture. Besides, the inclusion of fiber in R^2C further decreases the density. In FR^3C, these reduction percentages increase to 4.5, 7.5, 8.6, and 11.0 for 0%, 5%, 10%, and 15% CR content, respectively compared to the control specimen. The density range varies from 2200 kg/m^3 to 2400 kg/m^3 for R^2C, and 2100 kg/m^3 to 2350 kg/m^3 for FR^3C, whereas, the control specimen density is almost 2430 kg/m^3. Thus, relatively lightweight concrete can be produced by incorporating RCA, CR, and PP fiber in the concrete mixture which can reduce the self-weight of the concrete.

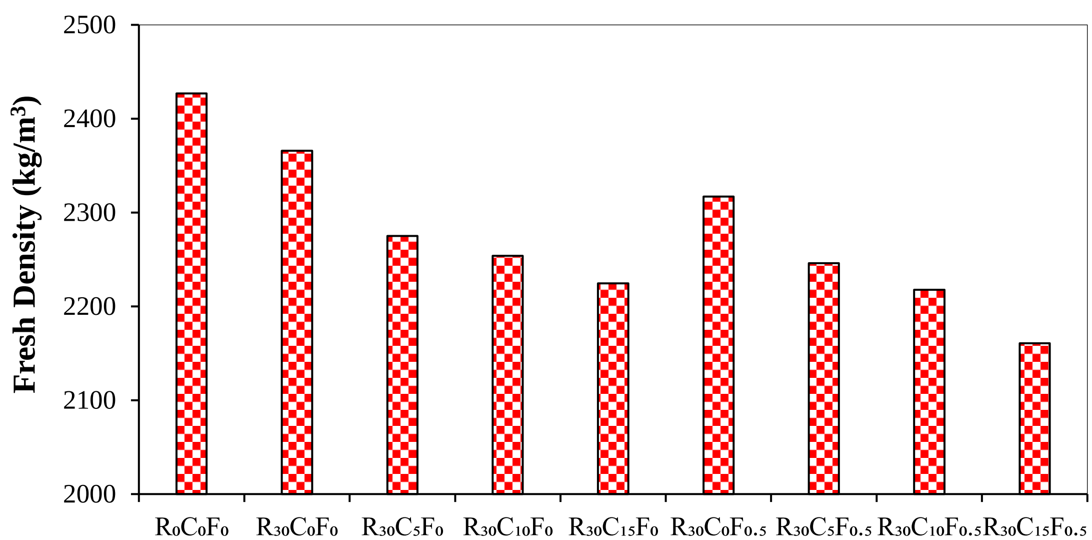

Figure 4.3 Fresh density of different concrete mixtures.

4.3 Hardened Properties

The following section presents the effect of RCA, CR, or fiber on various mechanical properties of different concrete mixtures.

4.3.1 Compressive Strength

The compressive strength of different concrete batches is summarized in Figure 4.4. In general, the concrete strength increases with increasing age. Approximately 49% of strength has been gained at 7 days and at 56 days the average strength has been increased by 14% compared to 28 days' strength in rubberized concrete (RuC). As the CR particles are hydrophobic in nature, proper hydration cannot be done at an early age. Thus, the strength gaining is comparatively slower than that of normal concrete or recycled aggregate concrete (RAC). From Figure 4.5 it is clearly seen that all RuC exhibits comparatively lower compressive strength. With increasing the percentage of CR content, the compressive strength of R^2C specimens′ decreases. The decreasing percentages are 11.7%, 18.5%, 25.8%, and 40.1% for 0%, 5%, 10%, and 15% CR content, respectively compared to the control mixture. As CR is a porous material and has a lower specific gravity and absorption capacity than NFA, it creates a weaker bond within the concrete matrix, thus creating a weaker ITZ (Interfacial Transition Zone). This strength reduction may also happen because of the various impurities presented in CR. However, higher than 25 MPa concrete can be produced by using 15% CR content, and it can be 30 MPa if the CR content is limited to 10%.

The inclusion of fiber in R^2C increases the compressive strength of FR^3C specimens. Approximately 15.9%, 13.6%, 9.7%, and 25.9% compressive strength can be increased at 56 days by adding 0.5% PP fiber in R^2C mixtures along with 0%, 5%, 10%, and 15% CR content, respectively. The same trend is also observed for 7 days and 28 days. Fiber can strongly bridge the cement paste and aggregate which needs additional strength to break, thus providing a higher strength of concrete. From the results of BN-1 and BN-2, it is observed that the replacement of NCA by RCA reduces the compressive strength since RCA induces a higher porosity that creates a weaker bond thereby a lower strength. Besides, the increased water absorption capacity and higher Los Angeles abrasion value (32%) of the RCA is the reason for its lower strength compared to natural aggregate concrete (NAC). BN-6 ($R_{30}C_0F_{0.5}$) provides the highest compressive strength which is 2.3% more than that of the control batch because it is a fiber-reinforced concrete without any CR content. However, more than 40 MPa concrete can be produced using 30% RCA and 5% CR content along with 0.5% PP fiber.

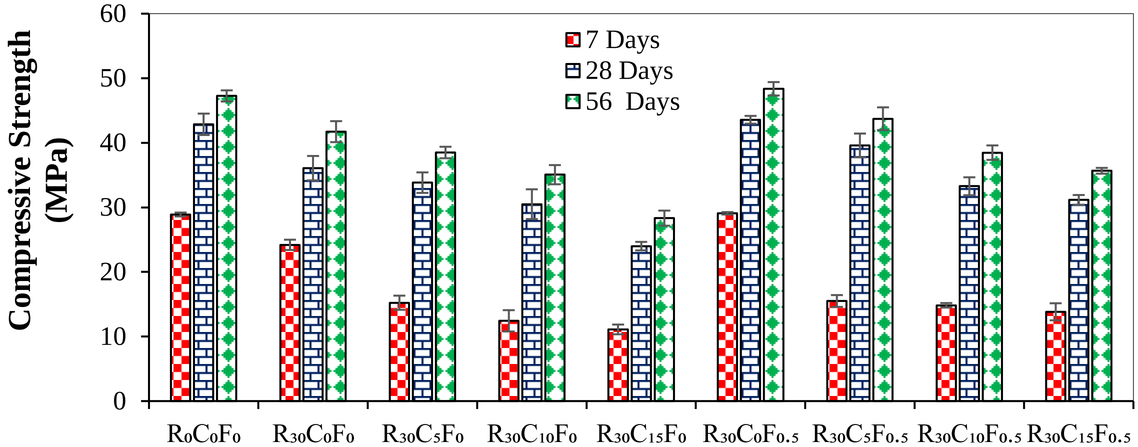

Figure 4.4 Compressive strength of different concrete batches at different ages.

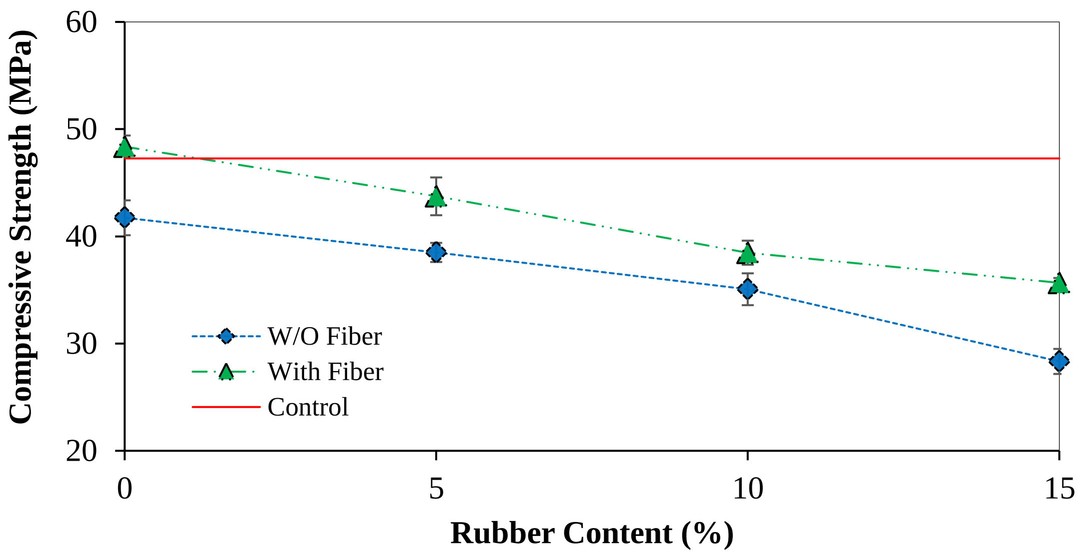

Figure 4.5 Effect of CR and PP fiber on compressive strength at 56 days.

4.3.2 Tensile Strength

Figure 4.6 represents the direct tensile strength of different concrete batches at 56 days. The tensile strengths are approximately 8% of the corresponding compressive strength. The splitting tensile strengths of FR^3C specimens are higher than that of R^2C specimens which implies that with the addition of fiber content the tensile strength increases. This is evident from the comparison between BN-2 ($R_{30}C_0F_0$), BN-6 ($R_{30}C_0F_{0.5}$); BN-3 ($R_{30}C_5F_0$), BN-7 ($R_{30}C_5F_{0.5}$), BN-4 ($R_{30}C_{10}F_0$), BN-8 ($R_{30}C_{10}F_{0.5}$), and BN-5 ($R_{30}C_{15}F_0$), BN-9 ($R_{30}C_{15}F_{0.5}$). Approximately 12.3%, 2.9%, 5.2%, and 16.7% tensile strength is increased by incorporating 0.5% PP fiber in R^2C mixtures with 0%, 5%, 10%, and 15% CR content, respectively. Fiber has a good tensile capacity and it bridges the aggregate and cement paste strongly, thus providing a higher concrete tensile strength. On the contrary, the concrete tensile strength drops with the increasing percentage of CR owing to the fragility of CR in tension. The hydrophobic nature of CR increases the amount of water content and air voids in the concrete mixture resulting in a lower strength for concrete. The tensile strength is decreased by 6.0%, 11.8%, 27.0% and 3.3%, 7.2%, 14.9% containing 5%, 10%, and 15% CR content in R^2C and FR^3C specimens, respectively compared to the control. As per ASTM C330-17 [205], the tensile strength of concrete with the combination of normal and lightweight aggregates should be a minimum of 2.3 MPa for a maximum density of 1840 kg/m^3, 2.1 MPa for a maximum density of 1760 kg/m^{3,} and 2.1 MPa for a maximum density of 1680 kg/m^3. All the combinations can satisfy this requirement.

Comparing BN-1 ($R_0C_0F_0$) and BN-2 ($R_{30}C_0F_0$) it is seen that the tensile strength is decreased by 4.9% for 30% RCA. The attached mortar on the surface of RCA creates a higher porosity that weakens the bonding capacity between the RCA and cement paste thereby providing a lower strength. Besides, the increased water absorption capacity and higher Los Angeles abrasion value of the RCA is another reason for lower strength compared to NAC. BN-6 ($R_{30}C_0F_{0.5}$) provides the highest tensile strength which is 6.7% higher than that of the control.

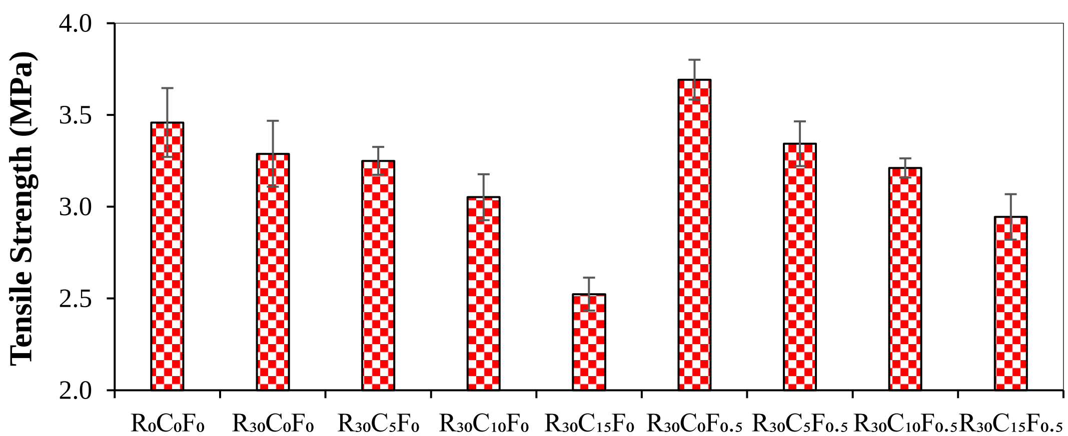

Figure 4.6 Tensile strength of different concrete batches.

4.3.3 Stress-Strain Behavior

The stress-strain behavior of NAC, RAC, R^2C, and FR^3C cylinder specimens under compression and dog bone specimens under direct tension are presented in Figure 4.7. Besides, the stress-strain responses of different concrete mixtures are summarized in Table 4.2. All the concrete specimens show a similar pattern of the stress-strain curves. All the compression curves are divided into three stages: elastic stage, elastoplastic stage, and fracture stage. The curves are linearly varied up to the elastic limit. After the elastic limit, the elastoplastic stage starts and is considered up to the ultimate point of stress. After that, the fracture stage starts and remains up to the breaking point. However, the dog bone specimens do not show any distinct fracture stage but rather suddenly break after reaching their ultimate point.

A significant difference is observed between R^2C and FR^3C specimens in strain capacity. Considering the compressive stress-strain behavior, the strain capacity increases with increasing the CR content, and it further increases with the addition of fiber. The axial strain corresponding to the peak stress is 0.00212, 0.00212, 0.00261, and 0.00279 for 0%, 5%, 10%, and 15% CR content in R^2C cylinders. After adding 0.5% PP fiber in R^2C mixtures, this strain exhibits as 0.00273, 0.00295, 0.00309, and 0.00325, respectively. In terms of fracture strain and transverse strain, a similar trend is also observed. Due to the soft nature of rubber particles and inherent mechanical properties compared to sand, they can experience higher deformation under compressive loading conditions. Besides, fiber can take the additional load and corresponding strain by making a strong bridging between the aggregates. The FR^3C specimens exhibit comparatively ductile behavior. As no aggregate spalling has occurred in the FR^3C specimens, it can take extra strain before fracture by providing a ductile behavior. Besides, the lower MoE of FR^3C specimens compared to R^2C specimens is another reason for this higher strain value (Figure 4.8). Fiber delays the first crack formation across the crack and retards visible cracking. So, larger deformation, and higher energy absorption can be achieved with the concrete containing rubber and fiber combinations. The transverse to axial strain ratio for R^2C is 0.28 whereas for FR^3C it is 0.23. Due to the strong bonding phenomena of fiber, it is effective in preventing a higher lateral strain.

From Table 4.2 it is observed that R^2C shows high Poisson's ratios due to its soft nature and enhanced energy absorption capacity. The Poisson's ratio increases with the increasing replacement level of rubber, which signifies better deformability and energy absorption capacity. On the contrary, it is seen that the Poisson's ratio decreases after adding PP fiber into the R^2C mixtures, which represents that fiber creates the concrete comparatively stiff. The Poisson's ratio of R^2C specimens varies from 0.24 to 0.30 and for FR^3C specimens it varies from 0.20 to 0.27 depending on the replacement level of CR content. Comparing $R_0C_0F_0$ and $R_{30}C_0F_0$ it is seen that the Poisson's ratio is increased after incorporating RCA into the mixture.

Considering the stress-strain behavior of dog bone specimens under tension, it is seen that an average 6.5% tensile strain is exhibited in the tensile test compared to axial strain. The tensile strain corresponding to peak stress is decreased with increasing the CR content. The tensile strain at the peak stress is 0.00019, 0.00017, 0.00014, and 0.00012 for 0%, 5%, 10%, and 15% CR content in R^2C specimens. After adding 0.5% PP fiber in R^2C mixtures, the strain capacity increases to 0.00025, 0.00020, 0.00017, and 0.00015, respectively. As fiber is strong in tension it provides higher tensile capacity. On the contrary, rubber is weak in tension.

Table 4.2 Summary of stress-strain responses of different concrete batches.

Batch No	**BN-1**	**BN-2**	**BN-3**	**BN-4**	**BN-5**	**BN-6**	**BN-7**	**BN-8**	**BN-9**
Batch Name	$R_0C_0F_0$	$R_{30}C_0F_0$	$R_{30}C_5F_0$	$R_{30}C_{10}F_0$	$R_{30}C_{15}F_0$	$R_{30}C_0F_{0.5}$	$R_{30}C_5F_{0.5}$	$R_{30}C_{10}F_{0.5}$	$R_{30}C_{15}F_{0.5}$
Peak Compressive Stress (MPa)	46.5	41.4	39.2	34.7	27.3	47.2	43.2	37.2	36.1
Modulus of Elasticity (GPa)	25.0	20.0	19.8	18.5	12.5	28.5	21.7	19.3	14.6
Axial Strain at Peak Compressive Stress (mm/mm)	0.00203	0.00212	0.00239	0.00261	0.00279	0.00273	0.00295	0.00309	0.00325
Ultimate Compressive Strain (mm/mm)	0.00213	0.00220	0.00247	0.00278	0.00293	0.00281	0.00312	0.00335	0.00344
Transverse Strain at Peak Compressive Stress (mm/mm)	0.00045	0.00051	0.00061	0.00071	0.00084	0.00054	0.00067	0.00074	0.00086
Poisson's ratio	0.22	0.24	0.25	0.27	0.30	0.20	0.23	0.24	0.27
Peak Tensile Stress (MPa)	3.50	3.27	3.20	3.05	2.42	3.78	3.48	3.21	2.83
Tensile Strain at Peak Tensile Stress (mm/mm)	0.00022	0.00019	0.00017	0.00014	0.00012	0.00025	0.00020	0.00017	0.00015

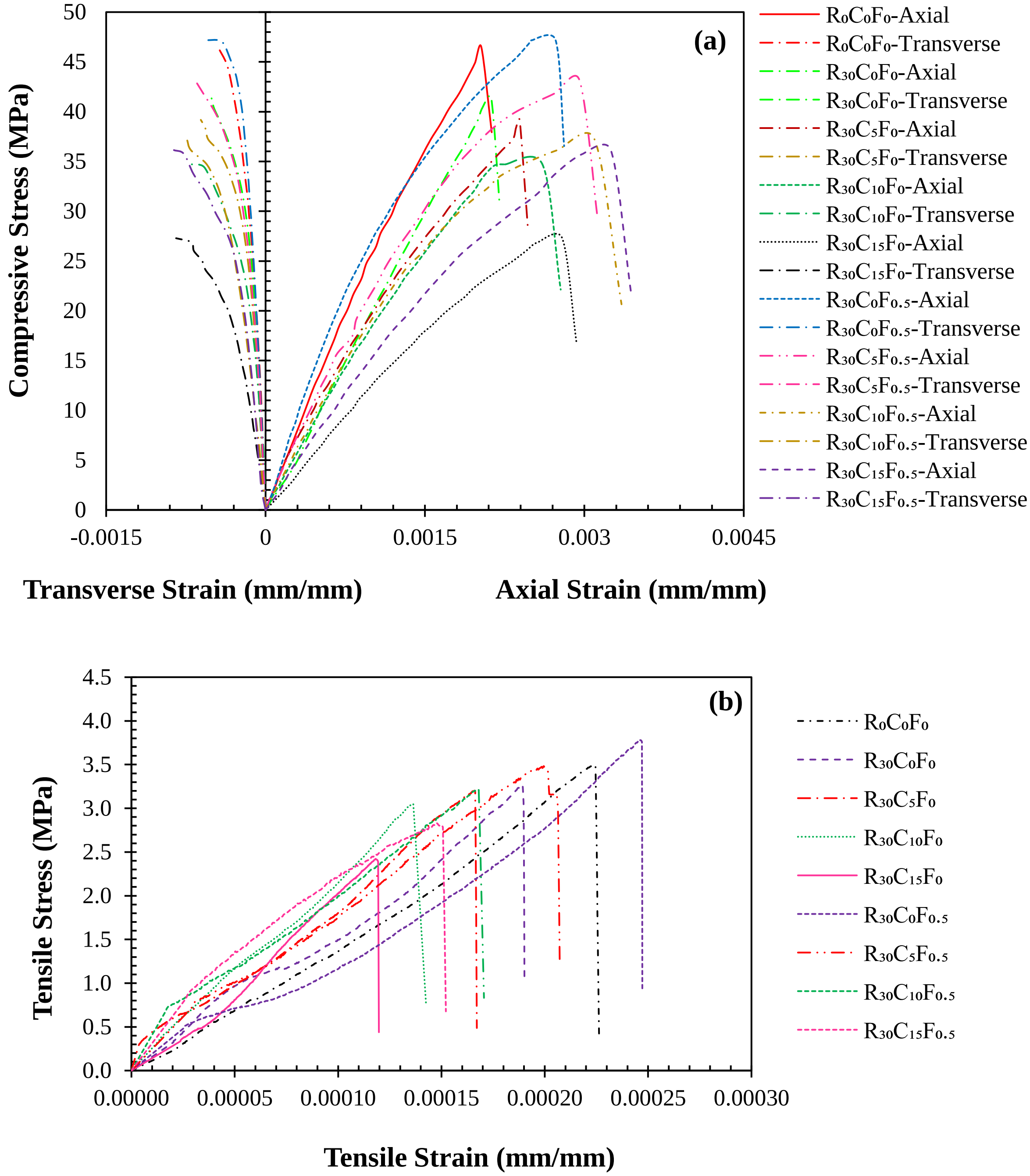

Figure 4.7 Stress-strain behavior of different concrete batches: (a) under compression, and (b) under direct tension.

4.3.4 Modulus of Elasticity

The variation in concrete modulus of elasticity (MoE) for various combinations are presented in Table 4.2 and Figure 4.8. The MoE mostly depends on the compressive strength, density, and CR content in the mixture. In general, the RuC specimens provide lower MoE compared to the control specimens. With increasing the CR content, the MoE decreases. The MoE of concrete containing 0%, 5%, 10%, and 15% CR content is 20 GPa, 19.8 GPa, 18.5 GPa, and 12.5 GPa. As CR is a soft material, it can deform easily and exhibits a lower stiffness which is the main reason for this reduction of MoE with CR content. This may also be due to the reduced density of R^2C specimens. However, after adding 0.5% PP fiber into the concrete mixture, the concrete becomes stiffer and exhibits a higher MoE. The MoE is increased by 42.5%, 9.4%, 4.5%, and 16.6% after adding fiber with 0%, 5%, 10%, and 15% CR content, respectively. Comparing BN-1 ($R_0C_0F_0$) and BN-2 ($R_{30}C_0F_0$) it is seen that the RAC specimens provide 20.1% lower MoE compared to NAC. BN-6 ($R_{30}C_0F_{0.5}$) provides the highest MoE which is 13.9% higher than that of control specimens as this is a fiber-reinforced concrete containing no CR content.

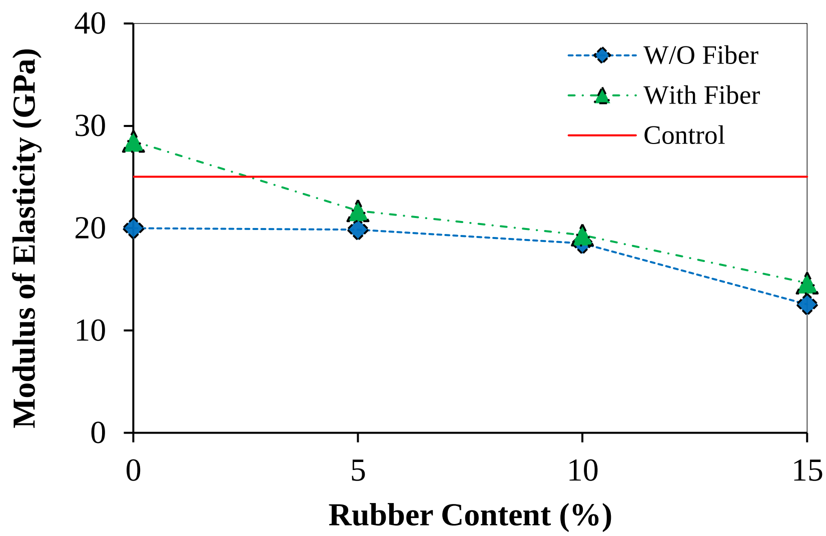

Figure 4.8 Modulus of Elasticity of different concrete batches.

4.3.5 Flexural Strength

The result of the quasi-static flexural strength is presented in Figure 4.9. Most of the concrete mixes show lower flexural strength than the control mix. The flexural strength is slightly decreased after incorporating RCA into the concrete mix by 0.5% ($R_0C_0F_0$ & $R_{30}C_0F_0$). With the incremental increases in CR replacement level, the flexural strength decreases. CR creates a weaker bond within the aggregate and cement paste, weakens the ITZ, and does not react uniformly with the matrix. The flexural strength is decreased by 14.1%, 20.5%, and 22.6% with the CR replacement level of 5%, 10%, and 15%, respectively. However, an increased flexural strength can be found after the inclusion of fiber in the concrete mixture. This occurs because fiber creates a good bridge between the aggregate and cement paste. After the beam was broken, it is seen that the bridging fibers are projecting outward and perpendicular to the cross-section. Approximately 8.6%, 16.0%, and 12.6% strength can be increased after adding 0.5% PP fiber. $R_{30}C_0F_{0.5}$ shows the highest flexural strength of 19.5% more than the control. As this is a fiber-reinforced concrete combination without any rubber particles, a strong bond is produced between aggregate and cement paste.

Figure 4.10 shows the load versus deflection responses at the mid-point of the different prism beams. From the figure, it is seen that the load-deflection curves R^2C and FR^3C beams are slightly different from the control one. The control specimen breaks suddenly and provides a lower deflection capacity in its plastic zone. On the contrary, load-deflection curves of R^2C and FR^3C specimens extend far beyond their plastic zone, thus providing a ductile behavior. However, this phenomenon is more prominent in FR^3C specimens compared to R^2C specimens. As fiber can form a bridge inside the densified concrete matrix on either side of the crack and can resist load against a larger deflection after it has reached its ultimate failure point. Thus, the load-deflection graph extends far beyond. Besides, fiber also creates a strong bond between aggregate and cement paste and acts as a barrier against crack propagation.

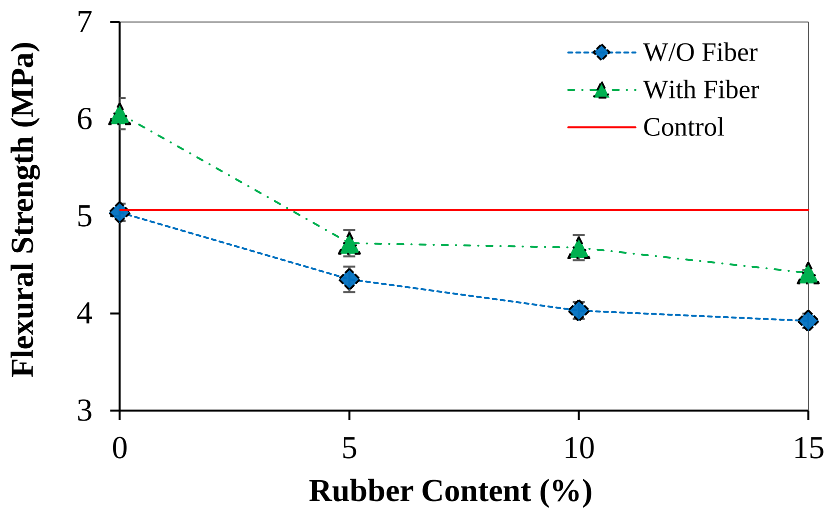

Figure 4.9 Flexural strength of different concrete batches.

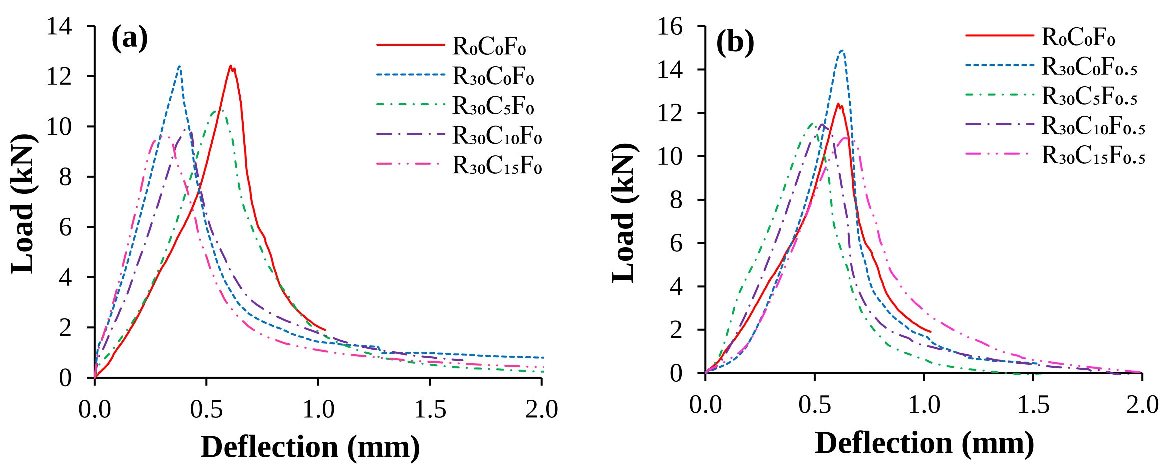

Figure 4.10 Load-deflection responses of different concrete beams under flexure test.

4.3.6 Hardened Density

Figure 4.11 compares the different concrete batches in terms of hardened concrete. Overall, it is observed that for all batches, the density is decreased compared to the control mixture. As the specific gravity of RCA, CR, and PP fiber is very low compared to NCA, NFA, and cement, they can produce a lower density concrete. The density increases with the maturity of concrete. When concrete is being cured, it assembles closer and the volume reduces as a result of the loss of water. Thus, the density increases. However, this incremental percentage is not significant. Approximately 1.5% and 0.5% density has been increased at 56 days compared to

7 days and 28 days. For the recycled aggregate concrete containing 0%, 5%, 10%, and 15% CR content, the density is decreased by 0.6%, 2.6%, 4.2%, and 8.1%, respectively at 56 days compared to control specimen. It is also found that the addition of PP fiber along with CR further reduces the concrete density. In that case, a reduction in density is 1.9%, 3.4%, 5.8%, and 8.7% observed, respectively. The same pattern is also observed at 7 days and 28 days. BN-5 ($R_{30}C_{15}F_0$) provides the lowest density among all R^2C specimens and BN-9 ($R_{30}C_{15}F_{0.5}$) is the lowest one among the FR^3C specimens.

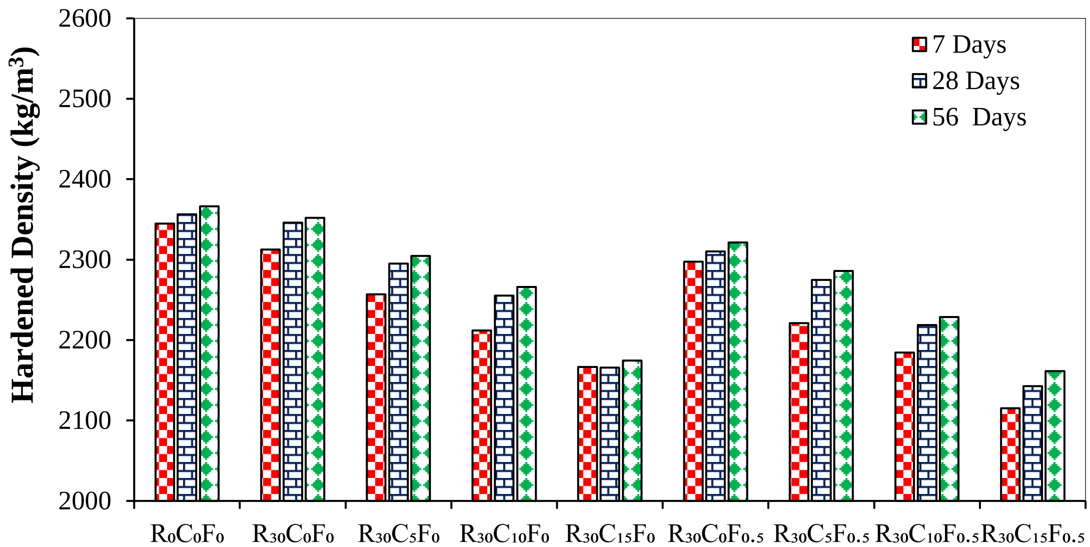

Figure 4.11 Hardened density of different concrete batches.

4.3.7 Ultrasonic Pulse Velocity

The ultrasonic pulse velocity (UPV) technique is used to examine the quality of concrete without any apparent damage to the concrete. Although there is no direct relationship exists between the compressive strength and the UPV value, the value of UPV is used for predicting the compressive strength [206].

Effect of Age on Ultrasonic Pulse Velocity

Figure 4.12 demonstrates the effect of age on UPV for various concrete batches. With increasing the maturity of concrete the UPV value increases. However, as noticed from the figure, the UPV values increase faster during the 7 to 28 days period. However, the incremental rate decreases with age until it levels off in later days. This phenomenon was also observed by Albano et al. [207]. As the hydration reaction is more prominent at the initial stage, more physical-chemical changes occur in the concrete at that stage. And with the increasing age, the hydration reaction occurs slowly, thus decreasing the propagation of pulse. Approximately 32% and 6% UPV value has been increased at 56 days compared to 7 days and 28 days.

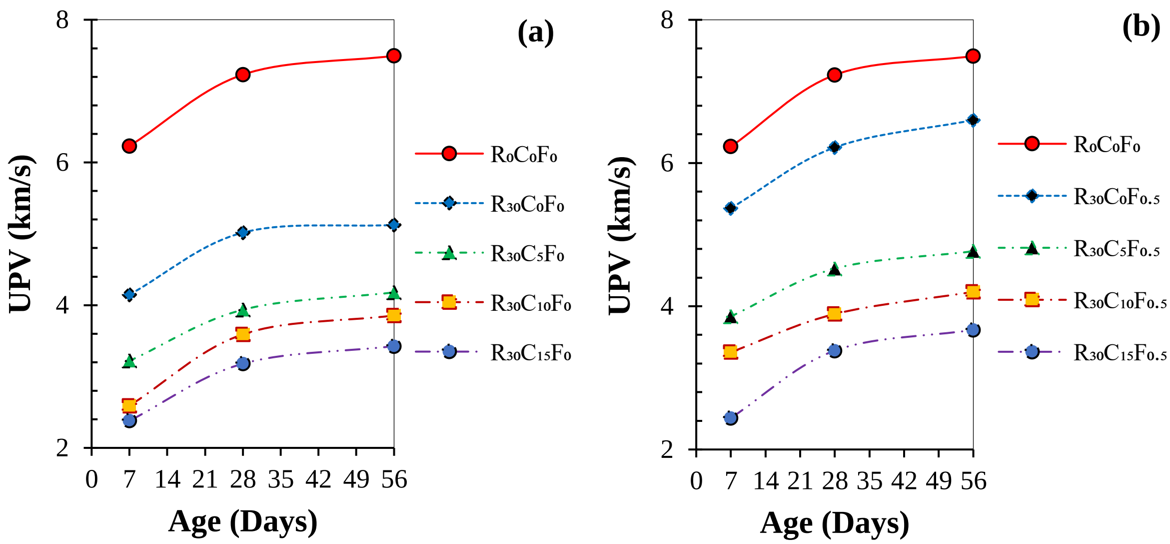

Figure 4.12 Variation in UPV values at different ages for different concrete batches: (a) without fiber and (b) with fiber.

Effect of Aggregate Type on Ultrasonic Pulse Velocity

Observing Figure 4.13 it is seen that all the combinations provide a lower UPV value than that of the control specimen. The inclusion of RCA, CR, and fiber reduces the UPV. According to Jones and Facaroau [208], the UPV is a function of elastic properties. When the wave passed through lower elastic materials, the UPV value decreased [207]. Thus, the UPV decreases for RAC, R^2C, and FR^3C due to their lower MoE and lower density. Besides, with increasing the CR content, the UPV decreases. The UPV is decreased by 31.6%, 42.2%, 48.6%, 54.3% and 11.9%, 36.4%, 43.9%, 51% containing 0%, 5%, 10%, and 15% CR content in R^2C and FR^3C specimens, respectively at 56 days. The UPV depends on the porosity, aggregate type, the density of the materials, etc. The surface of the CR particles is relatively smooth which does not provide significant frictional resistance between the aggregate particles, thus creates a higher void between the concrete mixes. Besides, the hydrophobic nature of CR increases the amount of water content and air voids in the concrete. These voids developed by the CR particles enfeeble the transmitted pulse because of the acoustic impedance.

However, the concrete containing fiber content provides a higher UPV value than that of specimens without any fiber. This is evident from the comparison between BN-2 ($R_{30}C_0F_0$), BN-6 ($R_{30}C_0F_{0.5}$); BN-3 ($R_{30}C_5F_0$), BN-7 ($R_{30}C_5F_{0.5}$), BN-4 ($R_{30}C_{10}F_0$), BN-8 ($R_{30}C_{10}F_{0.5}$), and BN-5 ($R_{30}C_{15}F_0$), BN-9 ($R_{30}C_{15}F_{0.5}$). Approximately 28.8%, 14.1%, 9.0%, and 7.1% UPV is increased by incorporating 0.5% PP fiber in R^2C mixtures with 0%, 5%, 10%, and 15% CR content, respectively at 56 days. As fiber reduces the air void into the concrete mixture the pulse velocity increases. Comparing BN-1 ($R_0C_0F_0$) and BN-2 ($R_{30}C_0F_0$) it is seen that at 56 days the RAC specimen exhibits approximately 31.6% lower UPV than that of the control due to the lower MoE and lower density of RAC.

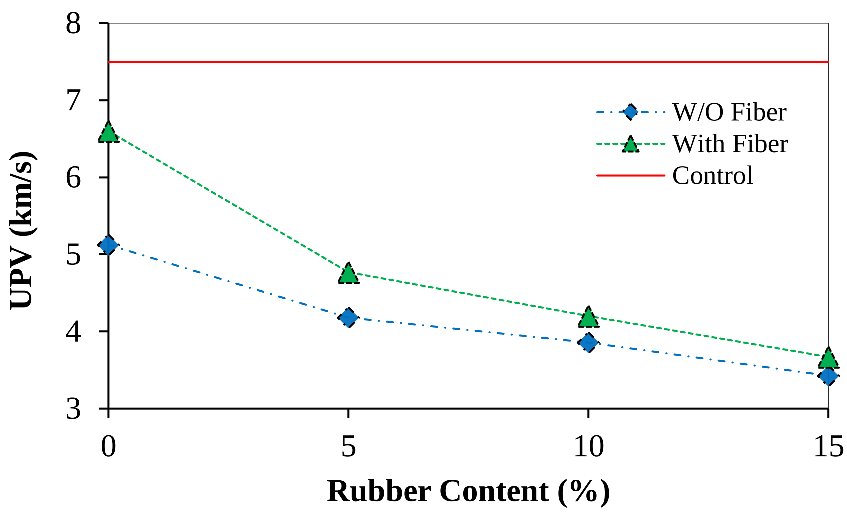

Figure 4.13 Effect of RCA, CR, and PP fiber on UPV at 56 days.

4.3.8 Surface Resistivity

The surface resistivity value of different concrete mixtures has been determined as per AASHTO TP 95 [201] and then correlated with the AASHTO TP 95 [201] guideline to get an idea about the chloride ion penetrability. Figure 4.14 presents the surface resistivity value of different concrete mixes. The result is consistent with the air content result. The inclusion of CR content into the concrete mixture increases the value of surface resistivity and it increases with increasing the percentage of CR content. The value is increased by 20.6%, 26.1%, 48.2%, 63.2% and 4.7%, 10.7%, 36.3%, 40.4% containing 0%, 5%, 10%, and 15% CR content in R^2C and FR^3C specimens, respectively. However, comparing the FR^3C specimens with R^2C specimens, the fiber-reinforced concrete provides a comparatively lower surface resistivity value. This is evident from the comparison between BN-2 ($R_{30}C_0F_0$), BN-6 ($R_{30}C_0F_{0.5}$); BN-3 ($R_{30}C_5F_0$), BN-7 ($R_{30}C_5F_{0.5}$), BN-4 ($R_{30}C_{10}F_0$), BN-8 ($R_{30}C_{10}F_{0.5}$), and BN-5 ($R_{30}C_{15}F_0$), BN-9 ($R_{30}C_{15}F_{0.5}$). Approximately 13.2%, 12.2%, 8.1%, and 14% value is decreased by incorporating 0.5% PP fiber in R^2C mixtures with 0%, 5%, 10%, and 15% CR content, respectively. Comparing BN-1 ($R_0C_0F_0$) and BN-2 ($R_{30}C_0F_0$) it is seen that the RAC specimen exhibits approximately 20.6% higher surface resistivity than that of the control one. Comparing the surface resistivity value with Table 4.3, the value for all combinations falls within the range of 37-254 kΩ.cm. Thus the chloride ion penetrability is assumed to be very low.

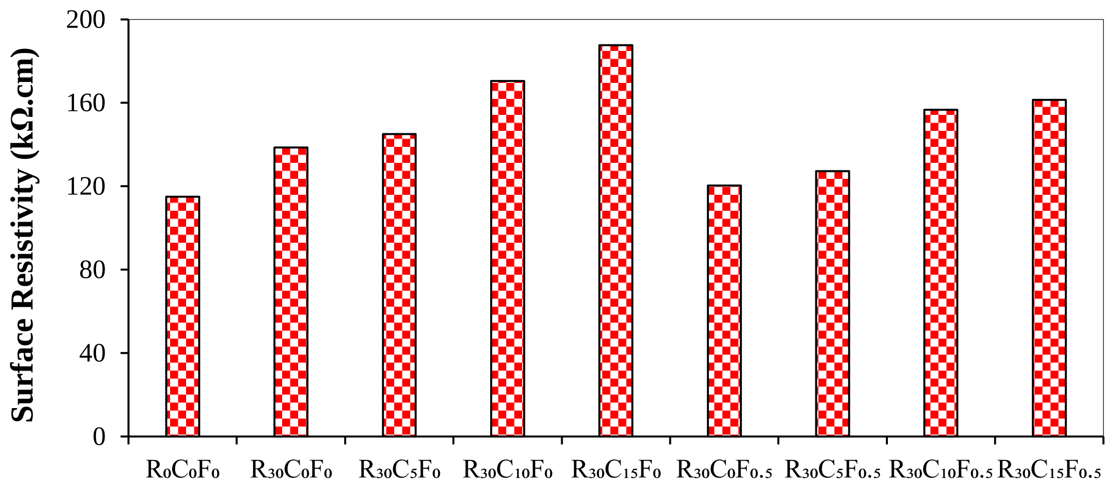

Figure 4.14 Surface resistivity of different concrete mixtures.

Table 4.3 Chloride ion penetrability classification as per AASHTO TP 95 [201].

Chloride Ion Penetrability	Specific Resistance (R) (kOhm-cm)
High	<12
Moderate	12-21
Low	21-37
Very Low	37-254
Negligible	>254

4.3.9 Failure Mode

The failure pattern of the concrete cylinder under the compression test is presented in Figure 4.15. Most of the rubberized recycled concrete (R^2C) cylinders showed shear failure whereas maximum fiber-reinforced rubberized recycled concrete (FR^3C) cylinders provided cone and shear failure. However, concrete cylinders with CR and fiber showed slow and gradual failure compared to the brittle failure of natural aggregate concrete (NAC) and recycled aggregate concrete (RAC). The failure of fiber-reinforced recycled concrete (FR^2C), R^2C, and FR^3C specimens were not as extensive as that of conventional concrete. The physical appearance of FR^3C specimens significantly differs from NAC, RAC, and R^2C samples. Several micro-cracks were observed on the surface of the FR^3C specimens as presented in Figure 4.15 (g-i). No visible macro-cracks were pointed out and provided no morphological change on the surface. On the contrary, the NAC, RAC, and R^2C specimens provide a number of macro-cracks.

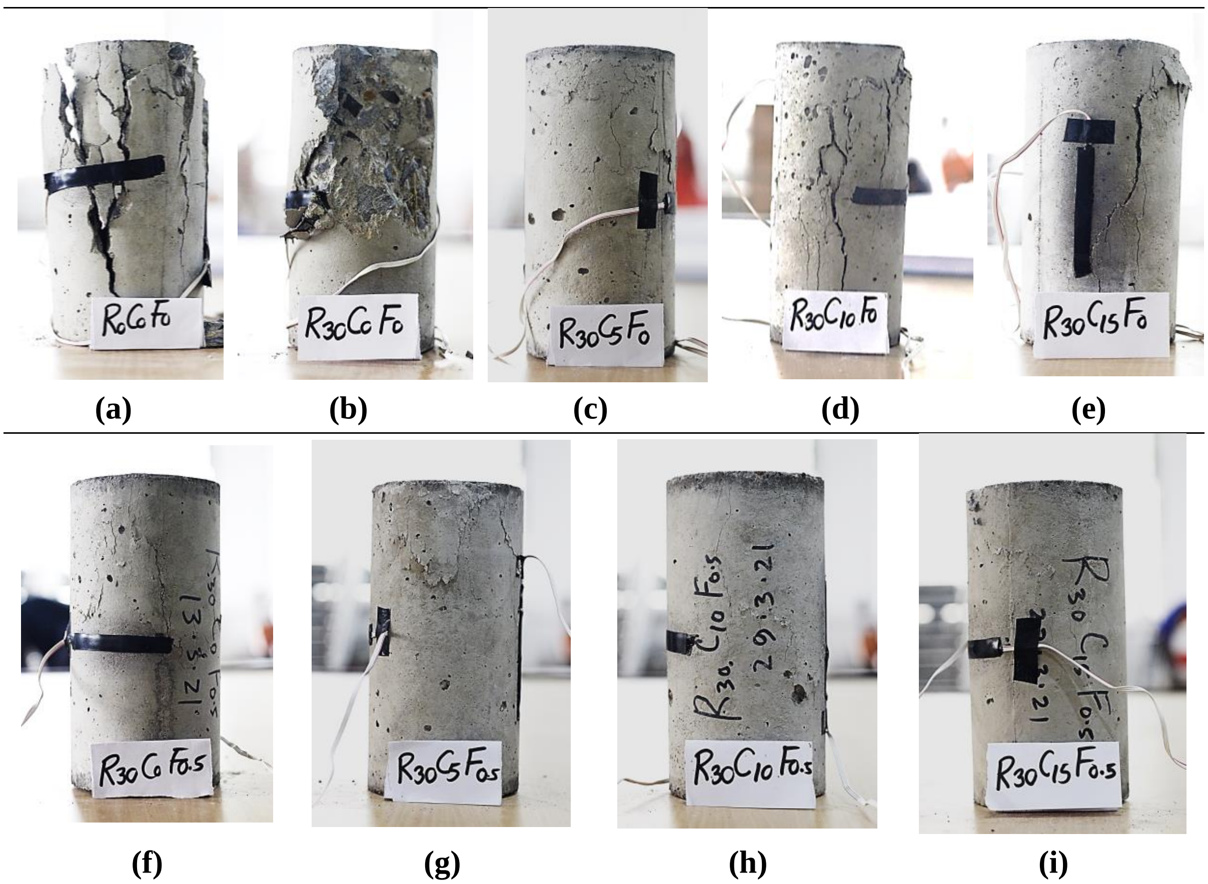

Figure 4.15 Failure pattern of the different concrete cylinders under compressive strength test at 56 days: (a) NAC, (b) RAC, (c-e) R^2C, (f) FR^2C, and (g-i) FR^3C.

The concrete cylinders are broken manually to examine the failure lines and the distribution of different aggregates. The failure lines propagate through the RCA and CR particles. The RCA particles contain attached mortar which weakens the ITZ and the CR particles are comparatively soft and relatively compressible compared to natural aggregates. Thus, when the cracks reach the tip of either RCA or CR, they can initially restrain due to higher strain capacity, and then the cracks are passed through them as shown in Figure 4.16 (a). On the other hand, fiber is too strong to prevent crack because it creates a strong bonding between aggregate and cement paste and holds the aggregate particle together to resist cracking (Figure 4.16 (b)).

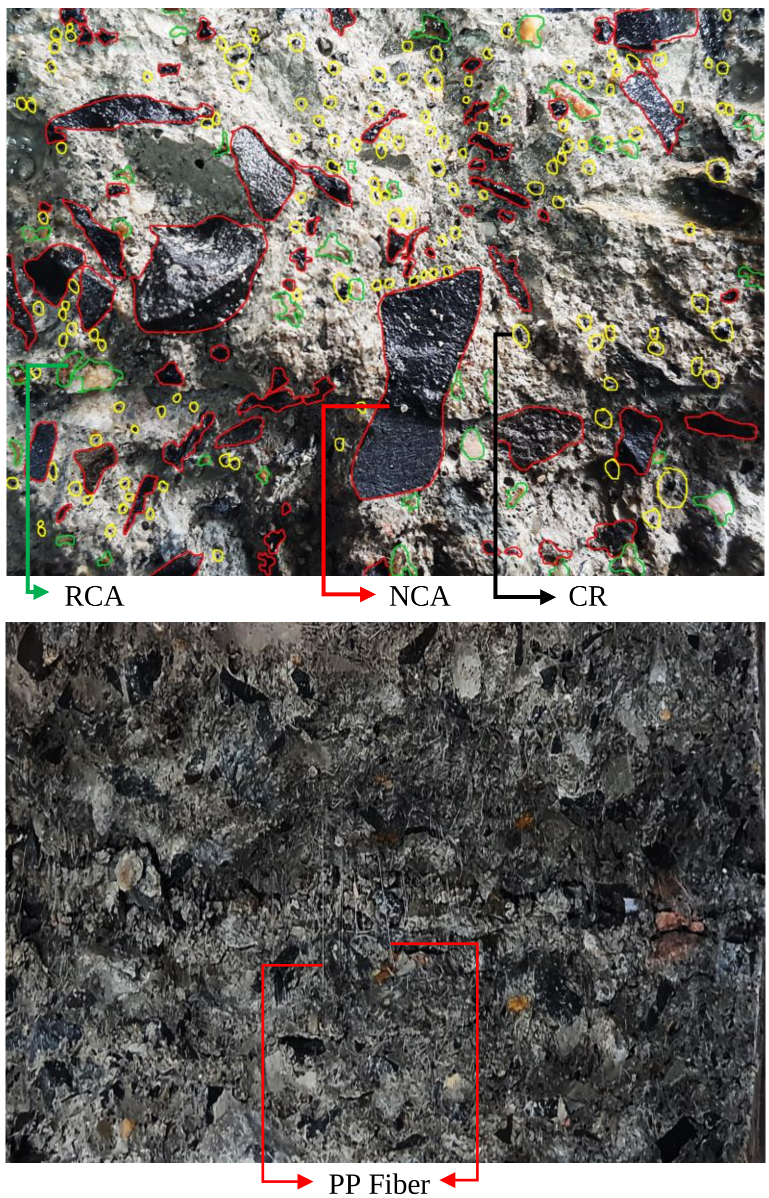

Figure 4.16 Inspection of RCA, CR, and PP fiber in the concrete.

Under the tensile strength test, the NCA, RAC and R^{2}C specimens failed suddenly whereas, in the FR^{3}C specimens, the fiber made a bridge between the aggregates and cement paste as presented in Figure 4.17 (e). Thus, the FR^{3}C specimens can take the additional load and resist more deformation. The failure pattern of the unreinforced concrete beams under the flexural strength test is presented in Figure 4.18. All the specimens provide flexural failure patterns. During the test, the control specimens suddenly split into two pieces. Thus, a sudden drop in the load-deflection curve is observed. However, the beams with CR and fiber, especially the fiber-reinforced beams didn't break completely upon reaching the maximum load and more ductile failure is observed. It can be concluded that concrete containing fiber is more ductile with higher toughness values compared to control concrete mixes. Later on, those beams are broken manually to examine the failure surfaces and found that the fibers are projecting outward & perpendicular to the cross-section as shown in Figure 4.18 (e).

(a) **(b)** **(c)** **(d)** **(e)**

Figure 4.17 Failure pattern of dog-bone specimens under direct tensile strength test: (a) NAC, (b) RAC, (c) R^{2}C, and (d-e) FR^{3}C.

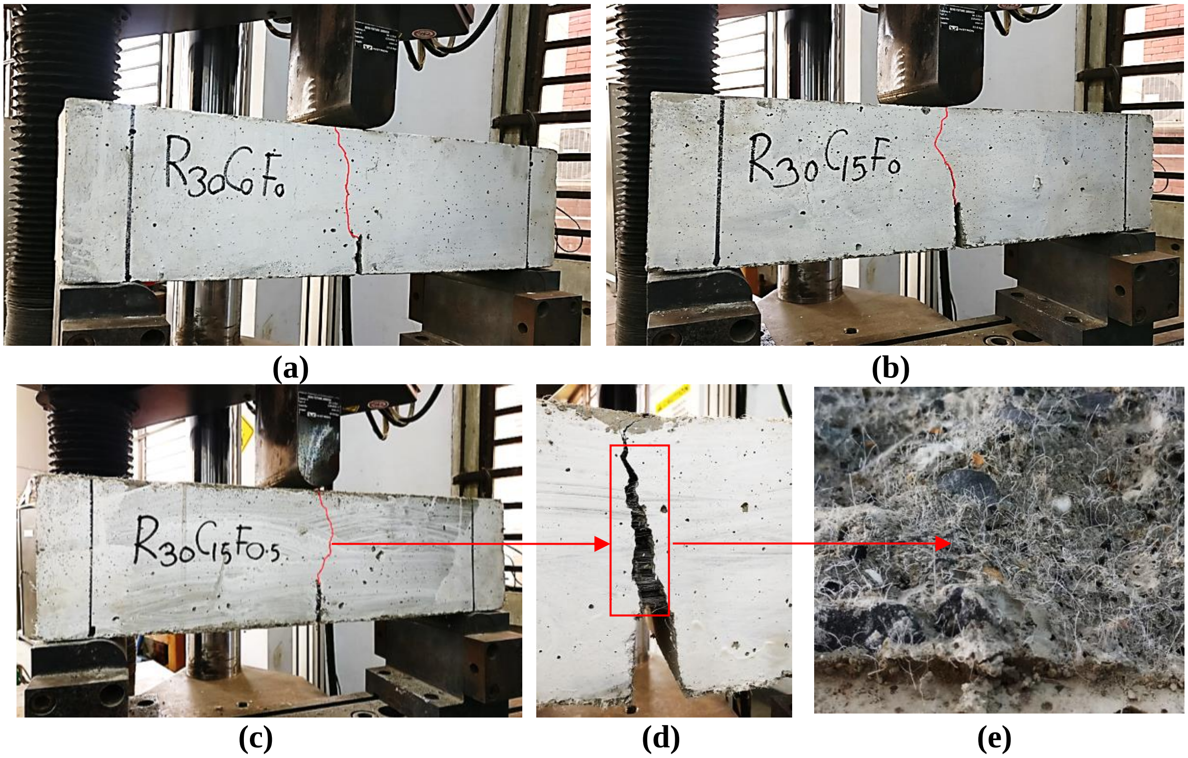

Figure 4.18 Failure pattern of the different concrete beams under flexural strength test: (a) RAC, (b) R^2C, and (c-e) FR^3C.

4.3.10 Prediction of Strength Equation using Regression Analysis

It is useful to have different empirical equations to predict various strengths of concrete. Though there are some available equations in various codes to predict different types of strength of concrete, none of them incorporate the effect of recycled aggregate like RCA and CR or any type of fiber. Using the experimental data regression analyses are performed and several equations are proposed to assess different mechanical properties of recycled concrete while considering the effect of CR and PP fiber.

Relationship Between Compressive and Tensile Strength

Analysis of experimental data reveals that the tensile strength mostly varied with the percentage of CR and inclusion of fiber content similar to the trend observed for the compressive strength. Therefore, an attempt is made to propose empirical equations to predict the tensile strength from the data of compressive strength while considering the effect of CR particles and fiber content. Two equations are developed for rubberized recycled concrete

(R^2C) without fiber (Eq. 4.1) and with fiber (Eq. 4.2) using multiple regression analyses of the experimental data.

Proposed Equation for RCA with CR (Without Fiber) : $f_{t,CR} = 0.51\sqrt{f_c{}'} - 0.0076CR$ (4.1)

Proposed Equation for RCA with CR (With Fiber) : $f_{t,CR.F} = 0.53\sqrt{f_c{}'} - 0.012CR$ (4.2)

ACI 318-14 [137] : $f_t = 0.556\sqrt{f_C'}$ (4.3)

fib2010 [143] : $f_t = 0.3(f_C')^{\frac{2}{3}}$ (4.4)

EC2 [209] : $f_t = 0.556\, \alpha_{sp}\sqrt{f_C'}$ (4.5)

where f_t = tensile strength in MPa, f_C' = compressive strength of concrete in MPa, α_{sp} = 0.9, and CR is the volumetric percentage of crumb rubber.

The experimental results are compared with the proposed equations and available design guidelines such as ACI 318-14, fib2010, and EC2 as presented in Eq. 4.3 – Eq. 4.5. It is to be noted that the reported equations (Eq. 4.1 and Eq. 4.2) are valid only for the prediction of tensile strength for R^2C and FR^3C within the range of CR between 0% to 15% and a constant RCA percentage (30%) and PP fiber content (0.5%). From Figure 4.19 it is seen that, though EC2 can predict the tensile strength with a low deviation, ACI 318 and fib2010 overestimate (theoretical vs experimental ratio is greater than 1) it by approximately 10%. However, the proposed equations can predict the tensile strength of R^2C and FR^3C more accurately. A good correlation is found between the experimental data and proposed equations, where the coefficients of determination (R^2) are 0.991 and 0.997 for R^2C and FR^3C, respectively.

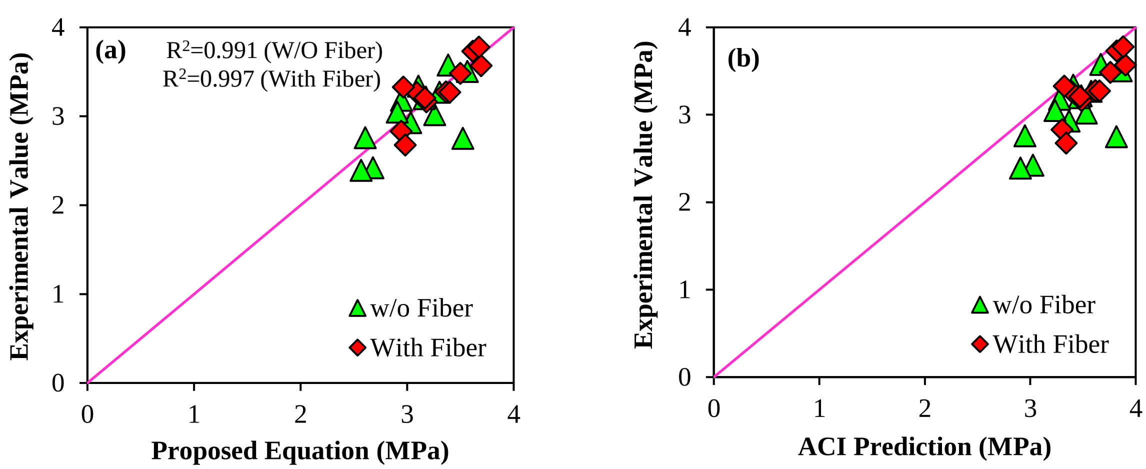

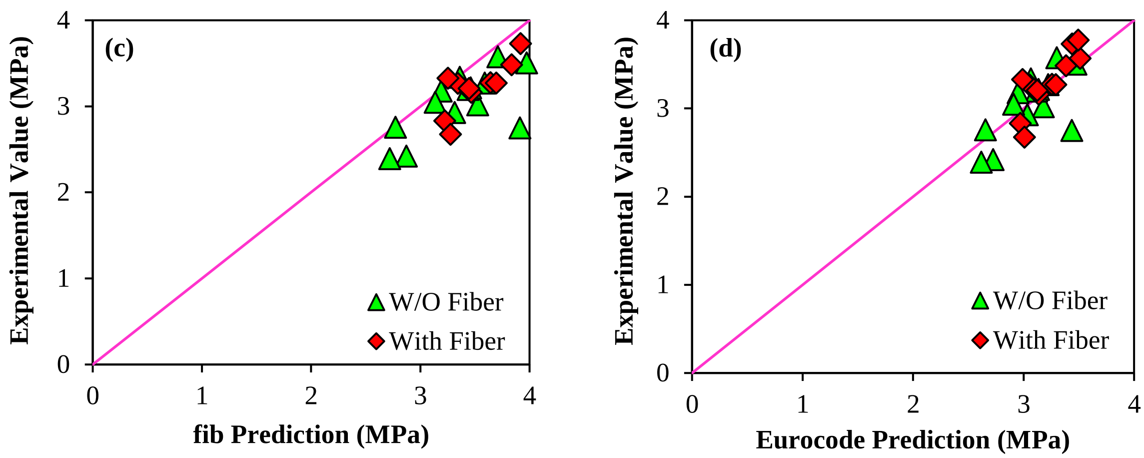

Figure 4.19 Comparison of experimental tensile strength with (a) proposed model, (b) ACI 318-14, (c) fib, and (d) EC2.

Relationship Between Compressive and Flexural Strength

The flexural strength also depends on the percentage of CR and the inclusion of fiber content like tensile strength. Thus, using the multiple regression analysis two equations are proposed for R^2C and FR^3C (Eq. 4.6 and Eq. 4.7), where the flexural strength is a function of compressive strength and CR percentage. The equations are valid for the range of CR content from 0% to 15% and for a constant RCA percentage (30%) and PP fiber content (0.5%). Figure 4.20 provides the comparison between the experimental data and forecasted values of flexural strength. As shown in the figures, the ACI 318 and CSA A23.3 underestimate (theoretical vs experimental ratio is less than 1) it by approximately 20% whereas the fib2010 overestimates it by approximately 12%. The proposed equations can predict the flexural strength more accurately. Good correlations are found with coefficients of determination (R^2) of 0.998 and 0.995 for R^2C and FR^3C, respectively.

Proposed Equation for RCA with CR (Without Fiber) : $f_{r,CR} = 0.74\sqrt{f_c{}'} - 0.015CR$ (4.6)

Proposed Equation for RCA with CR (With Fiber) : $f_{r,CR.F} = 0.82\sqrt{f_c{}'} - 0.044CR$ (4.7)

ACI 318-14 [137] : $f_r = 0.62\sqrt{f_c'}$ (4.8)

fib2010 [143] : $f_r = \frac{0.3((f_c')^{\frac{2}{3}})}{\alpha_{fl}}$ (4.9)

CSA A23.3-14[140] : $f_r = 0.6\lambda\sqrt{f_c'}$ (4.10) where f_r = flexural strength in MPa, f_c' = compressive strength of concrete in MPa, α_{fl} = $\frac{0.06h_b^{0.7}}{1+0.06h_b^{0.7}}$, h_b = beam depth in mm, λ = *1.0* for regular density concrete, and CR is the volumetric percentage of crumb rubber.

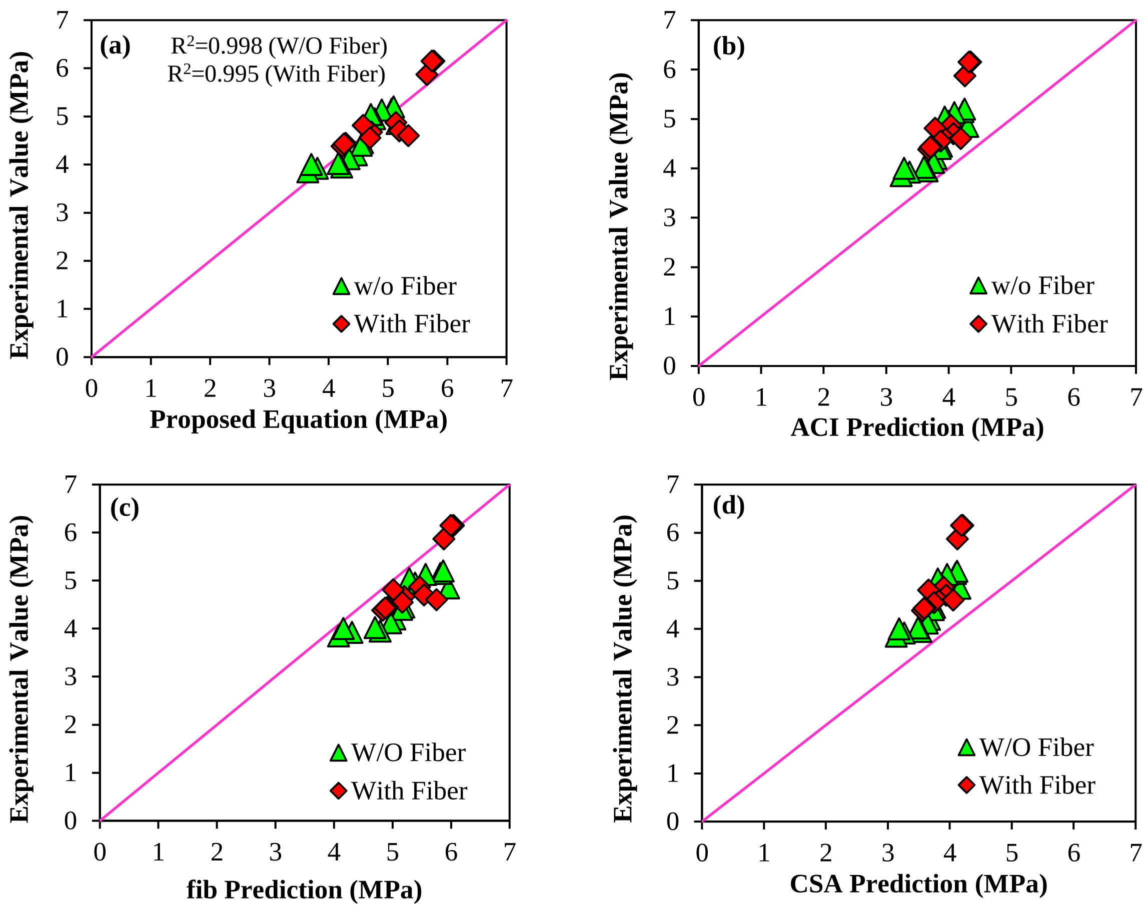

Figure 4.20 Comparison of experimental flexural strength with (a) proposed model, (b) ACI 318-14, (c) fib, and (d) CSA.

Relationship Between Compressive Strength and Modulus of Elasticity

The MoE not only depends on the CR and fiber content but also depends on the density of concrete. Incorporating this issue, a linear relationship is being made among the MoE, the compressive strength, the percentage of CR, and the density of concrete. Two proposed equations for R^2C and FR^3C are presented in Eq. 4.11 and Eq. 4.12. Figure 4.21 presents the comparison between the tested and predicted values of MoE. It is seen that all the available code equations overestimate the MoE of R^2C and FR^3C significantly (approximately 50%).

The proposed equations can predict the MoE with the R^2 value of 0.999 and 0.998 for R^2C and FR^3C, respectively.

Proposed Equation for RCA with CR (Without Fiber) : $E_{CR} = 13.7\sqrt{f_c'} - \left(\frac{w_c}{140}\right)^{1.5} + 0.076CR$ (4.11)

Proposed Equation for RCA with CR (With Fiber : $E_{CR.F} = 5.7\sqrt{f_c'} - \left(\frac{w_c}{455}\right)^{1.5} - 0.58CR$ (4.12)

ACI 318-14 [137] : $E = w_c^{1.5}\, 0.043\sqrt{f_c'}$ (4.13)

fib2010 [143] : $E = E_0\, \alpha_E \left(\frac{f_c}{10}\right)^{\frac{1}{3}}$ (4.14)

CSA A23.3-14[140] : $E = (3300\sqrt{f_c'} + 6900)\left(\frac{w_c}{2300}\right)^{1.5}$ (4.15)

where E = modulus of elasticity in GPa, w_c = density of concrete ranges from 1440 kg/m^3 to 2560 kg/m^3 for ACI 318-14 and 1500 kg/m^3 to 2500 kg/m^3 for CSA A23.3-14, f_c' = compressive strength of concrete in MPa, $E_0\, \alpha_E$ is 21500 MPa, and CR is the volumetric percentage of crumb rubber.

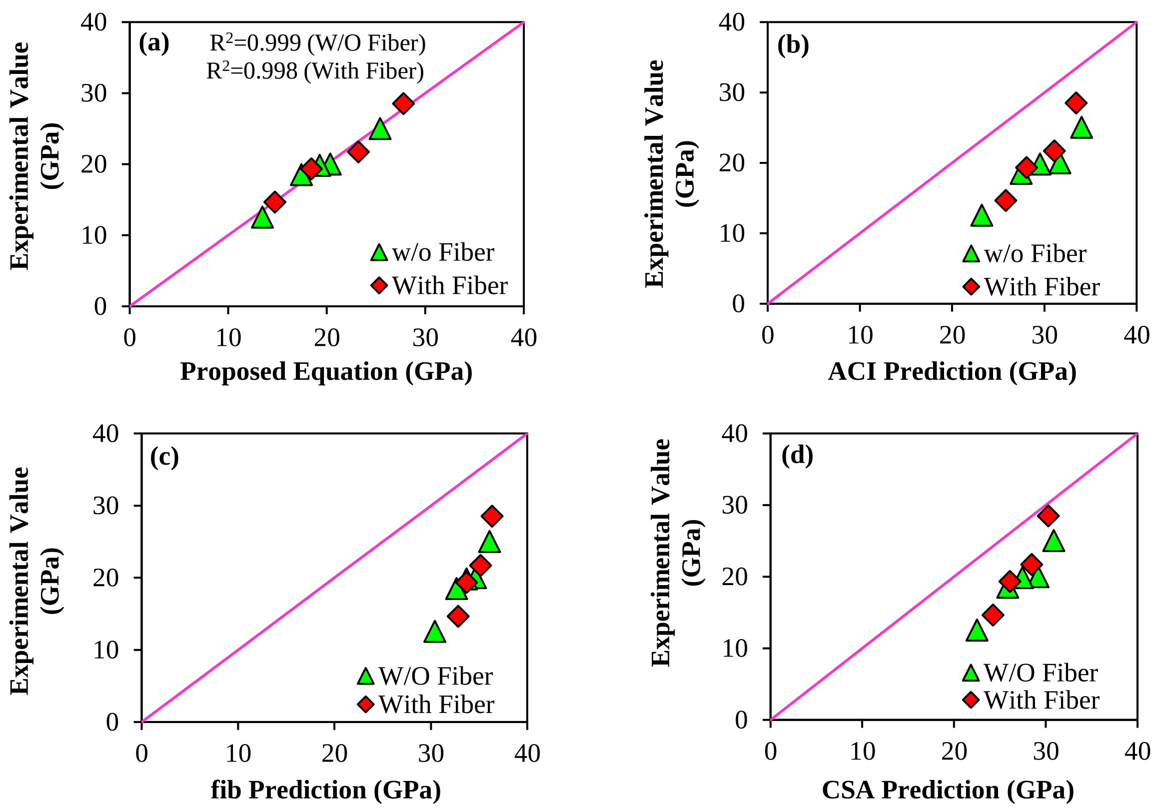

Figure 4.21 Comparison of experimental MoE with (a) proposed model, (b) ACI 318-14, (c) fib, and (d) CSA.

Prediction of Compressive Strength from Ultrasonic Pulse Velocity

The UPV depends on the porosity in concrete, elastic properties of the medium, size of ingredients, and the density of the materials. Considering that the compressive strength of R^2C and FR^3C can be predicted from the UPV, percentage of CR, and the density of concrete without any destructive testing. Most of the previous studies expressed the compressive strength of concrete as an exponential function of UPV [210-212]. Eq.16 and Eq. 4.17 have been proposed to predict the compressive strength of R^2C and FR^3C, respectively considering the UPV as an exponential function, concrete density, and the percentage of CR content. The R^2 value of the proposed equations is 0.998 and 0.996, respectively. It should be noted that the equations are valid for the range of CR content from 0% to 15% and for a constant RCA percentage (30%) and PP fiber content (0.5%).

Proposed Equation for RCA with CR (Without Fiber) : $f_c{'}_{CR} = 0.30e^V + \frac{wc}{122} + 0.042CR$ (4.16)

Proposed Equation for RCA with CR (With Fiber) : $f_c{'}_{CR.F} = 0.024e^V + \frac{wc}{58} - 0.34CR$ (4.17)

where f_C' = compressive strength of concrete in MPa, V = ultrasonic pulse velocity (UPV) in km/s, w_c = density of concrete in kg/m^3, and CR is the volumetric percentage of crumb rubber.

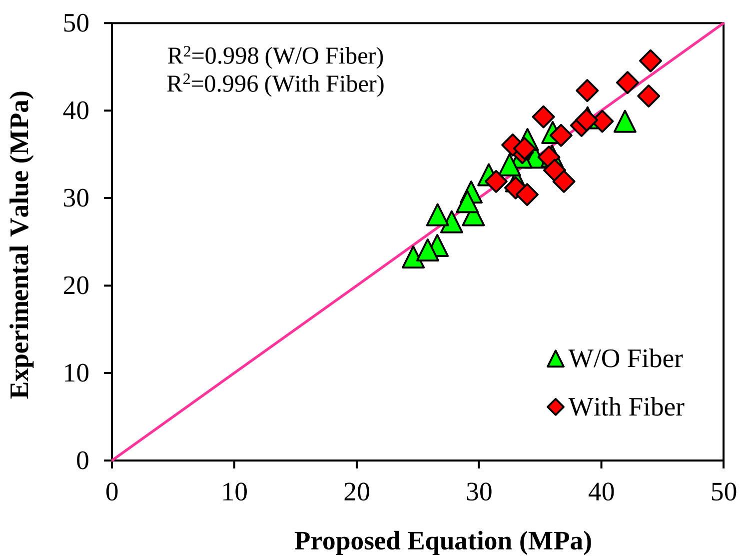

Figure 4.22 Comparison of compressive strength between experimental and regression models for R^2C and FR^3C.

Eq. 4.18 – Eq. 4.23 are used for determining statistical parameters for the proposed equations and Table 4.4 summarizes the statistical parameters of the proposed equations.

Performance factor, $PF = \frac{f_{exp}}{f_{pre}}$ (4.18)

Coefficient of Variation, $COV\ (\%) = \frac{f_{std\_PF}}{f_{avg\_PF}} \times 100$ (4.19)

$\text{Covariance} = \frac{\Sigma(f_{exp} - f_{exp\ \_avg}) \times (f_{pre} - f_{pre\_avg})}{n-1}$ (4.20)

Mean Absolute Error, $MAE = \frac{1}{n}\Sigma\left|f_{pre} - f_{exp}\right|$ (4.21)

Average Absolute Percentage Error, $AAPE = = \frac{1}{n}\Sigma\left|\frac{f_{exp} - f_{pre}}{f_{exp}}\right|$ (4.22)

Root Mean Squared Error, $RMSE = \sqrt{\frac{\Sigma((f_{exp} - f_{pre})^2}{n}}$ (4.23)

Table 4.4 Statistical parameters of the proposed equations.

Proposed Equation	Aggregate Type	Variables	PF				MAE	AAPE	RMSE	R^2
			Avg. PF	Std. PF	COV (%)	Covariance				
Tensile Strength	RCA, CR	f_c' and CR	1.00	0.09	9.32	0.10	0.22	0.07	0.30	0.991
	RCA, CR, Fiber		1.00	0.06	5.68	0.05	0.13	0.04	0.17	0.997
Flexural Strength	RCA, CR	f_c' and CR	1.00	0.05	5.07	0.23	0.20	0.05	0.22	0.998
	RCA, CR, Fiber		1.00	0.07	6.70	0.19	0.28	0.06	0.34	0.995
Modulus of Elasticity	RCA, CR	$f_{c'}$, Density, and CR	1.00	0.05	4.95	19.17	0.66	0.04	0.72	0.999
	RCA, CR, Fiber		1.00	0.05	4.95	32.21	0.81	0.04	0.95	0.998
Compressive Strength	RCA, CR	UPV, Density, and CR	1.00	0.05	5.08	22.54	1.38	30.70	1.57	0.998
	RCA, CR, Fiber		1.00	0.07	6.98	13.79	2.01	35.98	2.44	0.996

4.4 Cost Analysis

A cost-sensitivity analysis is carried out for R^2C and FR^3C mixtures to identify whether these new types of concrete are cost-effective or not. The cost and emission rate analysis are estimated based on a square column with a 15 cm width. The main variables in cost analysis are NCA, RCA, NFA, CR, and PP fiber. The prices of cement remain the same in all combinations. The cost of water is neglected for this comparison purpose. Besides, as RCA and CR is waste material, it is free of charge. Only the transportation and preparation cost is considered. As the PP fiber is not locally produced in Bangladesh, the fiber is imported from abroad. The cost of PP fiber is approximate US$12/kg. A 10% operation cost and 15% profit are considered from the total cost of all ingredients of the control mix.

The net present value (NPV) is calculated to determine the optimum mix design of all mixes based on initial cost and thermal resistance. The empirical equation (Eq. 4.24) proposed by Marie [84] is adopted to determine the thermal conductivity (λ) of different rubberized concrete mixtures. Then the thermal resistance (R) of the column per m^2 is calculated using Eq. 4.25 [213].

$$\lambda = 0.0733e^{0.0011w_c} \tag{4.24}$$

$$R = \frac{L}{\lambda} \tag{4.25}$$

Here λ is the thermal conductivity in W/m.K, w_c is the density of concrete in kg/m^3, R is the thermal resistance in m^2.K/W, and L is the width of the column in meter.

The electrical energy cost is calculated to determine the payback period and net present value using Eq. 4.26 to Eq. 4.30 adopted from Al-Osta et al. [213]. The energy consumed by air-conditioning (E) can be calculated as follows:

$$\mathrm{E} = \frac{0.024 \times D}{R \times C} \tag{4.26}$$

Here E is the energy consumed by air-conditioning in kWh/m^2, D is the degree-days (D was taken as 1431K for the study location of Dhaka city of Bangladesh), R is the thermal resistance of concrete in m^2.K/W, and C is an air-conditioning thermal efficiency coefficient (C = 2.16 adopted from Al-Osta et al. [213]).

Then the estimated energy is converted to energy costs (*EC*) which is estimated as follows:

$$EC = ET \times E \tag{4.27}$$

Here, *ET* is the energy tariff of the electricity in \$/kWh (1kWh =0.105\$ for Bangladesh), and E is the annual air conditioning system energy usage (kWh/m^2).

The payback period is determined by dividing the increased concrete cost by annual energy saving. Finally, the overall cost for a 15 cm wide concrete column per annum, involving initial and operating costs per m^2 is determined as follows:

$$NPV = PWF \times EC + BC \tag{4.28}$$

$$PWF = \frac{1}{i-e}\left(1 - \left(\frac{1+e}{1+i}\right)^n\right) \text{ for } e \neq i \tag{4.29}$$

$$PWF = n\,(i + e) \text{ for } e = i \tag{4.30}$$

Here, *PWF* (dimensionless) is the present worth factor, *BC* is the concrete column price per m^2 (\$/m^2), i = 2.5% (interest rate), e = 2% (energy inflation rate), and n = 30 years (concrete lifetime) is considered for calculating the NPV.

The cost analysis for one square meter of a column with different batches is summarized in Tables 4.5 and Table 4.6. Besides, the comparison of the total cost of 1 m^3 concrete for different mixtures is presented in Figure 4.23. It is observed that the inclusion of both CR and fiber increases the cost of concrete. The preparation cost of CR is comparatively high for manufacturing a small quantity. However, it is expected that for producing a bulk amount of CR, this cost will be decreased. Besides, the cost of PP fiber is much higher compared to other materials. Thus, the FR^{3}C mixtures provide a higher cost. Though the FR^{3}C mixtures exhibit higher costs, they can be more effective in terms of energy saving.

The annual energy cost for FR^{3}C mixtures varies from 8.79 \$/m^2 to 10.49 \$/m^2 whereas for R^{2}C mixtures it varies from 8.92 \$/m^2 to 10.84 \$/m^2. The FR^{3}C mixtures can save more energy compared to R^{2}C mixtures as presented in Figure 4.24 (a). Approximately 207.4%, 28.9%, 34.8%, 6.2% cost of energy can be saved by incorporating 0.5% PP fiber in R^{2}C mixtures with 0%, 5%, 10%, and 15% CR content, respectively. The cost associated with energy-saving is increased with increasing the percentage of CR content. The recycled concrete containing only

0%, 5%, 10%, and 15% CR content can save 0.17 $\$/m^2$, 0.72 $\$/m^2$, 1.15 $\$/m^2$, 2.09 $\$/m^2$ energy and the recycled concrete containing fiber can save 0.53 $\$/m^2$, 0.93 $\$/m^2$, 1.55 $\$/m^2$, 2.22 $\$/m^2$ energy, respectively. As FR^3C mixtures provide higher cost, a payback period of approximately 45 years, 26 years, 16 years, and 11 years is estimated for FR^3C mixtures containing 0%, 5%, 10%, and 15% CR content. On the contrary, no payback period may require for RAC as well as R^2C mixture containing 5% CR content. The NPV for R^2C mixtures varies from 260.49 $\$/m^2$ to 311.38 $\$/m^2$ whereas for FR^3C mixtures it varies from 265.11 $\$/m^2$ to 309.85 $\$/m^2$. From Figure 4.24 and Table 4.7, it is seen that with increasing the CR content the NPV decreases. Approximately 1.8%, 6.3%, 9.8%, 17.8% and 2.2%, 5.5%, 10.7%, 16.4% NPV is decreased with 0%, 5%, 10%, 15% CR content in R^2C and FR^3C mixtures, respectively. However, the difference in NVP between R^2C mixtures and FR^3C mixtures having a fixed amount of CR content is insignificant.

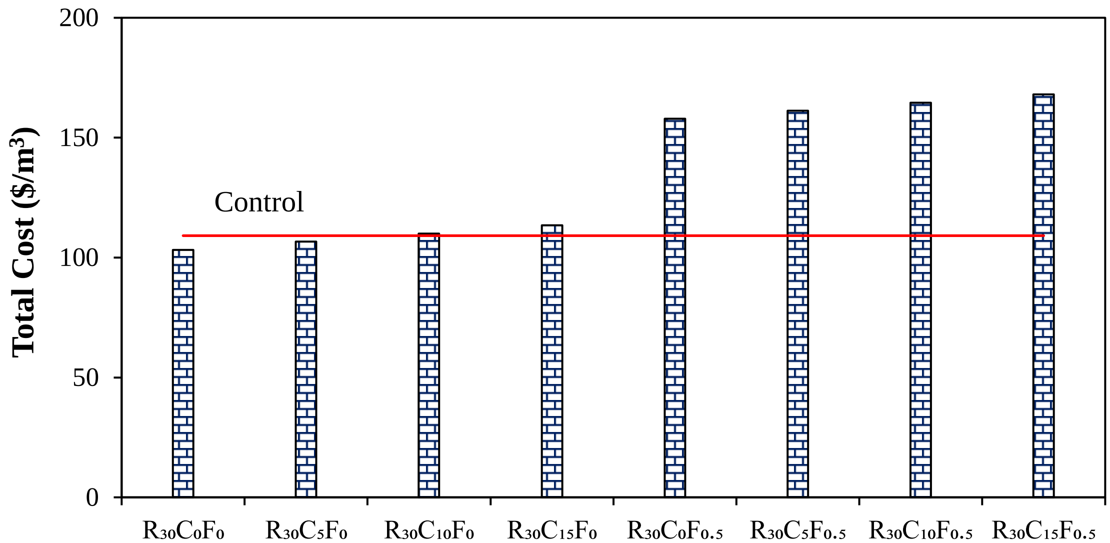

Figure 4.23 Comparison of the total cost of 1 m^3 concrete for different mixtures.

Table 4.5 Cost analysis for rubberized recycled concrete (R^2C).

Materials		$R_0C_0F_0$		$R_{30}C_0F_0$		$R_{30}C_5F_0$		$R_{30}C_{10}F_0$		$R_{30}C_{15}F_0$	
Units	$/kg	kg/m^3	$/m^3	kg/m^3	$/m^3	kg/m^3	$/m^3	kg/m^3	$/m^3	kg/m^3	$/m^3
Cement	0.108	456.0	49.25	456.0	49.25	456.0	49.25	456.0	49.25	456.0	49.25
Water	0.000	205.0	0.00	205.0	0.00	205.0	0.00	205.0	0.00	205.0	0.00
NCA	0.030	979.6	29.55	685.7	20.68	685.7	20.68	685.7	20.68	685.7	20.68
RCA	0.010	0.0	0.00	293.9	2.98	293.9	2.98	293.9	2.98	293.9	2.98
NFA	0.012	731.4	8.51	731.4	8.51	694.8	8.08	658.3	7.66	621.7	7.23
CR	0.240	0.0	0.00	0.0	0.00	15.9	3.82	31.8	7.63	47.7	11.45
PP Fiber	12.0	0.00	0.00	0.00	0.00	0.00	0.00	0.00	0.00	0.00	0.00
∑		2372	87.30	2372	81.42	2351	84.81	2331	88.20	2310	91.59
[a]Operation Cost/m^3 ($)		8.73		8.73		8.73		8.73		8.73	
[a]Profit ($)		13.10		13.10		13.10		13.10		13.10	
Total Cost ($/m^3)		109.13		103.24		106.63		110.02		113.41	
Compressive Strength at 56 days (MPa)		47.27		41.73		38.50		35.07		28.33	
Economy Index (Strength/Cost)		0.433		0.404		0.361		0.319		0.250	
[b]Cost of a Column with 15 cm Width ($/m^2)		16.37		15.49		15.99		16.50		17.01	

Table 4.6 Cost analysis for fiber-reinforced rubberized recycled concrete (FR^3C).

Materials		$R_0C_0F_0$		$R_{30}C_0F_{0.5}$		$R_{30}C_5F_{0.5}$		$R_{30}C_{10}F_{0.5}$		$R_{30}C_{15}F_{0.5}$	
Units	$/kg	kg/m^3	$/m^3	kg/m^3	$/m^3	kg/m^3	$/m^3	kg/m^3	$/m^3	kg/m^3	$/m^3
Cement	0.108	456.0	49.25	456.0	49.25	456.0	49.25	456.0	49.25	456.0	49.25
Water	0.000	205.0	0.00	205.0	0.00	205.0	0.00	205.0	0.00	205.0	0.00
NCA	0.030	979.6	29.55	685.7	20.68	685.7	20.68	685.7	20.68	685.7	20.68
RCA	0.010	0.0	0.00	293.9	2.98	293.9	2.98	293.9	2.98	293.9	2.98
NFA	0.012	731.4	8.51	731.4	8.51	694.8	8.08	658.3	7.66	621.7	7.23
CR	0.240	0.0	0.00	0.0	0.00	15.9	3.82	31.8	7.63	47.7	11.45
PP Fiber	12.0	0.00	0.00	4.55	54.60	4.55	54.60	4.55	54.60	4.55	54.60
∑		2372	87.30	2377	136.02	2356	139.41	2335	142.8	2315	146.2
[a]Operation Cost/m^3 ($)		8.73		8.73		8.73		8.73		8.73	
[a]Profit ($)		13.10		13.10		13.10		13.10		13.10	
Total Cost ($/m^3)		109.13		157.84		161.23		164.62		168.01	
Compressive Strength at 56 days (MPa)		47.27		48.37		43.73		38.48		35.67	
Economy Index (Strength/Cost)		0.433		0.306		0.271		0.234		0.212	
[b]Cost of a Column with 15 cm Width ($/m^2)		16.37		23.68		24.18		24.69		25.20	

Note:

[a] Operating cost/m^3 and Profit were considered 10% and 15% from the total cost of all components in the control mixture. Thus, these values were fixed and used for other mixes.

[b] The cost and emission rate analysis were estimated based on a 15 cm wide square column.

All the materials were collected from a local market, from December 2020 to March 2021, using local currency (BDT). For the analysis purpose, the local currency was converted to USD, as 1 BDT = 0.012 USD.

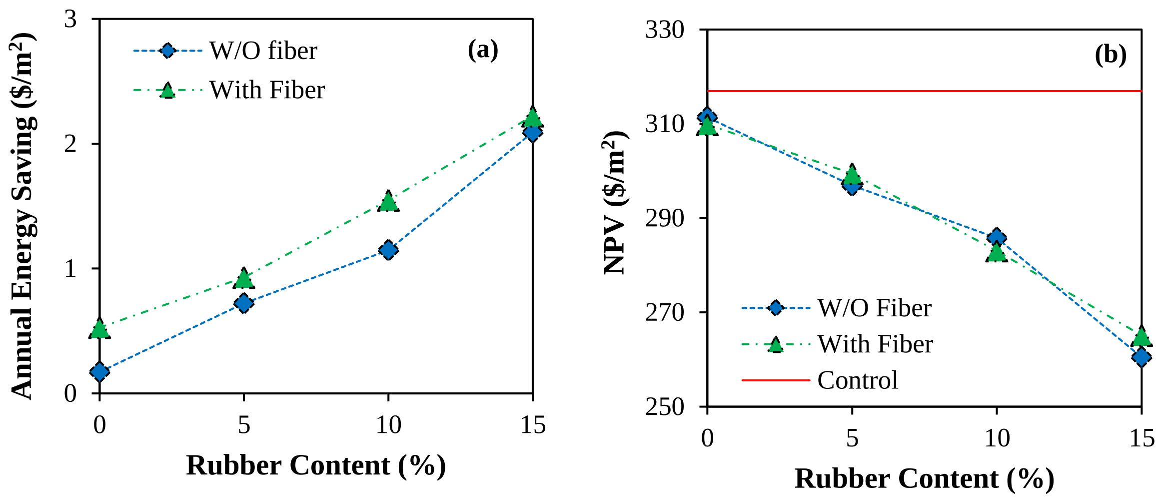

Figure 4.24 Comparison between R^2C mixtures and FR^3C mixtures in terms of (a) annual energy saving, and (b) NPV.

Table 4.7 Economic analysis for different batches of concrete.

Sample Type	Density at 56 days (kg/m³)	Thermal Conductivity (λ) (W/m.K)	Thermal Resistance (R) (m².K/W)	Annual Energy (E) (kWh/m²)	Annual Energy Cost (EC) ($/m²)	[a]Annual Energy Saving ($/m²)	Concrete Cost (BC) ($/m²)	[a]Increase in Concrete Cost ($/m²)	Simple Payback Period (yr)	[b]NPV ($/m²) (n=30 yrs)
$R_0C_0F_0$	2366	0.99	0.152	104.90	11.01	0.00	16.37	0.00	0.00	316.95
$R_{30}C_0F_0$	2352	0.97	0.154	103.26	10.84	0.17	15.49	0.00	0.00	311.38
$R_{30}C_5F_0$	2305	0.92	0.162	98.04	10.29	0.72	15.99	0.00	0.00	296.90
$R_{30}C_{10}F_0$	2266	0.89	0.169	93.96	9.87	1.15	16.50	16.50	14.37	285.75
$R_{30}C_{15}F_0$	2175	0.80	0.187	84.97	8.92	2.09	17.01	17.01	8.13	260.49
$R_{30}C_0F_{0.5}$	2321	0.94	0.159	99.87	10.49	0.53	23.68	23.68	44.84	309.85
$R_{30}C_5F_{0.5}$	2286	0.91	0.166	96.05	10.09	0.93	24.18	24.18	26.03	299.41
$R_{30}C_{10}F_{0.5}$	2229	0.85	0.176	90.16	9.47	1.55	24.69	24.69	15.96	283.04
$R_{30}C_{15}F_{0.5}$	2161	0.79	0.190	83.73	8.79	2.22	25.20	25.20	11.34	265.11

Note:

[a] Energy saving and increase in concrete cost were acquired with respect to the control mixture. The cost of electricity is 0.105 $/kWh.

[b] NPV = Net present value was examined over 30 years with discount rate and energy inflation rate equal to i = 2.5% and e = 2%, respectively.

Cost and energy values were also standardized to a 15 cm wide square column.

4.5 Emissions of Fuel Consumption

Increasing the thermal resistance of any structural element can minimize heat transfer, minimizing fuel consumption and air pollution. The present study evaluates the fuel consumption (m_{fA}) and the emission combustion rate of CO_2 (M_{CO_2}) and SO_2 (M_{SO_2}). The equations for calculating the m_{fA}, M_{CO_2}, and M_{SO_2} are adopted from Yildiz et al. [214] and Al-Osta et al. [213] (Eq. 4.31 to Eq. 4.40).

$$C_aH_bO_dS_eN_f + \alpha.X.(O_2 + 3.76N_2) \rightarrow a.co_2 + \left(\frac{b}{2}\right).H_2O + Y.O_2 + e.SO_2 + ZN_2 \quad (4.31)$$

$$X = a + \left(\frac{b}{4}\right) + e - \left(\frac{d}{2}\right) \quad (4.32)$$

$$Y = (\alpha - 1)(a + \frac{b}{4} + e - \frac{d}{2}) \quad (4.33)$$

$$Z = 3.76\alpha - 1\left(a + \frac{b}{4} + e - \frac{d}{2}\right) + \frac{f}{2} \quad (4.34)$$

$$M_{CO_2} = \frac{a.CO_2}{M} \equiv kgCO_2/kg\ fuel \quad (4.35)$$

$$M_{SO_2} = \frac{e.SO_2}{M} \equiv kgSO_2/kg\ fuel \quad (4.36)$$

$$M_{CO_2} = \frac{44.a}{M}.m_{fA} \quad (4.37)$$

$$M_{SO_2} = \frac{64.e}{M}.m_{fA} \quad (4.38)$$

$$M = 12.a + b + 16.d + 32.e + 14.f \quad (4.39)$$

$$m_{fA} = \frac{86400D}{R.LHV.\eta_s} \quad (4.40)$$

Here, M_{CO_2}, M_{SO_2}, and m_{fA} are in kg/m^2.yr, M is the weight of mol for fuel in kg/k.mol, D is the degree-days in Kelvin of the study location, R is the thermal resistance of column in W/m^2.K), LHV is the lower heating value for oil fuel in J/kg, and η_s is the space heating system efficiency. Table 4.8 shows the values of all parameters that were used in emission calculation.

Table 4.8 The parameters used in emission calculation [213].

Parameter	Value
Chemical Formula of Fuel-Oil	$C_{7.3125}H_{10.407}O_{0.04}S_{0.026}N_{0.02}$
LHV	40.604 × 106 J/kg
η_s	82 (%)
Degree-Days	1431 K

The oil fuel consumption and emission gases (CO_2 and SO_2 emissions) are predictable via the annual heating load obtained from dynamic methods. The yearly fuel consumption rate for different concrete mixtures is presented in Figure 4.25. The annual consumption of fuel is decreased with increasing the CR content. The inclusion of CR content by 0%, 5%, 10%, and 15% in R^2C mixture, the fuel consumption decreases 1.6%, 6.5%, 10.4%, 19.0% and for FR^3C mixture, it is decreased by 4.8%, 8.4%, 14.0%, 20.2%, respectively compared to the control mixture. Besides, it is also clear that incorporating fiber content can also decrease the fuel consumption rate by 3.3%, 2.0%, 4.0%, and 1.5% compared to R^2C mixtures with 0%, 5%, 10%, and 15% CR content, respectively. Comparing BN-1 and BN-2 is seen that the inclusion of 30% RCA can also decrease the fuel consumption by 1.6% compared to NAC.

In terms of CO_2 and SO_2 emission, it is seen that with increasing the CR content both the emissions decrease, and they further decrease after incorporating fiber content as presented in Figure 4.26. The CO_2 emission vary from 63.91 kg/m^2.yr to 77.67 kg/m^2.yr and the SO_2 emission vary from 0.33 kg/m^2.yr to 0.40 kg/m^2.yr for R^2C mixture which are higher than that of control mixture of 78.90 kg/m^2.yr and 0.41 kg/m^2.yr, respectively. On the other hand, adding fiber content in R^2C mixtures can further reduce emissions. For FR^3C mixtures, the CO_2 emission vary from 75.12 kg/m^2.yr to 62.97 kg/m^2.yr and the SO_2 emission vary from 0.33 kg/m^2.yr to 0.39 kg/m^2.yr. Besides, the RCA can also decrease the emission rate. The RCA, CR, and fiber emit the lowest CO_2 and SO_2 emissions due to their higher thermal resistance compared to the control mixture. Up to 19.0% and 20.2% emissions can be reduced using CR content without any fiber and with 0.5% fiber content, respectively.

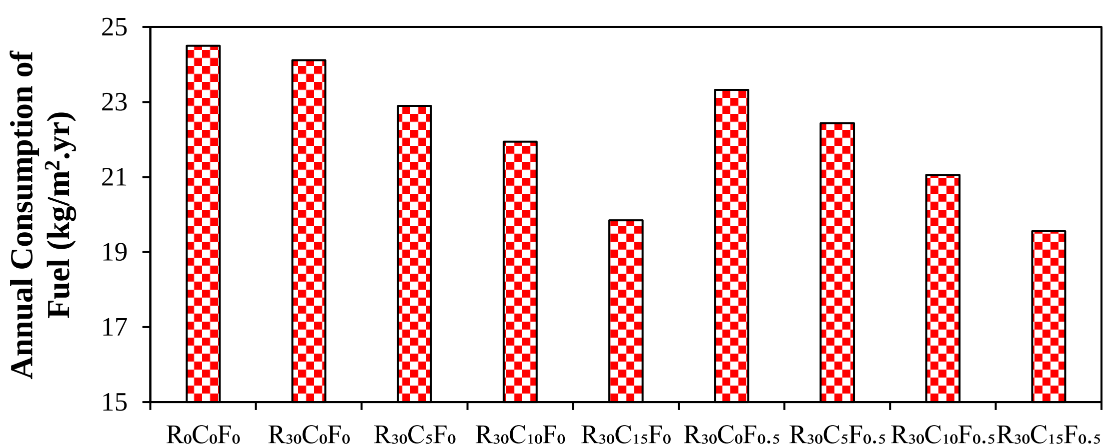

Figure 4.25 Annual fuel consumption due to different concrete types.

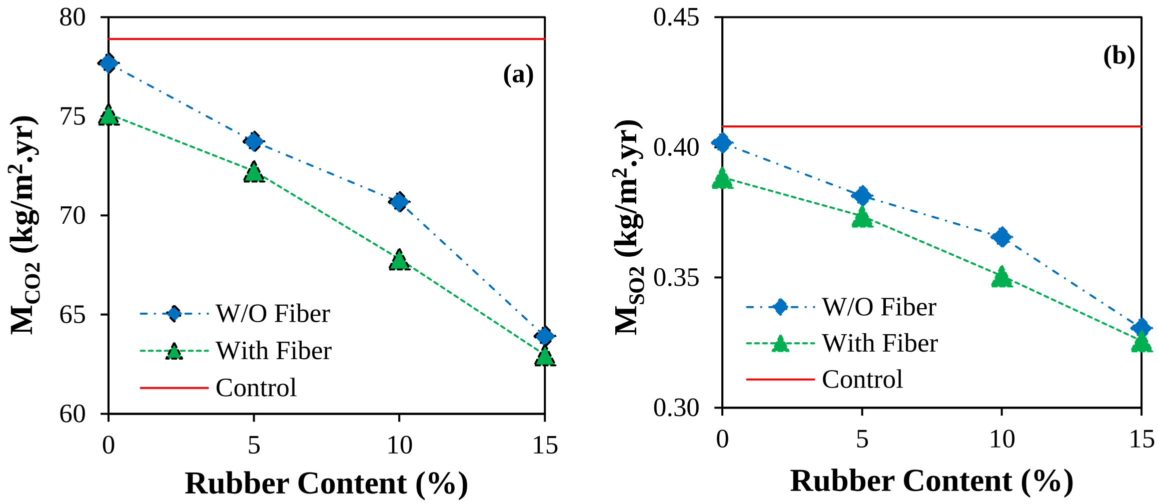

Figure 4.26 Annual emissions rate of different concrete mixes: (a) CO_2 emission, and (b) SO_2 emission.

4.6 Summary

To summarize, the inclusion of RCA, CR, or fiber decreases the slump value of the concrete mixture. The air content value of R^2C and FR^3C mixtures is comparatively higher than that of the control mixture. The compressive strength is decreased with increasing the CR percentage but the addition of fiber content can increase it. However, more than 40 MPa concrete can be produced using 30% RCA and 5% CR content along with 0.5% PP fiber. Though the R^2C and FR^3C specimens provide a lower modulus of elasticity (MoE), the FR^3C specimens exhibit comparatively higher MoE than that of the control specimen. All the R^2C and FR^3C specimens exhibit lower tensile strength and flexural strength. However, a marginal reduction is found in FR^3C specimens containing up to 5% CR content which is only 3.3% and 6.8% lower respectively than that of the control one. Approximately 8% density reduction can be achieved in R^2C and FR^3C depending on the percentage of CR and fiber content. Furthermore, the surface resistivity test reveals that for all the combinations of R^2C and FR^3C specimens, the chloride ion penetrability may be very low. With increasing the CR percentage level the UPV decreases but the addition of fiber content slightly increases the value. Both the R^2C and FR^3C mixtures save more energy cost and decrease the fuel consumption but the FR^3C mixtures can save more compared to R^2C mixtures.

Chapter 5

COMPRESSIVE BEHAVIORS OF COLUMNS

5. 1 Introduction

The present chapter presents the uniaxial compressive behavior of a total of 26 rubberized recycled concrete (R^2C) columns and fiber-reinforced rubberized recycled concrete (FR^3C) columns. The results are presented in terms of failure modes, load-deformation responses, axial capacity, strain in concrete and steel, contribution of concrete on axial capacity, volumetric strain, ductility, toughness, dilation ratio, influence of longitudinal reinforcement, influence of tie spacing, moment-curvature, and code provisions.

5.2 Cracking and Failure Mode

The post-failure overview of different tested columns is represented in Figures 5.1 to 5.4. Different failure modes were observed based on the inclusion of RCA or CR or fiber or transverse reinforcement spacing. Generally, the failure mode of R^2C columns followed this progression: (1) yielding of the longitudinal reinforcement, (2) crushing of concrete cover with a major or minor spall out, and (3) buckling of the longitudinal reinforcement or transverse reinforcement whereas the FR^3C columns did not experience any spalling of concrete.

Figure 5.1 displays the crack pattern of the columns containing 1.4% longitudinal reinforcement with 75 mm tie spacing. In the control column and recycled aggregate concrete (RAC) column, as the axial load increased, cracking initiated at the mid-height of the columns and then started to propagate towards the heads. The concrete cover spalled off for these columns after the longitudinal reinforcements yielded. Subsequently, the longitudinal reinforcement buckled at failure. Though in most of the columns, the cracking initiated from the mid-height of the columns, except for a few that were subjected to unintended eccentricities during loading. For these unintended eccentricities, the concrete was crushed locally near the heads of the specimens such as $R_{30}C_{10}F_0$-1.4-75 and $R_{30}C_5F_{0.5}$-1.4-75. The rubberized recycled concrete (R^2C) columns faced a little concrete separation from the surfaces. Besides, some distinct cracking lines were also observed. The propagation of the cracking lines represents the shear failure mode in R^2C columns. A higher crack length was also visualized. However, no concrete cover separation occurred in FR^3C columns. A zigzag failure pattern was followed by

FR^{3}C columns. The enhancement of bridging capacity due to fiber resisted a well-defined cracking width. Besides, the crack length was comparatively lower than that of R^{2}C columns. No distinct shear failure mode was observed in FR^{3}C columns.

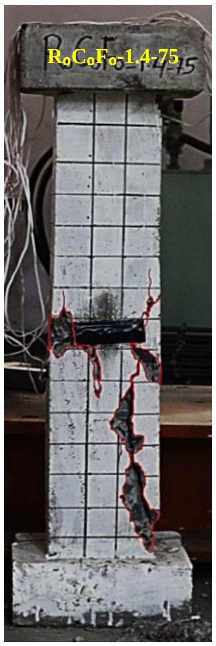

(a)

(b)

(c)

Figure 5.1 Failure mode of columns containing 1.4% longitudinal reinforcement with 75 mm tie spacing: (a) control column, (b) R^{2}C columns, and (c) FR^{3}C columns.

Figure 5.2 shows a photograph of a failed specimen of the columns containing 1.4% longitudinal reinforcement with 150 mm tie spacing. Upon attaining the peak load level, the large tie-spaced (150 mm) control column and R^2C columns failed suddenly and were accompanied by an explosive noise. Excessive buckling of the longitudinal and transverse steel bars occurred. Once the peak load was attained, the load dropped almost instantly without an early warning. The failure occurred in the entire lower half of these specimens, as shown in Figure 5.2 (a). Figure 5.4 (b) shows a close-up photograph of the failure area where a significant portion of concrete was spalled out from the surface of the columns, and the longitudinal bars are buckled and frayed. Besides, the concrete core was damaged. On the other hand, the specimens with smaller tie spacing (75 mm) experienced an increase in axial deformation without crushing the concrete core due to the confining action exerted by the closely spaced ties as displayed in Figure 5.4 (a). No visual buckling of the longitudinal reinforcement had observed along with a little concrete cover separation.

The FR^3C column specimens provided a ductile failure mode without separating any concrete cover as shown in Figure 5.2 (b). The failure modes were almost identical to the smaller tie-spaced columns. The cracking lines followed a zigzag pattern. Besides, no visible buckling of the longitudinal reinforcement had occurred. However, the FR^3C column containing a higher percentage of crumb rubber (CR) provided a large crack width compared to the column containing lower CR content. It can be concluded that, though rubberized concrete provides a brittle failure with a significant concrete spalling, it can be minimized by incorporating fiber into the concrete mixture.

To examine the effect of longitudinal reinforcement in FR^3C columns, 4 columns were tested with a higher percentage (2.0%) along with a large tie spacing (150 mm). The crack patterns of the columns after the failure are presented in Figure 5.3 (a). A comparatively small number of cracking lines were observed in the columns with a higher reinforcement ratio. The comparison between the failure mode of the column with a lower reinforcement ratio (1.4%) and a higher reinforcement ratio (2.0%) is presented in Figure 5.4 (e & f). No macro-crack was visualized in the higher reinforced concrete column. Only some hair-crack were observed.

The failure mode of unreinforced plain concrete columns is displayed in Figure 5.3 (b). The fiber-reinforced concrete exhibited gradual damage, while the control specimen and rubberized concrete (RuC) specimen provided a brittle failure mode. The RuC specimen was just divided into two pieces without providing any warning after reaching peak stress. A shear failure mode was observed as presented in Figure 5.4 (g) whereas higher energy was accumulated by the FR^{3}C specimen. A significant difference in post-peak behavior of the FR^{3}C specimen was observed compared to the RuC specimen.

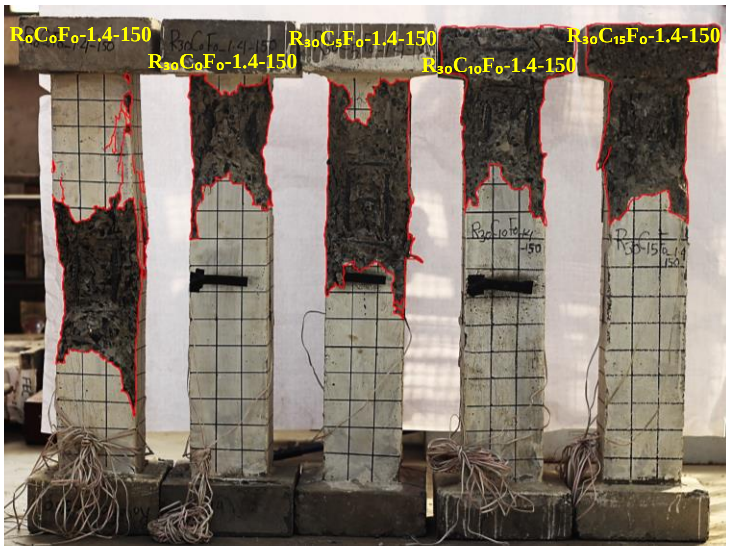

(a)

(b)

Figure 5.2 Failure mode of columns containing 1.4% longitudinal reinforcement with 150 mm tie spacing: (a) control column and R^{2}C columns, and (b) FR^{3}C columns.

(a)

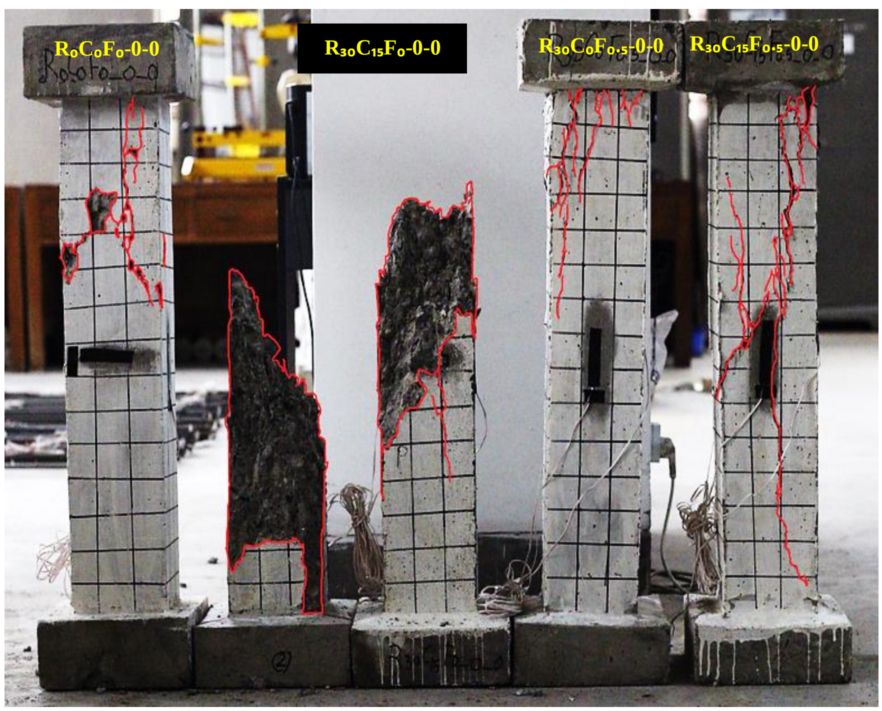

(b)

Figure 5.3 Failure mode of (a) control and FR^{3}C columns containing 2.0% longitudinal reinforcement with 150 mm tie spacing, and (b) plain concrete columns.

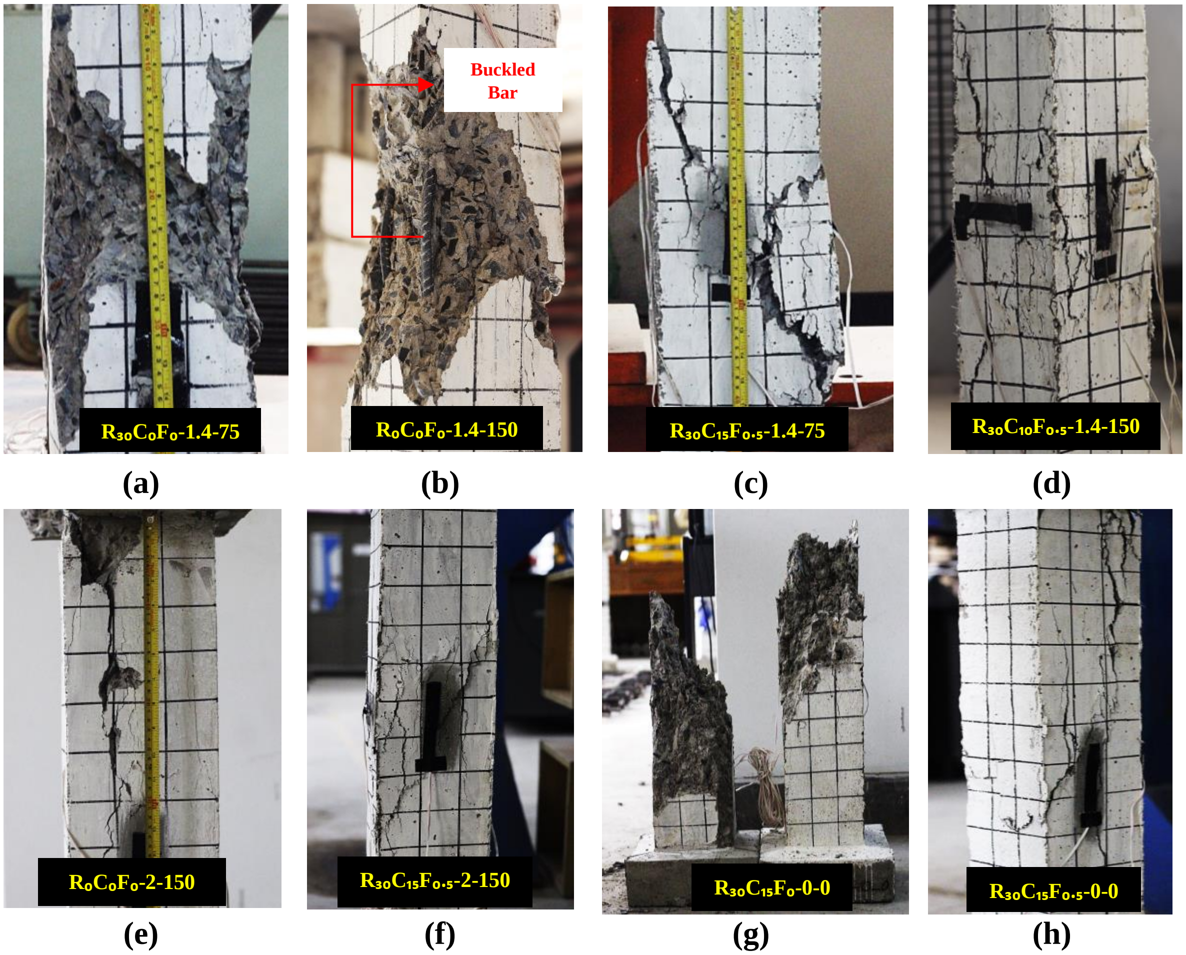

Figure 5.4 Close observation of crack patterns of the columns with different combinations.

5.3 Load Deformation Responses

The load-deformation curves of different reinforced concrete (RC) columns are presented in Figure 5.5. The curves are divided into three segments. The first segment corresponds to the behavior until the peak load, which is similar to the plain concrete column as shown in Figure 5.6, implying that transverse reinforcement does not affect this phase. The concrete cover was visually free of cracks in this segment, yet the peak load varies depending on the inclusion of CR and fiber content, longitudinal reinforcement ratio, and tie spacing. The second segment is very short and is characterized by a rapid drop in axial load. This starts once the load reaches the peak point, and finishes with passive-confinement activation (deformation increases in the transverse reinforcements). Transverse reinforcement plays a significant role in this phase. Thus, a cabalistic difference is observed among the curves of the columns with 75 mm tie spacing and 150 mm tie spacing in this stage. In stage is not so distinct for the curves of the columns containing 150 mm tie spacing due to the comparatively lower confinement effect. However, basically, in this phase, cracks began growing in the concrete cover, leading to gradual spalling that reduced the load-resisting cross-sectional area and resulted in strength degradation. The third phase is characterized by activation of transverse reinforcing associated with complete spalling of concrete cover and ended with the total failure of the column. The curves associated with the larger tie-spaced columns go straight down and the load drops abruptly whereas the lower tie-spaced columns' curve provides a more ductile phenomenon.

Table 5.1 summarizes the test result of the compression test of all RC columns. From the table, it is clear that the deformation capacity increases with increasing the CR content. For instance, in the R^2C columns with a longitudinal reinforcement ratio of 1.4% and tie spacing of 75 mm, the deformation corresponding to the peak load are 7.60 mm, 9.98 mm, 11.19 mm, and 11.56 mm for 0%, 5%, 10%, and 15% CR content, respectively which is a clear indication of higher deformation capacity of rubberized concrete. As rubber is a soft material with a lower elastic modulus, it can deform more compared to conventional concrete. However, the inclusion of fiber content in R^2C columns further increases the deformation capacity of FR^3C columns. For these FR^3C columns, the deformation corresponding to the peak load is 7.68 mm, 10.58 mm, 11.91 mm, and 11.97 mm for 0%, 5%, 10%, and 15% CR content, respectively which is 1.1%, 6.0% 6.4%, and 3.5% higher than that of corresponding R^2C columns. The bridging action of fiber can enhance the deformation capacity of the concrete. The same phenomenon is also observed in the case of ultimate deformation.

The tie spacing also affects the deformation capacity. The 150 mm tie-spaced columns exhibit comparatively lower deformation than those of 75 mm tie-spaced columns. Approximately 25%, 39.8%, 40.3%, and 28.8% lower deformation is found corresponding to peak load for 150 mm tie-spaced R^2C columns compared to 75 mm tie-spaced R^2C columns with 0%, 5%, 10%, and 15% CR content, respectively. For FR^3C columns, these reduction percentages are 12.1, 20.9, 26.4, and 26.2, respectively. With a higher tie spacing, the columns cannot resist higher deformation, rather they reach their peak points or fracture points by providing a lower deformation capacity. On the other hand, the increase in the longitudinal reinforcement ratio provides a positive impact on deformation capacity. The deformation corresponding to the peak load of the columns with a 2.0% longitudinal reinforcement ratio is increased from

8.77 mm and 8.83 mm to 9.88 mm and 11.21 mm for 10% and 15% CR content, respectively compared to the 1.4% longitudinal reinforcement ratio. However, for 5% CR content it is slightly decreased from 8.37 mm to 8.13 mm.

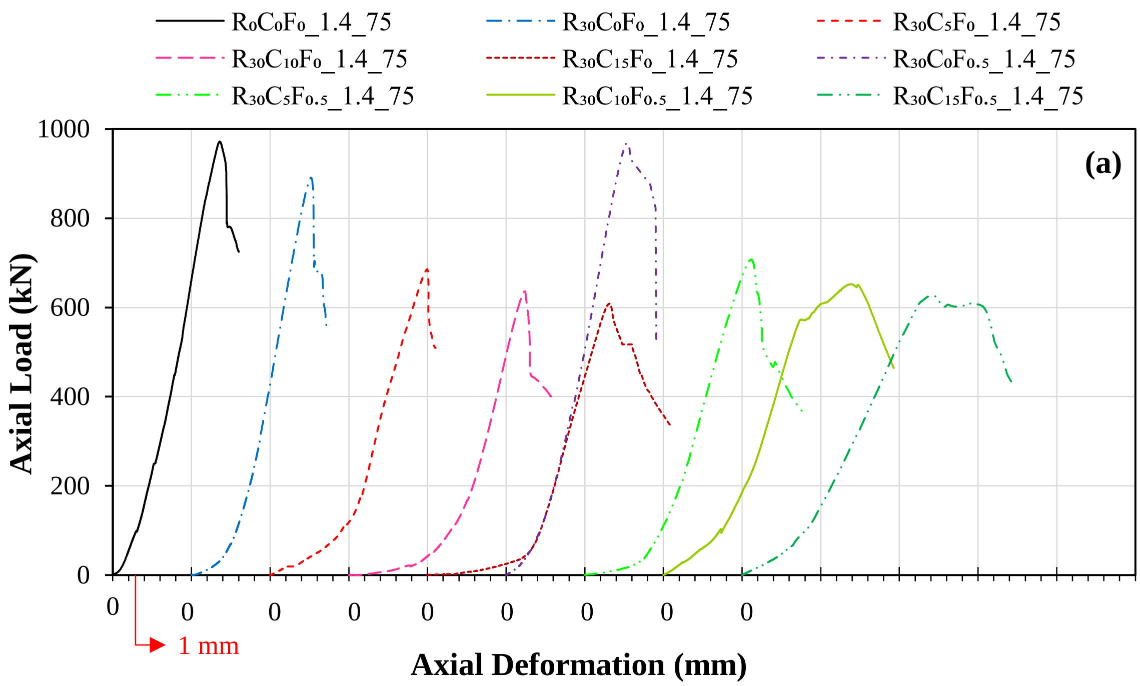

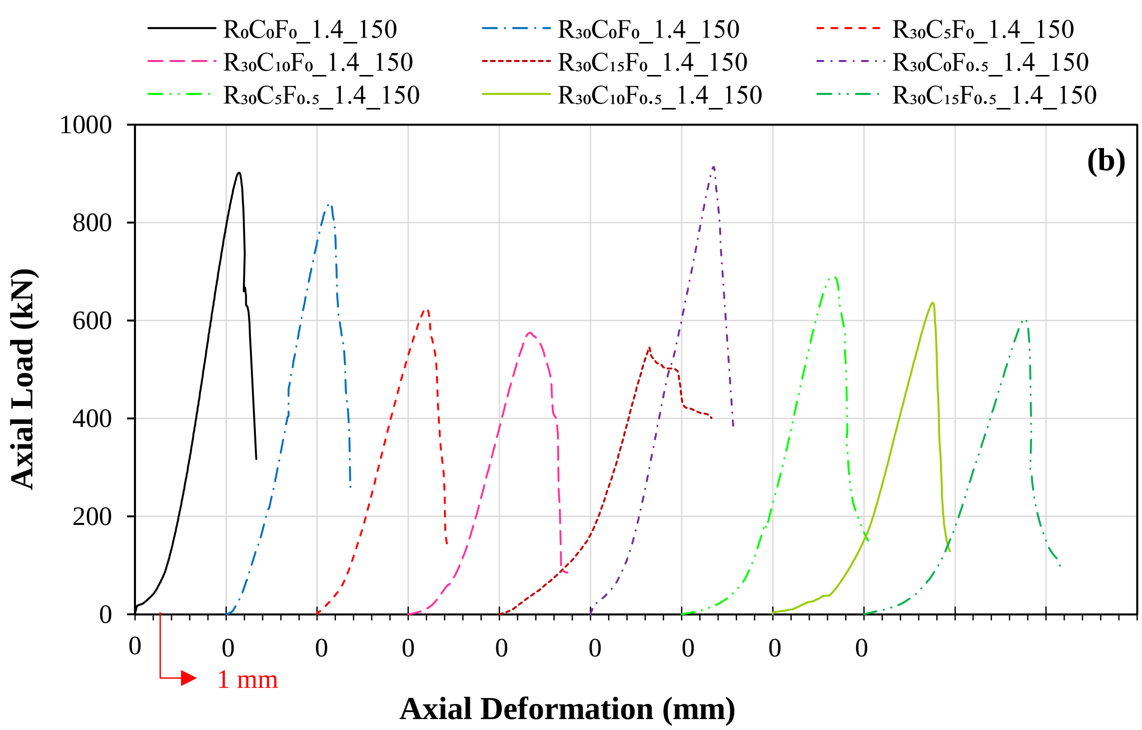

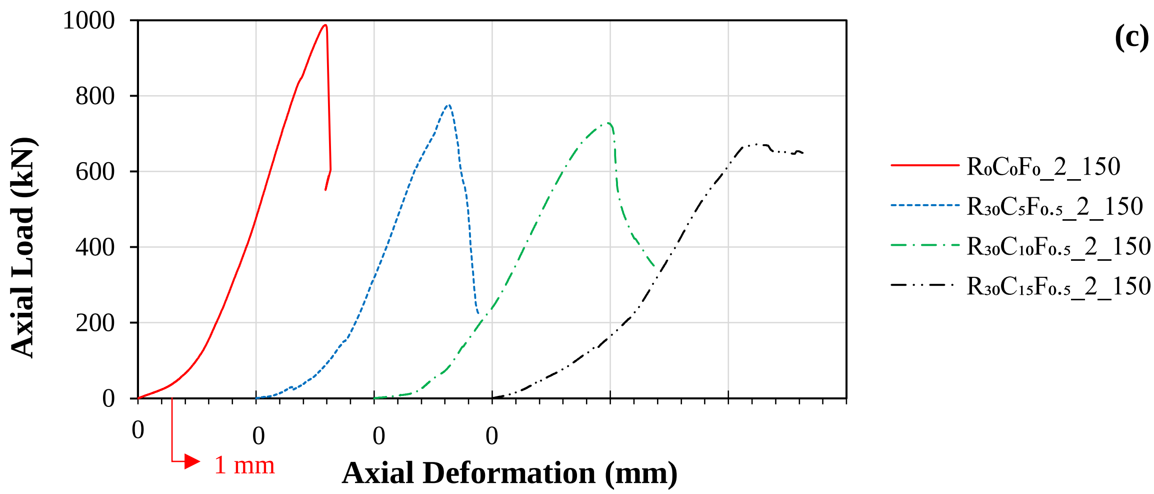

Figure 5.5 Load-deformation relationship of columns: (a) ρ = 1.4% with 75 mm tie spacing, (b) ρ = 1.4% with 150 mm tie spacing, and (c) ρ = 2.0% with 150 mm tie spacing.

Table 5.1 Test results of uniaxial compression test of RC columns.

Column Name	P_{peak} (kN)	$P_{F\text{-}Crack}$ (kN)	$P_{\Delta u}$ (kN)	Δ_{Peak} (mm)	Δ_y (mm)	Δ_u (mm)
$R_0C_0F_0$_1.4_75	971.7	449.1	724.7	6.79	3.95	8.02
$R_{30}C_0F_0$_1.4_75	891.2	301.7	555.5	7.60	4.34	8.59
$R_{30}C_5F_0$_1.4_75	685.7	147.7	509.6	9.98	4.90	10.52
$R_{30}C_{10}F_0$_1.4_75	636.1	51.4	390.8	11.19	5.41	13.03
$R_{30}C_{15}F_0$_1.4_75	608.1	24.0	334.1	11.56	5.89	15.48
$R_{30}C_0F_{0.5}$_1.4_75	968.3	384.9	525.8	7.68	4.31	9.55
$R_{30}C_5F_{0.5}$_1.4_75	707.2	47.3	361.7	10.58	3.98	13.89
$R_{30}C_{10}F_{0.5}$_1.4_75	652.1	97.0	464.1	11.91	3.72	14.65
$R_{30}C_{15}F_{0.5}$_1.4_75	626.4	68.7	422.0	11.97	3.26	17.35
$R_0C_0F_0$_1.4_150	902.0	416.1	317.2	5.73	3.42	6.66
$R_{30}C_0F_0$_1.4_150	840.6	404.5	260.4	5.70	3.42	6.93
$R_{30}C_5F_0$_1.4_150	625.8	306.6	130.2	6.01	3.41	7.18
$R_{30}C_{10}F_0$_1.4_150	575.1	218.3	85.1	6.68	3.85	8.74
$R_{30}C_{15}F_0$_1.4_150	545.0	141.2	401.1	8.23	4.63	11.64
$R_{30}C_0F_{0.5}$_1.4_150	913.9	497.2	385.4	6.75	4.30	7.83
$R_{30}C_5F_{0.5}$_1.4_150	688.8	175.4	150.6	8.37	4.49	10.23
$R_{30}C_{10}F_{0.5}$_1.4_150	636.6	41.5	128.8	8.77	3.19	10.72
$R_{30}C_{15}F_{0.5}$_1.4_150	604.3	52.0	91.9	8.83	3.06	10.91
$R_0C_0F_0$_2_150	987.5	847.2	588.0	7.93	6.83	8.07
$R_{30}C_5F_{0.5}$_2_150	776.1	154.7	218.7	8.13	3.82	9.46
$R_{30}C_{10}F_{0.5}$_2_150	727.9	136.9	351.3	9.88	3.8	11.8
$R_{30}C_{15}F_{0.5}$_2_150	671.9	141.2	309.3	11.21	4.55	14.24

Note:
P_{peak} = Peak Axial Load, $P_{F\text{-}Crack}$ = Load Corresponding to First Crack, $P_{\Delta u}$ = Load at Failure Point, Δ_{Peak} = Deformation Corresponding to Peak Axial Load, Δ_y = Deformation Corresponding to First Crack, and Δ_u = Deformation Corresponding to Failure Point.

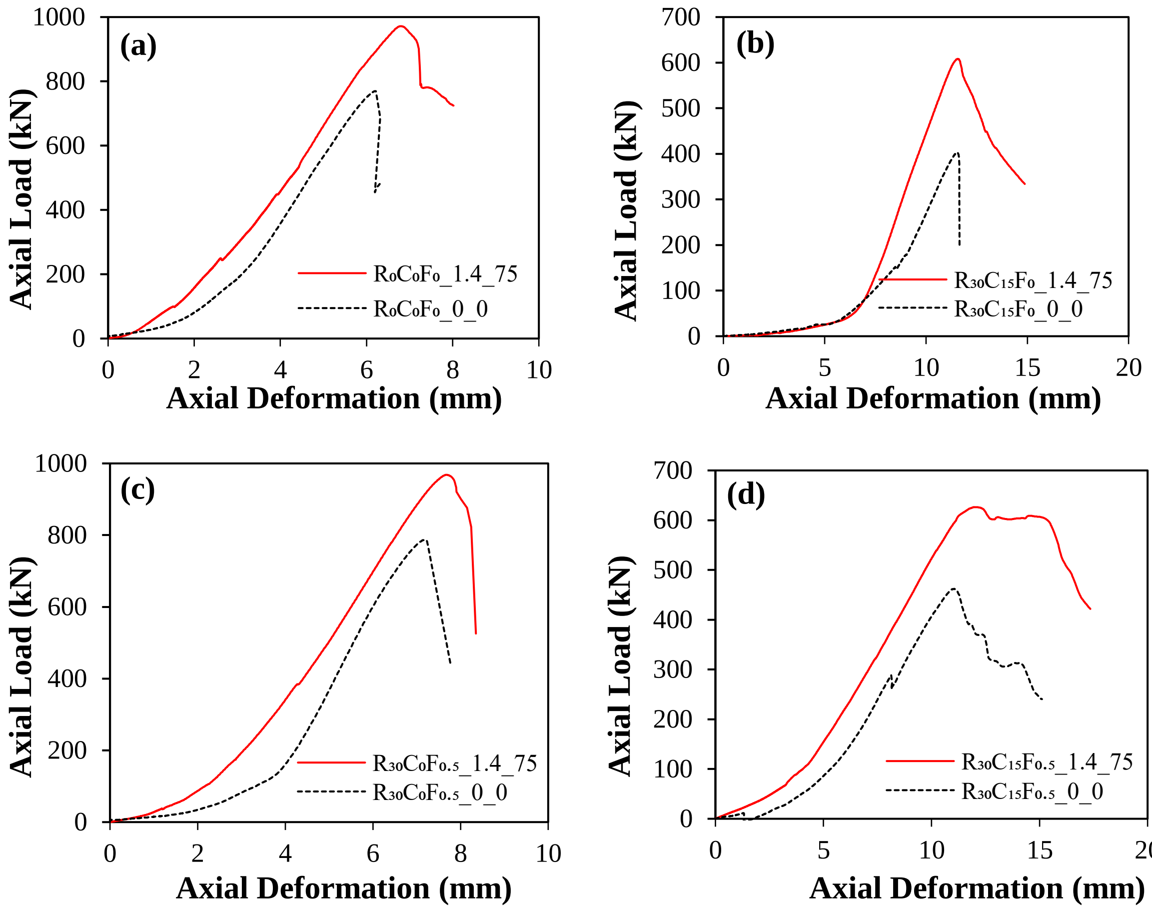

Figure 5.6 Comparison of load-deformation curves of RC columns with plain concrete columns: (a) NAC, (b) R^2C, (c) FR^2C, and (d) FR^3C.

5.4 Axial Capacity

Figure 5.7 compares the axial load carrying capacity of different RC columns as a function of CR content. Overall, it is seen that RAC, R^2C, and FR^3C columns provide lower axial capacity. However, it mostly depends on the percentage of CR content, longitudinal reinforcement ratio, and tie spacing. Figure 5.7 indicates that the compressive load-carrying capacity of column specimens decreases with an increase in CR content. For instance, the axial capacity of RC columns with a longitudinal reinforcement ratio of 1.4% along with 75 mm tie spacing decreases by 8.3%, 29.4%, 35.5%, and 37.4% after adding 0%, 5%, 10%, and 15% CR content into the R^2C mixture, respectively compared to the control column. However, the inclusion of 0.5% PP fiber in the same R^2C mixture increases the axial capacity by 8.7%, 3.1%, 2.5%, and 3.0% with 0%, 5%, 10%, and 15% CR content, respectively but still lower than the control one. Similarly, in columns with 150 mm tie spacing, the reduction percentage corresponding to 0%, 5%, 10%, and 15% CR content is 6.8%, 30.6%, 36.2%, and 39.6%, respectively for R^2C mixtures whereas for FR^3C mixtures these reduction percentage is slightly decreases. For FR^3C mixtures the axial capacity is increased by 8.7%, 10.1%, 10.7%, and 10.9% for 0%, 5%, 10%, and 15% CR content compared to corresponding column with R^2C mixture. This is in agreement with the results obtained from the compressive strength of tests as discussed in the previous chapter. Comparing 75 mm and 150 mm tie-spaced columns it is observed that the higher tie-spaced columns exhibit averagely 6.2% lower compressive load-carrying capacity due to the lower confinement of concrete. On the other hand, increasing the longitudinal reinforcement ratio from 1.4% to 2.0% increases the axial capacity of FR^3C columns by 9.5%, 12.7%, 14.3%, and 11.2% with 0%, 5%, 10%, and 15% CR content, respectively.

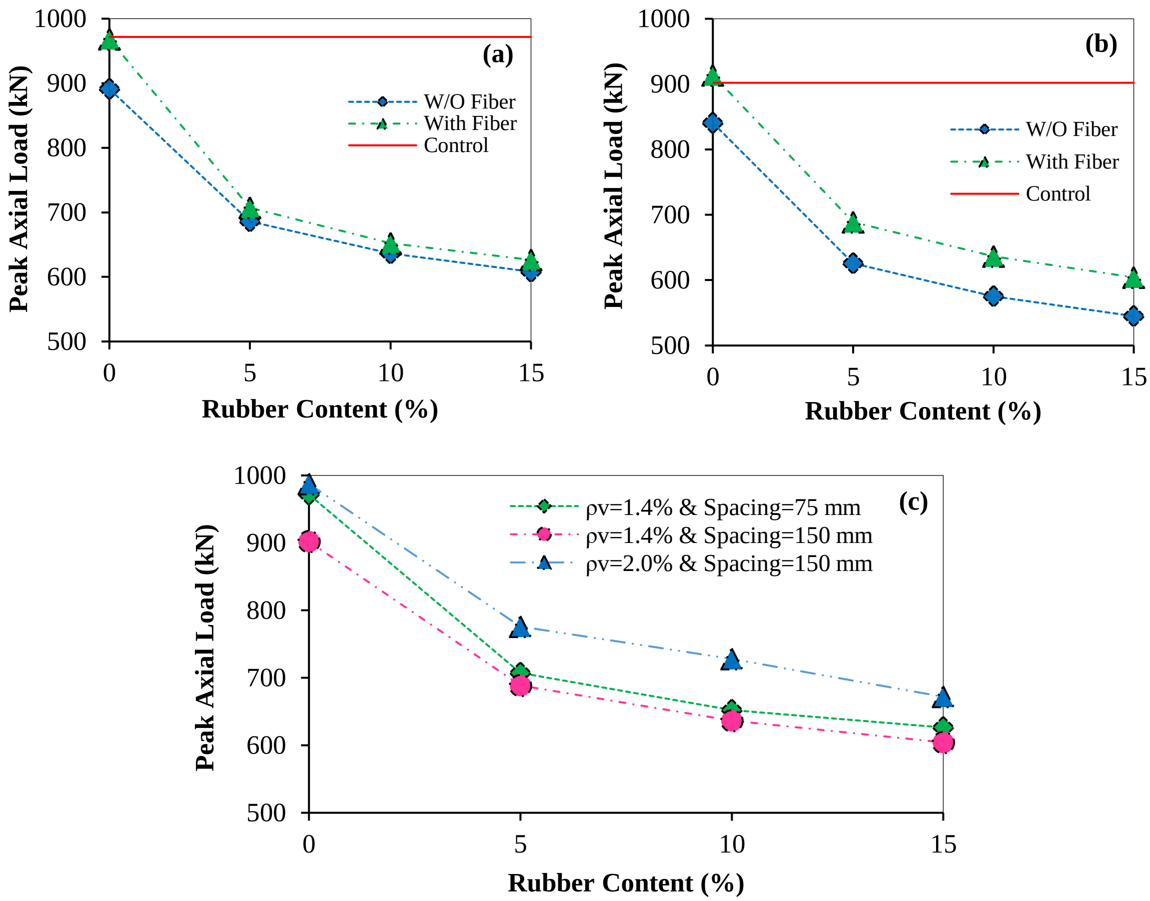

Figure 5.7 Axial capacity of RC columns: (a) ρ = 1.4% with 75 mm tie spacing, (b) ρ = 1.4% with 150 mm tie spacing, and (c) comparison between ρ = 1.4% and ρ = 2.0%.

5.5 Strain in Concrete and Reinforcement

The midpoint lateral deformations for different surfaces of column specimens and the typical axial load–strain curves are presented in ANNEX B. The locations of the LVDT and the strain gauges are discussed in the experimental details chapter (Figure 3.13). The points on the negative side of the graphs mean compression whereas the positive side's points are in tension. In terms of lateral deformation, all columns face both tension and compression in different faces. In terms of strain, the strain gauges in the longitudinal direction faced the compressive force whereas the transverse directional strain gauges faced either tensile force or compressive force.

In general, the deformation and strain value increases with increasing the load and the steel yields before the concrete crushes. From Table 5.2 it is seen that the failure of all the specimens seems to be ultimately caused by the buckling of the longitudinal bars rather than the crushing of the concrete core. The strain profiles reveal that the columns remain in compression in the middle section. Besides, in the comparison of the longitudinal compressive strain of concrete on two different sides of the columns, it is found that the tested columns were overall buckled either in the z–x plane or z–y plane. The pattern of all curves is identical and independent of RCA, CR, PP fiber, longitudinal reinforcement ratio, and tie spacing, and found that the sample for each type of column had a good consistency. Therefore, it can be confirmed that the materials used, the production of the specimens, and the test procedure were all well controlled. However, from Table 5.2 it is seen that the lateral deformation and concrete strain increase with increasing the CR content and it further increases after the inclusion of PP fiber in R^2C mixtures. As rubber is a soft material it can deform more compared to conventional aggregates. Besides, fiber improves the cementitious properties of the concrete which further increases the deformation capacity. In 75 mm tie-spaced columns, approximately 24% and 28% lateral deformation capacity can be increased using 15% CR content in RAC containing without any fiber and with 0.5% PP fiber, respectively compared to the control one. For 150 mm tie-spaced columns, these incremental percentages are 22% and 25%, respectively. This implies that rubber-mixed concrete columns are capable of absorbing a higher amount of energy before failure.

The lower confinement effect of 150 mm tie-spaced columns shows higher deformation and concrete strain compared to 75 mm tie-spaced columns. Approximately 5.6%, 6.2%, 2.8%, 3.0% and 3.6%, 4.9%, 2.7%, 2.2% higher lateral deformation can be found for 0%, 5%, 10%, 15% CR content containing without any fiber and with 0.5% PP fiber, respectively. The same trend is also observed for concrete strain. On the other hand, by increasing the longitudinal reinforcement ratio from 1.4% to 2.0%, the lateral deformation is decreased by 7.0%, 12.1%, 15.8%, and 16.9% for 0%, 5%, 10%, and 15% CR content, respectively. The axial strain of concrete in R^2C specimens varies from 0.00263 to 0.00330 for 75 mm tie-spaced columns and 0.00259 to 0.00315 for 150 mm tie-spaced columns. For FR^3C columns it is varied from 0.00269 to 0.00339 and 0.00264 to 0.00328 for 75 mm and 150 mm tie-spaced columns, respectively. The average lateral strains are approximately 26% and 28% of the axial concrete strain for 75 mm and 150 mm tie-spaced columns, respectively.

Both the axial and lateral strain of the reinforcing bar increases with increasing the CR content. The axial strain in the reinforcement of R^2C specimens varies from 0.00205 to 0.00267 for 75 mm tie-spaced columns and 0.00236 to 0.00274 for 150 mm tie-spaced columns. For FR^3C columns it is varied from 0.00203 to 0.00252 and 0.00227 to 0.00264 for 75 mm and 150 mm tie-spaced columns, respectively. It is found that the inclusion of fiber can slightly decrease the strain in reinforcement. Approximately 2.6% axial strain is decreased in 75 mm tie-spaced columns using 0.5% PP fiber whereas for 150 mm tie-spaced columns this reduction is about 3.2%. This may happen due to the higher strain resisting capacity of fiber which can lead to taking comparatively lower strain in the reinforcement. The same trend is also observed for lateral strain in the transverse reinforcing bar. The reinforcement in the larger tie-spaced columns (150 mm tie spacing) faces comparatively higher strain which is approximately 7.6% and 6.9% higher for R^2C columns and FR^3C columns compared to the smaller tie-spaced columns (75 mm tie spacing).

Table 5.2 Deflection and strain on concrete and steel bar corresponding to peak load.

Column Name	Lateral Deflection on Mid-Point of Column (mm)				Axial Strain on Concrete Surface (mm/mm)				Lateral Strain on Concrete Surface (mm/mm)	Axial Strain on Long Bar (mm/mm)	Lateral Strain on Trans Bar (mm/mm)	Poisson's ratio
	Min	Max	Avg	No of Readings	Min	Max	Avg	No of Readings				
$R_0C_0F_0$_1.4_75	1.96	5.73	3.80	4	0.00211	0.00298	0.00254	2	0.00057	0.00221	0.00055	0.22
$R_{30}C_0F_0$_1.4_75	1.98	6.23	3.81	4	0.00211	0.00315	0.00263	2	0.00062	0.00205	0.00045	0.24
$R_{30}C_5F_0$_1.4_75	2.10	4.64	4.02	4	0.00244	0.00344	0.00294	2	0.00077	0.00229	0.00061	0.26
$R_{30}C_{10}F_0$_1.4_75	2.79	5.87	4.37	4	0.00292	0.00311	0.00301	2	0.00082	0.00239	0.00063	0.27
$R_{30}C_{15}F_0$_1.4_75	2.09	6.27	4.71	4	0.00251	0.00408	0.00330	2	0.00095	0.00267	0.00080	0.29
$R_{30}C_0F_{0.5}$_1.4_75	3.06	5.28	3.96	4	0.00297	0.00241	0.00269	2	0.00063	0.00203	0.00040	0.23
$R_{30}C_5F_{0.5}$_1.4_75	2.50	5.58	4.12	4	0.00385	0.00252	0.00319	2	0.00080	0.00218	0.00049	0.25
$R_{30}C_{10}F_{0.5}$_1.4_75	2.19	6.01	4.56	4	0.00310	0.00349	0.00329	2	0.00086	0.00243	0.00059	0.26
$R_{30}C_{15}F_{0.5}$_1.4_75	2.22	6.76	4.88	4	0.00359	0.00318	0.00339	2	0.00097	0.00252	0.00073	0.28
$R_0C_0F_0$_1.4_150	2.10	6.00	3.99	4	0.00215	0.00282	0.00249	2	0.00062	0.00235	0.00068	0.25
$R_{30}C_0F_0$_1.4_150	3.12	5.21	4.02	4	0.00211	0.00307	0.00259	2	0.00067	0.00236	0.00076	0.26
$R_{30}C_5F_0$_1.4_150	2.39	5.28	4.26	4	0.00228	0.00354	0.00291	2	0.00081	0.00246	0.00084	0.28
$R_{30}C_{10}F_0$_1.4_150	3.42	5.86	4.50	4	0.00244	0.00345	0.00295	2	0.00085	0.00252	0.00089	0.29
$R_{30}C_{15}F_0$_1.4_150	3.33	6.42	4.85	4	0.00280	0.00350	0.00315	2	0.00095	0.00274	0.00095	0.30
$R_{30}C_0F_{0.5}$_1.4_150	3.19	6.27	4.10	4	0.00223	0.00305	0.00264	2	0.00069	0.00227	0.00066	0.26
$R_{30}C_5F_{0.5}$_1.4_150	3.00	5.40	4.32	4	0.00246	0.00372	0.00309	2	0.00084	0.00238	0.00078	0.27
$R_{30}C_{10}F_{0.5}$_1.4_150	2.93	6.21	4.69	4	0.00289	0.00354	0.00321	2	0.00091	0.00246	0.00083	0.28
$R_{30}C_{15}F_{0.5}$_1.4_150	2.15	7.10	4.99	4	0.00289	0.00366	0.00328	2	0.00099	0.00264	0.00088	0.30
$R_0C_0F_0$_2_150	1.73	5.61	3.71	4	0.00221	0.00246	0.00234	2	0.00051	0.00228	0.00058	0.22
$R_{30}C_5F_{0.5}$_2_150	5.36	2.45	3.80	4	0.00287	0.00316	0.00301	2	0.00070	0.00230	0.00066	0.23
$R_{30}C_{10}F_{0.5}$_2_150	1.23	6.06	3.95	4	0.00241	0.00399	0.00320	2	0.00081	0.00248	0.00072	0.25
$R_{30}C_{15}F_{0.5}$_2_150	2.04	6.30	4.14	4	0.00258	0.00392	0.00325	2	0.00089	0.00255	0.00077	0.27
$R_0C_0F_0$_0_0	1.39	5.30	2.57	4	0.00241	0.00257	0.00249	2	0.00050	-	-	0.20
$R_{30}C_{15}F_0$_0_0	1.21	5.18	2.79	4	0.00234	0.00267	0.00250	2	0.00068	-	-	0.27
$R_{30}C_0F_{0.5}$_0_0	1.35	4.49	2.67	4	0.00225	0.00247	0.00236	2	0.00050	-	-	0.21
$R_{30}C_{15}F_{0.5}$_0_0	4.41	2.46	2.86	4	0.00326	0.00290	0.00308	2	0.00085	-	-	0.27

5.6 Contribution of Concrete on Axial Capacity

Table 5.3 summarizes the contribution of concrete and steel to the axial capacity of different RC columns. The table reports the following results for each column: peak axial load P_{peak}; the axial strain on longitudinal reinforcement corresponding to peak load $\varepsilon_{S\text{-}peak}$; load carried by the reinforcement $P_{S\text{-}peak}$ (computed by multiplying the area of longitudinal reinforcement by the strain and modulus of elasticity of the bar material); the ratio between the load carried by the reinforcement and the peak load $P_{S\text{-}peak}/P_{peak}$; load carried by the concrete $P_{C\text{-}peak}$ (computed as the difference between the peak axial load and the load carried by the reinforcement); the ratio between the load carried by the concrete and the peak load $P_{C\text{-}peak}/P_{peak}$; and normalized concerning the net area of concrete multiplied by the average concrete compressive strength $P_{C\text{-}peak}/f'_c A_c$.

In control columns and RAC columns with 75 mm tie spacing, the concrete compressive stress at the peak is approximately $0.80 fc'$ (last column in Table 5.3), which is close to the value of $0.85 fc'$ as defined in ACI 318-14 [137]. However, for 150 mm tie-spaced columns, this value is reduced to about $0.72 fc'$. This may happen due to the comparatively larger tie spacing in the columns. However, for R^2C and FR^3C specimens, this ratio has been reduced further and varies from 0.52 to 0.68 and 0.52 to 0.78, respectively depending on the percentage of CR, tie spacing, and longitudinal reinforcement ratio. Thus, this is a clear indication of the inappropriateness of the existing equation of the normal concrete column. The existing equation needs some modification for rubberized concrete or fiber-reinforced rubberized concrete columns. From Figure 5.8 and Table 5.3 it is seen that the contribution of concrete to axial capacity decreases gradually with increasing the percentage of CR content. Besides, increasing the tie spacing can further decrease the concrete contribution and thus increase the steel contribution on axial capacity. For R^2C specimens, the concrete contribution varies from 70.5% to 84.6% of the peak load for 75 mm tie-spaced columns and 66.3% to 81.2% for 150 mm tie-spaced columns. However, incorporating the fiber content can slightly increase the concrete contribution and decrease the load on steel. For FR^3C specimens, the concrete contribution varies from 73.0% to 86.0% for 75 mm tie-spaced columns and 70.8% to 83.4% for 150 mm tie-spaced columns.

With increasing the longitudinal reinforcement ratio, the contribution of concrete decreases, and increases the steel contribution. The load carried by the longitudinal reinforcement ranges between approximately 23.2% to 29.2% of the peak load for the FR^{3}C columns of ρ =1.4%, whereas for the columns with ρ =2.0% it varies from 30.4% to 39.0% of the peak load. The results discussed previously are based on the assumption that the modulus of elasticity of a reinforcing bar in tension and compression are similar. The contribution of concrete to axial capacity is also validated with respect to plain concrete columns and presents the summary of the test results in Table 5.4. The variation in concrete contribution as calculated from strain gauge data and plain concrete data is lower than 10%.

Table 5.3 Summary of concrete and steel contribution on axial capacity of RC columns.

Column Name	P_{peak} (kN)	$\varepsilon_{S\text{-}peak}$ (mm/mm)	$P_{S\text{-}peak}$ (kN)	$P_{S\text{-}peak}/P_{peak}$ (%)	$P_{C\text{-}peak}$ (kN)	$P_{C\text{-}peak}/P_{peak}$ (%)	$P_{C\text{-}peak}/f'_cA_c$ (%)
$R_0C_0F_0$_1.4_75	971.7	0.00221	148.2	15.2	823.6	84.8	78.5
$R_{30}C_0F_0$_1.4_75	891.2	0.00205	137.1	15.4	754.0	84.6	81.4
$R_{30}C_5F_0$_1.4_75	685.7	0.00229	153.6	22.4	532.1	77.6	62.3
$R_{30}C_{10}F_0$_1.4_75	636.1	0.00239	160.1	25.2	476.0	74.8	61.2
$R_{30}C_{15}F_0$_1.4_75	608.1	0.00267	179.1	29.5	429.0	70.5	68.2
$R_{30}C_0F_{0.5}$_1.4_75	968.3	0.00203	135.6	14.0	832.6	86.0	77.6
$R_{30}C_5F_{0.5}$_1.4_75	707.2	0.00218	145.9	20.6	561.3	79.4	57.9
$R_{30}C_{10}F_{0.5}$_1.4_75	652.1	0.00243	162.6	24.9	489.5	75.1	57.3
$R_{30}C_{15}F_{0.5}$_1.4_75	626.4	0.00252	168.9	27.0	457.5	73.0	57.8
$R_0C_0F_0$_1.4_150	902.0	0.00235	157.3	17.4	744.7	82.6	71.0
$R_{30}C_0F_0$_1.4_150	840.6	0.00236	158.1	18.8	682.5	81.2	73.7
$R_{30}C_5F_0$_1.4_150	625.8	0.00246	164.9	26.3	460.9	73.7	54.0
$R_{30}C_{10}F_0$_1.4_150	575.1	0.00252	168.7	29.3	406.4	70.7	52.2
$R_{30}C_{15}F_0$_1.4_150	545.0	0.00274	183.6	33.7	361.3	66.3	57.5
$R_{30}C_0F_{0.5}$_1.4_150	913.9	0.00227	152.1	16.6	761.8	83.4	71.0
$R_{30}C_5F_{0.5}$_1.4_150	688.8	0.00238	159.7	23.2	529.1	76.8	54.5
$R_{30}C_{10}F_{0.5}$_1.4_150	636.6	0.00246	165.0	25.9	471.6	74.1	55.2
$R_{30}C_{15}F_{0.5}$_1.4_150	604.3	0.00264	176.6	29.2	427.7	70.8	54.1
$R_0C_0F_0$_2_150	987.5	0.00228	234.4	23.7	753.1	76.3	72.3
$R_{30}C_5F_{0.5}$_2_150	776.1	0.00230	236.2	30.4	539.9	69.6	56.0
$R_{30}C_{10}F_{0.5}$_2_150	727.9	0.00248	254.7	35.0	473.2	65.0	55.8
$R_{30}C_{15}F_{0.5}$_2_150	671.9	0.00255	262.0	39.0	409.9	61.0	52.1

Note:
P_{peak} = Peak Axial Load, $\varepsilon_{S\text{-}peak}$ = Axial Strain on Longitudinal Reinforcement Corresponding to Peak Load, $P_{S\text{-}peak}$ = Load Carried by Reinforcement, $P_{C\text{-}peak}$ = Load Carried by Concrete, f'_c = Compressive Strength of Concrete, and A_c = Cross-Sectional Area of Concrete.

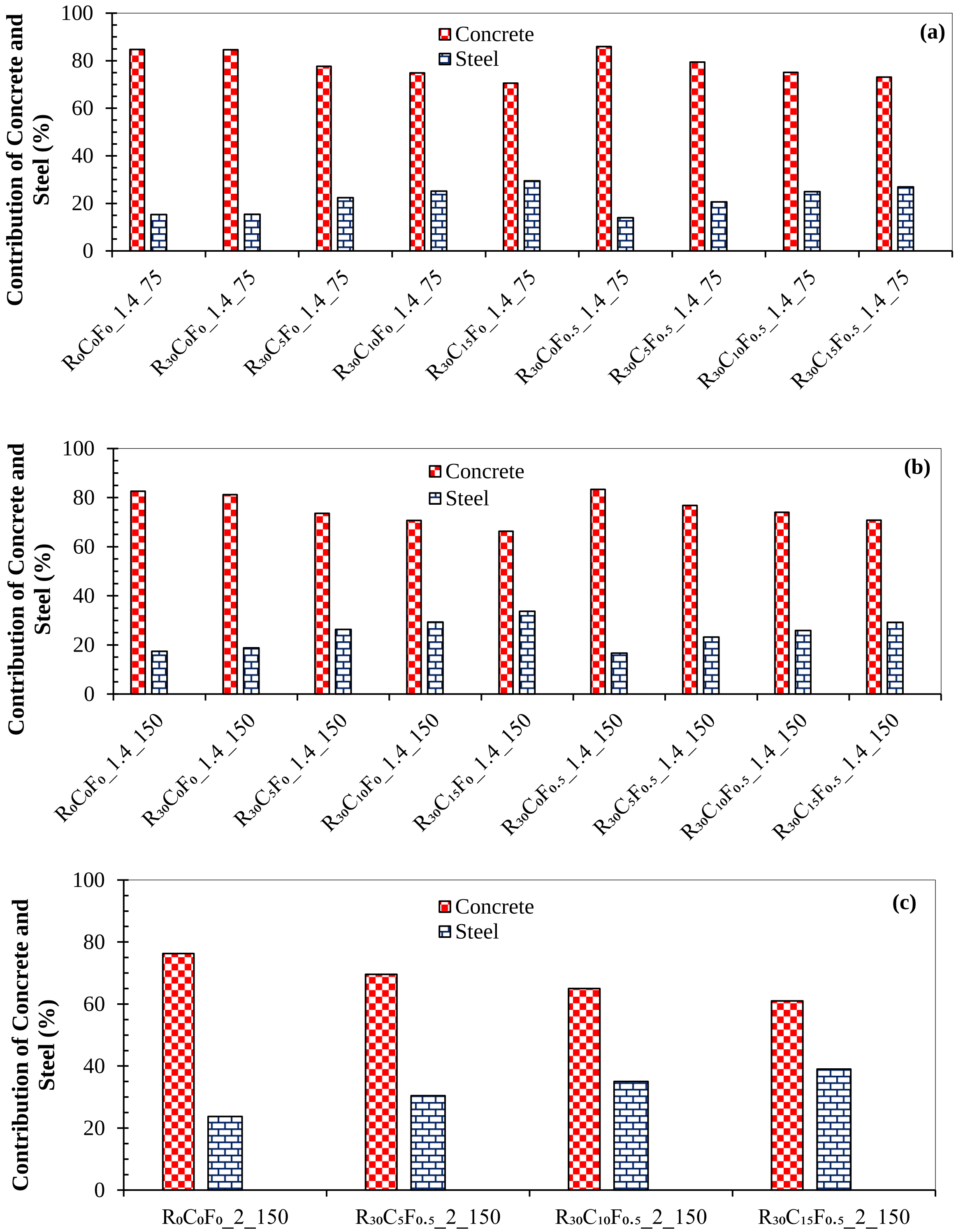

Figure 5.8 Contribution of concrete and steel on axial capacity of columns: (a) ρ = 1.4% with 75 mm tie spacing, (b) ρ = 1.4% with 150 mm tie spacing, and (c) ρ = 2.0% with 150 mm tie spacing.

Table 5.4 Contribution of concrete on axial capacity of different RC columns concerning plain concrete column.

Column Name	P_{peak} (kN)	$P_{C\text{-}peak}$ (kN)	Contribution of Concrete (%)		Variation (%)
			W.R.T. Plain Concrete Column	From Strain Data	
$R_0C_0F_0$_0_0	769.9	769.9	100.0	-	
$R_0C_0F_0$_1.4_75	971.7	823.6	79.2	84.8	7.0
$R_0C_0F_0$_1.4_150	902.0	744.7	85.3	82.6	-3.3
$R_{30}C_{15}F_0$_0_0	402.5	402.5	100.0	-	
$R_{30}C_{15}F_0$_1.4_75	608.1	429.0	66.2	70.5	6.6
$R_{30}C_{15}F_0$_1.4_150	545.0	361.3	73.9	66.3	-10.2
$R_{30}C_0F_{0.5}$_0_0	787.2	787.2	100.0	-	
$R_{30}C_0F_{0.5}$_1.4_75	968.3	832.6	81.3	86.0	5.8
$R_{30}C_0F_{0.5}$_1.4_150	913.9	761.8	86.1	83.4	-3.2
$R_{30}C_{15}F_{0.5}$_0_0	425.0	425.0	100.0	-	
$R_{30}C_{15}F_{0.5}$_1.4_75	626.4	457.5	67.8	73.0	7.7
$R_{30}C_{15}F_{0.5}$_1.4_150	604.3	427.7	70.3	70.8	0.6

5.7 Volumetric Strain

The true behavior of confined concrete can be captured by examining its volumetric response. In a triaxial state of stress, volumetric strain ε_v is defined as the volume change per unit volume as follows:

$$\varepsilon_v = \varepsilon_a + 2\varepsilon_l \tag{5.1}$$

where ε_a is the axial strain; and ε_l is the lateral strain of the column. It is assumed that a positive volumetric strain indicates volume reduction, whereas a negative value indicates expansion.

The volumetric strain response of different columns is shown in Figure 5.9 to Figure 5.11. The effect of CR, fiber, longitudinal reinforcement ratio and tie spacing is presented. In the figures, the initial slope of all curves is close to $(1 - 2\nu).\varepsilon_a$ (where ν is the Poisson's ratio of the concrete assumed to be equal to 0.20 and ε_a is the axial strain of concrete), which corresponds to the perfectly elastic condition. The curves deviate from this line and reach their maximum as the load approaches its peak value. This point corresponds to the onset of uncontrolled crack growth leading to failure.

From Figure 5.9 it is seen that the volumetric strain curve of plain concrete columns is almost close to the perfectly elastic curve. However, for the reinforced concrete columns, these curves deviate from the perfectly elastic curve. The larger tie-spaced columns show comparatively higher volumetric strain compared to smaller tie-spaced columns. Besides, the columns with larger tie spacing, the curve rapidly develops into failure. On the other hand, in the case of smaller tie spacing, the curves are more stable as presented in Figure 5.10. As the small spacing of the ties provides a lateral constraint against the cracked concrete core it delays unstable crack propagation. From Figure 5.10, it is also seen that the volumetric strain of rubberized recycled concrete (R^2C) columns are comparatively higher than that of recycled aggregate concrete (RAC) columns. The same case also happens for fiber-reinforced recycled concrete (FR^2C) columns and fiber-reinforced rubberized recycled concrete (FR^3C) columns. Figure 5.11 demonstrates that the columns containing a higher reinforcement ratio provide a lower volumetric strain and a more stable curve compared to the lower reinforcement ratio.

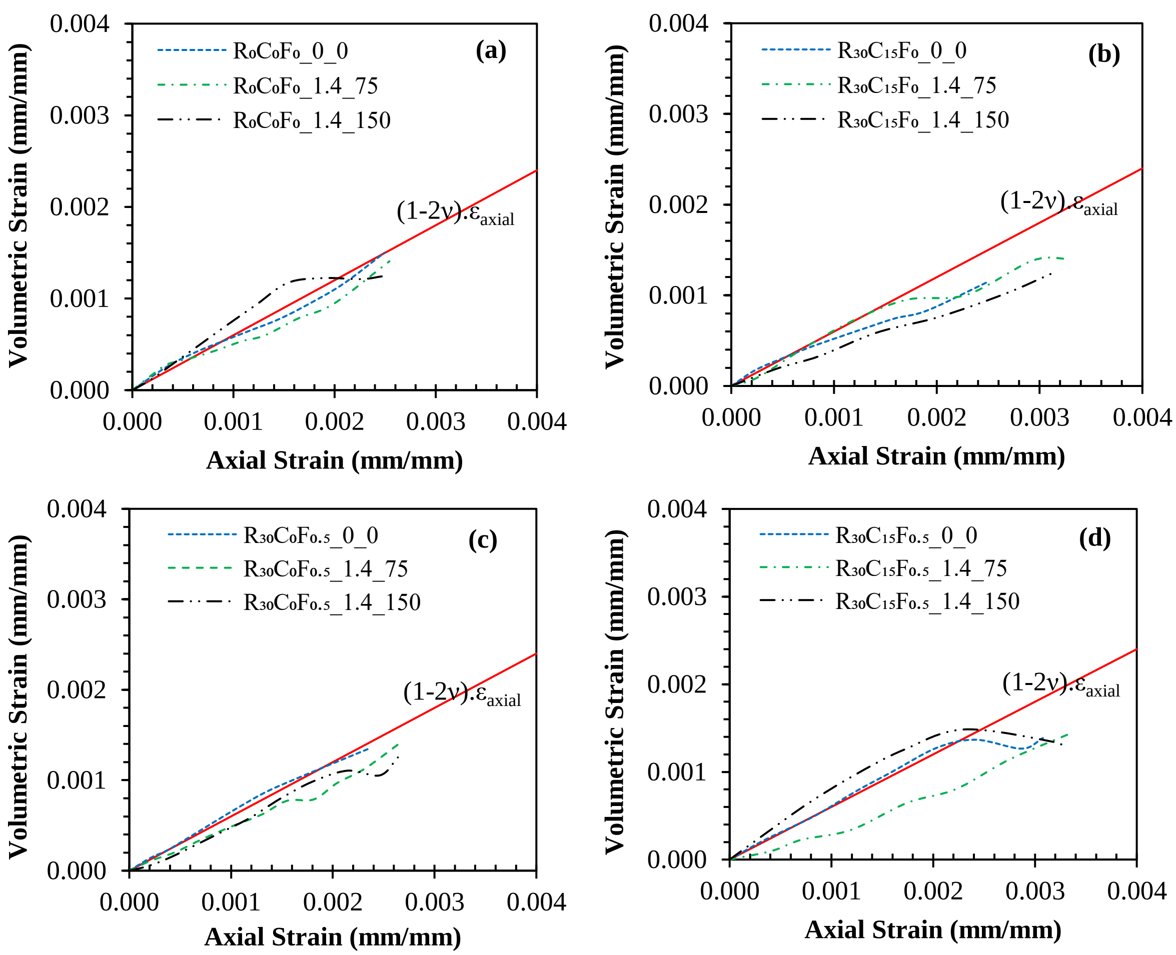

Figure 5.9 Effect of tie spacing on volumetric strain response: (a) control columns, (b) R^2C columns, (c) fiber-reinforced recycled concrete (FR^2C) columns, and (d) FR^3C columns.

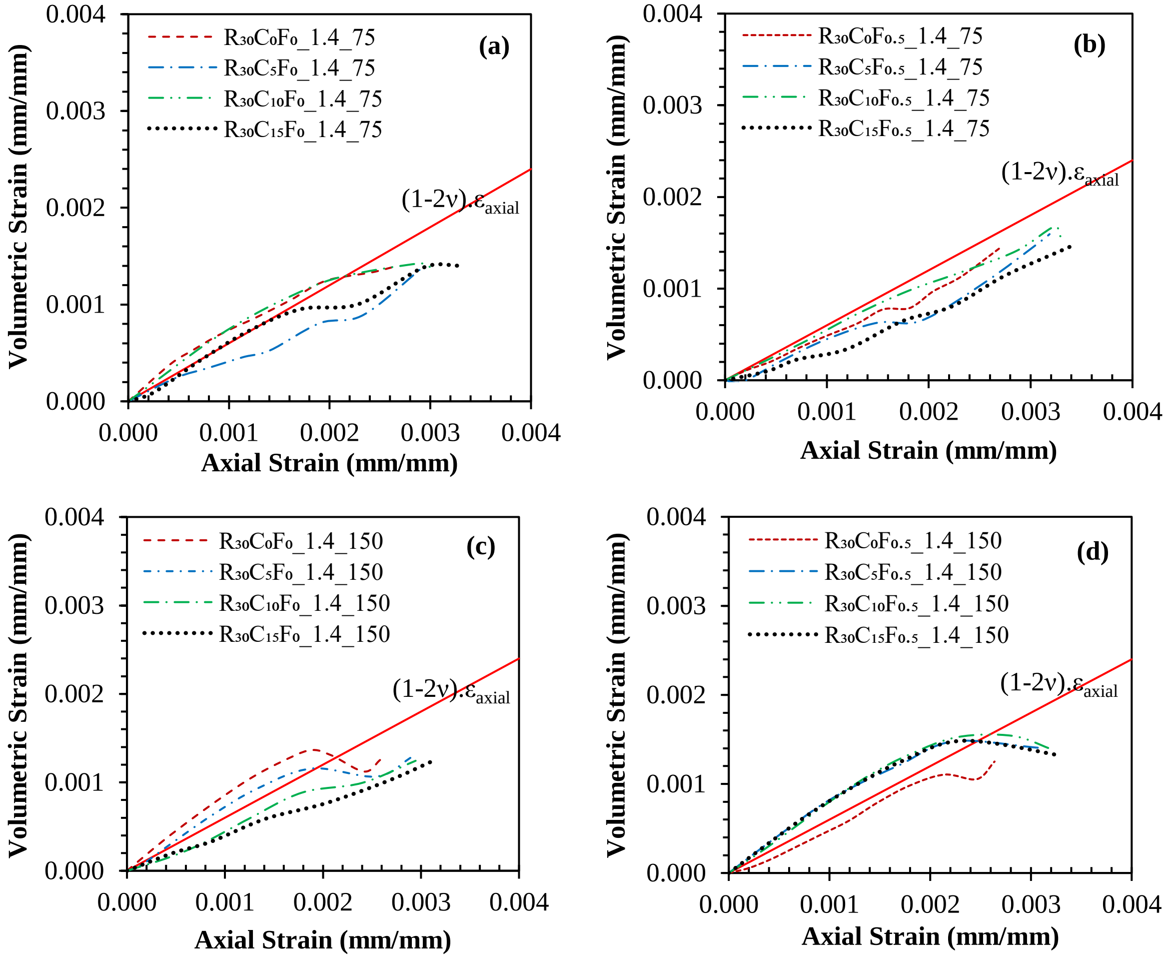

Figure 5.10 Volumetric strain response of (a) R^2C columns with 75 mm tie spacing, (b) FR^3C columns with 75 mm tie spacing, (c) R^2C columns with 150 mm tie spacing, and (d) FR^3C columns with 150 mm tie spacing.

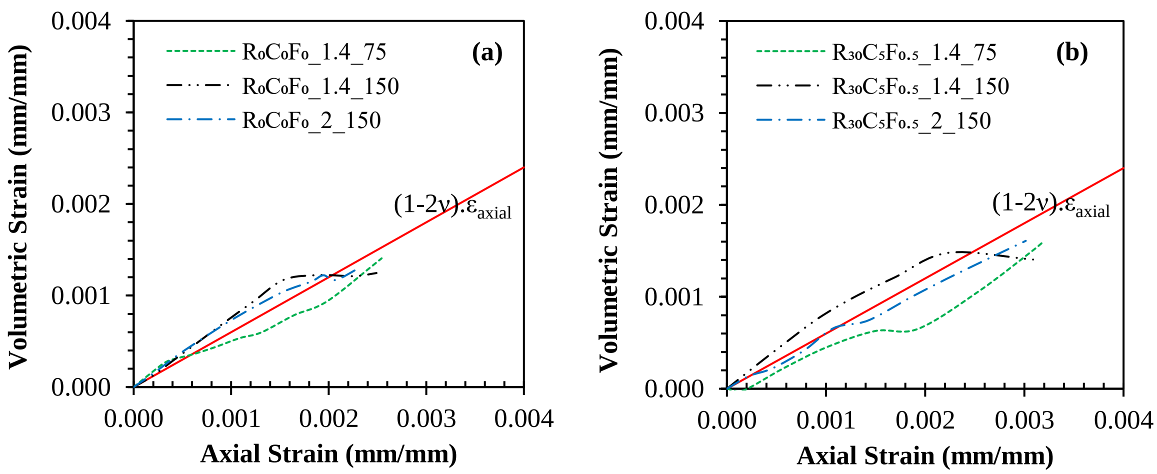

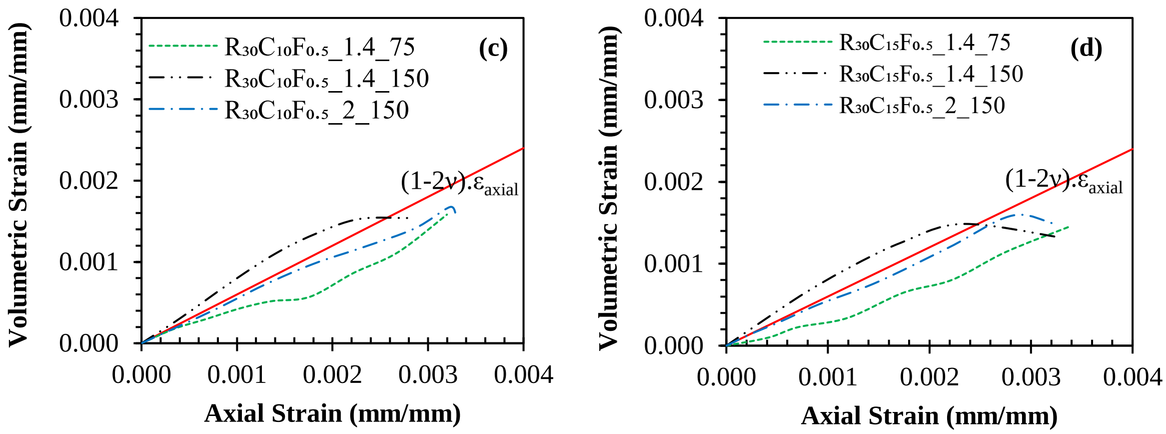

Figure 5.11 Effect of longitudinal reinforcement on volumetric strain of columns with (a) 0% CR, (b) 5% CR, (c) 10% CR, and (d) 15% CR content.

5.8 Ductility

The ductility value of different columns is determined from the load-deformation curves using the displacement ductility method proposed by Pessiki and Pieroni [215] and Choi and Yun [21]. The displacement ductility is the ratio of the axial deformation of the column under an axial load up to 85% of the maximum axial load on the descending portion of the load-deformation curve, i.e., $\Delta_{0.85}$ to the deformation corresponding to the yield point, Δ_y.

$$\mu = \frac{\Delta_{0.85}}{\Delta_y} \tag{5.2}$$

Figure 5.12 and Table 5.5 present the ductility value of different RC columns. Overall it is seen that the R^2C and FR^3C columns exhibit comparatively higher ductility than that of the control one. However, the ductility of RAC columns is almost similar to that of NAC columns. With increasing the CR content, the ductility value increases and it further increases after the inclusion of fiber content into the concrete mixtures. For R^2C columns with the longitudinal reinforcement ratio of 1.4% and 75 mm tie spacing, the ductility value increases 12.3%, 15.7%, and 20.2% for 5%, 10%, and 15% CR content, respectively compared to the control column. After adding 0.5% PP fiber the ductility value is increased almost 1.20, 1.52, 1.99, 2.67 times for 0%, 5%, 10%, and 15% CR content, respectively compared to the control specimen which is approximately 23.0%, 35.7%, 72.2%, and 122.3% higher than that of corresponding R^2C specimens. The same trend is also observed for 150 mm-tie spaced columns. As fiber can form a bridge inside the densified concrete matrix on either side of the crack it can resist load against a larger deflection after its yielding point. Fiber also creates a strong bond between aggregate and cement paste and acts as a barrier against crack propagation. Thus, the ductility value increases and resulted in a change in the failure mode by limiting the progression of cracks and enhancing the aggregate interlock along failure planes.

Due to the lower confinement effect of 150 mm tie-spaced columns, the ductility value is slightly decreased compared to 75 mm tie-spaced columns. This reduction is near to 1.1%, 8.0%, 4.9%, 2.8% for R^2C specimens and 17.3%, 27.6%, 22.9%, 39.7% for FR^3C specimens for 150 mm tie-spaced columns with 0%, 5%, 10%, 15% CR content, respectively. This lower ductility of larger tie-spaced columns also affects the failure mechanism. The larger tie-spaced columns failed suddenly without providing any significant warning compared to the smaller tie-spaced columns. From Figure 5.12 (c) it is seen that no significant difference has occurred in ductility after increasing the longitudinal reinforcement ratio from 1.4% to 2.0%.

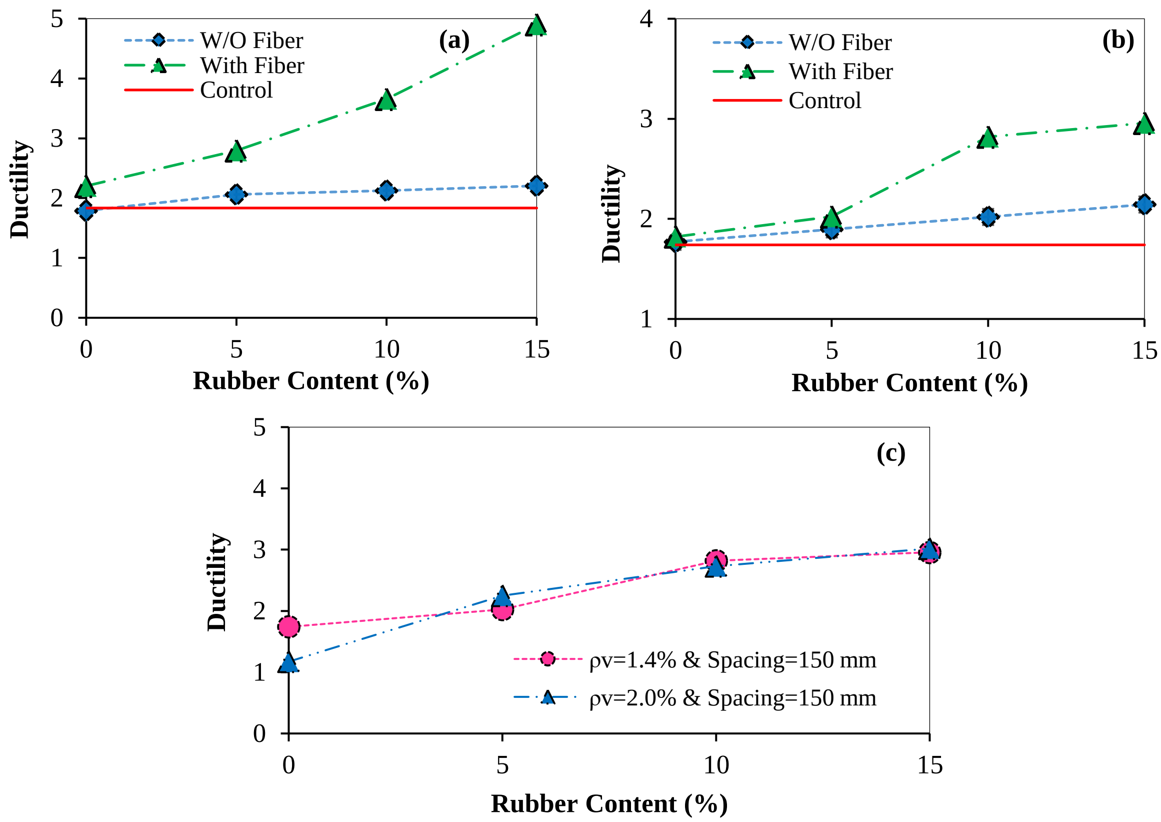

Figure 5.12 Variation in ductility of RC columns: (a) ρ = 1.4% with 75 mm tie spacing, (b) ρ = 1.4% with 150 mm tie spacing, (c) comparison between $\rho = 1.4\%$ and $\rho = 2.0\%$.

Table 5.5 Summary of ductility and toughness value of different RC columns.

Column Name	Δ_y (mm)	Δ_{Peak} (mm)	$\Delta_{0.85}$ (mm)	Δ_{peak}/Δ_y	μ	Toughness (kN.mm)
$R_0C_0F_0$_1.4_75	3.95	6.79	7.20	1.72	1.83	3202
$R_{30}C_0F_0$_1.4_75	4.34	7.60	7.78	1.75	1.79	2510
$R_{30}C_5F_0$_1.4_75	4.90	9.98	10.08	2.04	2.06	2537
$R_{30}C_{10}F_0$_1.4_75	5.41	11.19	11.48	2.07	2.12	2596
$R_{30}C_{15}F_0$_1.4_75	5.89	11.56	12.99	1.96	2.21	3529
$R_{30}C_0F_{0.5}$_1.4_75	4.31	7.68	9.50	1.78	2.20	3221
$R_{30}C_5F_{0.5}$_1.4_75	3.98	10.58	11.13	2.66	2.80	3364
$R_{30}C_{10}F_{0.5}$_1.4_75	3.72	11.91	13.61	3.20	3.66	4741
$R_{30}C_{15}F_{0.5}$_1.4_75	3.26	11.97	15.98	3.67	4.90	5535
$R_0C_0F_0$_1.4_150	3.42	5.73	6.00	1.67	1.74	2315
$R_{30}C_0F_0$_1.4_150	3.42	5.70	6.06	1.67	1.77	2297
$R_{30}C_5F_0$_1.4_150	3.41	6.01	6.46	1.76	1.89	2025
$R_{30}C_{10}F_0$_1.4_150	3.85	6.68	7.78	1.73	2.02	2144
$R_{30}C_{15}F_0$_1.4_150	4.63	8.23	9.93	1.78	2.14	2317
$R_{30}C_0F_{0.5}$_1.4_150	4.30	6.75	7.83	1.57	1.82	2690
$R_{30}C_5F_{0.5}$_1.4_150	4.49	8.37	9.09	1.86	2.02	2324
$R_{30}C_{10}F_{0.5}$_1.4_150	3.19	8.77	9.00	2.75	2.82	2417
$R_{30}C_{15}F_{0.5}$_1.4_150	3.06	8.83	9.05	2.88	2.96	2548
$R_0C_0F_0$_2_150	6.83	7.93	8.01	1.16	1.17	3073
$R_{30}C_5F_{0.5}$_2_150	3.82	8.13	8.58	2.13	2.25	2563
$R_{30}C_{10}F_{0.5}$_2_150	3.8	9.88	10.23	2.63	2.73	3164
$R_{30}C_{15}F_{0.5}$_2_150	4.55	11.21	13.73	2.46	3.02	4677

Note:
Δ_y = Deformation Corresponding to First Crack/Yielding Point, Δ_{Peak} = Deformation Corresponding to Peak Axial Load, $\Delta_{0.85}$ = Deformation Corresponding to 85% of the maximum axial load on the descending portion, and μ = Ductility.

5.9 Toughness

The toughness of the RC columns is calculated by summing up the area under the axial load versus the axial deformation curve up to 85% of the maximum axial load on the descending portion. The toughness value of different RC columns is summarized in Table 5.5 and presented in Figure 5.13. Overall it is seen that the R^2C columns exhibit comparatively lower toughness than that of the control specimens. However, adding fiber content into the concrete mixture improves the toughness value.

For R^2C columns with the longitudinal reinforcement ratio of 1.4% and 75 mm tie spacing, the toughness value is decreased by 21.6%, 20.8%, 18.9% for 0%, 5%, and 10% CR content, and then increased by 10.2% for 15% CR content compared to control specimen. As the axial capacity of R^2C specimens is comparatively lower than that of control columns, the area under the curves is reduced. However, though most of the R^2C specimens provide lower toughness, it increases with increasing the CR content. Thus, the columns with 15% CR content exhibit a higher toughness value than that of the control one due to the incremental tendency of deformation capacity with increasing the CR content. After adding 0.5% PP fiber the toughness value is increased almost 1.01, 1.05, 1.48, 1.73 times for 0%, 5%, 10%, and 15% CR content, respectively compared to the control specimen which is approximately 28.3%, 32.6%, 82.6%, and 56.8% higher than that of corresponding R^2C specimens. The same trend is also observed for 150 mm tie-spaced columns as presented in Table 5.5 and Figure 5.13.

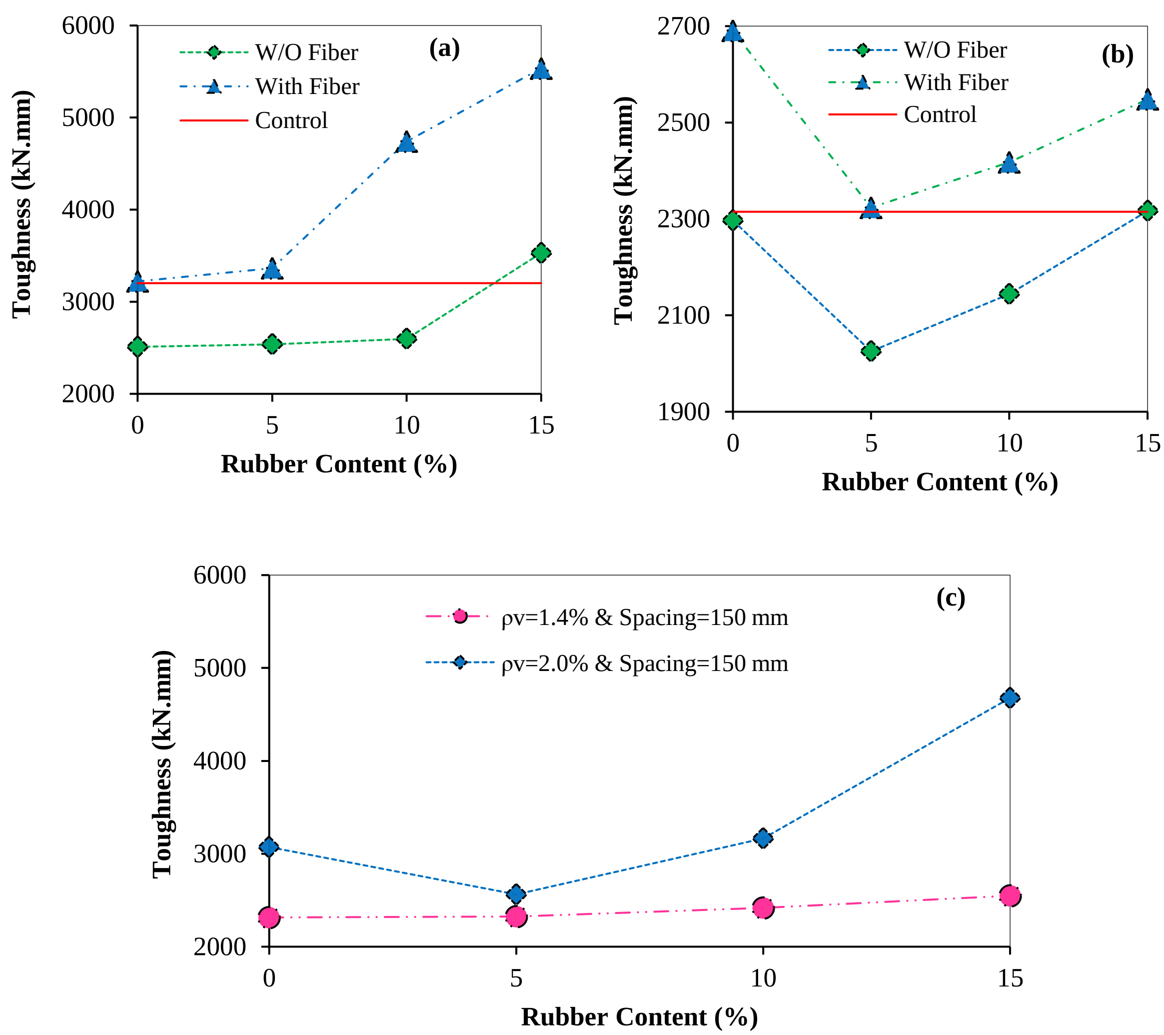

Figure 5.13 Variation in toughness of RC columns: (a) ρ = 1.4% with 75 mm tie spacing, (b) ρ = 1.4% with 150 mm tie spacing, and (c) comparison between ρ = 1.4% and ρ = 2.0%.

Comparing the 75 mm tie-spaced columns with 150 mm tie-spaced columns it is observed that the toughness value of larger tie-spaced columns is decreased significantly. The reduction percentage is almost 8.5, 20.2, 17.4, 34.4 for R^2C specimens and 16.5, 30.9, 49.0, 54.0 for FR^3C specimens for 0%, 5%, 10%, 15% CR content, respectively. On the other hand, an improved toughness value has been achieved by increasing the longitudinal reinforcement ratio from 1.4% to 2.0% as presented in Figure 5.13 (c). For the FR^3C columns having $\rho = 2.0\%$, the toughness value is increased by approximately 32.8%, 10.3%, 30.9%, and 83.5% compared to $\rho = 1.4\%$ for 0%, 5%, 10% and 15% CR content, respectively.

5.10 Dilation Ratio

The dilation ratio is defined as the ratio between the transverse strain and the axial strain of the column under any specific axial load. And this ratio corresponding to the peak load is termed Poisson's ratio (ν).

$$\nu = -\frac{\varepsilon_l}{\varepsilon_a} \tag{5.3}$$

Where ε_l is the lateral strain and ε_a is the axial strain of the column.

The dilation ratio vs axial strain of different columns is presented in Figure 5.14 and the variation in Poisson's ratio of different RC columns is shown in Figure 5.15. As seen in Figure 5.14, the dilation ratio for all the reinforced concrete columns ranges between 0.10 and 0.33 up to the peak axial strains of approximately 0.0035 whereas for plain concrete columns it varies between 0.10 and 0.30. In most cases, the dilation ratio increases with increasing the axial strain or axial load. However, from Figure 5.15 (a & b) it is seen that with increasing the CR content the Poisson's ratio increases which signifies better deformability and energy absorption capacity. On the contrary, the inclusion of fiber content makes the concrete comparatively stiff and as a result the Poisson's ratio slightly decreases. The Poisson's ratio of R^2C columns with the longitudinal reinforcement ratio of 1.4% and 75 mm tie spacing is 0.24, 0.26, 0.27, and 0.29 for 0%, 5%, 10%, and 15% CR content, respectively whereas for FR^3C columns this ratio is 0.23, 0.25, 0.26, 0.28, respectively. In the case of the specimens with larger tie spacing, the Poisson's ratio increases compared to the smaller tie spacing. Having the longitudinal reinforcement ratio (1.4%), the Poisson's ratio of R^2C columns with 150 mm tie spacing is 0.26, 0.28, 0.29, and 0.30 for 0%, 5%, 10%, and 15% CR content, respectively whereas for FR^{3}C columns this ratio is 0.26, 0.27, 0.28, 0.30, respectively. Investigating the effect of longitudinal reinforcement ratio on Poisson's ratio it is found that the Poisson's ratio decreases for a higher reinforcement ratio. The Poisson's ratio of FR^{3}C columns having a longitudinal reinforcement ratio of 2.0% and 150 mm tie spacing is 0.22, 0.23, 0.25, and 0.27 for 0%, 5%, 10%, and 15% CR content, respectively as presented in Figure 5.15 (c). From Figure 5.15 (d) it is noticed that the plain concrete columns provide a comparatively lower Poisson's ratio than that of RC columns.

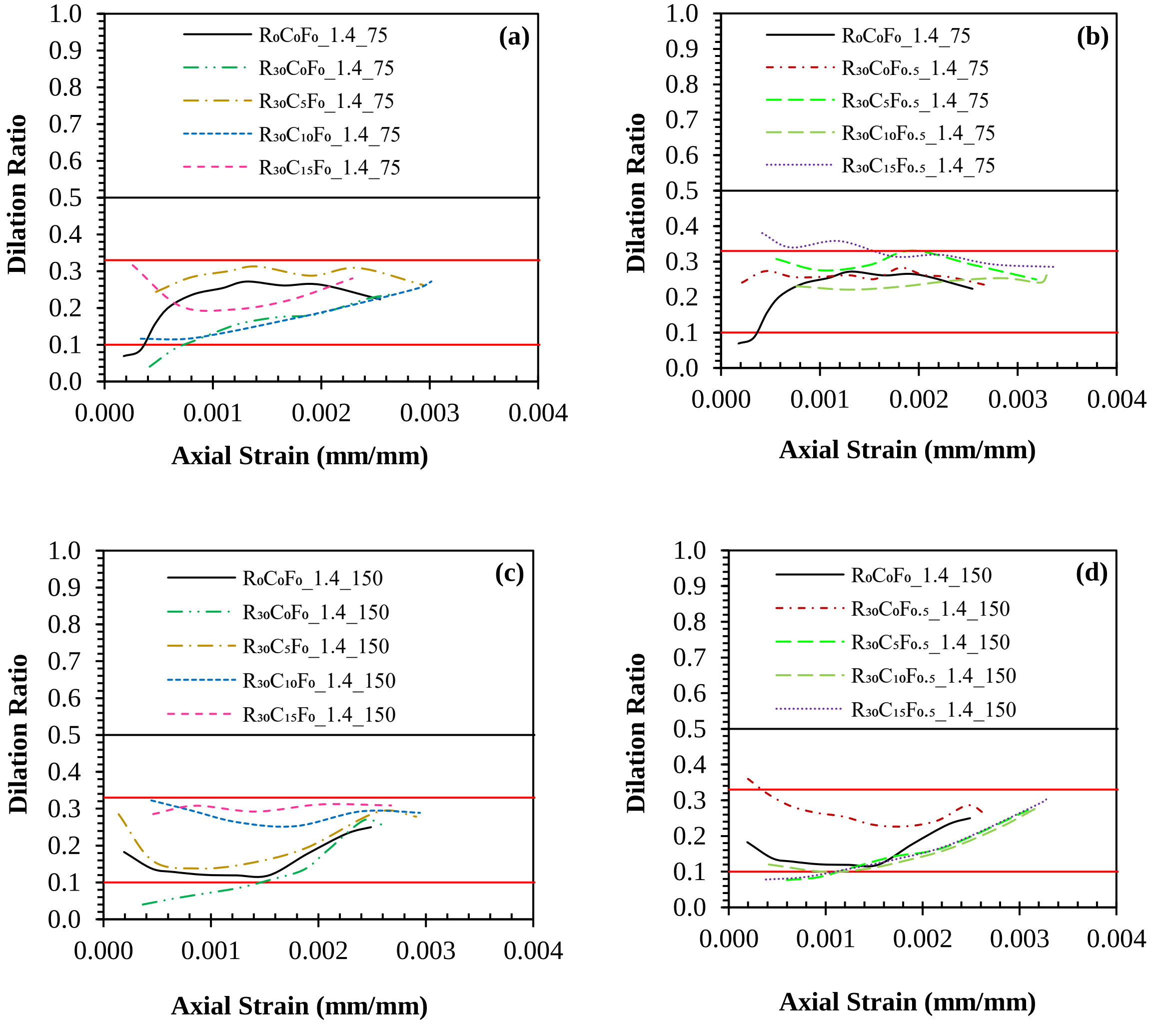

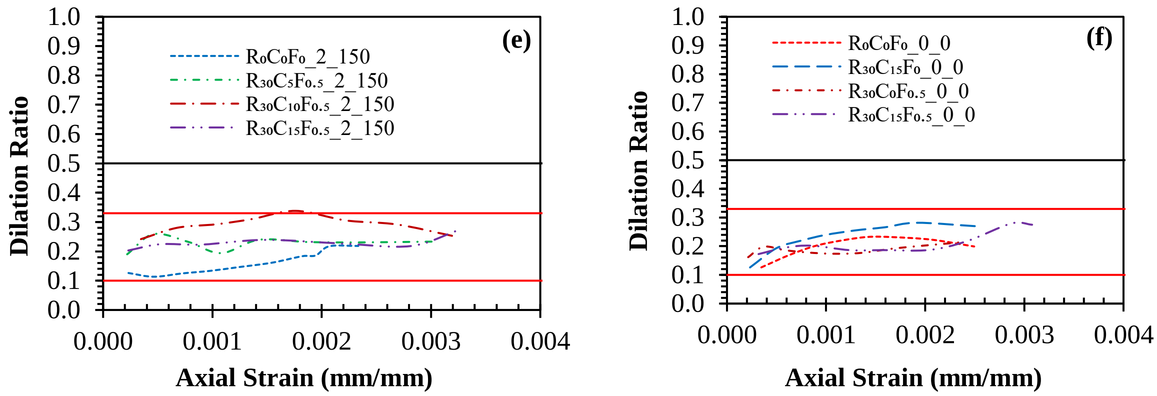

Figure 5.14 Dilation vs axial strain curves of columns: (a) R^2C with ρ = 1.4% and 75 mm tie spacing, (b) FR^3C with ρ = 1.4% and 75 mm tie spacing, (c) R^2C with ρ = 1.4% and 150 mm tie spacing, (d) FR^3C with ρ = 1.4% and 150 mm tie spacing, (e) FR^3C with ρ = 2.0% and 150 mm tie spacing, (f) plain concrete columns.

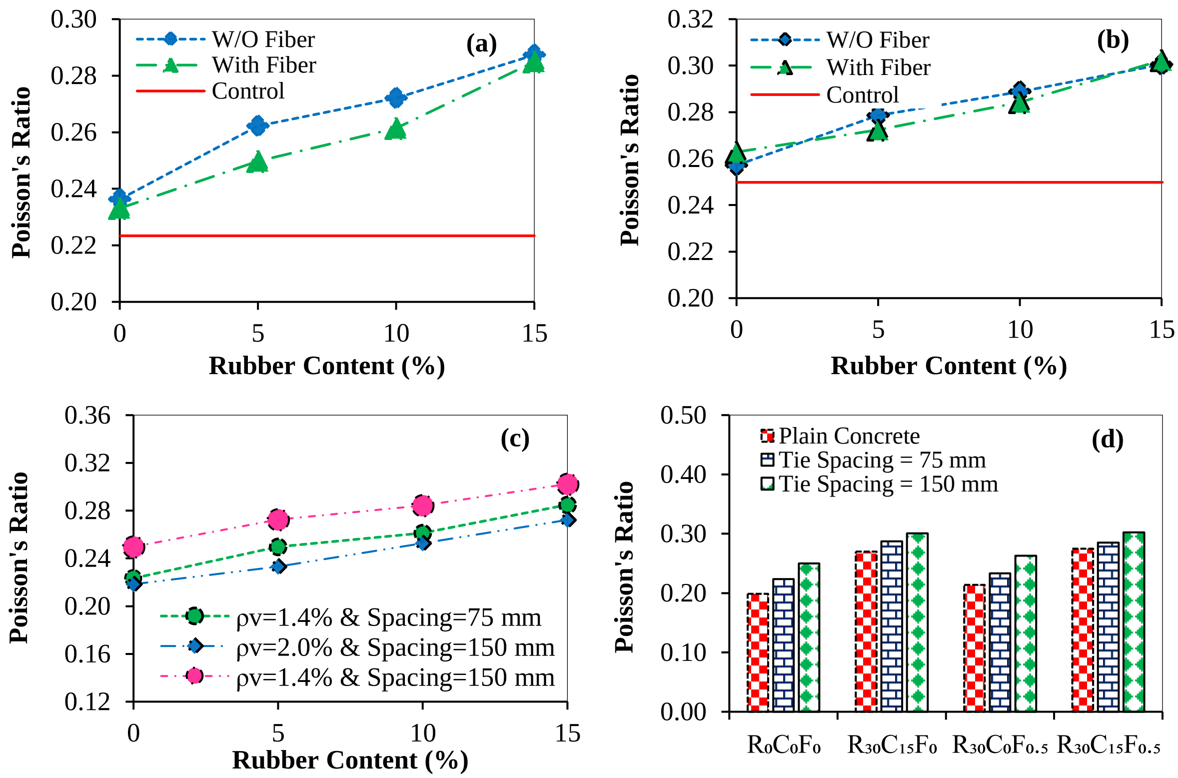

Figure 5.15 Variation in Poisson's ratio of different RC columns: (a) ρ = 1.4% with 75 mm tie spacing, (b) ρ = 1.4% with 150 mm tie spacing, (c) comparison of columns with ρ = 1.4% and ρ = 2.0%, and (d) comparison of RC columns with the plain concrete column.

5.11 Curvature Ductility

The moment-curvature relationships of different reinforced concrete columns are investigated by using software named Response 2000 [216]. The moment vs curvature graphs of different columns is presented in Figure 5.16. From the moment-curvature curves, the curvature ductility is calculated. The curvature ductility, μ_k is determined by using Eq. 5.4 which is an appropriate performance criterion for the seismic assessment of structural elements [24, 217]. It's a sectional property of the reinforced concrete column. The results of different sectional properties are summarized in Table 5.6.

$$\mu_k = \frac{\varphi_u}{\varphi_y} \tag{5.4}$$

where, φ_u and φ_y are ultimate curvature and yield curvature, respectively.

From Figure 5.16 it is seen that all the curves exhibit the same pattern up to the yield point. But after the yield point, the R^2C and FR^3C columns provide higher ductile phenomena. These curves go far longer compared to the control one after reaching their yield moments or even ultimate moments. From Figure 5.16 and Table 5.6 it is seen that the ultimate curvature moment decreases with increasing the CR content. However, the inclusion of fiber content can further increase the moment capacity. The longitudinal reinforcement ratio has a positive impact on the ultimate curvature moment. On the contrary, the tie spacing does not have any significant effect on the ultimate moment rather than the yield moment. The larger tie-spaced columns reach their yield point comparatively earlier than the smaller tie-spaced columns.

The variation in curvature ductility of different RC columns is presented in Figure 5.17. The results indicate that tire rubber concrete specimens can develop considerably higher curvature ductility compared to similar conventional concrete columns. Besides, the inclusion of fiber content into the rubberized concrete can further increase the curvature ductility. For 75 mm tie spaced columns with $\rho = 1.4\%$, the curvature ductility of R^2C columns containing 5% CR content is the same as the control one but then increases by 10% and 21% for 10% and 15% CR content. For FR^3C columns having the same ρ and tie spacing, this incremental percentage is 21.0, 33.1, and 33.1 for 5%, 10%, and 15% CR content, respectively. The larger tie-spaced (150 mm) columns provide lower curvature ductility compared to smaller tie-spaced (75 mm) columns. All 150 mm tie-spaced columns exhibit an average of 9% lower ductility compared to 75 mm tie-spaced columns. Moreover, the curvature ductility may further decrease for increasing the ρ value from 1.4% to 2.0%. The decreasing percentage is 24.9, 24.9, and 17.4 for 5%, 10%, and 15% CR content. Comparing the control column with the RAC column it is seen that the inclusion of RCA reduces the curvature ductility value. From the test results, it can be concluded that an enhancing curvature ductility can be achieved by maintaining a lower tie spacing along with a higher percentage of CR content which may further increase by incorporating fiber content into the column specimens. Having higher curvature ductility is usually accompanied by better seismic performance and less structural damage during strong earthquakes. Therefore, the rubberized concrete or fiber-reinforced rubberized concrete is shown to be a potentially suitable material for seismic applications.

Table 5.6 Summary of curvature ductility of different RC columns.

Column Name	Yield Moment (kN.m)	Yield Curvature (rad/m)	Ultimate Moment (kN.m)	Ultimate Curvature (rad/m)	Curvature Ductility
$R_0C_0F_0$_1.4_75	7.33	0.0258	8.95	0.098	3.80
$R_{30}C_0F_0$_1.4_75	7.19	0.0274	8.73	0.094	3.45
$R_{30}C_5F_0$_1.4_75	7.25	0.0261	8.59	0.099	3.80
$R_0C_{10}F_0$_1.4_75	7.13	0.0270	8.41	0.113	4.18
$R_0C_{15}F_0$_1.4_75	6.84	0.0270	7.99	0.124	4.59
$R_{30}C_0F_{0.5}$_1.4_75	7.17	0.0298	9.01	0.125	4.18
$R_{30}C_5F_{0.5}$_1.4_75	7.14	0.0273	8.81	0.126	4.60
$R_{30}C_{10}F_{0.5}$_1.4_75	7.09	0.0277	8.59	0.140	5.05
$R_{30}C_{15}F_{0.5}$_1.4_75	7.01	0.0277	8.45	0.140	5.05
$R_0C_0F_0$_1.4_150	7.39	0.0286	9.50	0.099	3.45
$R_{30}C_0F_0$_1.4_150	7.32	0.0314	8.73	0.099	3.14
$R_{30}C_5F_0$_1.4_150	7.18	0.0287	8.59	0.099	3.45
$R_0C_{10}F_0$_1.4_150	7.02	0.0297	8.41	0.113	3.80
$R_0C_{15}F_0$_1.4_150	6.91	0.0297	7.99	0.124	4.18
$R_{30}C_0F_{0.5}$_1.4_150	7.23	0.0328	9.01	0.125	3.80
$R_{30}C_5F_{0.5}$_1.4_150	7.11	0.0326	8.82	0.136	4.18
$R_{30}C_{10}F_{0.5}$_1.4_150	6.97	0.0304	8.59	0.140	4.59
$R_{30}C_{15}F_{0.5}$_1.4_150	6.90	0.0305	8.45	0.140	4.60
$R_0C_0F_0$_2_150	11.17	0.0315	12.72	0.074	2.36
$R_{30}C_5F_{0.5}$_2_150	10.72	0.0331	12.40	0.104	3.14
$R_{30}C_{10}F_{0.5}$_2_150	10.57	0.0335	11.99	0.116	3.45
$R_{30}C_{15}F_{0.5}$_2_150	10.17	0.0305	11.74	0.116	3.80

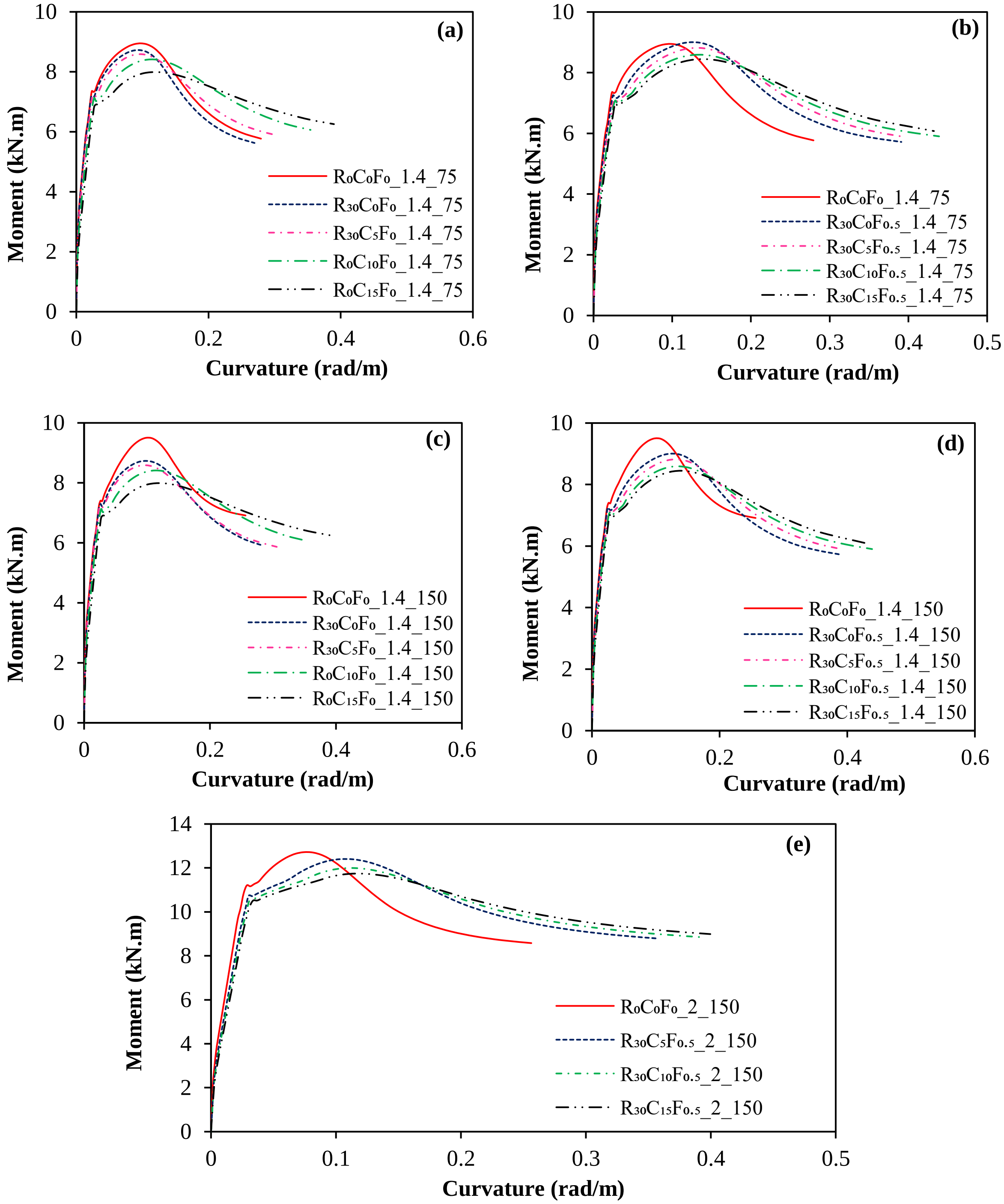

Figure 5.16 Moment–curvature relationships of different columns: (a) R^2C with ρ = 1.4% and 75 mm tie spacing, (b) FR^3C with ρ = 1.4% and 75 mm tie spacing, (c) R^2C with ρ = 1.4% and 150 mm tie spacing, (d) FR^3C with ρ = 1.4% and 150 mm tie spacing, (e) FR^3C with ρ = 2.0% and 150 mm tie spacing.

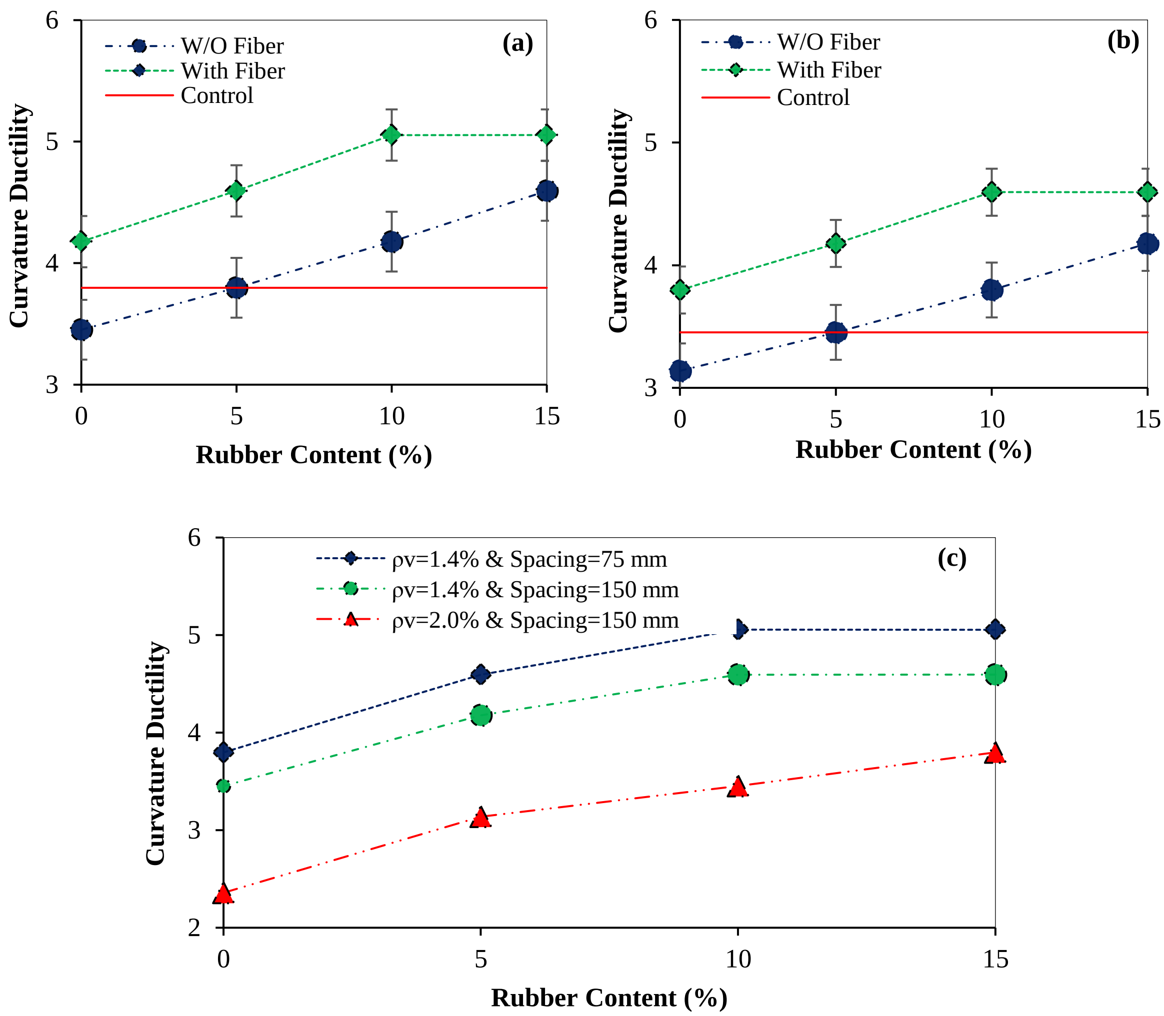

Figure 5.17 Variation in curvature ductility of RC columns: (a) ρ = 1.4% with 75 mm tie spacing, (b) ρ = 1.4% with 150 mm tie spacing, and (c) comparison between ρ = 1.4% and ρ = 2.0%.

5.12 Influence of Tie Spacing

Though the nominal capacity equation for conventional concrete ignores the tie-spacing effect, the behavior of R^2C and FR^3C columns significantly depends on it. Two different tie spacing has been considered such as 75 mm and 150 mm to maintain the same longitudinal reinforcement ratio of 1.4%. The large tie-spaced R^2C columns failed suddenly by providing an explosive noise. Besides, an excessive buckling of the longitudinal and transverse steel bars occurred. The concrete cover was spalled out from half of the entire specimens and the buckling of the transverse reinforcement was clearly visualized. Besides, the concrete core was damaged. On the contrary, the specimens with smaller tie spacing experienced no visual buckling of transverse reinforcement. Besides, no significant concrete core crushing has been observed due to the confining action exerted by the closely spaced transverse reinforcement. However, for FR^3C columns, the failure modes were almost identical to the smaller tie-spaced columns. The cracking lines followed a zigzag pattern. Besides, no visible buckling of the longitudinal reinforcement had occurred. From the load-deformation curves of larger tie-spaced columns, it is observed that once the peak load is attained, the load drops almost instantly without an early warning. Besides, the axial deformation capacity, as well as axial concrete strain, are also reduced. The 150 mm tie-spaced columns exhibit 25%, 39.8%, 40.3%, 28.8% and 12.1%, 20.9%, 26.4%, 26.2% lower peak point deformation for R^2C columns and FR^3C columns compared to 75 mm tie-spaced columns with 0%, 5%, 10%, and 15% CR content, respectively. The axial concrete strain in R^2C specimens varies from 0.00263 to 0.00330 for 75 mm tie-spaced columns and 0.00259 to 0.00315 for 150 mm tie-spaced columns. For FR^3C columns it is varied from 0.00269 to 0.00339 and 0.00264 to 0.00328 for 75 mm and 150 mm tie-spaced columns, respectively.

In terms of axial capacity, the axial capacity slightly decreases for larger tie-spaced columns. Approximately 5.7%, 8.7%, 9.6%, and 10.4% peak axial load is decreased for 0%, 5%, 10% and 15% CR content for R^2C columns and for FR^3C columns this reduction is about 5.6%, 2.6%, 2.4%, and 3.5%, respectively. However, the average reduction is near 6% due to increasing the tie spacing from 75 mm to 150 mm. Besides, increasing the tie spacing can decrease the concrete contribution and increase the steel contribution on axial capacity. Though the axial deformation capacity decreases for larger tie-spaced columns, the lateral deformation, and corresponding lateral concrete strain increase. The lateral deformation corresponding to the peak axial load is increased by 5.6%, 6.2%, 2.8%, 3.0% and 3.6%, 4.9%, 2.7%, 2.2% for 0%, 5%, 10%, 15% CR content containing without fiber and with 0.5% PP fiber, respectively.

Due to the lower confinement effect of larger tie-spaced columns, the ductility is decreased by 1.1%, 8.0%, 4.9%, 2.8% for R^2C specimens and 17.3%, 27.6%, 22.9%, 39.7% for FR^3C specimens for larger tie-spaced columns compared to lower tie-spaced columns with 0%, 5%, 10%, 15% CR content, respectively. The same pattern is also observed in toughness value and curvature ductility value. In terms of the Poisson’s ratio, it increases for larger tie-spaced columns compared to the smaller tie spacing. The Poisson's ratio varies from 0.22 to 0.29 for 75 mm tie-spaced columns whereas for 150 mm tie-spaced columns it varies from 0.25 to 0.30. depending on the percentage of CR content or inclusion of fiber content.

5.13 Influence of Longitudinal Reinforcement Ratio

In general, the longitudinal reinforcement ratio has a significant effect on different uniaxial compressive behaviors of RC columns. To investigate the effect of longitudinal reinforcement ratio in FR^3C columns, four RC columns were prepared with a longitudinal reinforcement ratio of 2.0%. In terms of failure mode, a comparatively small number of cracking lines were observed in the columns compared to a lower reinforcement ratio. Only a small number of hair-crack were observed. No macro-crack were visualized in the higher ρ reinforced concrete column. Thus, the deformation capacity is increased. As expected, the axial capacity is increased by 9.5%, 12.7%, 14.3%, and 11.2% with 0%, 5%, 10%, and 15% CR content, respectively by increasing the longitudinal reinforcement ratio from 1.4% to 2.0%. thus, the contribution of longitudinal reinforcement is increased on axial capacity and simultaneously decreased the concrete contribution. The axial load carried by the longitudinal reinforcement ranges between 30.4% to 39.0% for the columns with ρ =2.0% whereas for the columns with ρ =1.4% it varies from 23.2% to 29.2% of the peak axial load.

In terms of volumetric strain and dilation ratio, the columns containing a higher reinforcement ratio provide a lower volumetric strain and Poisson's ratio compared to the lower reinforcement ratio. The Poisson's ratio for 2% longitudinal steel-reinforced columns varies from 0.22 to 0.27 depending on the percentage of CR content whereas for 1.4% steel-reinforced columns it varies from 0.25 to 0.30. However, no significant difference has been observed in the ductility. On the contrary, the toughness value is increased by approximately 32.8%, 10.3%, 30.9%, and 83.5% for 0%, 5%, 10% and 15% CR content, respectively compared to the columns with ρ =1.4%. As the axial capacity and deformation capacity, both increase for 2% steel-reinforced columns. The area under the load-deformation curve is also increased. In terms of curvature ductility, it decreases for higher steel-reinforced columns. Approximately 31.7%, 24.9%, 24.9%, and 17.4% curvature ductility is decreased for 2% steel-reinforced columns having 0%, 5%, 10%, and 15% CR content, respectively compared to 1.4% steel-reinforced columns.

5.14 Code Provision for Ultimate Capacity

The compressive strength of plain concrete columns is generally lower than the compressive strength measured on standard 150 × 300 mm concrete cylinders. A reduction factor of 0.85 is suggested by the ACI 318 [137] or α_1 by CSA A23.3-14 [140] which is mainly attributed to the differences in size and shape of RC columns and the concrete cylinder. The nominal peak axial load RC column P_0 is defined as the sum of the forces carried by the concrete and the steel, as given by the following equations of Eq. 5.5 and Eq. 5.6.

ACI 318-14 [137] : $P_0 = 0.85 f_c' (A_g - A_s) + f_y A_s$ (5.5)

CSA A23.3-14[140] : $P_0 = \alpha_1 f_c' (A_g - A_s) + f_y A_s$ (5.6)

$$\alpha_1 = 0.85 - 0.0015 f_c' \geq 0.67 \quad (5.7)$$

Where P_0 is the nominal peak axial load in N, f_c' is the compressive concrete strength in MPa, A_g is the gross area of the column in mm^2, A_s is the total area of longitudinal reinforcement in mm^2, and f_y is the yield strength of the longitudinal reinforcement in MPa.

From Figure 5.18 it is seen that the existing equations can predict the nominal capacity of uniaxial loaded conventional columns and RAC columns accurately but overestimate the R^2C and FR^3C columns. The equations overestimate up to 40% depending on the percentage of CR, the inclusion of fiber content or not, tie spacing, and longitudinal reinforcement ratio.

From the previous discussion in the section "Contribution of Concrete on Axial Capacity", it is seen that the concrete contribution varies from 0.52 to 0.68 and 0.52 to 0.78 for R^2C and FR^3C specimens, respectively. Thus, this variation in predicting axial capacity mainly happened due to the variation in compressive strength of R^2C and FR^3C. Besides, the tie spacing may provide a significant role in the axial capacity of R^2C and FR^3C columns. Thus, the existing equations have been modified and incorporate the effect of CR and tie spacing. Eq. 5.8 has been proposed for R^2C columns and Eq. 5.9 has been proposed for FR^3C columns. In these equations, the reduction factor has been changed to 0.74 from 0.85. It should be noted that the equations are valid for the range of CR content from 0% to 15%, tie spacing from 75 mm to 150 mm, and for a constant RCA percentage (30%) and PP fiber content (0.5%).

Proposed Equation for RCA with CR (W/O Fiber): $P_0 = 0.79 f_c'(A_g - A_s) + 1.20 f_y A_s - \frac{CR}{0.00022} - \frac{S}{0.0013}$ (5.8)

Proposed Equation for RCA with CR (With Fiber): $P_0 = 0.71 f_c'(A_g - A_s) + 1.20 f_y A_s - \frac{CR}{0.00017} - \frac{S}{0.0019}$ (5.9)

Where *CR* is the volumetric percentage of crumb rubber, and *S* is the tie spacing in mm.

From Figure 5.18 it is seen that the proposed equations can predict the axial capacity of R^2C and FR^3C columns with good accuracy. The coefficients of determination (R^2) are found at 0.992 and 0.991 and coefficients of variation (COV) are found at 8.58% and 6.65% for R^2C and FR^3C columns, respectively. Thus, by reducing the reduction factor and considering the effect of CR and tie spacing it is possible to accurately predict the peak axial load of R^2C and FR^3C columns.

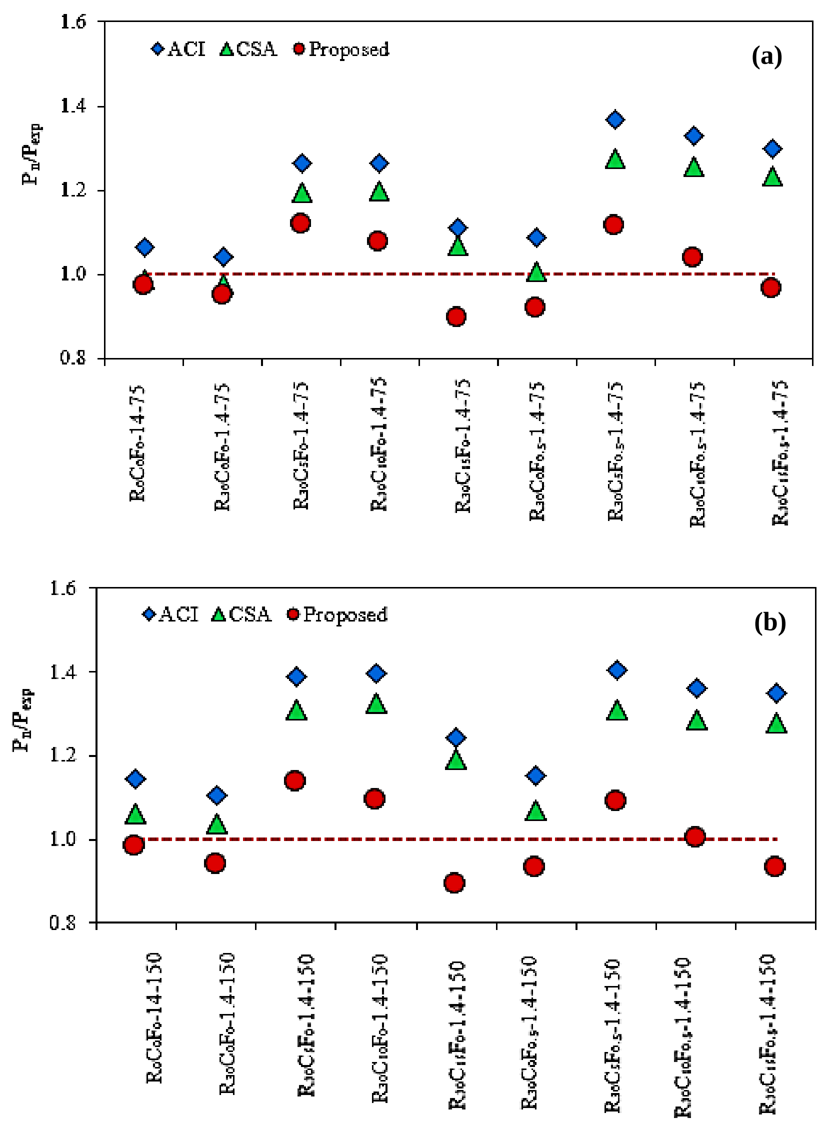

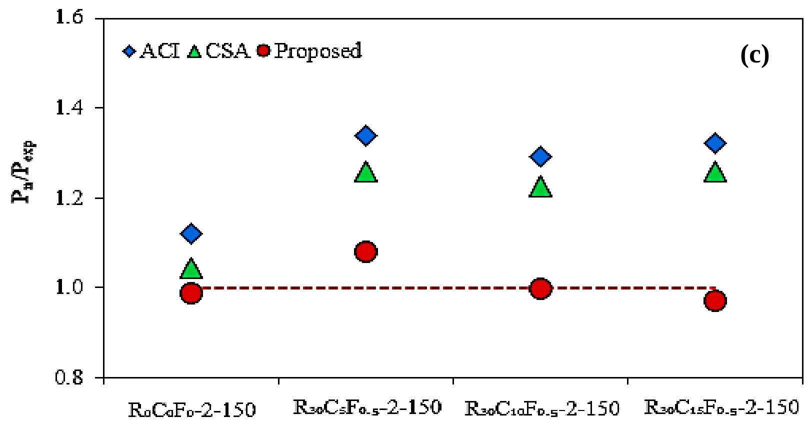

Figure 5.18 Comparison of nominal axial loads to experimental loads (a) 75 mm tie-spaced columns with ρ = 1.4%, (b) 150 mm tie-spaced columns with ρ = 1.4%,, and (c) 150 mm tie-spaced columns with ρ = 2.0%.

5.15 Summary

In conclusion, the axial capacity decreases with increasing the CR content and it is decreased by up to 37.4% and 35.5% for R^2C and FR^3C columns with 75 mm tie spacing and 39.6% and 33.0% for 150 mm tie-spaced columns. Though RAC, R^2C, and FR^3C columns provide lower axial capacity than that of the conventional column, the FR^3C columns exhibit comparatively higher axial capacity. Besides, the FR^3C columns provide more ductile phenomena without separating any concrete cover. Excessive buckling of the longitudinal and transverse steel bars, as well as the crushing of concrete core, occurs in larger tie-spaced columns. The lateral deformation and concrete strain are increased with increasing the CR percentage and after the inclusion of fiber content. In terms of ductility, the NAC and RAC columns exhibit almost similar ductility. However, the R^2C and FR^3C columns exhibit comparatively higher ductility than that of the conventional one and it is increased with increasing the CR percentage and the addition of fiber content. Approximately 167% and 70% higher ductility can be found using 0.5% fiber content in 75 mm and 150 mm tie spaced R^2C columns with 15% CR content. No significant variation in ductility is observed due to changing the longitudinal reinforcement ratio. The toughness value of R^2C columns is initially decreased for 0%, 5%, and 10% CR content but then increased for 15% CR content. On the contrary, all FR^3C columns exhibit a higher toughness value compared to the conventional column or R^2C columns.

Chapter 6

FREE VIBRATION RESPONSES OF COLUMNS

6.1 Introduction

This chapter presents the free vibration responses of different reinforced concrete (RC) columns containing recycled coarse aggregate (RCA), crumb rubber (CR), and fiber. Among twenty-six columns, nine columns having the longitudinal reinforcement ratio of 1.4% and tie spacing of 150 mm are used for the free vibration test. The effect of RCA, CR, and fiber on damping curve, damping ratio, damping coefficient, natural frequency, damping frequency, natural time-period, damping time-period, and horizontal displacement are investigated.

6.2 Data Acquisition and Processing

The accelerometer received time and acceleration arrays in the units of seconds and m/s^2, respectively. Therefore, no unit conversion of the raw data was required. Relative acceleration (between the top head acceleration and the bottom head acceleration) arrays were prepared from the raw acceleration output of the accelerometer. Before analyzing the results, noise cancellation of the raw data was required. For this purpose, first, the time series was truncated to a size equal to the power of 2. This will facilitate the frequency domain process that will be applied later. Then a "Bandpass" filter was designed with corner/ limiting frequencies that minimize the low and high-frequency noise while conserving the desired frequency range of concern. After removing the noise contamination of the raw data, Fast Fourier Transform (FFT) was applied to the acceleration data series. From the FFT analysis, the fundamental frequency and time period were obtained. The chosen filter's appropriateness and its cut-off frequencies were checked, and the filtering process was repeated if deemed necessary. The acceleration vs time data series obtained after noise cancelation was used to calculate the damping ratio. After that, from the filtered acceleration vs time data series, velocity vs time data series was obtained by integrating the acceleration data over time. Similarly, by the integration of velocity over time, displacement vs time data series was obtained. Figure 6.1 describes the whole data processing system.

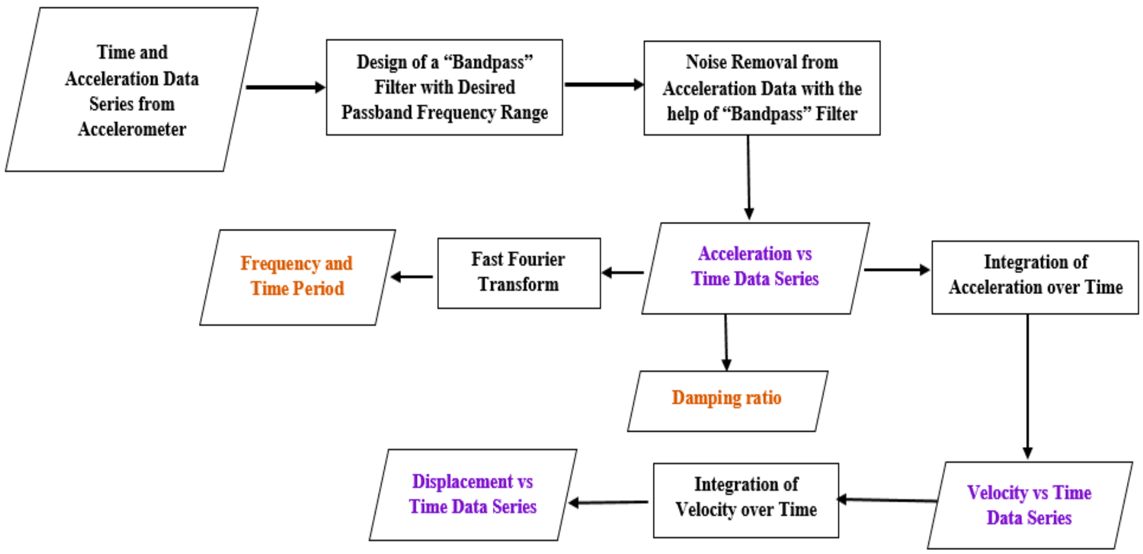

Figure 6.1 Flowchart of the data processing system.

6.3 Damping Curve

The acceleration vs time, velocity vs time, and displacement vs time responses of the columns for different combinations are shown in Figure 6.2. For better understanding, a small range of time is shown in Figure 6.3. From Figure 6.3 (a & b), it is evident that by using crumb rubber (CR) in recycled aggregate concrete (RAC) and fiber-reinforced recycled concrete (FR^2C), the damping is increased significantly compared to the columns containing no crumb rubber. The same phenomena can also be explained by Figure 6.4, where normalized peak acceleration values are plotted against the number of vibration cycles. It is observed that with increasing CR percentage (5%, 10%, and 15%) the acceleration response of the columns decreases quickly compared to the control column. Therefore, the damping curves quickly converge to zero acceleration which indicates a better damping property. From Figure 6.3 (c), it is seen that the RCA can also increase the damping property. However, a significant improvement in the damping curve is observed in Figure 6.3 (d) due to the addition of fiber content in rubberized recycled concrete (R^2C).

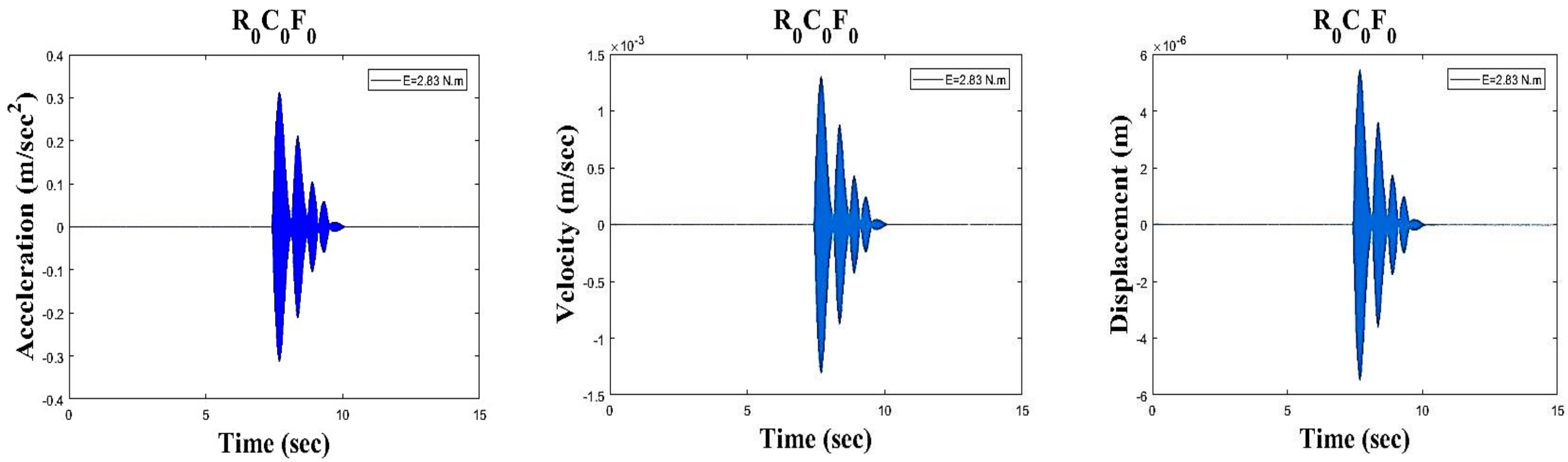

R0C0F0
E=2.83 N.m
Acceleration (m/sec2)
Time (sec)
R0C0F0
×10-3
E=2.83 N.m
Velocity (m/sec)
Time (sec)
R0C0F0
×10-6
E=2.83 N.m
Displacement (m)
Time (sec)

(a)

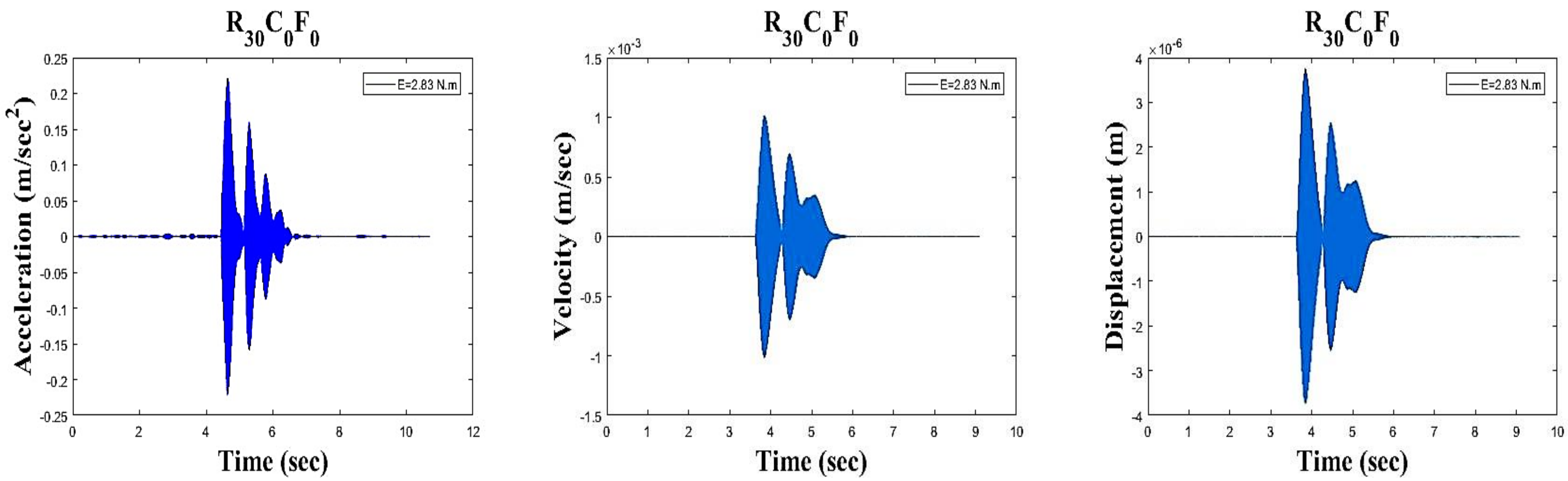

R30C0F0
E=2.83 N.m
Acceleration (m/sec2)
Time (sec)
R30C0F0
×10-3
E=2.83 N.m
Velocity (m/sec)
Time (sec)
R30C0F0
×10-6
E=2.83 N.m
Displacement (m)
Time (sec)

(b)

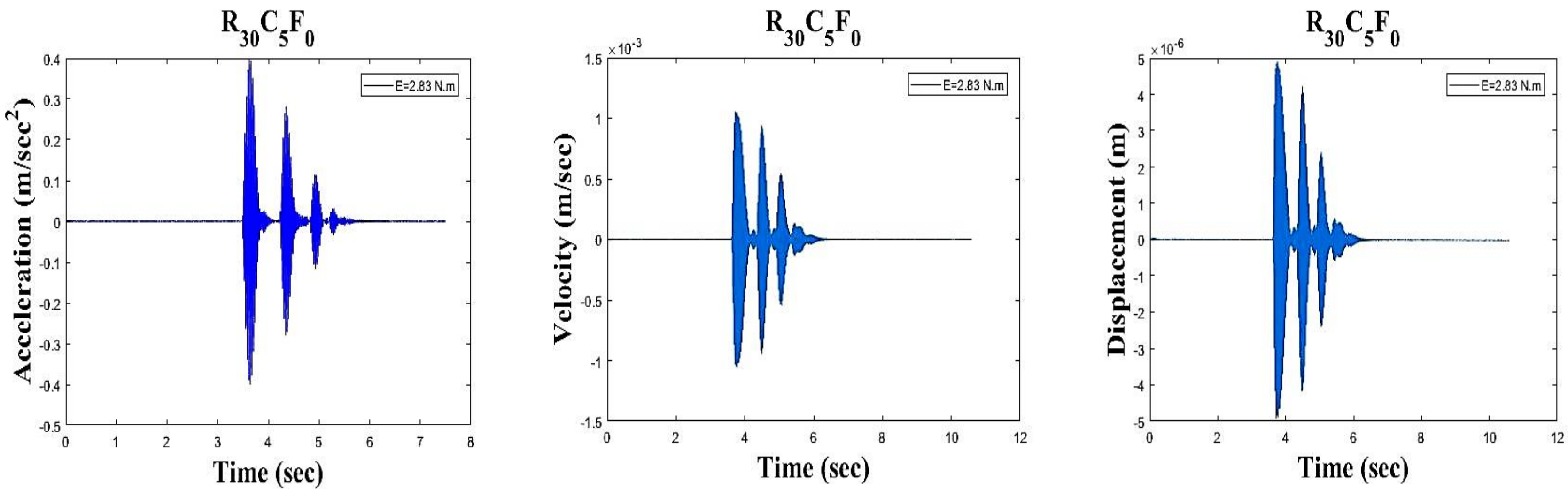
R30C5F0
Acceleration (m/sec2)
Time (sec)
E=2.83 N.m
R30C5F0
Velocity (m/sec)
Time (sec)
E=2.83 N.m
R30C5F0
Displacement (m)
Time (sec)
E=2.83 N.m

(c)

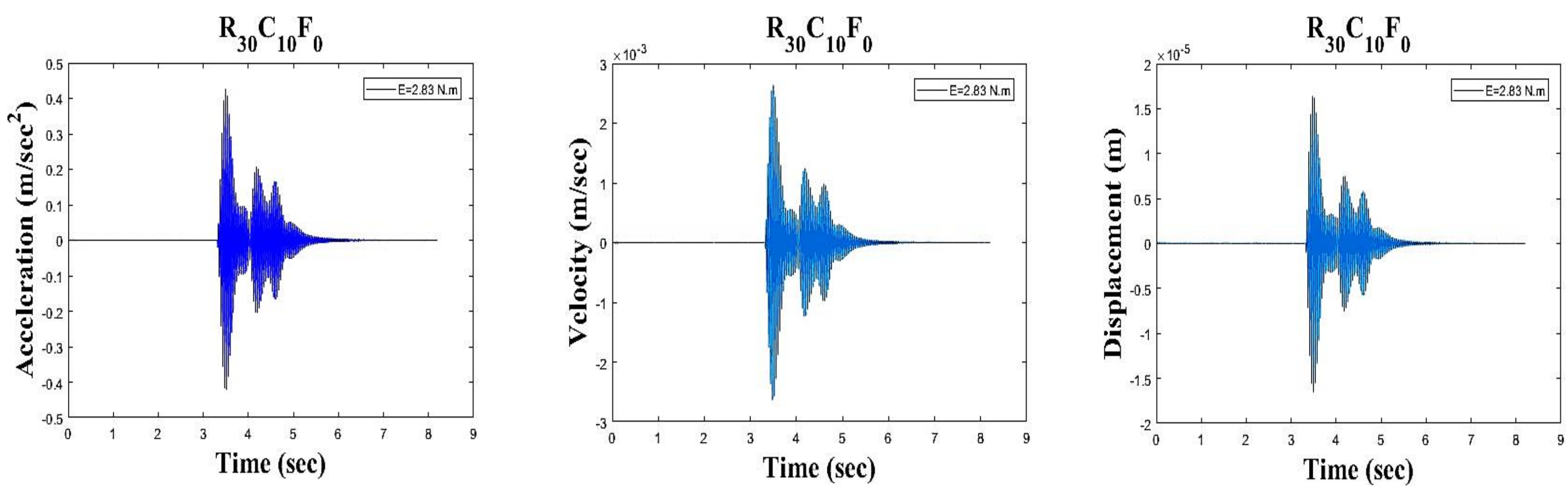
R30C10F0
Acceleration (m/sec2)
Time (sec)
E=2.83 N.m
R30C10F0
Velocity (m/sec)
Time (sec)
E=2.83 N.m
R30C10F0
Displacement (m)
Time (sec)
E=2.83 N.m

(d)

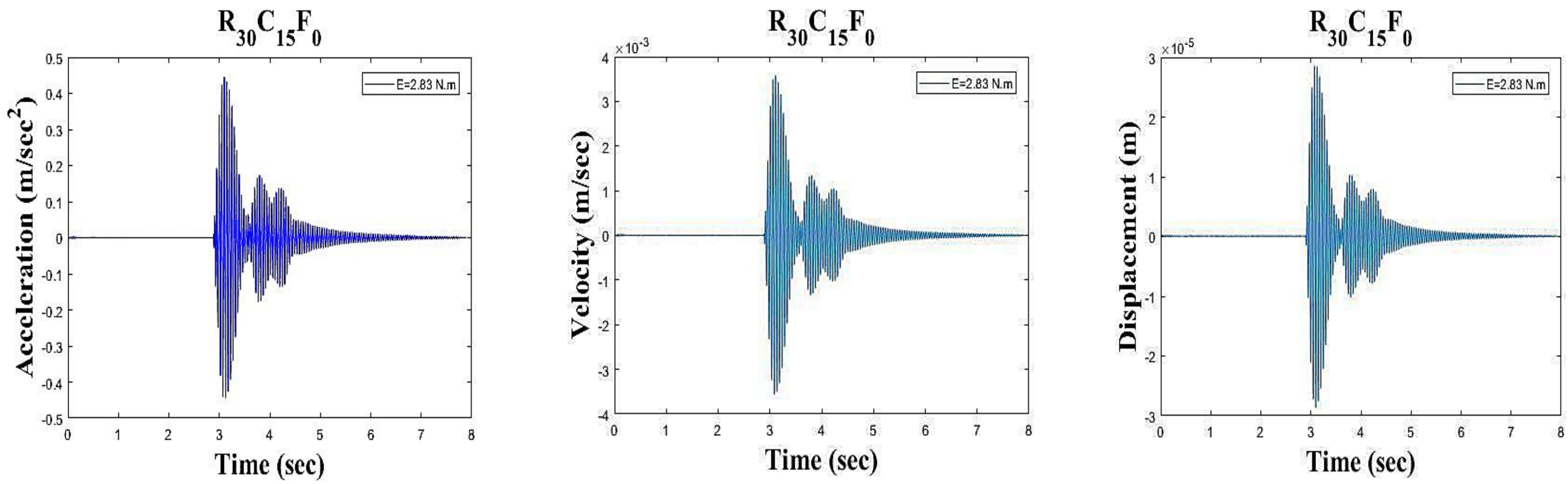

R30C15F0
Acceleration (m/sec2)
Time (sec)
E=2.83 N.m
R30C15F0
×10-3
Velocity (m/sec)
Time (sec)
E=2.83 N.m
R30C15F0
×10-5
Displacement (m)
Time (sec)
E=2.83 N.m

(e)

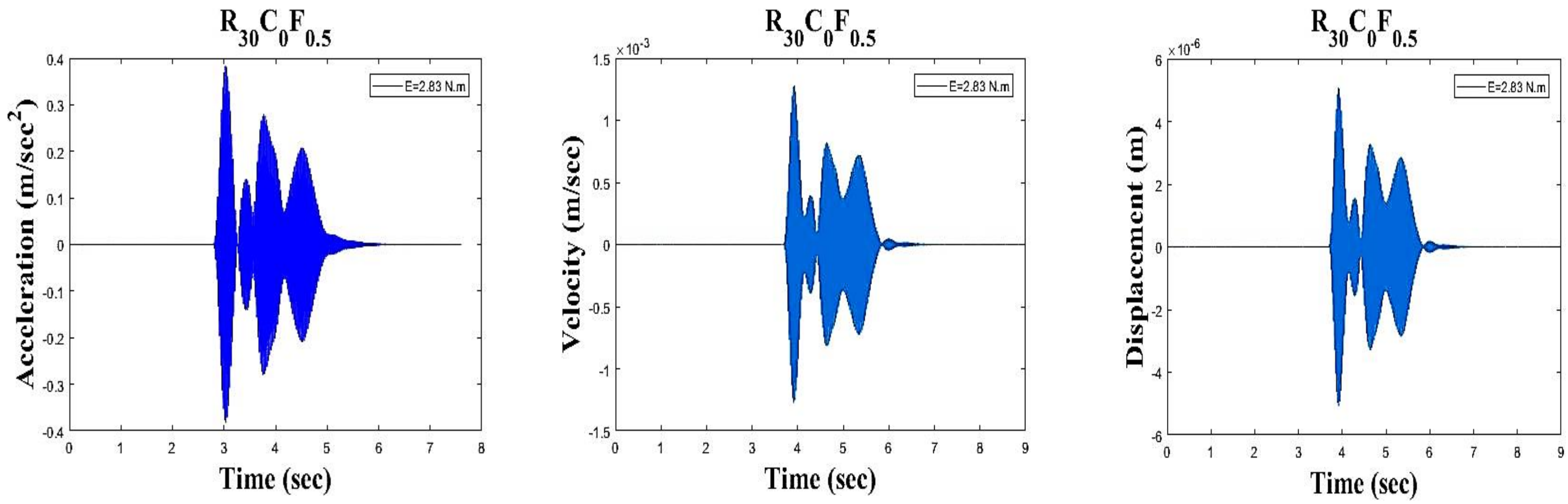

R30C0F0.5
Acceleration (m/sec2)
Time (sec)
E=2.83 N.m
R30C0F0.5
×10-3
Velocity (m/sec)
Time (sec)
E=2.83 N.m
R30C0F0.5
×10-6
Displacement (m)
Time (sec)
E=2.83 N.m

(f)

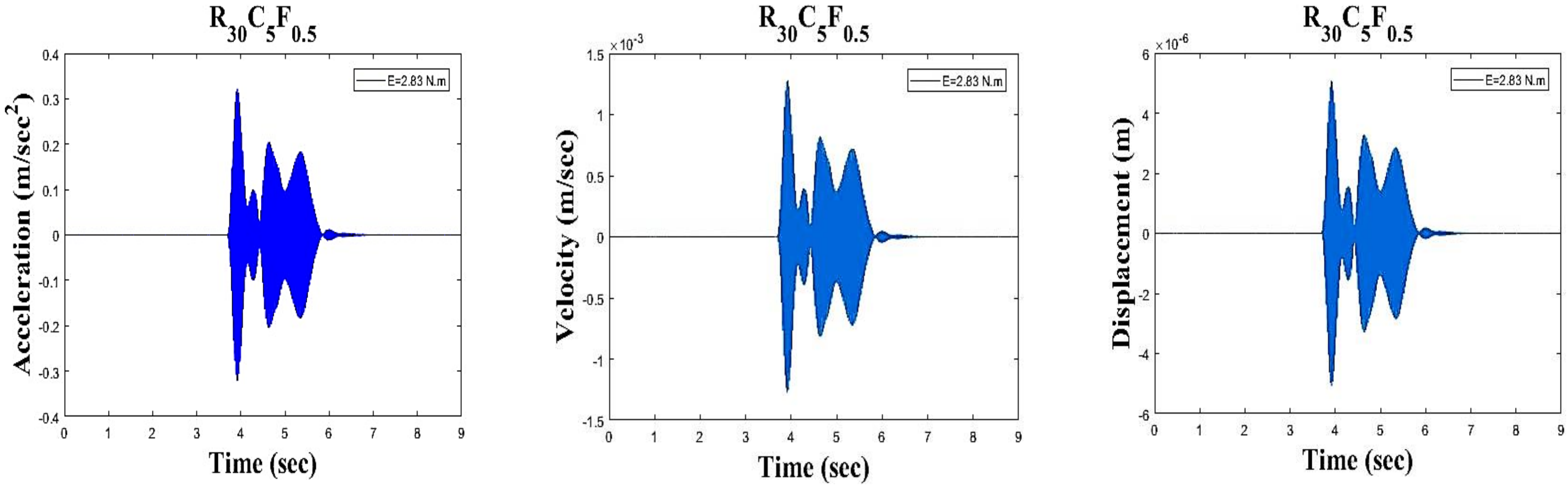

R30C5F0.5
Acceleration (m/sec2)
Time (sec)
E=2.83 N.m
R30C5F0.5
Velocity (m/sec)
×10-3
Time (sec)
E=2.83 N.m
R30C5F0.5
Displacement (m)
×10-6
Time (sec)
E=2.83 N.m

(g)

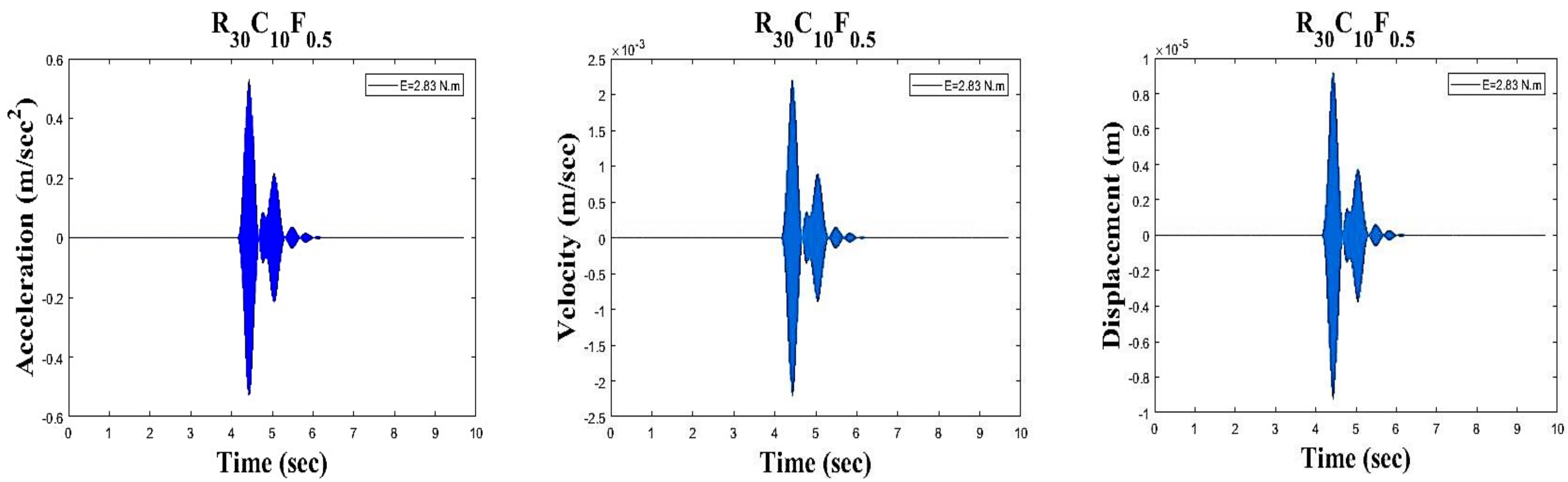

R30C10F0.5
Acceleration (m/sec2)
Time (sec)
E=2.83 N.m
R30C10F0.5
Velocity (m/sec)
×10-3
Time (sec)
E=2.83 N.m
R30C10F0.5
Displacement (m)
×10-5
Time (sec)
E=2.83 N.m

(h)

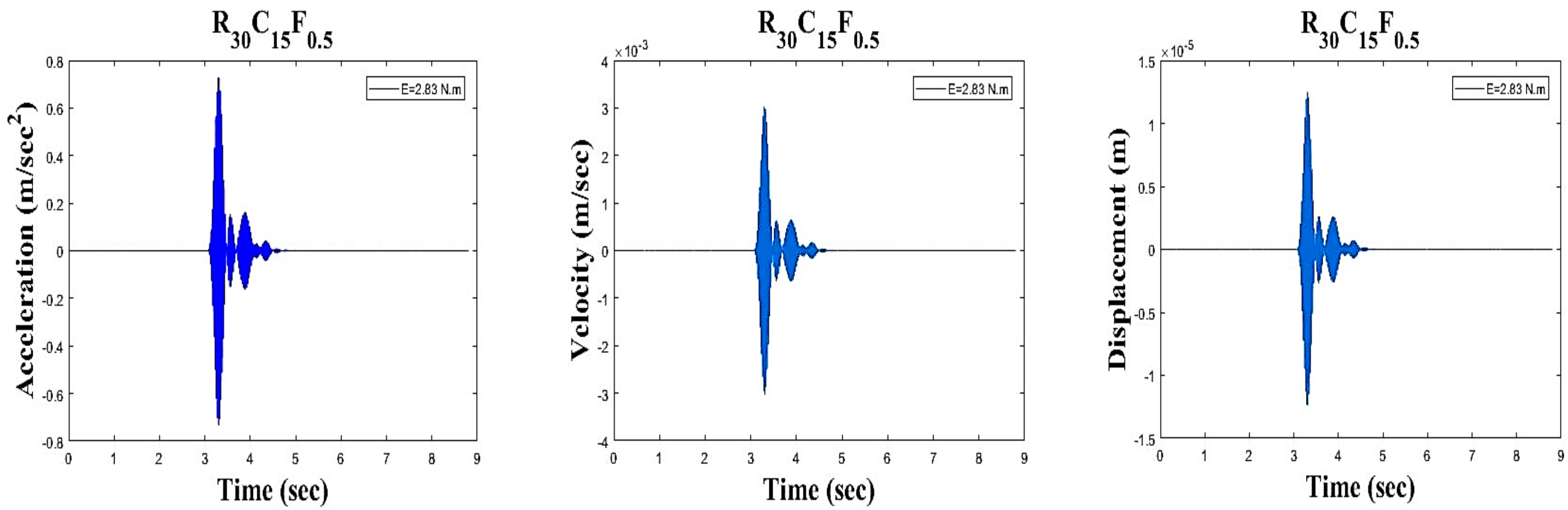

(i)

Figure 6.2 Typical damping curve of columns in the time domain for different combinations: (a) $R_0C_0F_0$, (b) $R_{30}C_0F_0$, (c) $R_{30}C_5F_0$, (d) $R_{30}C_{10}F_0$, (e) $R_{30}C_{15}F_0$, (f) $R_{30}C_0F_{0.5}$, (g) $R_{30}C_5F_{0.5}$, (h) $R_{30}C_{10}F_{0.5}$, and (i) $R_{30}C_{15}F_{0.5}$.

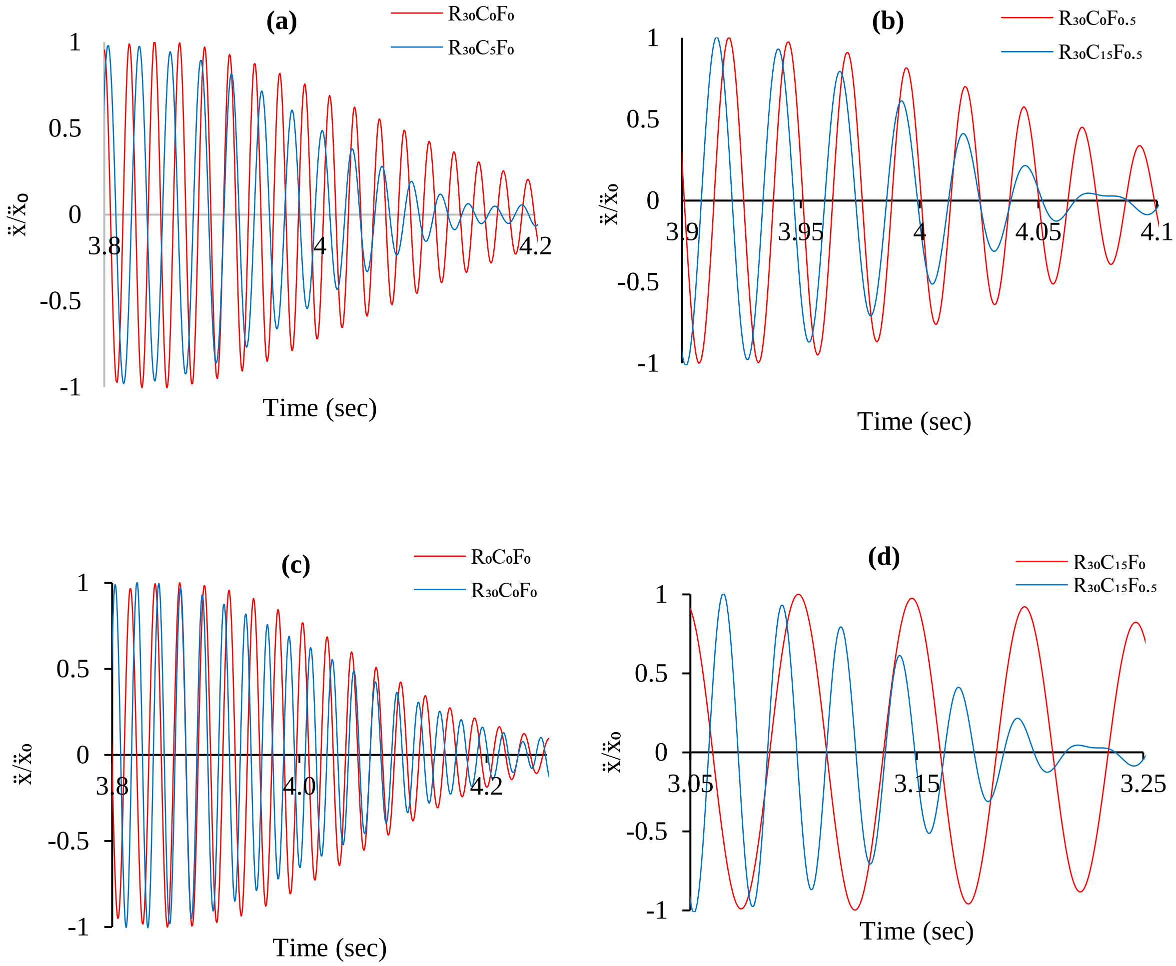

Figure 6.3 Decay of acceleration curves in the time domain for (a) RAC and R^2C column, (b) FR^2C (Fiber-Reinforced Recycled Concrete) and FR^3C column, (c) control and RAC column, and (d) R^2C and FR^3C column.

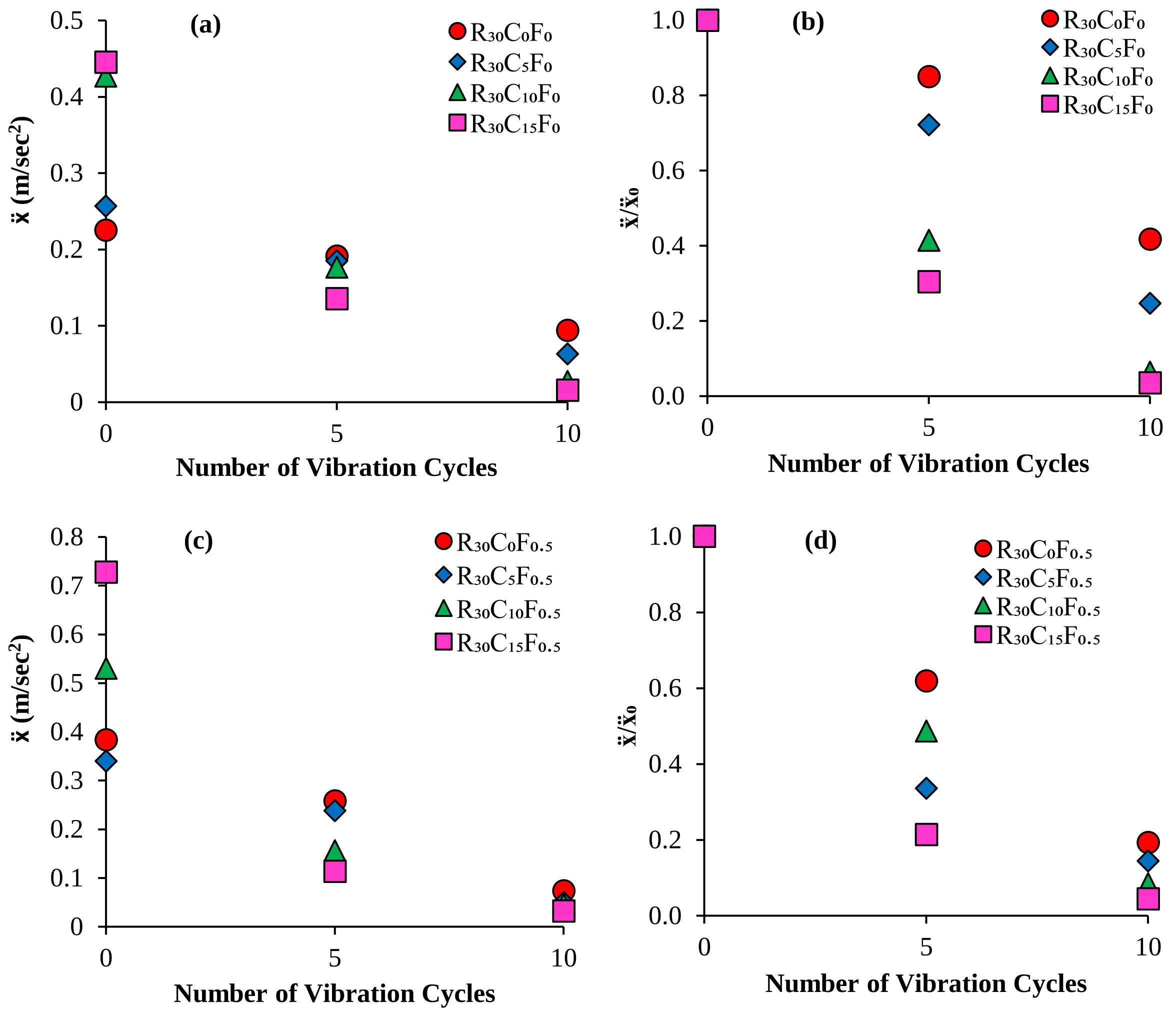

Figure 6.4 Decay of the acceleration of different columns: (a & c) as measured and (b & d) normalized by its initial maximum value.

6.4 Maximum Acceleration

The value of the maximum acceleration of different columns under different impact energy is presented in Figure 6.5. Three different impact energy such as 1.54 N.m, 2.13 N.m, and 2.83 N.m has been imposed on the top head of the columns. As depicted in the figure, the acceleration amplitude is increased with increasing the impact energy. However, conventional concrete and recycled aggregate concrete (RAC) are not very sensitive to induced energy. No significant difference (less than 2%) is observed in acceleration amplitude for different imposed energy. On the contrary, the R^2C and FR^3C specimens are more affected by the imposed energy. As rubber is a soft material, it can displace more compared to conventional aggregate under the same impact force. Besides, due to the inherent damping properties of rubber, it can dissipate higher energy. For R^2C columns having 0%, 5%, 10%, 15% CR content the acceleration amplitude is increased by 6%, 10%, 6%, 21% and 22%, 23%, 27%, 36% when the imposed energy is increased from 1.54 N.m to 2.13 N.m and 2.83 N.m, respectively. For FR^3C columns this amplitude is increased by 41%, 4%, 20%, 11% and 66%, 17%, 48%, 11% for 2.13 N.m and 2.83 N.m, respectively.

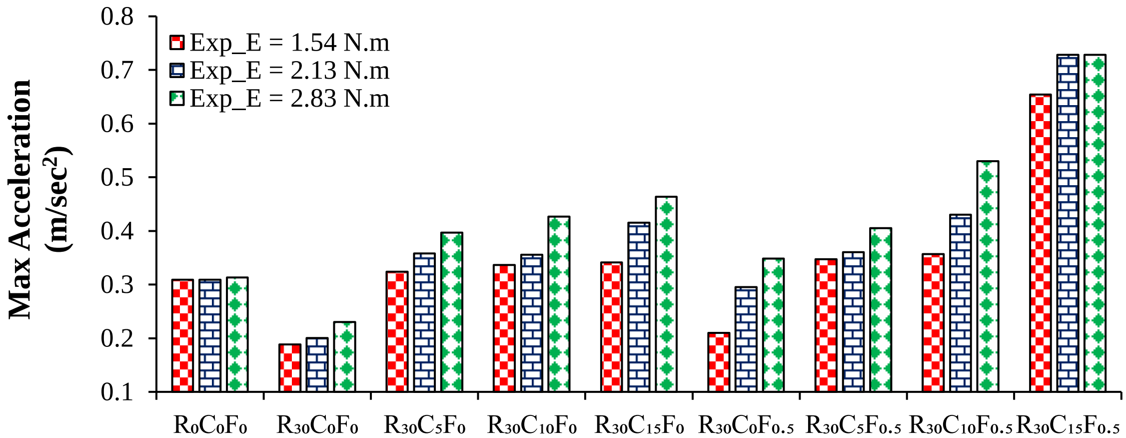

Figure 6.5 Effect of impact energy on the maximum acceleration of columns.

6.5 Maximum Horizontal Displacement

The horizontal displacement of columns is consistent with the behavior of acceleration. The horizontal displacement value is increased by incorporating CR into the concrete mixture and it increases with increasing the CR content. After the inclusion of fiber content in the R^2C mixtures, it further increases for FR^3C mixtures. The displacement value corresponding to 2.83 N.m impact energy is increased by 12%, 17%, 91% for R^2C columns and 14%, 138%, 153% for FR^3C columns with 5%, 10% and 15% CR content, respectively compared to control one. As rubber is a soft material with a lower elastic modulus, it can deform more compared to conventional concrete. Besides, the fiber also creates the concrete more flexible. However, for the RAC column, the displacement value is decreased by 21%. The same trend is also observed for 1.54 N.m and 2.13 N.m. As expected, the displacement value associated with higher impact energy is comparatively higher than that of lower impact energy. However, this incremental percentage is comparatively lower for conventional concrete and RAC than that of R^2C and FR^3C columns. For instance, for the control column and RAC column, the displacement value is increased by 20% and 18% when the impact energy is increased from 1.54 N.m to 2.13 N.m, and for 2.83 N.m it is increased by 33% and 37%. On the contrary, for R^2C columns, it increases up to 24% and 45%, and for FR^3C columns it increases up to 54% and 97 % for 2.13 N.m and 2.83 N.m impact energy, respectively depending on the percentage of CR content.

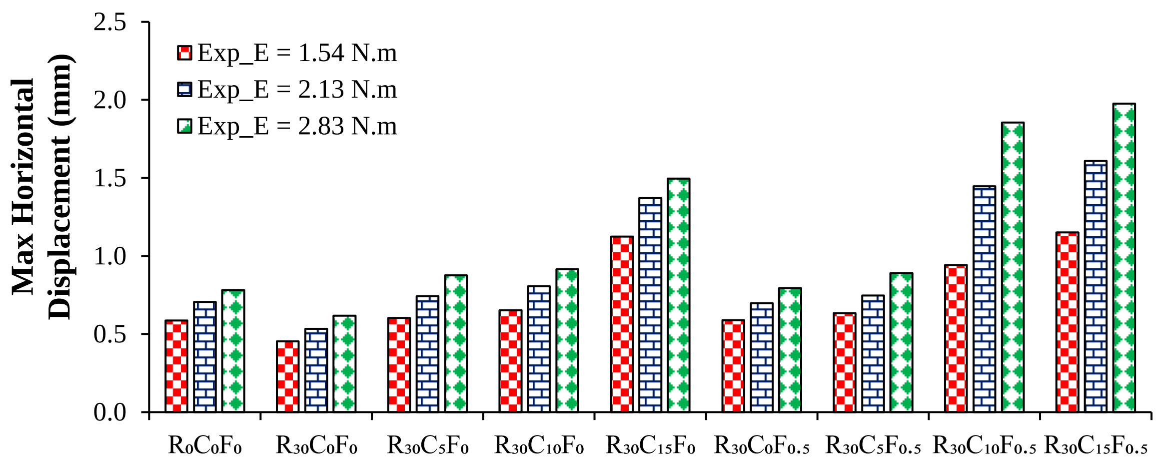

Figure 6.6 Effect of impact energy on the maximum horizontal displacement of columns.

6.6 Natural Frequency

The natural frequency of the column is calculated from the received acceleration data by using Fast Fourier Transform (FFT). The frequency curves for different combinations of columns are shown in Figure 6.8. The experimental natural frequency is then compared with the theoretical frequency. The theoretical natural frequency is calculated using Eq. 6. 1 to Eq. 6.3.

$$f = \frac{\omega_n}{2\pi} \tag{6.1}$$

$$\omega_n = \sqrt{\frac{k}{m}} \tag{6.2}$$

$$k = \frac{3EI}{L^3} \tag{6.3}$$

Where f is the natural frequency in Hz, ω_n is the angular frequency in rad/sec, k is the stiffness of column in N/m, m is the mass of the column in kg, E is the modulus of elasticity of concrete in MPa, I is the moment of inertia of area of the column in m^4, and L is the length of the column in m.

The variation in natural frequency among the specimens is summarized in Table 6.1 and for the comparison purpose, the natural frequency of various columns against 2.83 N.m impact energy is presented in Figure 6.7. Overall it is seen that the natural frequency of most of the columns is lower than that of control specimens. The figure also depicts a decrease in the natural frequency with the addition of CR content. On the contrary, the inclusion of fiber increases the natural frequency. The stiffness of the rubberized concrete is comparatively lower than that of fiber-reinforced concrete and the stiffness has a proportional relation with the frequency (Eq. 6.2). Thus, the R^2C columns provide a lower natural frequency than those of FR^3C columns. Under the impact energy of 2.83 N.m, the natural frequency is decreased by 4%, 25%, and 43% for 5%, 10%, and 15% CR content for R^2C columns compared to the 0% CR content. For FR^3C columns, it is decreased by 1%, 7%, and 15%, respectively. On the other hand, after the inclusion of 0.5% PP fiber into the concrete mixture the natural frequency of FR^3C is increased by 12%, 16%, 40%, and 67% compared to the corresponding R^2C columns with 0%, 5%, 10%, and 15% CR content, respectively. The same pattern is also observed with other impact energy. However, changing the impact energy does not significantly affect the natural frequency. The variation is found less than 5% which implies that the natural frequency of any structure does not depend on the external force rather it is an inherent property of a structure. Comparing the experimental result with the theoretical result it is found that the theoretical equation overestimates the natural frequency. The reason for this diversity is the difficulty to apply a frictionless impact load as the load is applied manually by a hammer.

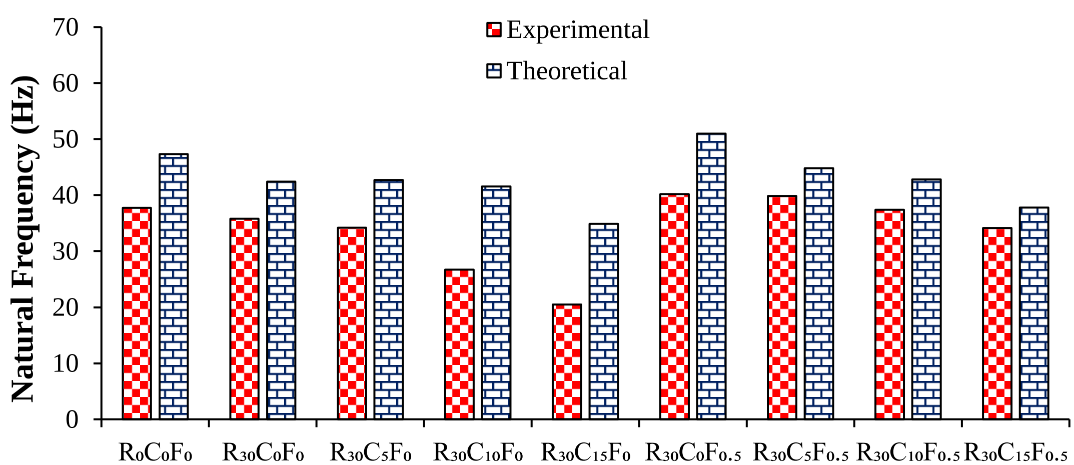

Figure 6.7 Natural frequency of different combinations of columns.

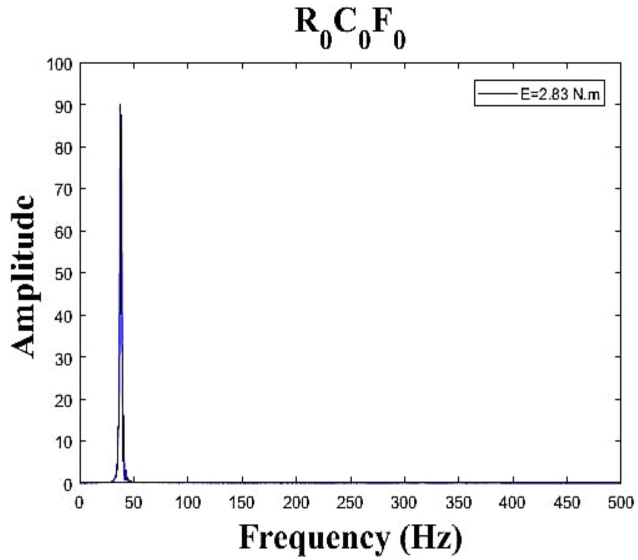

(a) $R_0C_0F_0$

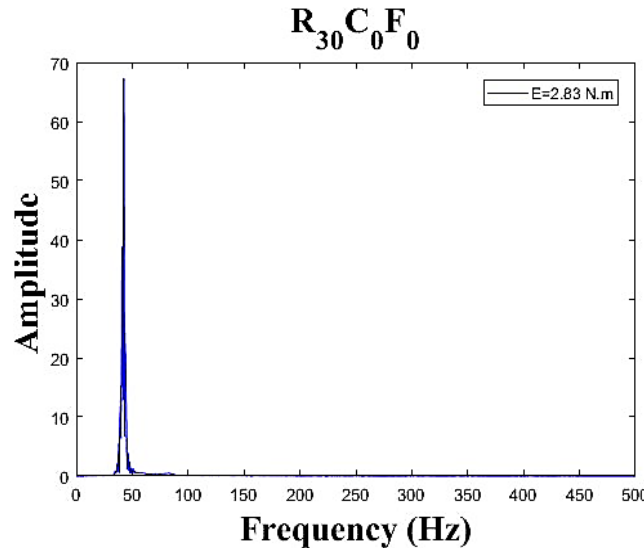

(b) $R_{30}C_0F_0$

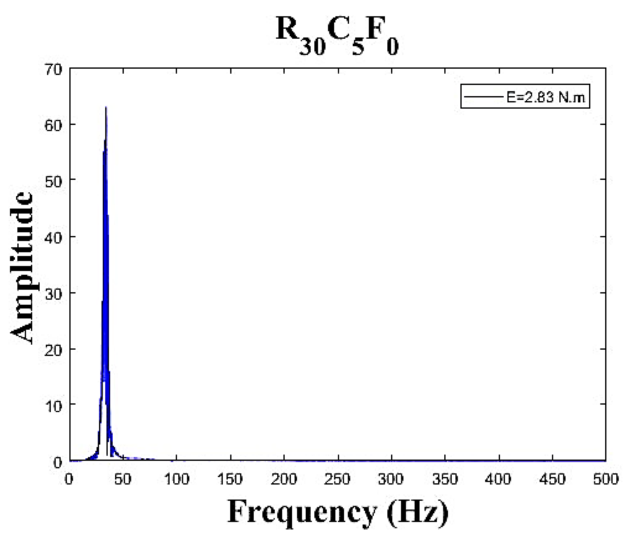

(c) $R_{30}C_5F_0$

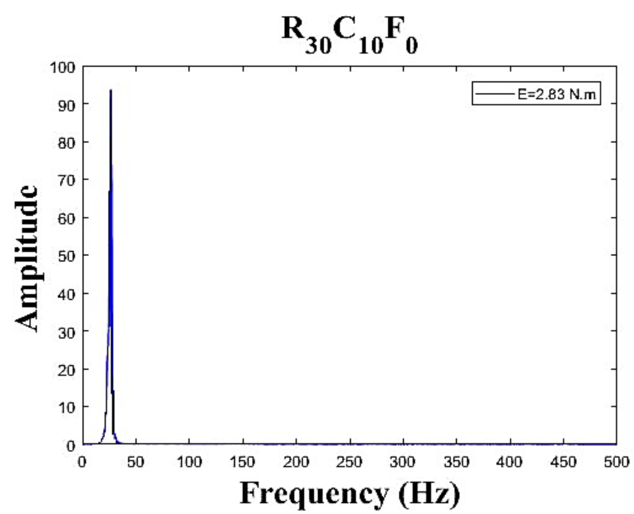

(d) $R_{30}C_{10}F_0$

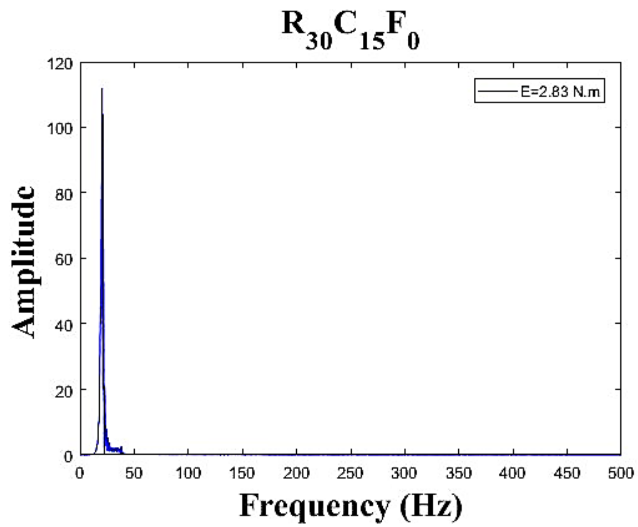

(e) $R_{30}C_{15}F_0$

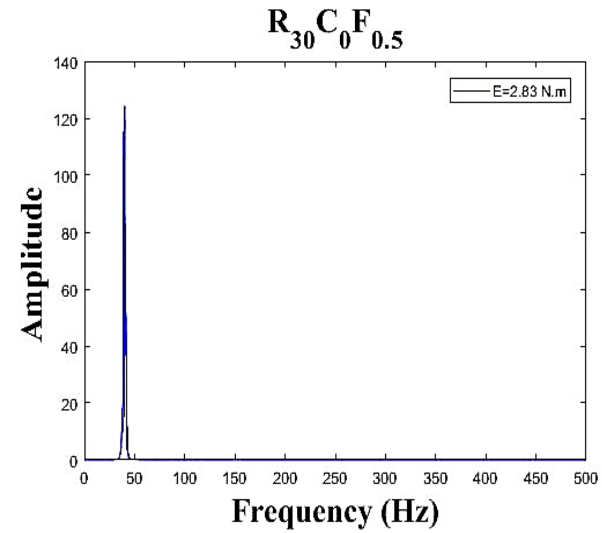

(f) $R_{30}C_0F_{0.5}$

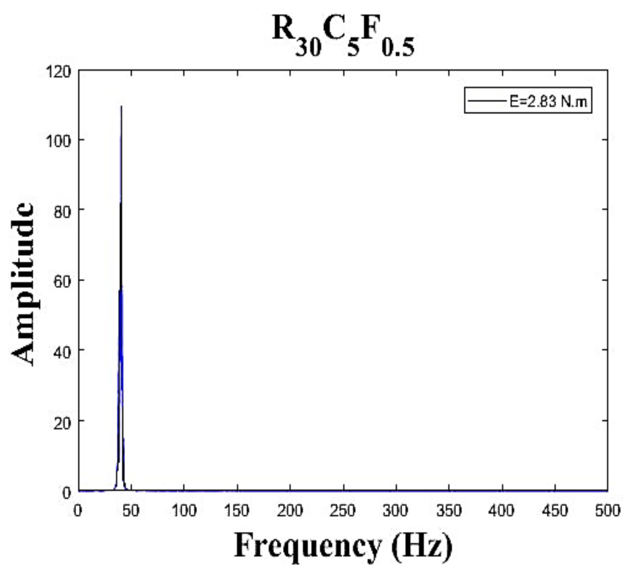

(g) $R_{30}C_5F_{0.5}$

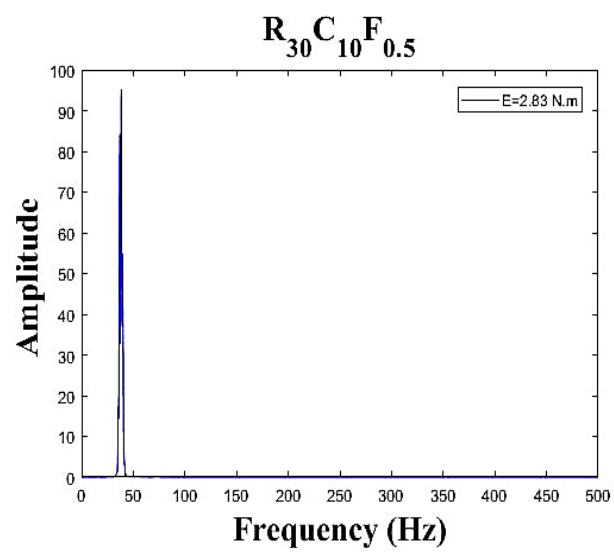

(h) $R_{30}C_{10}F_{0.5}$

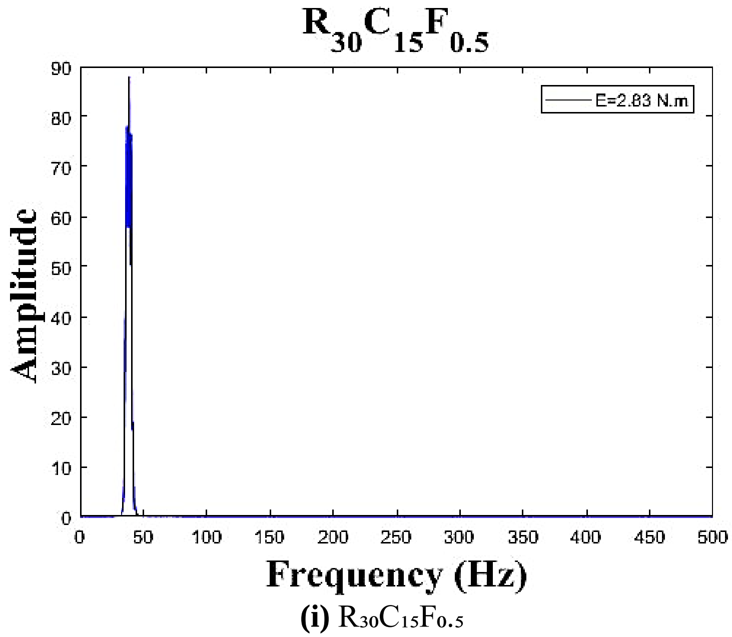

(i) $R_{30}C_{15}F_{0.5}$

Figure 6.8 Natural frequency curves for different combinations of columns.

Table 6.1 Summary of different frequencies of various columns.

Batch No		BN-1	BN-2	BN-3	BN-4	BN-5	BN-6	BN-7	BN-8	BN-9
Batch Name		$R_0C_0F_0$	$R_{30}C_0F_0$	$R_{30}C_5F_0$	$R_{30}C_{10}F_0$	$R_{30}C_{15}F_0$	$R_{30}C_0F_{0.5}$	$R_{30}C_5F_{0.5}$	$R_{30}C_{10}F_{0.5}$	$R_{30}C_{15}F_{0.5}$
Natural Frequency (f_n) (Hz)	Exp_E = 1.54 N.m	39.63	35.46	35.22	26.08	20.89	40.07	40.41	38.84	35.99
	Exp_E = 2.13 N.m	39.65	35.95	34.46	26.57	21.04	39.59	38.82	38.72	36.03
	Exp_E = 2.83 N.m	37.76	35.77	34.22	26.69	20.49	40.20	39.84	37.37	34.14
	Theoretical	47.35	42.44	42.68	41.54	34.88	50.98	44.81	42.79	37.78
Angular Frequency (ω_n) (rad/sec)	Exp_E = 1.54 N.m	249.02	222.81	221.31	163.88	131.28	251.80	253.87	244.03	226.14
	Exp_E = 2.13 N.m	249.14	225.88	216.55	166.95	132.18	248.76	243.90	243.26	226.39
	Exp_E = 2.83 N.m	237.26	224.73	215.01	167.72	128.73	252.60	250.31	234.83	214.50
	Theoretical	297.48	266.67	268.19	261.02	219.14	320.32	281.52	268.87	237.35
Damping Frequency (ω_d) (rad/sec)	Exp_E = 1.54 N.m	248.99	222.78	221.27	163.84	131.24	251.77	253.73	243.80	225.84
	Exp_E = 2.13 N.m	249.11	225.84	216.48	166.89	132.13	248.74	243.68	243.02	225.90
	Exp_E = 2.83 N.m	237.22	224.68	214.92	167.63	128.62	252.49	250.05	234.55	213.98

6.7 Damping Frequency

Using the natural frequency (f) or angular frequency (ω_n) the damping frequency (ω_d) can be determined using Eq. 6.4.

$$\omega_d = \omega_n\sqrt{1-\zeta^2} \tag{6.4}$$

Where ω_d is the damping frequency in rad/sec, ω_n is the angular frequency in rad/sec, and ζ is the damping ratio.

The variation in damping frequency among different columns and the effect of impact energy on it is presented in Figure 6.9. As the damping frequency mostly depends on the natural frequency, the result is consistent with the natural frequency. No significant effect is observed due to the variation in impact energy. However, the CR and fiber content plays the main role in changing the damping frequency. The addition of CR content decreases the damping frequency and this decreasing percentage is increased with increasing the CR content. On the contrary, the inclusion of fiber increases the damping frequency. In Eq. 6.4, the effect of ζ is quite small as the ζ^2 value is $\ll$1. Thus, the percentage variation is similar to that of natural frequency.

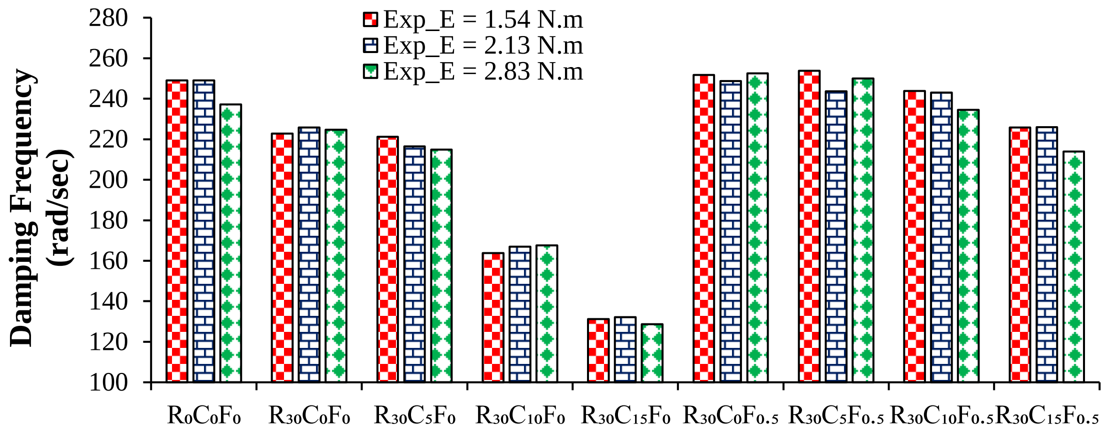

Figure 6.9 Damping frequency of different combinations of columns.

6.8 Damping Ratio

The damping in a single degree of freedom system can be classified into two damping mechanisms such as viscous damping and hysteretic damping. In this study, the viscous damping is discussed that can be determined using two common methods namely, the logarithmic decrement method and the half-power bandwidth method. The logarithmic decrement technique obtains the damping properties of a structure from a free vibration test using data in the time domain. However, the half-power bandwidth method uses the transfer function of the structure to determine the amount of damping using data in the frequency domain. Eq. 6.5 and Eq. 6.6 are used to calculate the damping ratio using the logarithmic decrement method and half-power bandwidth method, respectively. More details for each method can be found in Chopra 1995 [218].

$$\zeta = \frac{1}{2\pi n} \ln \frac{\ddot{x}_0}{\ddot{x}_n} \tag{6.5}$$

where ζ is the damping ratio, $\ddot{x}_0$ is the initial amplitude of acceleration in the free vibration response decay in the time domain, and $\ddot{x}_n$ is the amplitude of acceleration after n cycles.

$$\zeta = \frac{f_b - f_a}{2 f_n} \tag{6.6}$$

where f_b and f_a are the frequencies associated with the half-power points $\left(\frac{A_p}{\sqrt{2}}\right)$ on either side of the peak amplitude (A_p) in the frequency domain, and f_n is the natural frequency of the structure in Hz.

The average damping ratio for three tests of different columns is presented in Figure 6.10 and Table 6.2. Figure 6.2 and Figure 6.3 show that the actual response of the columns is not strictly exponential; hence, variation in the value of the damping ratio occurs with the change in the number of cycles used to calculate the damping. In the current study, a base of 5 and 10 cycles is used to define the damping ratio and is denoted by ζ_5 and ζ_{10}. The logarithmic decrement damping ratio is denoted as $\zeta_{5\text{-log. Dec}}$ or $\zeta_{10\text{-log. Dec}}$ and half-power bandwidth damping ratio is denoted as $\zeta_{half\text{-}power}$. From Figure 6.10, it is seen that the values of both damping ratios are very close. The effect of CR, fiber, the number of vibration cycles, impact energy and maximum amplitude is discussed in the following sub-sections.

Table 6.2 Damping ratio and damping coefficient of different combinations of columns.

Batch No			BN-1	BN-2	BN-3	BN-4	BN-5	BN-6	BN-7	BN-8	BN-9
Batch Name			$R_0C_0F_0$	$R_{30}C_0F_0$	$R_{30}C_5F_0$	$R_{30}C_{10}F_0$	$R_{30}C_{15}F_0$	$R_{30}C_0F_{0.5}$	$R_{30}C_5F_{0.5}$	$R_{30}C_{10}F_{0.5}$	$R_{30}C_{15}F_{0.5}$
Damping Ratio	$\zeta_{5\text{-log. Dec.}}$ (%)	Exp_E = 1.54 N.m	1.00	1.16	1.24	2.10	2.30	1.36	2.22	2.41	2.95
		Exp_E = 2.13 N.m	1.16	1.24	2.10	2.15	2.35	1.47	2.35	2.56	2.94
		Exp_E = 2.83 N.m	1.26	1.55	2.23	2.27	2.40	1.58	2.55	2.80	3.77
	$\zeta_{10\text{-log. Dec.}}$ (%)	Exp_E = 1.54 N.m	1.38	1.73	1.91	2.15	2.43	1.40	3.33	4.35	5.11
		Exp_E = 2.13 N.m	1.68	1.83	2.44	2.54	2.64	1.42	4.25	4.48	6.58
		Exp_E = 2.83 N.m	1.73	2.14	3.00	3.15	4.00	2.95	4.51	4.89	6.94
	$\zeta_{half\text{-}power}$ (%)	Exp_E = 2.83 N.m	2.04	2.09	3.19	3.31	4.10	3.01	4.69	5.05	6.90
Damping Coeff	C_5 ($N.sec^2/m$)	Exp_E = 1.54 N.m	289.44	300.29	312.06	384.66	325.05	392.59	635.51	646.71	713.90
		Exp_E = 2.13 N.m	336.50	324.10	515.87	401.23	333.89	417.51	645.86	685.12	711.93
		Exp_E = 2.83 N.m	349.56	404.96	546.20	425.77	333.34	455.79	721.63	725.37	865.59
	C_{10} ($N.sec^2/m$)	Exp_E = 1.54 N.m	400.93	445.90	480.73	393.71	344.07	404.43	954.36	1169.57	1236.43
		Exp_E = 2.13 N.m	486.83	479.38	600.40	475.17	376.38	403.94	1169.38	1199.64	1594.43
		Exp_E = 2.83 N.m	477.25	557.69	733.29	591.03	555.11	852.22	1274.02	1266.04	1594.46

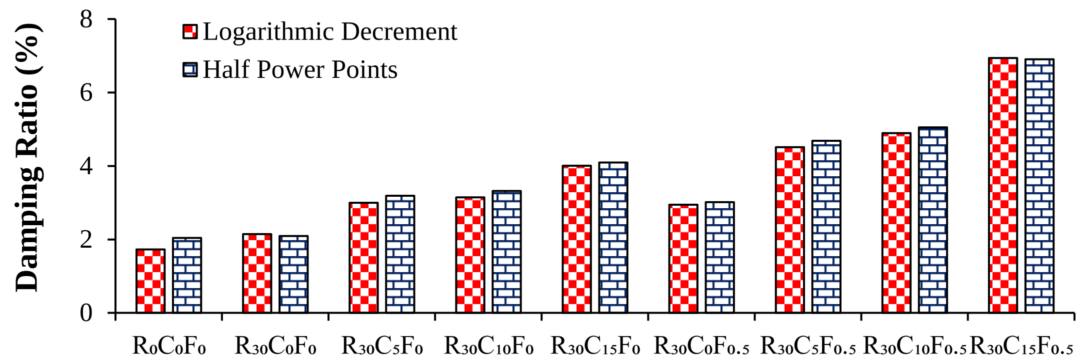

Figure 6.10 Damping ratio of different combinations of columns.

6.8.1 Effect of Crumb Rubber on Damping Ratio

The effect of CR on the damping ratio of different columns is summarized in Table 6.2. For the comparison purpose, the damping ratio against the impact energy of 2.83 N.m is presented in Figure 6.11. The figure shows an increasing trend of the damping ratio (ζ) with the increase in CR content. The ζ_5 Value is increased by approximately 23%, 77%, 80%, and 90% for 0%, 5%, 10%, and 15% CR content, respectively in R^2C columns compared to the conventional concrete whereas for FR^3C columns these incremental percentages are 25, 102, 122, and 199, respectively. In the case of ζ_{10}, these percentages are 24%, 73%, 82%, and 131% for R^2C columns and 71%, 161%, 183%, and 301% for FR^3C columns, respectively. The same trend is also observed for other impact energy (1.54 N.m and 2.13 N.m). As rubber is a soft material with high damping properties, the rubberized concrete can dissipate more energy and return to its initial position quickly compared to conventional concrete. A higher damping ratio of concrete would improve the seismic safety of concrete structures such as bridges and buildings.

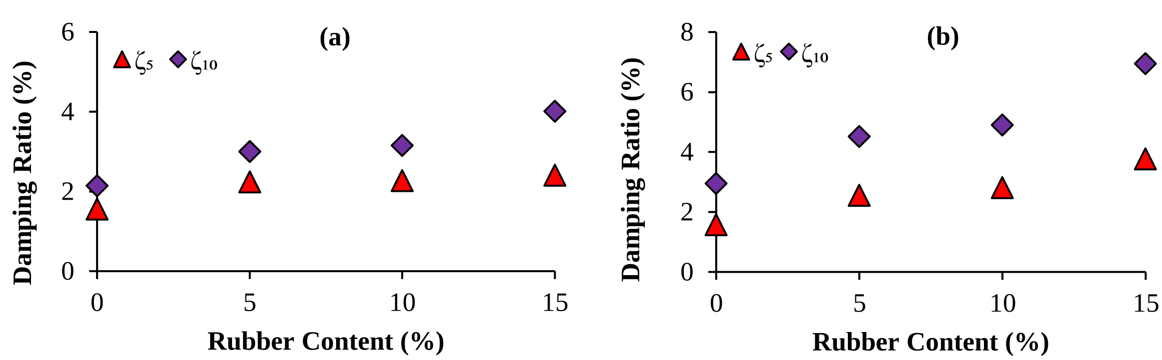

Figure 6.11 Effect of CR on damping ratio of concrete: (a) without fiber and (b) with fiber.

6.8.2 Effect of Fiber on Damping Ratio

The effect of fiber on the damping ratio of different columns under different impact energy is summarized in Table 6.2 and the value against the impact energy of 2.83 N.m is presented in Figure 6.12. Though the CR content increases the damping ratio, it can be further increased by incorporating fiber content into the concrete mixture. The ζ_5 value of FR^3C against the impact energy of 2.83 N.m is increased by 2%, 14%, 23%, and 57% compared to R^2C with 0%, 5%, 10%, and 15% CR content, respectively. At the same time, the ζ_{10} value is increased by 38%, 50%, 55%, and 74%, respectively. The same trend is also observed with other the impact energy. This was due to the bridging action of PP fiber in concrete. Besides, this bridging action leads to absorbing more energy in the process of bonding, sliding, and pulling out between fiber and concrete matrix. With the addition of rubber content, the damping capacity is also increased in fiber-reinforced rubberized recycled concrete (FR^3C).

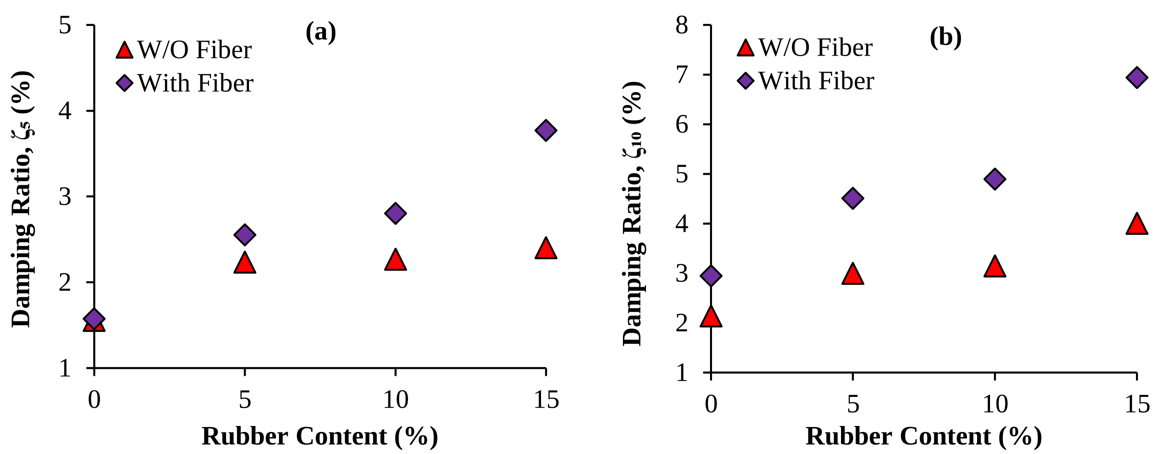

Figure 6.12 Effect of fiber on damping ratio of concrete: (a) ζ_5, and (b) ζ_{10}.

6.8.3 Effect of Impact Energy on Damping Ratio

To investigate the effect of impact energy on free vibrational responses of R^2C and FR^3C columns three different impact energy such as 1.54 N.m, 2.13 N.m, and 2.83 N.m has been imposed on the top head of the columns. As illustrated in Figure 6.13, a variation has occurred in the damping ratio for different imposed energy. This effect of the imposed energy on the damping ratio can be expressed by the variation of the maximum amplitude of the received accelerations. The damping ratio is increased with increasing the impact energy. As depicted in the figure, the conventional concrete and recycled aggregate concrete (RAC) are not very sensitive to the induced energy. The R^2C and FR^3C specimens, on the contrary, is more affected by the imposed energy. The ζ_5 value of R^2C specimens is increased by an average of 15% and 24% for increasing the impact energy from 1.54 N.m to 2.13 N.m, and 2.83 N.m, respectively. For FR^3C specimens, these incremental percentages are 15% and 50%, respectively. The same trend is also observed for the ζ_{10} value. Approximately 4% and 20% higher ζ_{10} value is found for 2.13 N.m and 2.83 N.m impact energy compared to 1.54 N.m energy for R^2C specimens and 18% and 36% for FR^3C specimens, respectively.

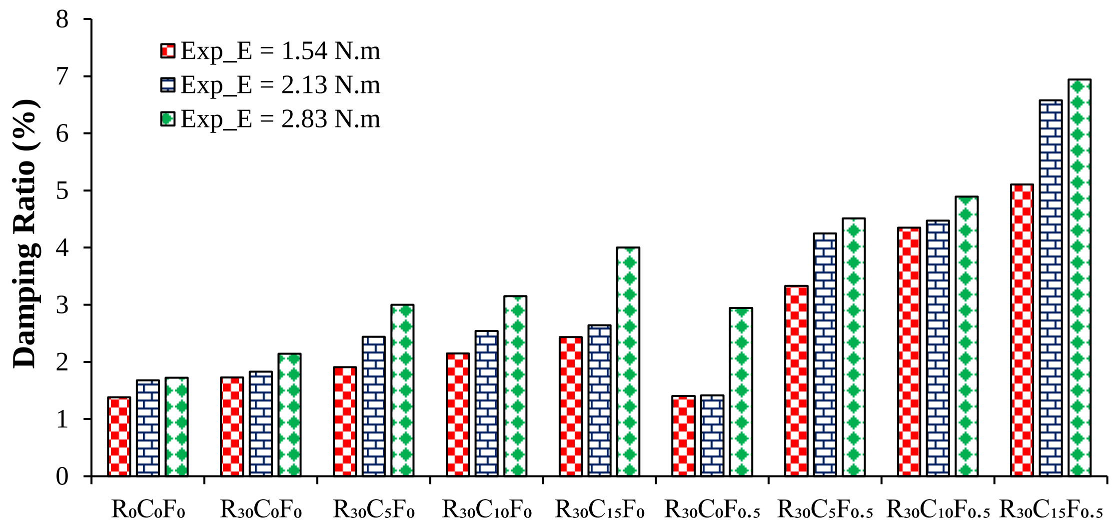

Figure 6.13 Effect of impact energy on damping ratio (ζ_{10}) of different columns.

6.8.4 Effect of Number of Vibration Cycles on Damping Ratio

Previous researchers have found that the calculated damping ratio depends on the number of cycles used in the calculations, i.e. n parameter in Eq. 6.5 [68]. In this study, the damping ratio is calculated using 5 and 10 vibration cycles. Though conventional concrete and some R^2C specimens provided more than 15 vibration cycles against a single impact, FR^3C specimens did not provide more than 12. Thus for damping calculation, the n value is limited to 10. Figure 6.14 shows the change in damping ratio with changing the number of vibration cycles from 5 to 10. As shown in the figure, the damping calculations are sensitive to the number of vibration cycles which is increased for 10 cycles compared to 5 cycles. However, for FR^3C columns this variation is comparatively higher than those of R^2C columns. Approximately 38%, 35%, 39%, 67% and 87%, 77%, 75%, 84% variation is observed for R^2C and FR^3C columns with 0%, 5%, 10%, and 15% CR content, respectively against 2. 83 N.m impact energy. On the other hand, for normal concrete, this variation is only 37%. The same behavior is also observed with other impact energy. As FR^{3}C specimens belong to a higher damping property, they try to come back to their original position comparatively faster by providing a higher energy dissipation. Thus, a higher slope is created in acceleration-time curves. That's why this higher variation may occur for FR^{3}C specimens.

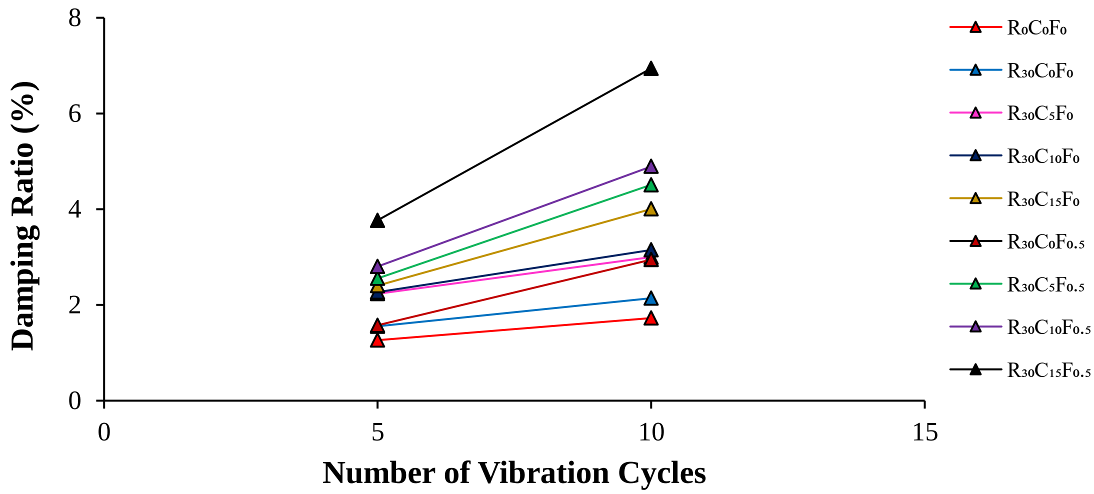

Figure 6.14 Effect of the number of vibration cycles on damping ratio of columns.

6.8.5 Effect of Amplitude on Damping Ratio

The effect of acceleration amplitude on the damping ratio of concrete under impact energy of 2.83 N.m is presented in Figure 6.15. From the figure, it is seen that the higher CR reinforced concrete column provides a higher amplitude and the column providing a higher amplitude exhibits a higher damping ratio. For R^{2}C columns having 0%, 5%, 10% and 15% CR content the acceleration amplitude is 0.230 m/s^2, 0.397 m/s^2, 0.427 m/s^2, and 0.464 m/s^2, respectively and their corresponding damping ratio (ζ_{10}) is 2.14%, 3.0%, 3.15%, and 4.0%. And for FR^{3}C columns, the acceleration amplitude is 0.349 m/s^2, 0.405 m/s^2, 0.530 m/s^2, and 0.729 m/s^2, for 0%, 5%, 10%, and 15% CR content and their corresponding damping ratio is 2.95%, 4.51%, 4.89%, and 6.94%, respectively. The same behavior is also observed for other impact energy.

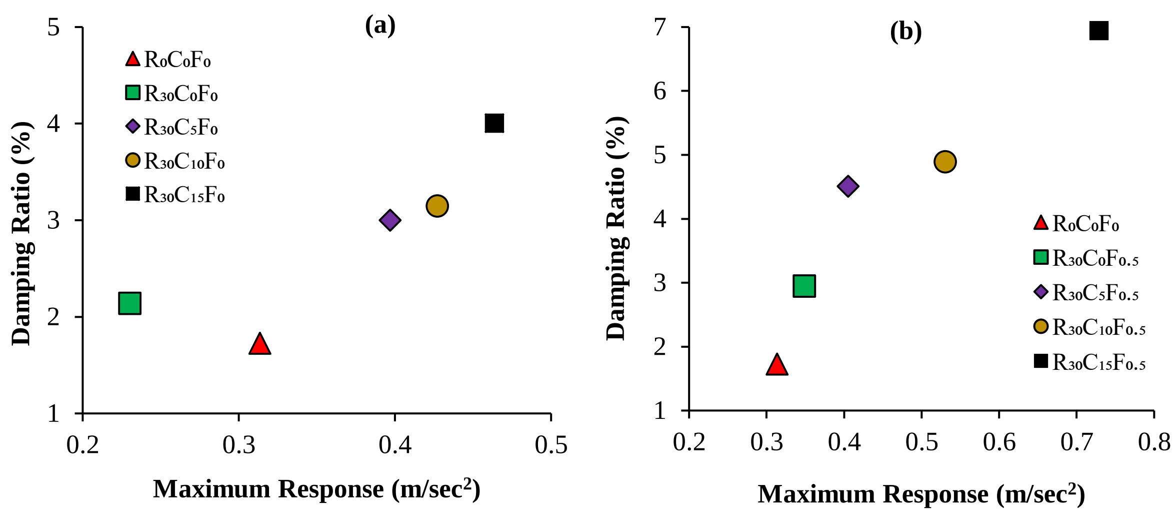

Figure 6.15 Effect of acceleration amplitude on damping ratio of concrete: (a) without fiber and (b) with fiber.

6.8.6 Repeatability of Test

The effectiveness of dynamic testing is determined by its repeatability. For this purpose, under a fixed impact energy, the hammer is dropped three times, and the average value is reported. Thus, for three impact energy, a total of nine drops of the hammer are imposed on one column. So, the total number of hammer drops is eighty-one for nine columns. Good repeatability has been found for all columns. For instance, Figure 6.16 checks the variation in damping ratio under the repeatability test at 2.83 N.m energy induced in the column and for the different number of cycles. The figure shows that the variation in damping ratio among the drops is not significant. The average coefficient of variance (COV) for ζ_5 is found at 17% and 19% for R^2C and FR^3C columns and for ζ_{10} this COV is 12% and 13%, respectively. The reason for this diversity is due to the difficulty in eliminating the effect of amplitude in such a test where the impact load is applied manually by a hammer.

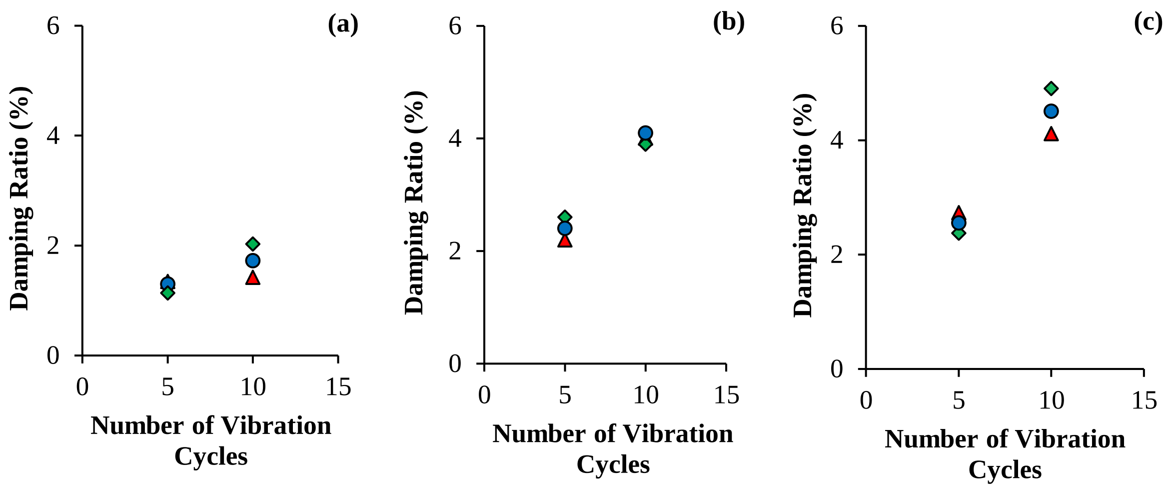

Figure 6.16 Repeatability of the tests for (a) normal concrete (i.e. $R_0C_0F_0$), (b) R^2C (i.e. $R_{30}C_{15}F_0$), and (c) FR^3C (i.e. $R_{30}C_5F_{0.5}$).

6.9 Damping Coefficient

The damping coefficient is a material property that can be measured from the damping ratio and angular frequency by using Eq. 6.7. The coefficient indicates whether a material will bounce back or return energy to a system.

$$C = 2m\omega_n\zeta \tag{6.7}$$

Where C is the damping coefficient in N.sec^2/m, m is the mass of the column in kg, ω_n is the angular frequency in rad/sec, and ζ is the damping ratio.

Two different damping coefficients have been calculated such as C_5 and C_{10} considering two damping ratios of ζ_5 and ζ_{10}. The calculated damping coefficient of different columns is summarized in Table 6.2. For the comparison purpose, C_{10} values are presented in Figure 6.17. As shown in the figure, the damping coefficient is increased with increasing the impact energy due to the higher damping ratio for higher impact energy. Besides, the damping coefficient for R^2C is increased up to 5% CR content and then decreased for 10% and 15% CR content but still higher than the control one. As already mentioned, the damping coefficient depends on the damping ratio, mass as well as frequency. Though the damping ratio is increased for CR content, the mass and frequency are decreased. Thus, for a higher CR content the damping coefficient decreases. On the contrary, FR^3C columns exhibit a higher damping coefficient compared to control column and R^2C columns and it increases with increasing the CR content. This may happen due to the much higher damping ratio of FR^3C columns compared to others. Approximately 79%, 165%, 167%, and 234% higher damping coefficient (C_{10}) is found compared to control one for 0.5% PP fiber with 0%, 5%, 10% and 15% CR content under 2.83 N.m impact energy. On the contrary, for R^2C columns, these incremental percentages are only 17%, 54%, 24%, and 16%, respectively. Thus, the FR^3C columns can easily diminish the response of unwanted vibration or shock due to this higher damping coefficient in the material.

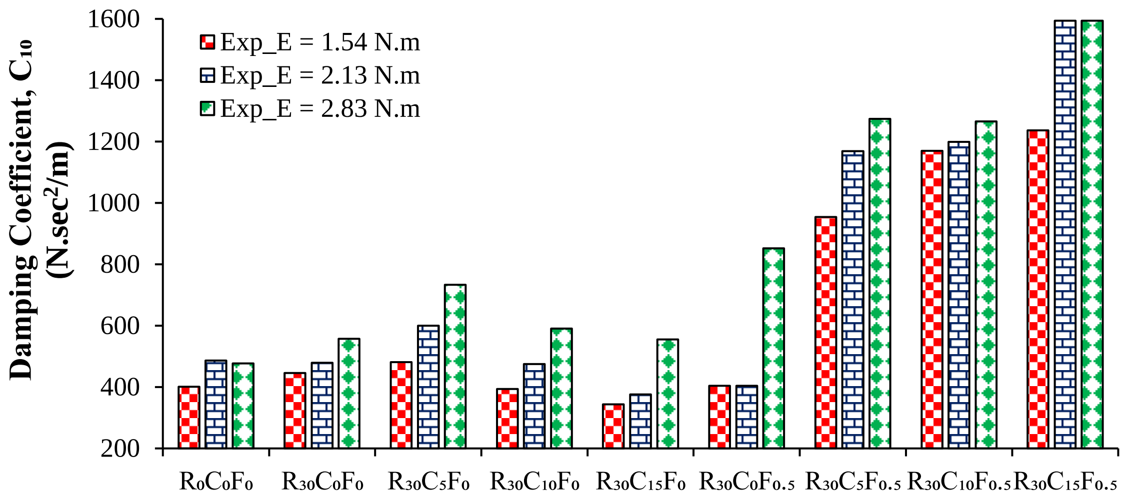

Figure 6.17 Damping coefficient of different combinations of columns.

6.10 Natural Time Period

The time period is an inherent property of a building or structure that is mainly controlled by its mass (*m*) and stiffness (*k*). The experimental and theoretical time period of the columns is determined from the natural frequency or angular frequency using Eq. 6.8 and Eq. 6.9.

$$T_n = \frac{1}{f_n} \tag{6.8}$$

$$f_n = \frac{\omega_n}{2\pi} \tag{6.9}$$

Where T_n is the natural time period in sec, and f_n is the natural frequency in Hz.

The natural time period of different columns under three impact loading is summarized in Table 6.3. However, for the comparison purpose, the time period against 2.83 N.m impact energy is presented in Figure 6.18. As the time period is inversely proportional to the frequency it follows the opposite trend of the natural frequency. The figure depicts that an increasing time period can be achieved by using CR content in the concrete mixture. Approximately 4%, 32%, 75% and 0%, 8%, 16% time period is increased with 5%, 10%, 15% CR content compared to 0% CR content for R^2C and FR^3C columns under 2.83 N.m impact energy. As previously mentioned that the time period depends on the stiffness and mass of any structure. Due to the softness of the rubber particles, the rubberized concrete provides a lower stiffness in the column. Besides, the rubber particles also reduce the mass of the column. Thus, the time period increases. However, the change in time period along with CR content is more prominent for R^2C than that of FR^3C. Besides, the addition of fiber content decreases the time period. As fiber creates the column stiffer, thus time period reduces. Comparing the R^2C columns with FR^3C columns, the FR^3C columns provides 11%, 14%, 27%, and 41% lower time period for 0%, 5%, 10%, and 15% CR content, respectively. The same trend is also observed with 1.54 N.m and 2.13 N.m impact energy.

No significant variation is observed due to the change in impact force. Almost the same value or less than 4% variation is observed for changing the impact energy which implies that the natural time period does not depend on the external force rather it only depends on the mass and stiffness of the system. Comparing the experimental time period with the time period calculated by theoretical equations, it is found that the theoretical equation overestimates the natural frequency. The overestimation factor is comparatively less for FR^3C columns compared to R^2C columns. As previously mentioned that the reason for this diversity is the difficulty to apply a frictionless impact load as the load is applied manually by a hammer. Finally, it is recommended that an improved time period can be achieved by using either R^2C or FR^3C mixture in any structure compared to the conventional concrete.

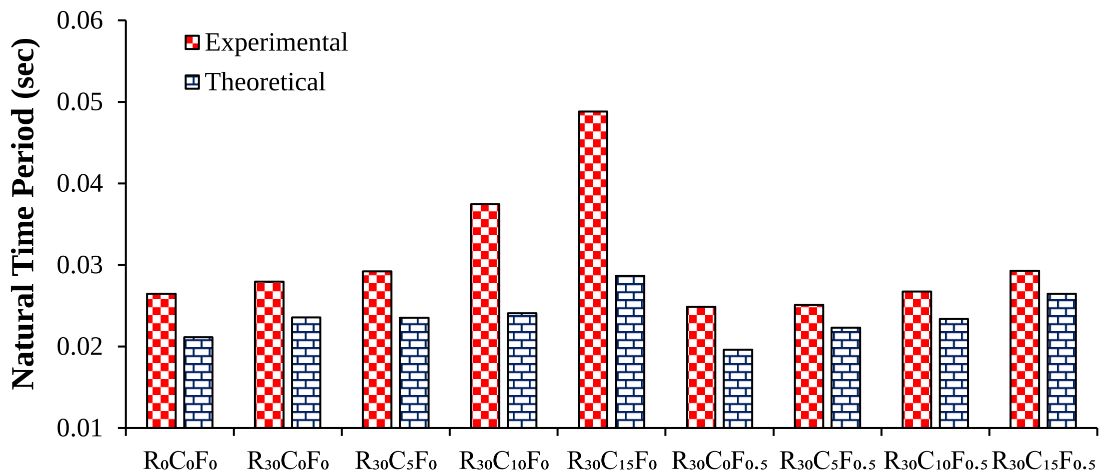

Figure 6.18 Natural time period of different combinations of columns.

Table 6.3 Summary of different time periods of various columns.

Batch No / **Batch Name**		**BN-1** $R_0C_0F_0$	**BN-2** $R_{30}C_0F_0$	**BN-3** $R_{30}C_5F_0$	**BN-4** $R_{30}C_{10}F_0$	**BN-5** $R_{30}C_{15}F_0$	**BN-6** $R_{30}C_0F_{0.5}$	**BN-7** $R_{30}C_5F_{0.5}$	**BN-8** $R_{30}C_{10}F_{0.5}$	**BN-9** $R_{30}C_{15}F_{0.5}$
Natural Time Period (T_n) (sec)	Exp_E = 1.54 N.m	0.025	0.028	0.028	0.038	0.048	0.025	0.025	0.026	0.028
	Exp_E = 2.13 N.m	0.025	0.028	0.029	0.038	0.048	0.025	0.026	0.026	0.028
	Exp_E = 2.83 N.m	0.026	0.028	0.029	0.037	0.049	0.025	0.025	0.027	0.029
	Theoretical	0.021	0.024	0.024	0.024	0.029	0.020	0.022	0.023	0.026
Damping Time Period (T_d) (sec)	Exp_E = 1.54 N.m	0.025	0.028	0.028	0.038	0.048	0.025	0.025	0.026	0.028
	Exp_E = 2.13 N.m	0.025	0.028	0.029	0.038	0.048	0.025	0.026	0.026	0.028
	Exp_E = 2.83 N.m	0.026	0.028	0.029	0.037	0.049	0.025	0.025	0.027	0.029

6.11 Damping Time Period

Using the damping frequency as described previously the damping time period is calculated using Eq. 6.10.

$$T_d = \frac{2\pi}{\omega_d} \tag{6.10}$$

Where T_d is the damping time period in sec, and ω_d is the damping frequency in rad/sec.

The effect of impact energy on the damping time period and its variation among different columns are presented in Figure 6.19. As the damping time period depends on the damping frequency and they are inversely proportional to each other, it follows the opposite trend to the damping frequency. No significant variation is observed due to the change in impact energy. However, the CR and fiber content plays the main role main in changing the d damping time period. The FR^{3}C columns belong comparatively lower damping time period than those of R^{2}C columns. As the stiffness of the FR^{3}C columns is higher due to the inclusion of fiber content, the time period reduces. However, due to the softness of the rubber particles, the time period increases with the addition of CR content. The column containing 15% CR content provides the maximum damping time period which is approximately 90% higher than that of the control column.

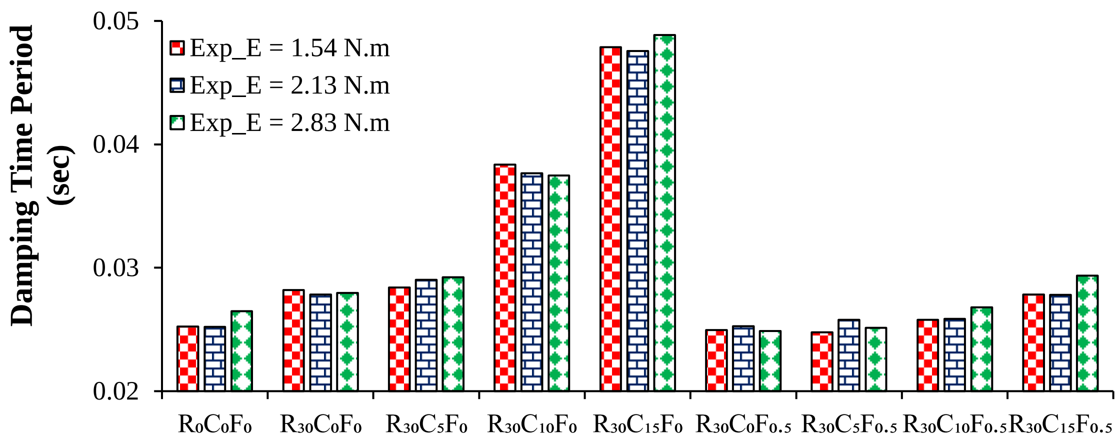

Figure 6.19 Damping time period of different combinations of columns.

6.12 Summary

To summarize the free vibrational responses, the damping ratio of all RAC, R^{2}C, and FR^{3}C columns are higher than that of the conventional column. With increasing the CR content, the damping ratio increases and it is increased further with the addition of fiber. Up to 131% and 301% damping ratio is increased for R^{2}C columns and FR^{3}C columns depending on the percentage of CR content. The natural frequency is decreased with the addition of CR content and subsequently, the time period is increased. Though the addition of fiber content decreases the time period of FR^{3}C columns, it is still higher than that of the conventional column. No significant effect is observed in natural frequency and time period due to changing the impact force whereas increasing the imposed energy from 1.54 N.m to 2.13 N.m and 2.83 N.m the damping ratio is increased by an averagely of 4%, 18% and 20%, 36% for R^{2}C and FR^{3}C columns, respectively.

Chapter 7
CONCLUSIONS AND RECOMMENDATIONS

7.1 Introduction

Concrete is the 2nd most consumed substance in the world behind water. The scarcity of natural aggregates has led researchers to find out alternative sustainable solutions. Every year huge amount of waste concrete is generated from concrete structures which cause environmental degradation. On the other hand, a large amount of waste tires is reached their end life, consequently increasing environmental loads. Thus, the necessity for research on alternative materials arises.

This study investigates the combined effect of recycled coarse aggregate (RCA) derived from the waste building structures, crumb rubber (CR) from waste tires, and polypropylene (PP) fiber on the mechanical properties of rubberized recycled concrete (R^2C) and fiber-reinforced rubberized recycled concrete (FR^3C). Besides, using these new types of concrete, twenty-six one-third scale tied reinforced concrete columns were prepared to investigate the uniaxial compressive behavior of columns. The columns were sufficiently stocky by ignoring the slenderness effects. The failure pattern, load-deformation responses, axial capacity, ductility, toughness, the influence of tie spacing, and longitudinal reinforcement ratio were investigated. Besides, the applicability of these newly developed R^2C and FR^3C columns was evaluated by comparing them with the existing design standards developed for conventional reinforced concrete columns. An extensive regression analysis has been carried out to predict different mechanical properties of R^2C and FR^3C considering the effect of CR and fiber and the axial capacity of reinforced concrete (RC) columns made with these new types of concrete. Finally, different free vibration responses such as damping ratio, natural frequency, and time period were determined through a free vibration test of these R^2C and FR^3C columns. This chapter summarizes the conclusion of this study. Besides, research contribution, limitations, and recommendations for future study are also presented.

7.2 Conclusions

Based on experimental programs carried out in this research the following conclusions can be drawn:

7.2.1 Mechanical Properties of Concrete

1. Both the R^2C and FR^3C mixtures exhibited a reduced slump compared to the control mixture. The slump value was decreased by up to 54.5% and 69.7% for R^2C and FR^3C mixtures depending on the percentage of CR content.
2. The highest air content value was found at 2.95% and 2.60% in R^2C and FR^3C mixtures with 15% CR content whereas the control one exhibited 2.20% air content.
3. The addition of RCA and CR decreased the compressive strength and the decreasing percentage was increased with increasing the CR content both in R^2C and FR^3C specimens. However, the inclusion of fiber content in R^2C mixtures positively increased the compressive strength. More than 40 MPa concrete can be produced using 30% RCA and 5% CR content along with 0.5% PP fiber.
4. Though all the R^2C and FR^3C specimens provided comparatively lower tensile strength and flexural strength, the FR^3C specimens containing only 5% CR content showed a marginal reduction which was merely 3.3% and 6.8% lower respectively than that of the control one.
5. The R^2C and FR^3C specimens had a lower modulus of elasticity (MoE) than that of the control specimen. The MoE was decreased by 20.7%, 26.1%, 49.9% and 13.3%, 22.8%, 41.5% for R^2C and FR^3C specimens with 5%, 10%, and 15% CR content, respectively compared to the control one.
6. Approximately 8% density reduction can be achieved in R^2C and FR^3C depending on the percentage of CR and fiber content. Furthermore, the surface resistivity test revealed that for all the combinations of R^2C and FR^3C specimens, the chloride ion penetrability would be very low.
7. All the R^2C and FR^3C specimens exhibited lower UPV values than that of conventional concrete. However, though increasing the percentage of CR content simultaneously decreased the UPV, the addition of fiber increased it by approximately 28.8%, 14.1%, 9.0%, and 7.1% for 0%, 5%, 10%, and 15% CR content mixtures, respectively.

8. The FR^3C specimens exhibited comparatively ductile behavior without providing any aggregate spalling. Besides, no visible macro-cracks were pointed out after the compression test and provided no morphological change on the surface. Fiber delayed the first crack formation across the crack and retarded visible cracking. On the contrary, the NAC, RAC, and R^2C specimens provided several macro-cracks.
9. All available equations for predicting the tensile strength, flexural strength, compressive strength, or MoE of conventional concrete under-predicted or over-predicted the experimental results of R^2C and FR^3C. However, the proposed equations can predict these mechanical properties of R^2C and FR^3C more accurately as they consider the effect of RCA, CR, and fiber.
10. The total cost of R^2C was quite similar to the conventional concrete. On the contrary, due to the higher production cost of both CR and fiber compared to the conventional aggregates, FR^3C mixtures exhibited higher costs. However, both the R^2C and FR^3C mixtures save more energy costs and decrease the fuel consumption but the FR^3C mixtures can save more compared to R^2C mixtures. No payback period was required for RAC as well as R^2C mixture containing up to 5% CR content.

7.2.2 Compressive Behaviors Columns

1. For 75 mm tie-spaced columns, the NAC and RAC columns faced a large concrete separation from the surfaces whereas no significant spalled-off of concrete cover occurred in R^2C and FR^3C columns. However, in 150 mm tie-spaced R^2C columns, almost half of the entire column was damaged. Excessive buckling of the longitudinal and transverse steel bars, as well as the crushing of the concrete core, occurred. On the other hand, in both cases, the FR^3C columns provided more ductile phenomena without separating any concrete cover. The columns with a higher reinforcement ratio (2.0%) exhibited a higher crack resisting capacity.

2. The axial deformation corresponding to the peak point was increased up to 70% and 76% for R^2C and FR^3C columns compared to the control column depending on the percentage of CR content in 75 mm tie-spaced columns. For 150 mm tie-spaced columns, it was increased up to 44% and 54%, respectively.

3. The axial capacity was decreased by up to 37.4% and 35.5% for R^2C and FR^3C columns with 75 mm tie spacing and 39.6% and 33.0% for 150 mm tie-spaced columns depending on the percentage of CR content. However, the FR^3C columns exhibited comparatively higher axial capacity than those of R^2C columns. Besides, increasing the longitudinal reinforcement ratio from 1.4% to 2.0% the axial capacity was increased on average by 10%.

4. The axial strain of the longitudinal reinforcement was decreased by an average of 2.6% and 3.2% due to the addition of 0.5% PP fiber in 75 mm and 150 mm tie-spaced FR^3C columns.

5. The strength reduction factor for R^2C and FR^3C specimens varied from 0.52 to 0.68 and 0.52 to 0.78, respectively depending on the percentage of CR, tie spacing, and longitudinal reinforcement ratio.

6. The NAC and RAC columns exhibited almost similar ductility. However, up to 167% and 70% higher ductility was found in 75 mm and 150 mm tie-spaced FR^3C columns depending on the percentage of CR content. No significant variation in ductility was observed due to changing the longitudinal reinforcement ratio.

7. The toughness value of R^2C columns was decreased for 0%, 5%, and 10% CR content compared to the control one but then increased by 10.2% and 0.5% for 15% CR content in 75 mm and 150 mm tie-spaced columns. However, all FR^3C columns exhibited a higher toughness value and it was increased up to 1.73 times and 1.16 times for 75 mm and 150 mm tie-spaced columns depending on the percentage of CR content.

8. The plain concrete columns provided a comparatively lower Poisson's ratio than that of RC columns. Besides, the higher reinforcement ratio decreased the Poisson's ratio but the larger tie spacing increased it.

9. Though the existing equations can predict the nominal capacity of NAC and RAC columns accurately, they overestimate R^2C and FR^3C columns by an average of 38%.

7.2.3 Free Vibration Responses of Columns

1. The acceleration amplitude was increased by up to 21% and 41% for R^2C and FR^3C columns with increasing the imposed energy from 1.54 N.m to 2.13 N.m. And for 2.83 N.m it was increased by 36% and 66%, respectively. On the other hand, for the NAC and RAC columns, this increasing percentage was less than 2%.
2. All the R^2C and FR^3C columns had a lower natural frequency than that of the conventional column. For 5%, 10%, and 15% CR content the natural frequency was decreased by 4%, 25%, and 43% for R^2C columns and 1%, 7%, and 15% for FR^3C columns, respectively compared to the 0% CR content. The magnitude of the impact energy did not have any significant effect on the natural frequency.
3. The damping ratio of RAC, R^2C, and FR^3C columns were higher than that of the conventional column. With increasing the CR content, the damping ratio was increased and it was further increased for the fiber content. Approximately 131% and 301% higher damping ratio (ζ_{10}) was found with 15% CR content in R^2C and FR^3C columns.
4. With increasing the imposed energy from 1.54 N.m to 2.13 N.m the damping ratio (ζ_{10}) was increased by an average of 4% and 18% for R^2C and FR^3C columns whereas for 2.83 N.m it was increased by averagely 20% and 36%, respectively.
5. The damping coefficient for R^2C was increased up to 5% CR content and then decreased for 10% and 15% CR content but still higher than the control one. On the contrary, FR^3C columns exhibited a higher damping coefficient compared to control column and R^2C columns and it was increased with increasing the CR content.
6. No significant variation (less than 4%) was observed in the time period for changing the impact force. An increasing time period can be achieved with the addition of CR content in the concrete mixture and it was increased with increasing the CR content. The change in time period along with CR content was more prominent for R^2C columns than that of FR^3C columns. Though the addition of fiber content decreased the time period of FR^3C columns compared to R^2C columns, it was still higher than that of the conventional column.

7.3 Research Contribution

This experimental work investigates the acceptability of using different waste materials such as recycled coarse aggregate (RCA), crumb rubber (CR) along with polypropylene (PP) fiber in structural members. Based on the experimental results, it can be concluded that though different mechanical properties of concrete degrade after incorporating CR particles into the concrete mixture, it can be improved by using PP fiber content. More than 40 MPa concrete can be produced using 30% RCA and 5% CR content along with 0.5% PP fiber. Besides, a marginal reduction in other properties is found in this combination. Using the fiber content in the rubberized recycled concrete (R^2C) column significantly changed the failure mode. A higher ductility, toughness as well as an improved damping property is found for fiber-reinforced rubberized recycled concrete (FR^3C) columns. As the available equations for the conventional concrete either underestimate or overestimate different properties of R^2C and FR^3C or the axial capacity of R^2C and FR^3C columns, the proposed equations can predict them more accurately.

This study will facilitate engineers to determine the suitability of different combinations of RCA and CR with or without fiber depending on their intended use in practical applications. As this type of concrete can offer excellent vibration damping it can be used in foundation pads for heavy machinery, railway stations, as well as runway where a higher energy absorption and impact resistance capacity is required. Furthermore, the roadside barriers of highways and bridges, bridge piers, and bridge abutments may also be the application fields where toughness, ductility as well as energy dissipation are the primary concerns. Moreover, this study will effectively contribute toward alleviating the concerns regarding the disposal of waste materials along with mitigating the demand for natural aggregates and the associated environmental costs.

7.4 Limitations of This Study

Because of the unavailability of proper equipment, materials, and time restriction, this study has the following limitations:

1. Due to the lower capacity of UTM, all the columns were converted to a one-third scale. However, large-scale columns should be tested to predict their actual behaviors.

2. The CR used in this study was untreated. The CR particles should be treated with NaOH solution.
3. Due to time limitations, the number of combinations had to be reduced in this study. For obtaining the more optimum result further extensive study is needed.
4. The SEM (Scanning Electron Microscopy) test should be done to identify the actual phenomena at ITZ (Interfacial Transition Zone).
5. The proposed equations are valid for the range of CR content from 0% to 15% and for a constant RCA percentage of 30% and PP fiber content of 0.5%.

7.5 Recommendations for Future Research.

As RCA and CR have the structural potential for use as aggregate, they can use as sustainable construction materials. Since the application of fiber-reinforced rubberized recycled concrete (FR^3C) is an almost new concept in construction industries, therefore it needs more research on the different properties of R^2C and FR^3C before establishing them as safe and viable alternatives to natural aggregate concrete. Some future research may include:

1. Shake table testing should be performed to investigate different seismic performances of various structural elements and frames made with R^2C and FR^3C before using them in earthquake-resistant buildings.
2. Extensive investigation should be needed on the compressive behavior of R^2C and FR^3C columns under different eccentric loading conditions.
3. Long-term mechanical behavior of R^2C and FR^3C as well as their performance in high-strength concrete should be investigated.
4. Various durability properties under severe environmental exposure conditions along with their actual influence on the life cycle are required to be studied to assess the feasibility of using such waste as an environmentally friendly alternative to traditional materials.
5. Fire and blast resistance of R^2C and FR^3C based concrete structures should be investigated.
6. Shear behavior of reinforced concrete beams made with R^2C and FR^3C are needed to be studied.

7. No extensive investigation on bond behavior between steel and R^2C & FR^3C has been done. Thus, the future researcher can focus on it.
8. Incorporating machine learning (ML) techniques such as artificial neural network (ANN), random forest, and support vector machines the mechanical properties of R^2C and FR^3C like compressive strength, tensile strength, and MoE can predict. It is high time to conduct future research on ML techniques as very few publications have addressed this region so far [219-221].
9. Studying the possibility of optimizing the production process of RCA and CR particles need to be investigated to accomplish essential adjustments in their physical characteristics, like angularity, rough surfaces, flakiness, elongation, density, hydrophobicity, and impurities.

REFERENCES

[1] Mohammed, T. U., Hasnat, A., Awal, M. A., and Bosunia, S. Z., "Recycling of brick aggregate concrete as coarse aggregate," *Journal of Materials in Civil Engineering*, vol. 27, no. 7, p. B4014005, 2015.

[2] Huda, S. B., and Alam, M. S., "Mechanical behavior of three generations of 100% repeated recycled coarse aggregate concrete," *Construction and building materials*, vol. 65, pp. 574-582, 2014.

[3] McMillan, M., "Waste Management Industry Survey: Business and Government Sectors," in *Statistics Canada*, 2008.

[4] Xiao, J. Z., Li, W. G., Fan, Y. H., and Huang, X., "An overview of study on recycled aggregate concrete in China (1996–2011)," *Construction and Building Materials,* vol. 31, pp. 364–83, 2012.

[5] Matias, D., Brito, J., Rosa, A., and Pedro, D., "Mechanical properties of concrete produced with recycled coarse aggregates – Influence of the use of superplasticizers," *Construction and Building Materials,* vol. 44, pp. 101-109, 2013.

[6] USTMA, "2017 U.S. Scrap Tire Management Summary," in *U.S Tire Manufacturers Association (USTMA),* Washington DC, U.S.A, 2018.

[7] Thomas, B. S., Gupta, R. C., Kalla, P., and Cseteneyi, L., "Strength, abrasion and permeation characteristics of cement concrete containing discarded rubber fine aggregates," *Construction and Building Materials,* vol. 59, pp. 204-212, 2014.

[8] ACI Committee 555, "Removal and reuse of hardened concrete," in *American Concrete Institute*, Farmington Hills, MI, 2001.

[9] CSA A23.1/23.2, "Concrete Materials and Methods of Concrete Construction/Methods of Test and Standard Practices for Concrete," in *Canadian Standards Association*, Canada, 2014.

[10] ASTM C33, "Standard Specification for Concrete Aggregates," in *ASTM International*, West Conshohocken, PA, 2018.

[11] Ajdukiewicz, A. and Kliszczewicz, A., "Influence of recycled aggregates on mechanical properties of HS/HPC," *Cement and Concrete Composites*, vol. 24, no. 2, pp. 269–79, 2002.

[12] Ismail, M. K., and Hassan, A. A. A., "Performance of full-scale self-consolidating rubberized concrete beams in flexure," *ACI Materials Journal*, vol. 113, no. 2, pp. 207-218, 2016.

[13] Shahjalal, M., Islam, K., Rahman, J., Ahmed, K. S., Karim, M. R., and Billah, A. H. M. M., "Flexural response of fiber reinforced concrete beams with waste tires rubber and recycled aggregate," *Journal of Cleaner Production*, vol. 278, p. 123842, 2021.

[14] Zheng, L., Huo, X. S., and Yuan, Y., "Strength, modulus of elasticity, and brittleness index of rubberized concrete," *Journal of Materials in Civil Engineering,* vol. 20, no. 11, pp. 692-699, 2008.

[15] Shahjalal, M., Hossain, F. M. Z., Islam, K., Tiznobaik, M., and Alam, M. S., "Experimental Study on the Mechanical Properties of Recycled Aggregate Concrete Using Crumb Rubber and Polypropylene Fiber," *CSCE Annual Conference*, Canada, 2019.

[16] Hossain, F. M. Z., Shahjalal, M., Islam, K., Tiznobaik, M., and Alam, M. S., "Mechanical properties of recycled aggregate concrete containing crumb rubber and polypropylene fiber," *Construction and Building Materials,* vol. 225, pp. 983-996, 2019.

[17] Slater, E., Moni, M., and Alam, M. S., "Predicting the shear strength of steel fiber reinforced concrete beams," *Construction and Building Materials*, vol. 26, no. 1, pp. 423-436, 2012.

[18] Wang, J., Dai, Q., Si, R., and Guo, S., "Mechanical, durability, and microstructural properties of macro synthetic polypropylene (PP) fiber-reinforced rubber concrete," *Journal of Cleaner Production,* vol. 234, pp. 1351-1364, 2019.

[19] Ochi, T., Okubo, S., and Fukui, K., "Development of recycled PET fiber and its application as concrete-reinforcing fiber," *Cement and Concrete Composites*, vol. 29, no. 6, pp. 448-55, 2007.

[20] Shen, L., Worrell, E., and Patel, M. K., "Open-loop recycling: A LCA case study of PET bottle-to-fibre recycling," *Resources Conservation and Recycling*, vol. 55, no. 1, pp. 34–52, 2010.

[21] Choi, W., and Yun, H., "Compressive behavior of reinforced concrete columns with recycled aggregate under uniaxial loading," *Engineering structures,* vol. 41, pp. 285-293, 2012.

[22] Zhou, J. H., He, H. J., Meng, X. H., and Huan, S., "Experimental study of recycled concrete columns under large eccentric compression," in *12th international conference on engineering, science, construction, and operations in challenging, environments*, United States, 2010.

[23] Hassanli, R., Youssf, O., Vincent, T., Mills, J. E., Manalo, A., and Gravina, R., "Experimental study on compressive behavior of FRP-confined expansive rubberized concrete," *Journal of Composites for Construction,* vol. 24, no. 4, p. 04020034, 2020.

[24] Son, K. S., Hajirasouliha, I., and Pilakoutas, K., "Strength and deformability of waste tyre rubber-filled reinforced concrete columns," *Construction and Building Materials*, vol. 25, pp. 218–226, 2011.

[25] Xue, J. and Shinozuka, M., "Rubberized concrete: A green structural material with enhanced energy-dissipation capability," *Construction and Building Materials,* vol. 42 pp. 196–204, 2013.

[26] Klee, H., "The cement sustainability initiative: recycling concrete," *World Business Council for Sustainable Development (WBCSD): Geneva, Switzerland*, 2009.

[27] Behera, M., Bhattacharyya, S. K., Minocha, A. K., Deoliya, R., and Maiti, S., "Recycled aggregate from C&D waste & its use in concrete–A breakthrough towards sustainability in construction sector: A review," *Construction and building materials*, vol. 68, pp. 501-516, 2014.

[28] Martín-Morales, M., Zamorano, M., Ruiz-Moyano, A., and Valverde-Espinosa, I., "Characterization of recycled aggregates construction and demolition waste for concrete production following the Spanish Structural Concrete Code EHE-08," *Construction and building materials,* vol. 25, no. 2, pp. 742-748, 2011.

[29] Abbas, A., Fathifazl, G., Isgor, O. B., Razaqpur, A. G., Fournier, B., and Foo, S., "Environmental benefits of green concrete," in *EIC Climate Change Technology*, 2006: IEEE, pp. 1-8.

[30] Verian, K. P., Ashraf, W., and Cao, Y., "Properties of recycled concrete aggregate and their influence in new concrete production," *Resources, Conservation and Recycling*, vol. 133, pp. 30-49, 2018.

[31] Tamanna, K., *Mechanical properties of rubberized concrete containing recycled concrete aggregate and polypropylene fiber*, Master of Applied Science, Civil Engineering, University of British Columbia, Canada, 2018.

[32] Duan, Z. H., and Poon, C. S., "Properties of recycled aggregate concrete made with recycled aggregates with different amounts of old adhered mortars," *Materials & Design*, vol. 58, pp. 19-29, 2014.

[33] ECCO, "Recycling Concrete Saves Resources, Eliminates Dumping," in *Environmental Council of Concrete Organization*, Illinois, 2018.

[34] Verian, K. P., Whiting, N. M., Jitendra, J., Olek, J., and Snyder, M. B., "Using Recycled Concrete as Aggregate in Concrete Pavements to Reduce Materials Cost," in *Joint Transportation Research Program, Indiana Department of Transportation and Purdue University*, West Lafayette, Indiana, 2013.

[35] Sgobba, S., Borsa, M., Molfetta, M., and Marano, G. C., "Mechanical performance and medium-term degradation of rubberised concrete," *Construction and Building Materials*, vol. 98, pp. 820-831, 2015.

[36] Khaloo, A. R., Dehestani, M., and Rahmatabadi, P., "Mechanical properties of concrete containing a high volume of tire–rubber particles," *Waste Management*, vol. 28, no. 12, pp. 2472-2482, 2008.

[37] Ismail, M. K. and Hassan, A. A. A., "Shear behaviour of large-scale rubberized concrete beams reinforced with steel fibres," *Construction and Building Materials*, vol. 140, pp. 43-57, 2017.

[38] Mendis, A. S. M., Al-Deen, S., and Ashraf, M., "Flexural shear behaviour of reinforced Crumbed Rubber Concrete beam," *Construction and Building Materials*, vol. 166, pp. 779-791, 2018.

[39] Aslani, F., Ma, G., Wan, D. L. Y., and Muselin, G., "Development of high-performance self-compacting concrete using waste recycled concrete aggregates and rubber granules," *Journal of Cleaner Production*, vol. 182, pp. 553-566, 2018.

[40] Najim, K. B. and Hall, M. R., "A review of the fresh/hardened properties and applications for plain- (PRC) and self-compacting rubberised concrete (SCRC)," *Construction and Building Materials*, vol. 24, pp. 2043–2051, 2010.

[41] Oikonomou, N. D., "Recycled concrete aggregates," *Cement and concrete composites*, vol. 27, no. 2, pp. 315-318, 2005.

[42] Su, H., *Properties of concrete with recycled aggregates as coarse aggregate and as-received/surface-modified rubber particles as fine aggregate*, Ph.D., Department of Civil Engineering, University of Birmingham, 2015.

[43] Bai, G., Zhu, C., Liu, C., and Liu, B., "An evaluation of the recycled aggregate characteristics and the recycled aggregate concrete mechanical properties," *Construction and Building Materials*, vol. 240, p. 117978, 2020.

[44] Estanqueiro, B., Dinis Silvestre, J., de Brito, J., and Duarte Pinheiro, M., "Environmental life cycle assessment of coarse natural and recycled aggregates for concrete," *European Journal of Environmental and Civil Engineering*, vol. 22, no. 4, pp. 429-449, 2018.

[45] Evangelista, B. L., Rosado, L. P., and Penteado, C. S. G., "Life cycle assessment of concrete paving blocks using electric arc furnace slag as natural coarse aggregate substitute," *Journal of cleaner production*, vol. 178, pp. 176-185, 2018.

[46] Marinković, S. B., Malešev, M., and Ignjatović, I., "Life cycle assessment (LCA) of concrete made using recycled concrete or natural aggregates," *Eco-Efficient Construction and Building Materials*, pp. 239-266, 2014.

[47] Hossain, M. U., Poon, C. S., Lo, I. M. C., and Cheng, J. C. P., "Comparative environmental evaluation of aggregate production from recycled waste materials and virgin sources by LCA," *Resources, Conservation and Recycling*, vol. 109, pp. 67-77, 2016.

[48] Ganjian, E., Khorami, M., and Maghsoudi, A. A., "Scrap-tyre-rubber replacement for aggregate and filler in concrete," *Construction and building materials*, vol. 23, no. 5, pp. 1828-1836, 2009.

[49] Baoshan, H., Guoqiang, L., Su-Seng, P., and John, E., "Investigation into Waste Tire Rubber-Filled Concrete," *Journal of Materials in Civil Engineering*, vol. 16, no. 3, pp. 187–94, 2004.

[50] Emiroglu, M., Kelestemur, M. H., and Yildiz, S., "An investigation on ITZ microstructure of the concrete containing waste vehicles tire," in *Proceedings of 8th International Fracture Conference*, Istanbul/TURKEY, 2007.

[51] Mhaya, A. M., Huseien, G. F., Abidin, A. R. Z., and Ismail, M., "Long-term mechanical and durable properties of waste tires rubber crumbs replaced GBFS modified concretes," *Construction and Building Materials*, vol. 256, p. 119505, 2020.

[52] Rashad, A. M., "A comprehensive overview about recycling rubber as fine aggregate replacement in traditional cementitious materials," *International Journal of Sustainable Built Environment*, vol. 5, no. 1, pp. 46-82, 2016.

[53] Roychand, R., Gravina, R. J., Zhuge, Y., Ma, X., Youssf, O., and Mills, J. E., "A comprehensive review on the mechanical properties of waste tire rubber concrete," *Construction and Building Materials*, vol. 237 p. 117651, 2020.

[54] Siddique, R. and Cachim, P., "Waste and supplementary cementitious materials in concrete: Characterisation, properties and applications," *Woodhead Publishing*, pp. 51-77, 2018.

[55] Gerges, N. N., Issa, C. A., and Fawaz, S. A., "Rubber concrete: Mechanical and dynamical properties," *Case Studies in Construction Materials*, vol. 9, p. e00184, 2018.

[56] Meherier, M. S., *Investigation of mechanical and durability properties of cement mortar and concrete with varying replacement levels of crumb rubber as fine aggregate*, Master of Applied Science, Civil Engineering, University of British Columbia, Canada, 2016.

[57] Gupta, T., Chaudhary, S., and Sharma, R. K., "Assessment of mechanical and durability properties of concrete containing waste rubber tire as fine aggregate," *Construction and Building Materials*, vol. 73, pp. 562-574, 2014.

[58] Angelin, A. F., Da Silva, F. M., Barbosa, L. A. G., Lintz, R. C. C., De Carvalho, M. A. G., and Franco, R. A. S., "Voids identification in rubberized mortar digital images using K-Means and Watershed algorithms," *Journal of Cleaner Production* vol. 164, pp. 455-464, 2017.

[59] Shahjalal, M., Islam, K., Ahmed, K. S., K., T., and Alam, M. S., "Mechanical Characterization of Rubberized Fiber Reinforced Recycled Aggregate Concrete for

Bridge Barriers," in *IABSE-JSCE Joint Conference on Advances in Bridge Engineering-IV*, Dhaka, Bangladesh, 2020.

[60] Chen, J. H., Chen, K. S., and Tong, L. Y., "On the pyrolysis kinetics of scrap automotive tires," *Journal of Hazardous Materials,* vol. 84, no. 1, pp. 43-55, 2001.

[61] Copetti, C. M., Borges, P. M., Squiavon, J. Z., Silva, S. R., and Andrade, J. J. O., "Evaluation Of Tire Rubber Surface Pre-Treatment And Silica Fume On Physical-Mechanical Behavior And Microstructural Properties Of Concrete," *Journal of Cleaner Production,* vol. 256, p. 120670, 2020.

[62] Muñoz-Sánchez, B., Arévalo-Caballero, M. J., and Pacheco-Menor, M. C., "Influence of acetic acid and calcium hydroxide treatments of rubber waste on the properties of rubberized mortars," *Materials and Structures,* vol. 50, no. 1, p. 75, 2016.

[63] Ahmed, H., Tiznobaik, M., and Alam, M. S., "Mechanical and Durability Properties of Rubberized Recycled Aggregate Concrete," *CSCE Annual Conference,* Canada, 2019.

[64] Mavroulidou, M. and Figueiredo, J., "Discarded tyre rubber as concrete aggregate: a possible outlet for used tyres," *Global NEST Journal,* vol. 12, no. 4, pp. 359-367, 2010.

[65] Wong, S. and Ting, S., "Use of recycled rubber tires in normal-and high-strength concretes," *ACI Materials Journal,* vol. 106, no. 4, p. 325, 2009.

[66] Alfayez, S. F., *Eco-Effifficient Preplaced Recycled Aggregate Concrete Incorporating Recycled Tire Waste Rubber Granules and Steel Wire Fibre Reinforcement*, Master of Engineering Science, Civil and Environmental Engineering Department, The University of Western Ontario, 2018.

[67] Gesoğlu, M., Güneyisi, E., Khoshnaw, G., and İpek, S., "Abrasion and freezing–thawing resistance of pervious concretes containing waste rubbers," *Construction and Building Materials,* vol. 73, pp. 19-24, 2014.

[68] Moustafa, A. and ElGawady, M. A., "Dynamic Properties of High Strength Rubberized Concrete," *ACI Symposium Publication,* vol. 314, pp. 1-22, 2017.

[69] Presti, D. L., "Recycled tyre rubber modified bitumens for road asphalt mixtures: A literature review," *Construction and Building Materials,* vol. 49, pp. 863-881, 2013.

[70] Reda-Taha, M. M., El-Dieb, A. S., Abd.El-Wahab, M. A., and Abdel-Hameed, M. E., "Mechanical, fracture, and microstructural investigations of rubber concrete," *Journal of Materials in Civil Engineering,* vol. 20, no. 10, pp. 640-649, 2008.

[71] Eldin, N. N. and Senouci, A. B., "Measurement and prediction of the strength of rubberized concrete," *Cement and Concrete Composites,* vol. 16, no. 4, pp. 287-298, 1994.

[72] Khatib, Z. K., and Bayomy, F. M., "Rubberized Portland cement concrete," *Journal of materials in civil engineering,* vol. 11, no. 3, pp. 206-213, 1999.

[73] Bravo, M. and de Brito, J., "Concrete made with used tyre aggregate: durability-related performance," *Journal of Cleaner Production,* vol. 25, pp. 42-50, 2012.

[74] Thomas, B. S., Gupta, R. C., and Panicker, V. J., "Recycling of waste tire rubber as aggregate in concrete: durability-related performance," *Journal of Cleaner Production,* vol. 112, pp. 504-513, 2016.

[75] Hanai, J. B., and Holanda, K. M. A., "Similarities between punching and shear strength of steel fiber reinforced concrete (SFRC) slabs and beams," *RIEM-IBRACON Structures and Materials Journal,* vol. 1, no. 1, 2008.

[76] Banthia, N. and Soleimani, S. M., "Flexural response of hybrid fiber-reinforced cementitious composites," *ACI Materials Journal,* vol. 102, no. 6, p. 382, 2005.

[77] Pająk, M. and Ponikiewski, T., "Flexural behavior of self-compacting concrete reinforced with different types of steel fibers," *Construction and Building Materials,* vol. 47, pp. 397-408, 2013.

[78] Banthia, N. and Trottier, J., "Test methods for fexural toughness characterization of fiber reinforced concrete: Some concerns and a proposition," *Materials Journal,* vol. 92, no. 1, pp. 48-57, 1995.

[79] Pelisser, F., Zavarise, N., Longo, T. A., and Bernardin, A. M., "Concrete made with recycled tire rubber: Effect of alkaline activation and silica fume addition," *Journal of Cleaner Production,* vol. 19, no. 6, pp. 757-763, 2011.

[80] Benazzouk, A. and Queneudec, M., "Durability of cement-rubber composites under freeze thaw cycles," *Proceeding of International Congress of Sustainable Concrete Construction,* vol. 5, pp. 355-362, 2002.

[81] Mohseni, E., Saadati, R., Kordbache, N., Parpinchi, Z. S., and Tang, W., "Engineering and microstructural assessment of fibre-reinforced self-compacting concrete containing recycled coarse aggregate," *Journal of Cleaner Production,* vol. 168, pp. 605-613, 2017.

[82] Richardson, A. E., Coventry, K. A., and Ward, G., "Freeze/thaw protection of concrete with optimum rubber crumb content," *Journal of Cleaner Production*, vol. 23, no. 1, pp. 96-103, 2012.

[83] Batayneh, M. K., Marie, I., and Asi, I., "Promoting the use of crumb rubber concrete in developing countries," *Waste Management*, vol. 28, no. 11, pp. 2171-2176, 2008.

[84] Marie, I., "Thermal conductivity of hybrid recycled aggregate–Rubberized concrete," *Construction and Building Materials*, vol. 133, pp. 516-524, 2017.

[85] Henry, M., Yamashita, H., Nishimura, T., and Kato, Y., "Properties and mechanical–environmental efficiency of concrete combining recycled rubber with waste materials," *International Journal of Sustainable Engineering*, vol. 5, no. 1, pp. 66-75, 2012.

[86] Guo, Y., Zhang, J., Chen, G., and Xie, Z., "Compressive behaviour of concrete structures incorporating recycled concrete aggregates, rubber crumb and reinforced with steel fibre, subjected to elevated temperatures," *Journal of cleaner production*, vol. 72, pp. 193-203, 2014.

[87] Chen, A., Han, X., Chen, M., Wang, X., Wang, Z., and Guo, T., "Mechanical and stress-strain behavior of basalt fiber reinforced rubberized recycled coarse aggregate concrete," *Construction and Building Materials*, vol. 260, p. 119888, 2020.

[88] Jalal, M., Pouladkhan, A., Harandi, O. F., and Jafari, D., "Comparative study on effects of Class F fly ash, nano silica and silica fume on properties of high performance self compacting concrete," *Construction and Building Materials*, vol. 94, no. 3, pp. 90–104, 2015.

[89] Krishna, C. P. S. S., *Workability and Air Void Related Problems in Plain and Fly Ash Cementitious Systems*, M.S.C.E. Thesis, Civil Engineering Department, Purdue University, 2011.

[90] Gesoglu, M., Güneyisi, E., Hansu, O., İpek, S., and Asaad, D. S., "Influence of waste rubber utilization on the fracture and steel–concrete bond strength properties of concrete," *Construction and Building Materials*, vol. 101, pp. 1113-1121, 2015.

[91] Raffoul, S., Garcia, R., Pilakoutas, K., Guadagnini, M., and Medina, N. F., "Optimisation of rubberised concrete with high rubber content: An experimental investigation," *Construction and Building Materials*, vol. 124, pp. 391-404, 2016.

[92] Bompa, D. V., Elghazouli, A. Y., Xu, B., Stafford, P. J., and Ruiz-Teran, A. M., "Experimental assessment and constitutive modelling of rubberised concrete materials," *Construction and Building Materials,* vol. 137, pp. 246-260, 2017.

[93] Feng, L., Liang-yu, M., Guo-Fang, N., and Li-Juan, L., "Fatigue performance of rubber-modified recycled aggregate concrete (RRAC) for pavement," *Construction and Building Materials* vol. 95, pp. 207–217, 2015.

[94] Hesami, S., Hikouei, I. S., and Emadi, S. A. A., "Mechanical behavior of self-compacting concrete pavements incorporating recycled tire rubber crumb and reinforced with polypropylene fiber," *Journal of cleaner production,* vol. 133, pp. 228-234, 2016.

[95] Li, L., Tu, G., Lan, C., and Liu, F., "Mechanical characterization of waste-rubber-modified recycled-aggregate concrete," *Journal of Cleaner Production,* vol. 124, pp. 325-338, 2016.

[96] Li, L., Ruan, S., and Zeng, L., "Mechanical properties and constitutive equations of concrete containing a low volume of tire rubber particles," *Construction and Building Materials,* vol. 70, pp. 291-308, 2014.

[97] Chen, A., Wang, J., and Ma, Y., "Test of frost resistance for steel fiber rubber recycled concrete," *Acta Materiae Compositae Sinica*, vol. 32, no. 4, pp. 933–941, 2015.

[98] Yongggui, W., Hughes, P., Haicheng, N., and Yuhui, F., "A new method to improve the properties of recycled aggregate concrete: composite addition of basalt fiber and nano-silica," *Journal of Cleaner Production,* vol. 236, p. 117602, 2019.

[99] Xie, J., Fang, C., Lu, Z., Li, Z., and Li, L., "Effects of the addition of silica fume and rubber particles on the compressive behaviour of recycled aggregate concrete with steel fibres," *Journal of cleaner production,* vol. 197, pp. 656-667, 2018.

[100] Aslani, F. and Kelin, J., "Assessment and development of high-performance fibre-reinforced lightweight self-compacting concrete including recycled crumb rubber aggregates exposed to elevated temperatures," *Journal of Cleaner Production,* vol. 200, pp. 1009-1025, 2018.

[101] Turatsinze, A. and Garros, M., "On the modulus of elasticity and strain capacity of self-compacting concrete incorporating rubber aggregates," *Resources, conservation and recycling,* vol. 52, no. 10, pp. 1209-1215, 2008.

[102] Benazzouk, A., Douzane, O., Langlet, T., Mezreb, K., Roucoult, J. M., and Quéneudec, M., "Physico-mechanical properties and water absorption of cement composite containing shredded rubber wastes," *Cement and Concrete Composites*, vol. 29, no. 10, pp. 732-740, 2007.

[103] Gupta, T., Siddique, S., Sharma, R. K., and Chaudhary, S., "Effect of elevated temperature and cooling regimes on mechanical and durability properties of concrete containing waste rubber fiber," *Construction and Building Materials*, vol. 137, pp. 35–45, 2017.

[104] Hilal, N. N., "Hardened properties of self-compacting concrete with different crumb rubber size and content," *International Journal of Sustainable Built Environment*, vol. 6, no. 1, pp. 191-206, 2017.

[105] Sofi, A., "Effect of waste tyre rubber on mechanical and durability properties of concrete–A review," *Ain Shams Engineering Journal*, vol. 9, no. 4, pp. 2691-2700, 2018.

[106] Jian-he, X., Yong-chang, G., Li-sha, L., and Zhi-hong, X., "Compressive and flexural behaviours of a new steel-fibre-reinforced recycled aggregate concrete with crumb rubber," *Construction and Building Materials* vol. 79, pp. 263–272, 2015.

[107] Al-Tayeb, M. M., Kang, J. F., and Jiang, Y. Q., "Improvement of cracking-resistance and flexural behavior of cement-based materials by addition of rubber particles," *Journal of Wuhan University of Technology-Mater. Sci.*, vol. 23, no. 4, pp. 579–583, 2008.

[108] Zheng, W. H., Li, L. J., and Liu, F., "The compressive and flexural deformation of rubberized concrete," *Advanced Materials Research*, vol. 168–170, pp. 1788–1791, 2011.

[109] Ding, Y., Zhang, F., Torgal, F., and Zhang, Y., "Shear behaviour of steel fibre reinforced self-consolidating concrete beams based on the modified compression field theory," *Composite Structures*, vol. 94, no. 8, pp. 2440-2449, 2012.

[110] Ning, X., Ding, Y., Zhang, F., and Zhang, Y., "Experimental study and prediction model for flexural behavior of reinforced SCC beam containing steel fibers," *Construction and Building Materials*, vol. 93, pp. 644-653, 2015.

[111] Tahenni, T., Chemrouk, M., and Lecompte, T., "Effect of steel fibers on the shear behavior of high strength concrete beams," *Construction and Building Materials,* vol. 105, pp. 14-28, 2016.

[112] MH/T 5004-2010, "Specifications for Airport Cement Concrete Pavement Design," *Civil Aviation Administration of China,* 2010.

[113] Dilbas, H., Simsek, M., and Cakir, O., "An investigation on mechanical and physical properties of recycled aggregate concrete (RAC) with and without silica fume," *Construction and Building Materials*, vol. 61, pp. 50-59, 2014.

[114] Topcu, I. B. and Sengel, S., "Properties of concretes produced with waste concrete aggregate," *Cement and Concrete Research,* vol. 34, no. 8, pp. 1307–1312, 2004.

[115] Graeff, A., Pilakoutas, K., Neocleous, K., Vania, M., and Peres, N., "Fatigue resistance and cracking mechanism of concrete pavements reinforced with recycled steel fibres recovered from post-consumer tyres," *Engineering Structure,* vol. 45, pp. 385-395, 2012.

[116] Turatsinze, A., Granju, J. L., and Bonnet, S., "Positive synergy between steel-fibres and rubber aggregates: effect on the resistance of cement-based mortars to shrinkage cracking," *Cement and Concrete Research,* vol. 36, no. 9, pp. 1692-1697, 2006.

[117] Zhang, P., Zhao, Y., Li, Q., Wang, P., and Zhang, T., "Flexural Toughness of Steel Fiber Reinforced High Performance Concrete Containing Nano-SiO_2 and Fly Ash," *The Scientific World Journal* vol. 2014, 2014.

[118] Tamanna, K., Tiznobaik, M., Rockson, C., N., B., and Alam, M. S., "Experimental Investigation of the Flexural Behaviour of Rubberized Concrete Containing Recycled Concrete Aggregate," in *CSCE Annual Conference*, Canada, 2019.

[119] Bui, N. K., Satomi, T., and Takahashi, H., "Mechanical properties of concrete containing 100% treated coarse recycled concrete aggregate," *Construction and Building Materials*, vol. 163, pp. 496-507, 2018.

[120] Zhu, Y., Kou, S., Poon, C., Dai, J., and Li, Q., "Influence of silane-based water repellent on the durability properties of recycled aggregate concrete," *Cement and Concrete Composites*, vol. 35, no. 1, pp. 32-38, 2013.

[121] Xuan, D., Zhan, B., and Poon, C. S., "Durability of recycled aggregate concrete prepared with carbonated recycled concrete aggregates," *Cement and Concrete Composites,* vol. 84, pp. 214-221, 2017.

[122] Youssf, O., Hassanli, R., Mills, J. E., Skinner, W., Ma, X., Zhuge, Y., Roychand, R., and Gravina, R., "Influence of mixing procedures, rubber treatment, and fibre additives on rubcrete performance," *Journal of Composites Science,* vol. 3, no. 2, p. 41, 2019.

[123] Siddique, R. and Naik, T. R., "Properties of concrete containing scrap-tire rubber–an overview," *Waste Management,* vol. 24, no. 6, pp. 563-569, 2004.

[124] Mohammadi, I., Khabbaz, H., and Vessalas, K., "Enhancing mechanical performance of rubberised concrete pavements with sodium hydroxide treatment," *Materials and Structures,* vol. 49, no. 3, pp. 813-827, 2016.

[125] ACPA, "Production of RCA," *Available: http://1204075.sites.myregisteredsite.com/downloads/TS/EB043P/TS043.2P.pdf (Accessed June 04, 2017),* 2010.

[126] Tang, W., Khavarian, M., Yousefi, A., Chan, R. W. K., and Cui, H., "Influence of surface treatment of recycled aggregates on mechanical properties and bond strength of self-compacting concrete," *Sustainability,* vol. 11, no. 15, p. 4182, 2019.

[127] Su, H., Yang, J., Ghataora, G. S., and Dirar, S., "Surface modified used rubber tyre aggregates: effect on recycled concrete performance," *Magazine of Concrete Research,* vol. 67, no. 12, pp. 680-691, 2015.

[128] Dong, Q., Huang, B., and Shu, X., "Rubber modified concrete improved by chemically active coating and silane coupling agent," *Construction and Building Materials,* vol. 48, pp. 116-123, 2013.

[129] Najim, K. B. and Hall, M. R., "Crumb rubber aggregate coatings/pre-treatments and their effects on interfacial bonding, air entrapment and fracture toughness in self-compacting rubberised concrete (SCRC)," *Materials and Structures,* vol. 46, no. 12, pp. 2029-2043, 2013.

[130] Onuaguluchi, O. and Panesar, D. K., "Hardened properties of concrete mixtures containing pre-coated crumb rubber and silica fume," *Journal of Cleaner Production,* vol. 82, pp. 125-131, 2014.

[131] Emam, E. and Yehia, S., "Experimental study on enhanced crumb rubber concrete," *International Journal of Scientific and Engineering Research,* vol. 9, no. 2, pp. 1240-1247, 2018.

[132] Guo, Y. C., Zhang, J. H., Chen, G., Chen, G. M., and Xie, Z. H., "Fracture behaviors of a new steel fiber reinforced recycled aggregate concrete with crumb rubber," *Construction and Building Materials* vol. 53, pp. 32–39, 2014.

[133] Netinger, I., Kesegic, I., and Guljas, I., "The effect of high temperatures on the mechanical properties of concrete made with different types of aggregates," *Fire Safety Journal,* vol. 46, no. 7, pp. 425-430, 2011.

[134] Lau, A. and Anson, M., "Effect of high temperatures on high performance steel fibre reinforced concrete," *Cement and Concrete Research,* vol. 36, no. 9, pp. 1698-1707, 2006.

[135] Mendis, A. S. M., Al-Deen, S., and Ashraf, M., "Behaviour of similar strength crumbed rubber concrete (CRC) mixes with different mix proportions," *Construction and Building Materials,* vol. 137, pp. 354–366, 2017.

[136] Mutsuddy, R., *Bond Performance between Lightweight Concrete with Crumb Rubber and Glass Fibre Reinforced Polymer Bar*, Ph.D. in Structural Engineering, Department of Civil and Environmental Engineering, University of Alberta, Canada, 2017.

[137] ACI 318-14, "Building Code Requirements for Structural Concrete and Commentary," in *American Concrete Institute*, Farmington Hills, MI, 2014.

[138] ACI 209, "Prediction of Creep, Shrinkage and Temperature Effects in Concrete Structures," in *American Concrete Institute*, Farmington Hills, MI, 2008.

[139] EN1992-1-1, "Design of concrete structures: General rules and rules for buildings," in *European Standard*, 1992.

[140] CSA A23.3-14, "Design of Concrete Structures," in *Canadian Standards Association*, Canada, 2014.

[141] AS 3600, "Concrete Structures: Design Properties of materials," in *Australian Standard*, Australia, 2009.

[142] ACI 363, "State-of-the-Art Report on High-Strength Concrete," in *American Concrete Institute,* Farmington Hills, MI, 1997.

[143] fib, "fib Model Code for Concrete Structures," in *International Fedaration for Structural Concrete*, 2010.

[144] Al-Tayeb, M. M., Bakar , B. H. A., Ismail, H., and Akil, H. M., "Effect of partial replacement of sand by recycled fine crumb rubber on the performance of hybrid rubberized-normal concrete under impact load: experiment and simulation," *Journal of Cleaner Production,* vol. 59, pp. 284-289, 2013.

[145] Grinys, A., Sivilevicius, H., Pupeikis, D., and Ivanauskas, E., "Fracture of concrete containing crumb rubber," *Journal of Civil Engineering and Management,* vol. 19, no. 3, pp. 447–55, 2013.

[146] Xie, J., Guo, Y., Liu, L., and Xie, Z., "Compressive and flexural behaviours of a new steel-fibre-reinforced recycled aggregate concrete with crumb rubber," *Construction and Building materials,* vol. 79, pp. 263-272, 2015.

[147] Martínez-Lage, I., Vázquez-Burgo, P., and Velay-Lizancos, M., "Sustainability evaluation of concretes with mixed recycled aggregate based on holistic approach: technical, economic and environmental analysis," *Waste Management,* vol. 104, pp. 9-19, 2020.

[148] Andersson, R., Stripple, H., Gustafsson, T., and Ljungkrantz, C., "Carbonation as a method to improve climate performance for cement based material," *Cement and Concrete Research*, vol. 124, p. 105819, 2019.

[149] Yang, K.-H., Seo, E.-A., and Tae, S.-H., "Carbonation and CO2 uptake of concrete," *Environmental Impact Assessment Review*, vol. 46, pp. 43-52, 2014.

[150] Li, W., Wang, Q., Jin, J., and Li, S., "A life cycle assessment case study of ground rubber production from scrap tires," *The International Journal of Life Cycle Assessment,* vol. 19, no. 11, pp. 1833-1842, 2014.

[151] Xiao, J., Wang, C., Ding, T., and Akbarnezhad, A., "A recycled aggregate concrete high-rise building: Structural performance and embodied carbon footprint," *Journal of Cleaner Production,* vol. 199, pp. 868-881, 2018.

[152] Kim, T. H., and Chae, C. U., "Environmental impact analysis of acidification and eutrophication due to emissions from the production of concrete," *Sustainability,* vol. 8, no. 6, p. 578, 2016.

[153] Piotrowska, K., Kruszelnicka, W., Bałdowska-Witos, P., Kasner, R., Rudnicki, J., Tomporowski, A., Flizikowski, J., and Opielak, M., "Assessment of the Environmental Impact of a Car Tire throughout Its Lifecycle Using the LCA Method," *Materials,* vol. 12, no. 24, p. 4177, 2019.

[154] Moro, C., Francioso, V., Schrager, M., and Velay-Lizancos, M., "TiO2 nanoparticles influence on the environmental performance of natural and recycled mortars: A life cycle assessment," *Environmental Impact Assessment Review,* vol. 84, p. 106430, 2020.

[155] Ajdukiewicz, A. B. and Kliszczewicz, A. T., "Comparative tests of beams and columns made of recycled aggregate concrete and natural aggregate concrete," *Journal of Advanced Concrete Technology,* vol. 5, no. 2, pp. 259-273, 2007.

[156] Islam, M. M., Choudhury, M. S. I., and Amin, A. F. M. S., "Dilation effects in FRP-confined square concrete columns using stone, brick, and recycled coarse aggregates," *Journal of Composites for Construction,* vol. 20, no. 1, 2015.

[157] Choudhury, M. S. I., Amin, A. F. M. S., Islam, M. M., and Hasnat, A., "Effect of confining pressure distribution on the dilation behavior in FRP-confined plain concrete columns using stone, brick and recycled aggregates," *Construction and Building Materials,* vol. 102, pp. 541–551, 2016.

[158] Breccolotti, M. and Materazzi, A. L., "Structural reliability of eccentrically-loaded sections in RC columns made of recycled aggregate concrete," *Engineering Structures,* vol. 32, pp. 3704–3712, 2010.

[159] Eltayeb, E., Ma, X., Zhuge, Y., Youssf, O., Mills, J. E., Xiao, J., and Singh, A., "Structural performance of composite panels made of profiled steel skins and foam rubberised concrete under axial compressive loads," *Engineering Structures,* vol. 211, p. 110448, 2020.

[160] Raza, A., Ali, B., and Aslam, H. M. U., "Axial performance of hybrid fiber reinforced concrete columns having GFRP longitudinal bars and spirals," *Journal of Building Engineering,* vol. 35, p. 102017, 2021.

[161] Chao, S.-H., Shamshiri, M., Liu, X., Palacios, G., Schultz, A. E., and Nojavan, A., "Seismically Robust Ultra-High-Performance Fiber-Reinforced Concrete Columns," *ACI Structural Journal*, vol. 118, no. 2, pp. 17-32, 2021.

[162] Zheng, L., Huo, X. S., and Yuan, Y., "Experimental investigation on dynamic properties of rubberized concrete," *Construction and Building Materials,* vol. 22, pp. 939–947, 2008.

[163] Moustafa, A., Gheni, A., and ElGawady, M. A., "Shaking-Table Testing of High Energy–Dissipating Rubberized Concrete Columns," *Journal of Bridge Engineering,* vol. 22, no. 8, p. 04017042, 2017.

[164] Pitilakis, D., Anastasiadis, A., Vratsikidis, A., Kapouniaris, A., Massimino, M. R., Abate, G., and Corsico, S., "Large-scale field testing of geotechnical seismic isolation of structures using gravel-rubber mixtures," *Earthquake Engineering & Structural Dynamics,* vol. 50, no. 10, pp. 1–20, 2021.

[165] Youssf, O., ElGawady, M. A., and Mills, J. E., "Experimental Investigation of Crumb Rubber Concrete Columns under Seismic Loading," *Structures,* vol. 3, pp. 13–27, 2015.

[166] Mo, J., Zeng, L., Liu, Y., Ma, L., Liu, C., Xiang, S., and Cheng, G., "Mechanical properties and damping capacity of polypropylene fiber reinforced concrete modified by rubber powder," *Construction and Building Materials,* vol. 242, p. 118111, 2020.

[167] KS F 2573:2014, "Recycled aggregates for concrete," in *Korean Standards Association*, Seoul, Korea, 2014.

[168] ASTM C114 -18, "Standard Test Methods for Chemical Analysis of Hydraulic Cement," in *ASTM International*, West Conshohocken, PA, 2018.

[169] ASTM C188-17, "Standard Test Method for Density of Hydraulic Cement," in *ASTM International*, West Conshohocken, PA, 2017.

[170] ASTM C204-18, "Standard Test Methods for Fineness of Hydraulic Cement by Air-Permeability Apparatus," in *ASTM International*, West Conshohocken, PA, 2018.

[171] ASTM C187 -16, "Standard Test Method for Amount of Water Required for Normal Consistency of Hydraulic Cement Paste," in *ASTM International*, West Conshohocken, PA, 2016.

[172] ASTM C191-19, "Standard Test Methods for Time of Setting of Hydraulic Cement by Vicat Needle," in *ASTM International*, West Conshohocken, PA, 2019.

[173] ASTM C109-13, "Standard Test Method for Compressive Strength of Hydraulic Cement Mortars (Using 2-in. or [50-mm] Cube Specimens)," *ASTM International*, vol. West Conshohocken, PA, 2013.

[174] ASTM C125-20, "Standard Terminology Relating to Concrete and Concrete Aggregates," in *ASTM International*, West Conshohocken, PA, 2020.

[175] ASTM C127-15, "Standard Test Method for Relative Density (Specific Gravity), and Absorption of Coarse Aggregate," in *ASTM International*, West Conshohocken, PA, 2015.

[176] ASTM C128-15, "Standard Test Method for Relative Density (Specific Gravity), and Absorption of Fine Aggregate," in *ASTM International*, West Conshohocken, PA, 2015.

[177] ASTM C136-14, "Standard Test Method for Sieve Analysis of Fine and Coarse Aggregates," in *ASTM International*, West Conshohocken, PA, 2014.

[178] ASTM C29-17, "Standard Test Method for Bulk Density ("Unit Weight") and Voids in Aggregate," in *ASTM International*, West Conshohocken, PA, 2017.

[179] ASTM C131-20, "Standard Test Method for Resistance to Degradation of Small-Size Coarse Aggregate by Abrasion and Impact in the Los Angeles Machine," in *ASTM International*, West Conshohocken, PA, 2020.

[180] BS 812-105.2, "Testing aggregates. Methods for determination of particle shape. Elongation index of coarse aggregate," in *British Standards Institution*, UK 1990.

[181] BS 812-105.1, "Testing aggregates. Methods for determination of particle shape. Flakiness index," in *British Standards Institution*, UK, 1989.

[182] ASTM A615-20, "Standard Specification for Deformed and Plain Carbon-Steel Bars for Concrete Reinforcement," in *ASTM International*, West Conshohocken, PA, 2020.

[183] BSI-BS 6543, "BS 6543—guide to the use of industrial byproducts and waste materials in building and civil engineering," in *British Standards Institution*, London, 1985.

[184] Hendriks, C. F. and Pieterson, H. S., "Sustainable raw materials—construction and demolition waste. RILEM report," *RILEM Publication Series*, vol. 22, 1998.

[185] DM, "New technical standard for civil construction," in *Italian Ministry of Infrastructure*, 2008.

[186] Alam, M. S., Slater, E., and Billah, A. H. M. M., "Green concrete made with RCA and FRP scrap aggregate: Fresh and hardened properties," *Journal of Materials in Civil Engineering*, vol. 25, pp. 1783-94, 2013.

[187] Huda, S. B., and Alam, M. S., "Mechanical and freeze-thaw durability properties of recycled aggregate concrete made with recycled coarse aggregate," *Journal of Materials in Civil Engineering*, vol. 27, no. 10, p. 04015003, 2015.

[188] Limbachiya, M., Leelawat, T., and Dhir, R., "Use of recycled concrete aggregate in high-strength concrete," *Materials and Structures*, vol. 33, p. 574, 2000.

[189] Etxeberria, M., Vazquez, E., Marí, A., and Barra, M., "Influence of amount of recycled coarse aggregates and production process on properties of recycled aggregate concrete," *Cement and Concrete Research*, vol. 37, pp. 735-42, 2007.

[190] Mohod, M. V., "Performance of polypropylene fibre reinforced concrete," *IOSR Journal of Mechanical and Civil Engineering*, vol. 12, no. 1, pp. 28-36, 2015.

[191] ASTM C31-19, "Standard Practice for Making and Curing Concrete Test Specimens in the Field," in *ASTM International*, West Conshohocken, PA, 2019.

[192] Liu, T., Wang, Z., Guo, J., and Wang, J., "Shear Strength of Dry Joints in Precast UHPC Segmental Bridges: Experimental and Theoretical Research," *Journal of Bridge Engineering*, vol. 24, no. 1, p. 04018100, 2019.

[193] JCI-S-002-2003, "Method of test for load-displacement curve of fiber reinforced concrete by use of notched beam," in *Japan Concrete Institute Standard*, Japan, 2003.

[194] ACI 318/318R, "Building Code Requirements for Reinforced Concrete," in *American Concrete Institute*, Farmington Hills, MI, 2014.

[195] Manzur, T., Khomeni, A., Baten, B., and Hossain, K. M. A., "Investigating significance of various parameters affecting capacity of core drilled columns for safe core extraction," *Engineering Structures*, vol. 200 p. 109722, 2019.

[196] ASTM C143-15, "Standard Test Method for Slump of Hydraulic-Cement Concrete," in *ASTM International*, West Conshohocken, PA, 2015.

[197] ASTM C231-17, "Standard Test Method for Air Content of Freshly Mixed Concrete by the Pressure Method," in *ASTM International*, West Conshohocken, PA, 2017.

[198] ASTM C39-18, "Standard Test Method for Compressive Strength of Cylindrical Concrete Specimens," in *ASTM International*, West Conshohocken, PA, 2018.

[199] ASTM C469-14, "Standard Test Method for Static Modulus of Elasticity and Poisson's Ratio of Concrete in Compression," in *ASTM International*, West Conshohocken, PA, 2014.

[200] ASTM C597-16, "Standard Test Method for Pulse Velocity Through Concrete," in *ASTM International*, West Conshohocken, PA, 2016.

[201] AASHTO TP 95, "Standard Method of Test for Surface Resistivity of Concrete's Ability to Resist Chloride Ion Penetration," in *American Association of State Highway and Transportation Official*, Washington, DC, 2011.

[202] ASTM C642-13, "Standard Test Method for Density, Absorption, and Voids in Hardened Concrete," in *ASTM International*, West Conshohocken, PA, 2013.

[203] Bartos, P. J. M., Sonebi, M., and Tamimi, A. K., "Workability and Rheology of Fresh Concrete: Compendium of Tests," in *Report of Technical Committee TC145 WSM*, 2002.

[204] EN 206-1, "Concrete-Part 1: Specification, performance, production and conformity," in *European Standard*, 2000.

[205] ASTM C330–17, "Standard Specification for Lightweight Aggregates for Structural Concrete," *ASTM International,* vol. West Conshohocken, PA, 2017.

[206] Neville, A. M., "Properties of Concrete," Fifth Ed.: Pearson Education Limited, 2011.

[207] Albano, C., Camacho, N., Hernandez, M., and Matheus, A., "Influence of content and particle size of waste pet bottles on concrete behavior at different w/c ratios," *Waste Management,* vol. 29, no. 10, pp. 2707-2716, 2009.

[208] Jones, R. and Facaroau, I., "Incerearea Nedistructiva a Betonului," *Editure Technica*, vol. Bucauresti, 1971.

[209] Eurocode 2, "EN 1992-1-1, Design of Concrete Structures – Part 1–1: General Rules and Rules for Buildings," in *Thomas Telford*, London, UK, 2005.

[210] Babu, D. S., Babu, K. G., and Wee, T. H., "Properties of lightweight expanded polystyrene aggregate concretes containing fly ash," *Cement and Concrete Research,* vol. 35, no. 6, pp. 1218-1223, 2005.

[211] Mohammed, T. U., and Rahman, M. N., "Effect of types of aggregate and sand-to-aggregate volume ratio on UPV in concrete," *Construction and Building Materials,* vol. 125 pp. 832-841, 2016.

[212] Ravindrarajah, R. S. and Tuck, A., "Properties of hardened concrete containing treated expanded polystyrene beads," *Cement and Concrete Composites*, vol. 16, no. 4, pp. 273-277, 1994.

[213] Al-Osta, M. A., Al-Tamimi, A. S., Al-Tarbi, S. M., Al-Amoudi, O. S. B., Al-Awsh, W. A., and Saleh, T. A., "Development of sustainable concrete using recycled high-density polyethylene and crumb tires: Mechanical and thermal properties," *Journal of Building Engineering,* vol. 45, p. 103399, 2022.

[214] Yildiz, A., Gurlek, G., Erkek, M., and Özbalta, N., "Economical and environmental analyses of thermal insulation thickness in buildings," *Journal of Thermal Science and Technology,* vol. 28, no. 2, pp. 25-34, 2008.

[215] Pessiki, S. and S., P., "Axial load behavior of large-scale spirally-reinforced highstrength concrete columns," *ACI Structural Journal*, vol. 94, no. 3, pp. 304–14, 1997.

[216] Response-2000, "Response-2000 v1.0, An utility designed to calculate the strength of traditional columns and more," University of Toronto, Canada, 2001.

[217] Memari, A. M., Motlagh, A. Y., and Scanlon, A., "Seismic evaluation of an existing reinforced concrete framed tube building based on inelastic dynamic analysis," *Engineering Structures*, vol. 22, no. 6, pp. 621–637, 2000.

[218] Chopra, A. K., "Dynamics of structures," in *5th Edition,* Pearson: Prentice Hall, 2017.

[219] Bachir, R., Mohammed, A. M. S., and Habib, T., "Using Artificial Neural Networks Approach to Estimate Compressive Strength for Rubberized Concrete," *Periodica Polytechnica Civil Engineering*, vol. 62, no. 4, pp. 858–865, 2018.

[220] Behnood, A., Olek, J., and Glinicki, M. A., "Predicting modulus elasticity of recycled aggregate concrete using M50 model tree algorithm," *Construction and Building Materials*, vol. 94, pp. 137–147, 2015.

[221] Zhang, J., Ma, G., Huang, Y., Sun, J., Aslani, F., and Nener, B., "Modelling uniaxial compressive strength of lightweight self-compacting concrete using random forest regression," *Construction and Building Materials* vol. 210, pp. 713–719, 2019.

APPENDIX A

Table A.1 Summary of fresh properties of different concrete mixtures.

Batch No		BN-1	BN-2	BN-3	BN-4	BN-5	BN-6	BN-7	BN-8	BN-9
Batch Name		$R_0C_0F_0$	$R_{30}C_0F_0$	$R_{30}C_5F_0$	$R_{30}C_{10}F_0$	$R_{30}C_{15}F_0$	$R_{30}C_0F_{0.5}$	$R_{30}C_5F_{0.5}$	$R_{30}C_{10}F_{0.5}$	$R_{30}C_{15}F_{0.5}$
Slump (mm)		165.0	150.0	130.0	90.0	75.0	85.0	75.0	60.0	50.0
	% Change		-9.1	-21.2	-45.5	-54.5	-48.5	-54.5	-63.6	-69.7
Air Content (%)		2.20	2.42	2.65	2.80	2.95	2.35	2.40	2.52	2.60
	% Change		10.0	20.5	27.3	34.1	6.8	9.1	14.5	18.2
Fresh Density (kg/m^3)		2427	2366	2275	2254	2225	2317	2246	2218	2161
	% Change		-2.5	-6.3	-7.1	-8.3	-4.5	-7.5	-8.6	-11.0

Table A.2 Summary of compression test results of different concrete batches.

Batch No		BN-1	BN-2	BN-3	BN-4	BN-5	BN-6	BN-7	BN-8	BN-9
Batch Name		$R_0C_0F_0$	$R_{30}C_0F_0$	$R_{30}C_5F_0$	$R_{30}C_{10}F_0$	$R_{30}C_{15}F_0$	$R_{30}C_0F_{0.5}$	$R_{30}C_5F_{0.5}$	$R_{30}C_{10}F_{0.5}$	$R_{30}C_{15}F_{0.5}$
7 Days		22.20	19.80	14.60	10.60	11.90	21.00	16.30	14.50	14.10
	Individual	19.90	18.30	14.60	12.90	10.40	21.80	15.70	14.80	12.40
		19.60	19.50	16.50	13.80	11.00	20.40	14.50	15.20	15.00
	Average	28.90	24.20	15.23	12.43	11.10	29.08	15.50	14.83	13.83
	SD	0.30	0.79	1.10	1.65	0.75	0.19	0.92	0.35	1.32
	COV	0.01	0.03	0.07	0.13	0.07	0.01	0.06	0.02	0.10
	% Change		-16.3	-47.3	-57.0	-61.6	0.6	-46.4	-48.7	-52.1
	Fracture Type	Cone and Shear	Cone and Shear	Shear	Shear	Shear	Cone and Shear	Cone and Shear	Cone and Shear	Cone and Shear
	Failure Type	Combined	Combined	Combined	Combined	Combined	Combined	Combined	Combined	Combined
28 Days		44.60	38.23	32.00	32.70	24.60	44.20	38.30	34.70	31.20
	Individual	41.30	35.30	34.70	30.70	23.30	43.50	38.80	33.20	31.90
		42.70	34.70	34.80	28.10	24.10	43.00	41.70	31.93	30.40
	Average	42.87	36.08	33.83	30.50	24.00	43.57	39.60	33.28	31.17
	SD	1.66	1.89	1.59	2.31	0.66	0.60	1.84	1.39	0.75
	COV	0.04	0.05	0.05	0.08	0.03	0.01	0.05	0.04	0.02
	% Change		-15.8	-21.1	-28.8	-44.0	1.6	-7.6	-22.4	-27.3
	Fracture Type	Cone and Shear	Cone and Shear	Shear	Cone and Shear	Shear	Columnar	Cone and Shear	Columnar	Cone and Shear
	Failure Type	Combined	Combined	Combined	Combined	Combined	Combined	Combined	Combined	Combined
56 Days		48.20	43.50	37.50	36.70	29.60	49.20	42.30	39.30	35.20
	Individual	46.50	41.40	39.20	34.70	27.30	47.20	43.20	37.20	36.10
		47.10	40.30	38.80	33.80	28.10	48.70	45.70	38.93	35.70
	Average	47.27	41.73	38.50	35.07	28.33	48.37	43.73	38.48	35.67
	SD	0.86	1.63	0.89	1.48	1.17	1.04	1.76	1.12	0.45
	COV	0.02	0.04	0.02	0.04	0.04	0.02	0.04	0.03	0.01
	% Change		-11.7	-18.5	-25.8	-40.1	2.3	-7.5	-18.6	-24.5
	Fracture Type	Cone and Shear	Shear	Shear	Columnar	Shear	Cone and Shear	Columnar	Cone and Shear	Shear
	Failure Type	Combined	Combined	Combined	Combined	Combined	Combined	Combined	Combined	Combined

Table A.3 Summary of tensile test results of different concrete batches.

Batch No	**BN-1**	**BN-2**	**BN-3**	**BN-4**	**BN-5**	**BN-6**	**BN-7**	**BN-8**	**BN-9**
Batch Name	**$R_0C_0F_0$**	**$R_{30}C_0F_0$**	**$R_{30}C_5F_0$**	**$R_{30}C_{10}F_0$**	**$R_{30}C_{15}F_0$**	**$R_{30}C_0F_{0.5}$**	**$R_{30}C_5F_{0.5}$**	**$R_{30}C_{10}F_{0.5}$**	**$R_{30}C_{15}F_{0.5}$**
Individual	3.50	3.48	3.34	2.93	2.42	3.57	3.28	3.16	2.83
	3.62	3.27	3.22	3.18	2.59	3.73	3.27	3.27	3.08
	3.253	3.12	3.20	3.05	2.56	3.78	3.48	3.21	2.93
Average	3.46	3.29	3.25	3.05	2.52	3.69	3.34	3.21	2.94
SD	0.19	0.18	0.08	0.13	0.09	0.11	0.12	0.05	0.12
COV	0.05	0.05	0.02	0.04	0.04	0.03	0.04	0.02	0.04
% Change		-4.9	-6.0	-11.8	-27.0	6.7	-3.3	-7.2	-14.9

Table A.4 Summary of flexural test results of different concrete batches.

Batch No	**BN-1**	**BN-2**	**BN-3**	**BN-4**	**BN-5**	**BN-6**	**BN-7**	**BN-8**	**BN-9**
Batch Name	**$R_0C_0F_0$**	**$R_{30}C_0F_0$**	**$R_{30}C_5F_0$**	**$R_{30}C_{10}F_0$**	**$R_{30}C_{15}F_0$**	**$R_{30}C_0F_{0.5}$**	**$R_{30}C_5F_{0.5}$**	**$R_{30}C_{10}F_{0.5}$**	**$R_{30}C_{15}F_{0.5}$**
Individual	4.85	5.13	4.20	4.12	3.92	6.15	4.87	4.67	4.38
	5.15	4.95	4.45	3.95	3.85	5.87	4.70	4.81	4.44
	5.20	5.04	4.40	4.02	4.00	6.15	4.60	4.55	4.43
Average	5.07	5.04	4.35	4.03	3.92	6.06	4.72	4.68	4.42
SD	0.19	0.09	0.13	0.09	0.08	0.16	0.14	0.13	0.03
COV	0.04	0.02	0.03	0.02	0.02	0.03	0.03	0.03	0.01
% Change		-0.5	-14.1	-20.5	-22.6	19.5	-6.8	-7.7	-12.8

Table A.5 Summary of the hardened density of different concrete batches.

Batch No		**BN-1**	**BN-2**	**BN-3**	**BN-4**	**BN-5**	**BN-6**	**BN-7**	**BN-8**	**BN-9**
Batch Name		**$R_0C_0F_0$**	**$R_{30}C_0F_0$**	**$R_{30}C_5F_0$**	**$R_{30}C_{10}F_0$**	**$R_{30}C_{15}F_0$**	**$R_{30}C_0F_{0.5}$**	**$R_{30}C_5F_{0.5}$**	**$R_{30}C_{10}F_{0.5}$**	**$R_{30}C_{15}F_{0.5}$**
7 Days	Hardened Density (kg/m^3)	2353	2302	2173	2172	2110	2280	2189	2206	2091
		2327	2320	2266	2270	2216	2336	2132	2158	2108
		2355	2316	2331	2194	2173	2275	2343	2189	2146
	Average	2345	2313	2257	2212	2166	2297	2221	2184	2115
	% Change		-1.4	-3.8	-5.7	-7.6	-2.0	-5.3	-6.8	-9.8
28 Days	Hardened Density (kg/m^3)	2329	2361	2327	2218	2279	2333	2263	2193	2153
		2394	2338	2283	2219	1985	2273	2284	2220	2064
		2346	2339	2275	2329	2234	2325	2276	2243	2212
	Average	2356	2346	2295	2255	2166	2310	2275	2219	2143
	% Change		-0.4	-2.6	-4.3	-8.1	-2.0	-3.5	-5.8	-9.1
56 Days	Hardened Density (kg/m^3)	2358	2351	2301	2239	2253	2362	2274	2161	2169
		2411	2336	2318	2217	2063	2248	2357	2224	2128
		2330	2368	2295	2343	2208	2354	2227	2300	2187
	Average	2366	2352	2305	2266	2175	2321	2286	2229	2161
	% Change		-0.6	-2.6	-4.2	-8.1	-1.9	-3.4	-5.8	-8.7

Table A.6 Summary of ultrasonic pulse velocity of different concrete batches.

Batch No		BN-1	BN-2	BN-3	BN-4	BN-5	BN-6	BN-7	BN-8	BN-9
Batch Name		$R_0C_0F_0$	$R_{30}C_0F_0$	$R_{30}C_5F_0$	$R_{30}C_{10}F_0$	$R_{30}C_{15}F_0$	$R_{30}C_0F_{0.5}$	$R_{30}C_5F_{0.5}$	$R_{30}C_{10}F_{0.5}$	$R_{30}C_{15}F_{0.5}$
7 Days	Individual	6.40	5.19	3.67	2.70	2.44	4.79	3.55	3.79	2.18
		6.20	3.69	3.95	2.57	2.39	5.66	3.50	3.20	2.24
		6.09	3.56	2.04	2.50	2.31	5.66	4.53	3.08	2.91
	Average	6.23	4.15	3.22	2.59	2.38	5.37	3.86	3.36	2.44
	% Change		-33.42	-48.32	-58.41	-61.79	-13.79	-38.07	-46.09	-60.82
28 Days	Individual	7.40	5.19	3.82	3.70	3.18	5.79	3.55	3.79	3.44
		7.20	5.30	3.95	3.57	3.24	6.20	4.50	3.80	3.39
		7.09	4.56	4.04	3.50	3.12	6.66	5.53	4.08	3.31
	Average	7.23	5.02	3.94	3.59	3.18	6.22	4.53	3.89	3.38
	% Change		-30.62	-45.57	-50.33	-56.03	-14.00	-37.41	-46.18	-53.25
56 Days	Individual	7.62	6.29	4.03	3.92	3.49	5.88	3.82	3.89	3.74
		7.52	5.05	4.18	3.90	3.52	6.97	4.81	4.15	3.65
		7.34	4.04	4.33	3.75	3.26	6.95	5.68	4.56	3.62
	Average	7.49	5.12	4.18	3.86	3.43	6.60	4.77	4.20	3.67
	% Change		-31.6	-44.2	-48.6	-54.3	-11.9	-36.4	-43.9	-51.0

Table A.7 Summary of surface resistivity of different concrete mixtures.

Batch No	BN-1	BN-2	BN-3	BN-4	BN-5	BN-6	BN-7	BN-8	BN-9
Batch Name	$R_0C_0F_0$	$R_{30}C_0F_0$	$R_{30}C_5F_0$	$R_{30}C_{10}F_0$	$R_{30}C_{15}F_0$	$R_{30}C_0F_{0.5}$	$R_{30}C_5F_{0.5}$	$R_{30}C_{10}F_{0.5}$	$R_{30}C_{15}F_{0.5}$
Surface Resistivity (kΩ.cm)	111.0	134.0	138.6	164.6	188.0	119.5	122.8	151.1	167.8
	120.0	148.0	170.1	169.6	170.0	115.7	127.0	150.0	165.4
	114.0	134.0	126.4	177.1	205.0	126.0	132.1	169.0	151.1
Average	115.0	138.7	145.0	170.4	187.7	120.4	127.3	156.7	161.4
% Change		20.6	26.1	48.2	63.2	4.7	10.7	36.3	40.4
Chloride Ion Penetrability	Very Low	Very Low	Very Low	Very Low	Very Low	Very Low	Very Low	Very Low	Very Low

Table A.8 Summary of emissions of fuel consumption.

Sample Type	M (kg/kmol)	Thermal Resistance (R) (m^2.K/W)	Annual Consumption of Fuel (m_{FA}) (kg/m^2.yr)	M_{CO2} (kg/m^2.yr)	M_{SO2} (kg/m^2.yr)
$R_0C_0F_0$		0.152	24.50	78.90	0.41
$R_{30}C_0F_0$		0.154	24.12	77.67	0.40
$R_{30}C_5F_0$		0.162	22.90	73.73	0.38
$R_{30}C_{10}F_0$		0.169	21.94	70.67	0.37
$R_{30}C_{15}F_0$	99.91	0.187	19.84	63.91	0.33
$R_{30}C_0F_{0.5}$		0.159	23.32	75.12	0.39
$R_{30}C_5F_{0.5}$		0.166	22.43	72.24	0.37
$R_{30}C_{10}F_{0.5}$		0.176	21.06	67.81	0.35
$R_{30}C_{15}F_{0.5}$		0.190	19.55	62.97	0.33

APPENDIX B

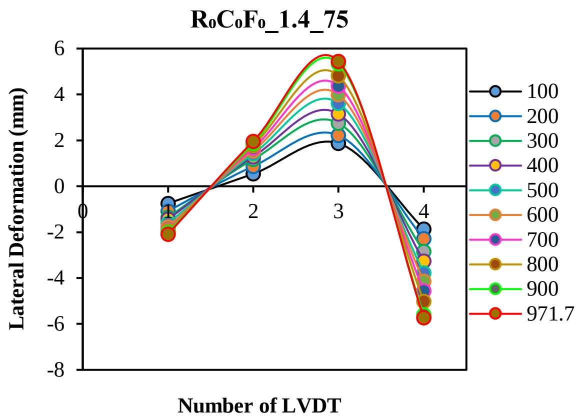

(a-1)

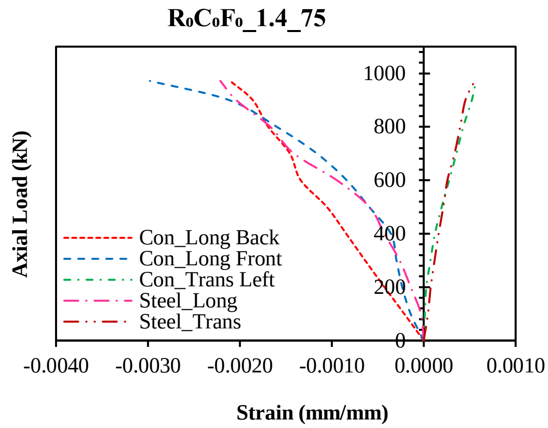

(b-1)

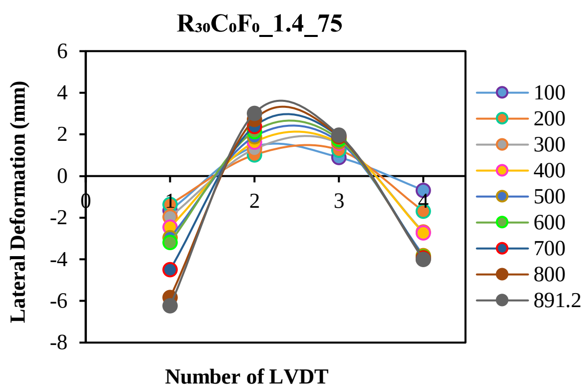

(a-2)

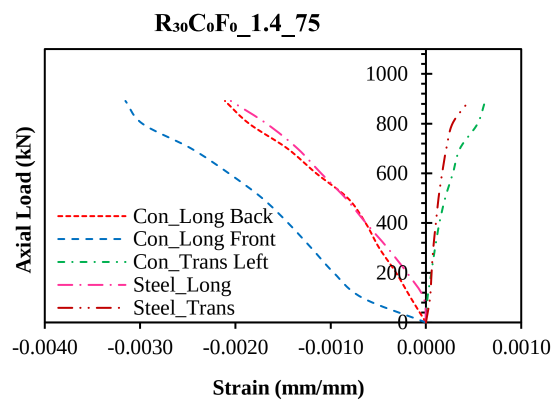

(b-2)

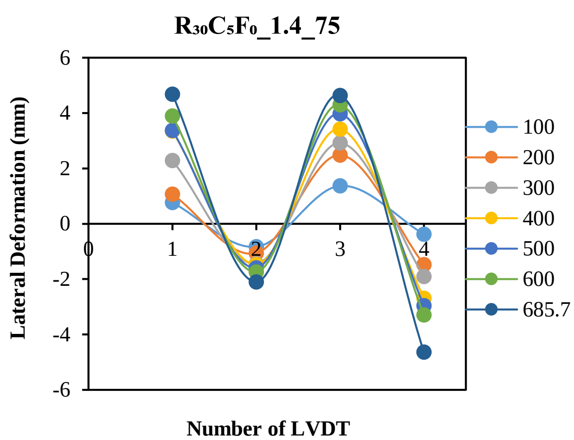

(a-3)

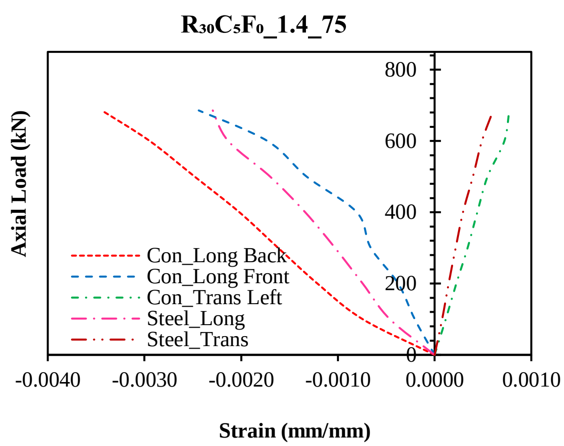

(b-3)

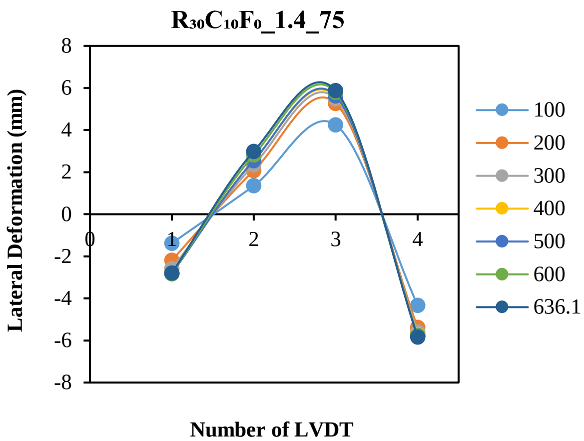

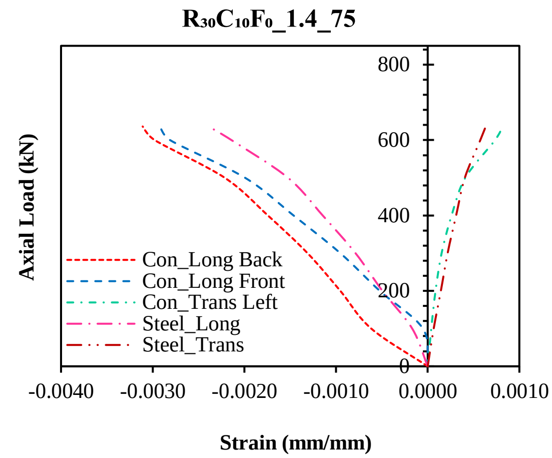

(a-4)

(b-4)

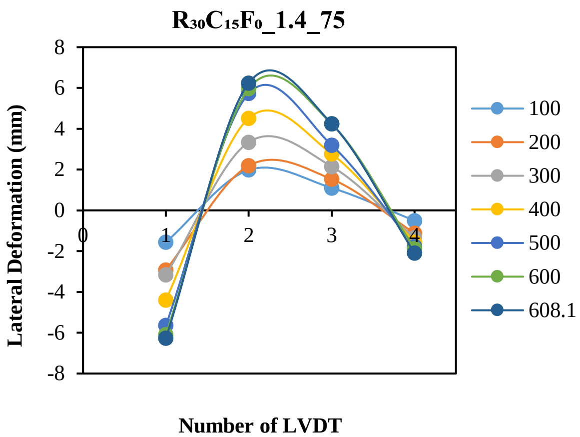

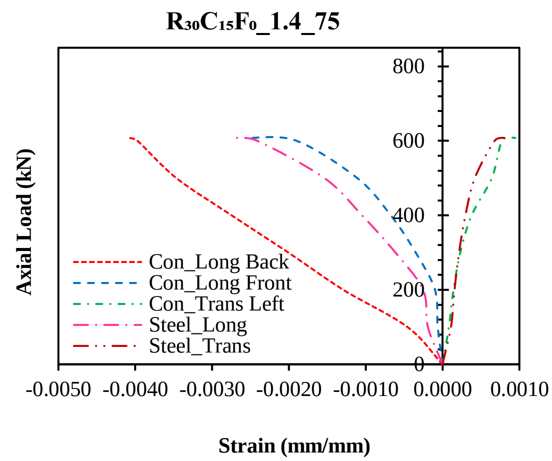

(a-5)

(b-5)

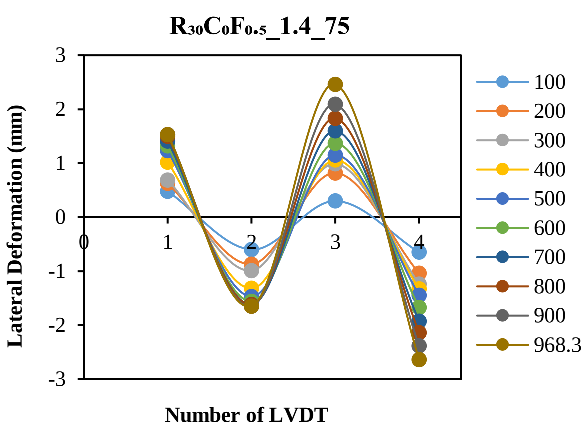

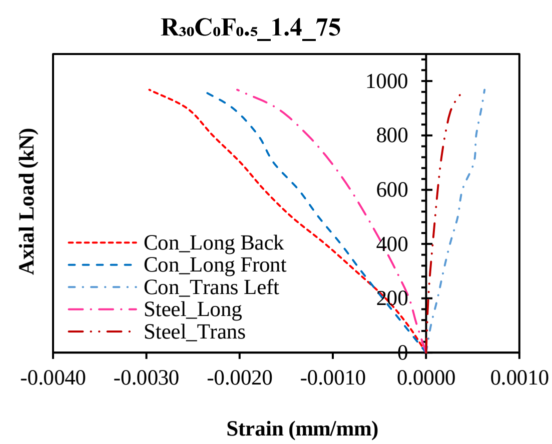

(a-6)

(b-6)

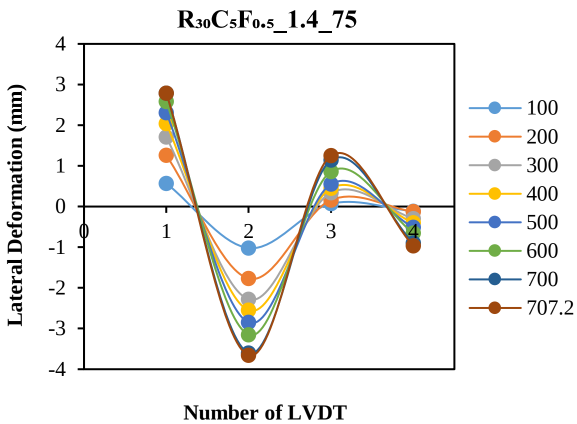

(a-7)

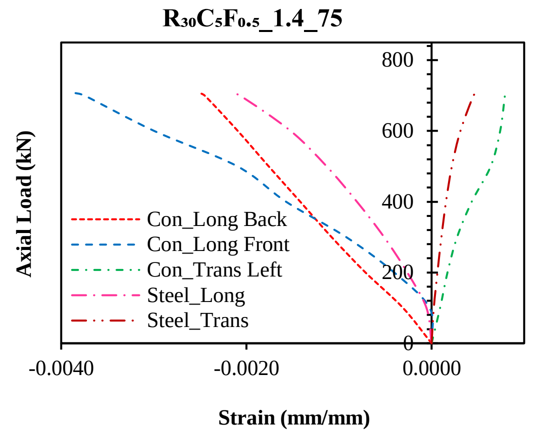

(b-7)

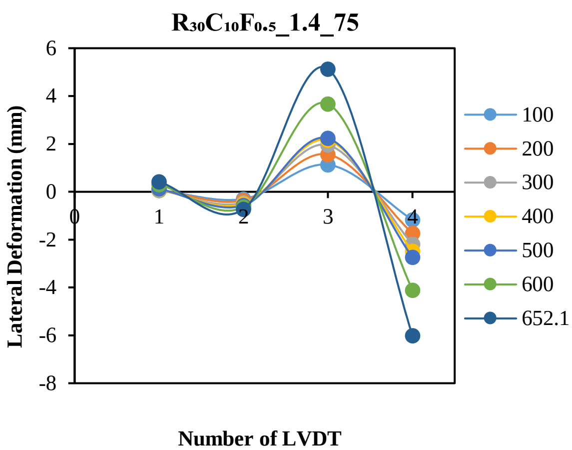

(a-8)

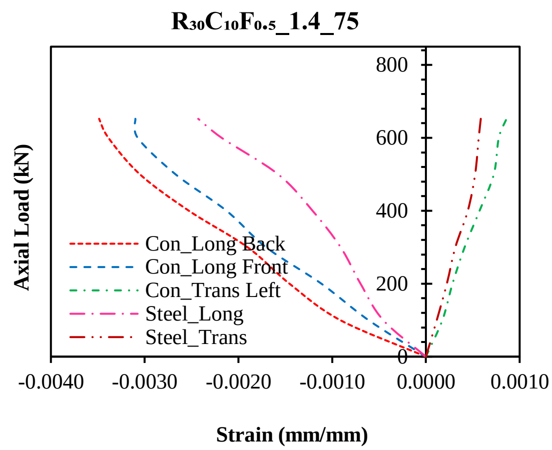

(b-8)

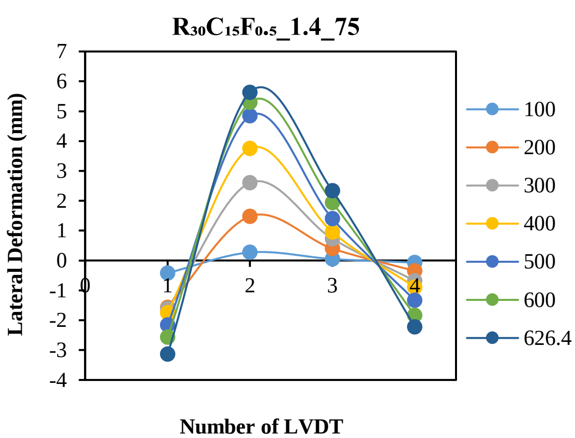

(a-9)

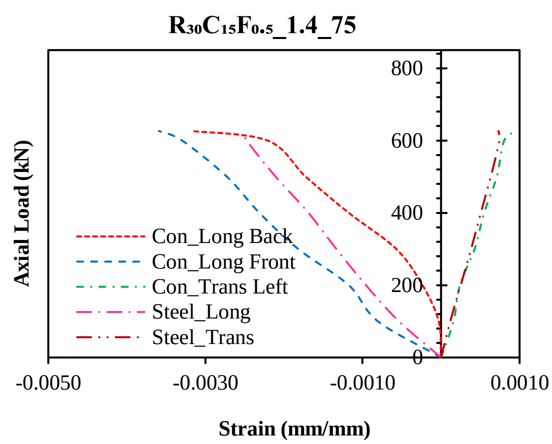

(b-9)

Figure B.1 Lateral deformations and strain value for different columns with ρ = 1.4% and 75 mm tie spacing: (a) Lateral deformation at the midpoint of the columns on different surfaces and (b) axial load vs strain curves.

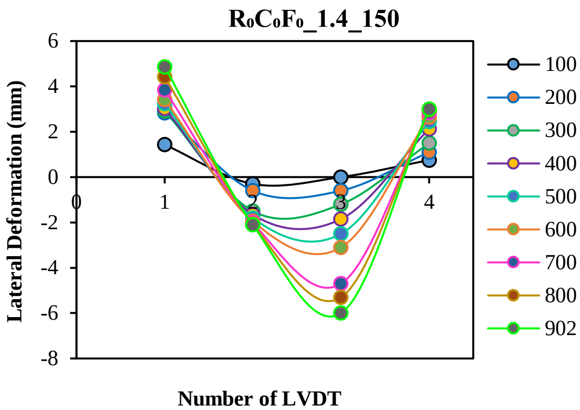

(a-1)

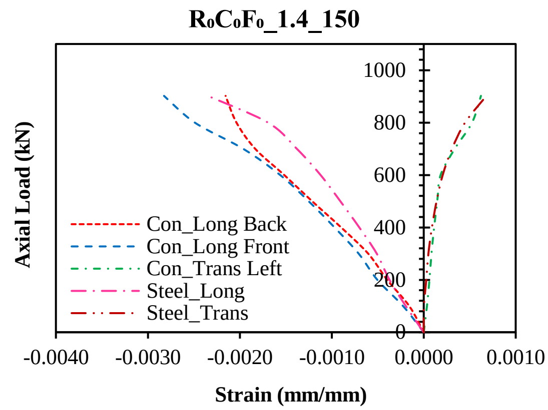

(b-1)

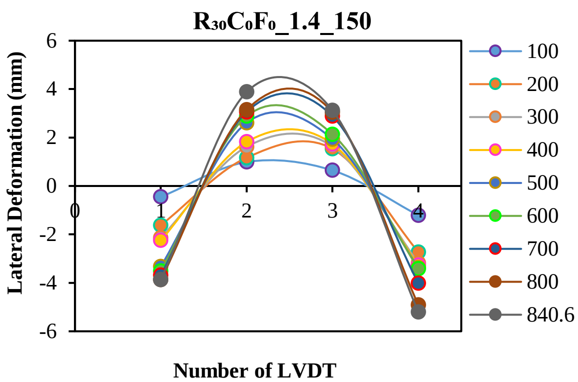

(a-2)

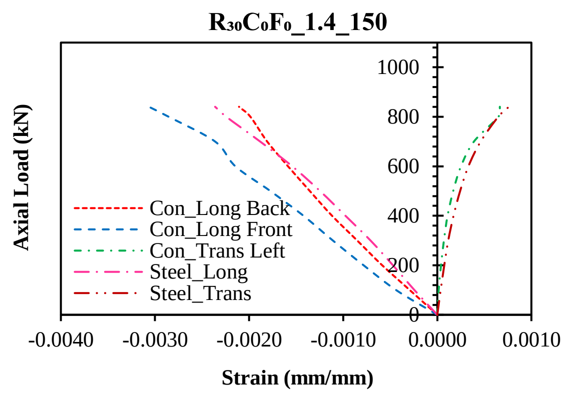

(b-2)

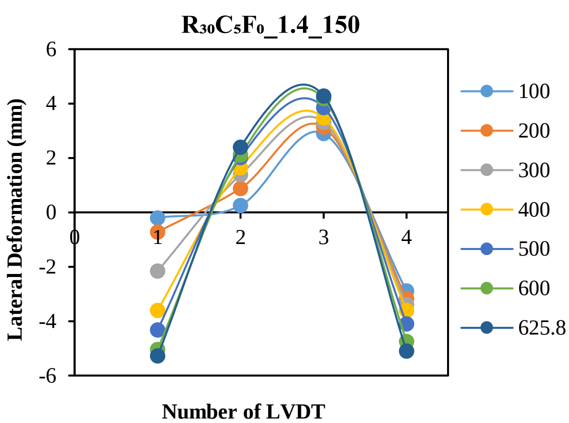

(a-3)

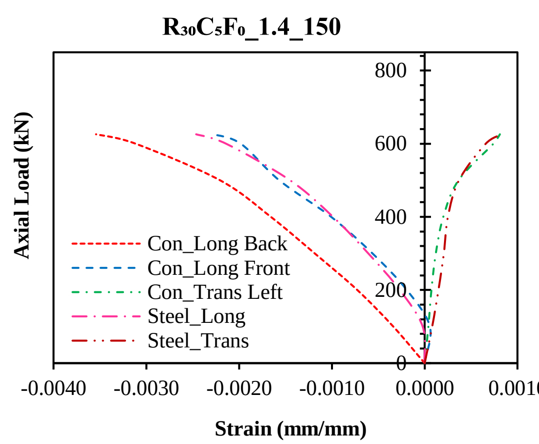

(b-3)

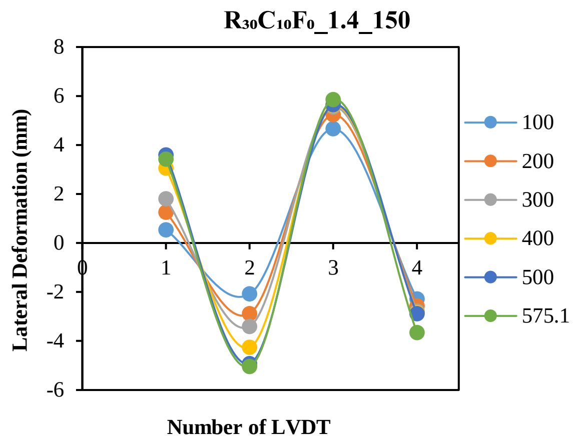

(a-4)

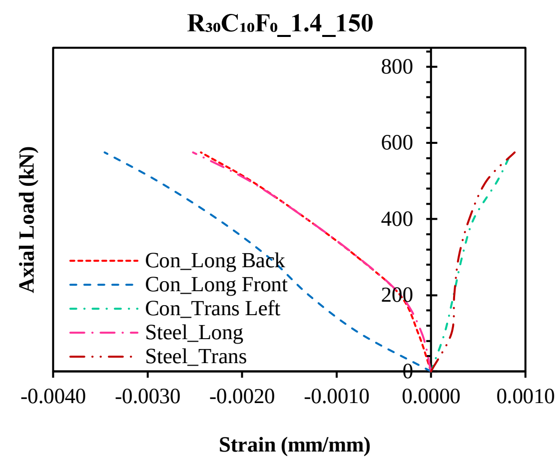

(b-4)

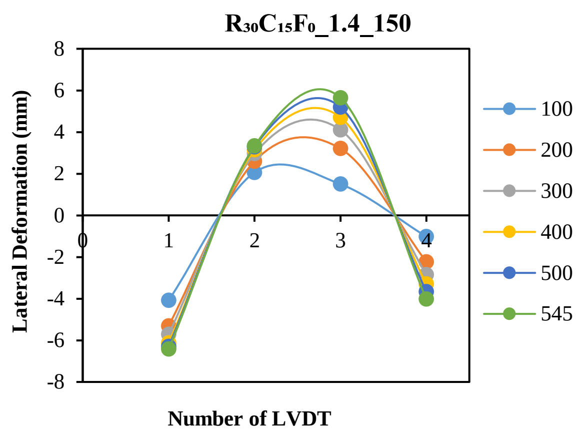

(a-5)

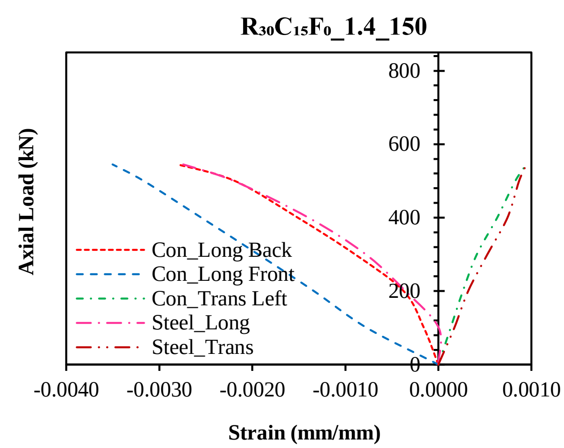

(b-5)

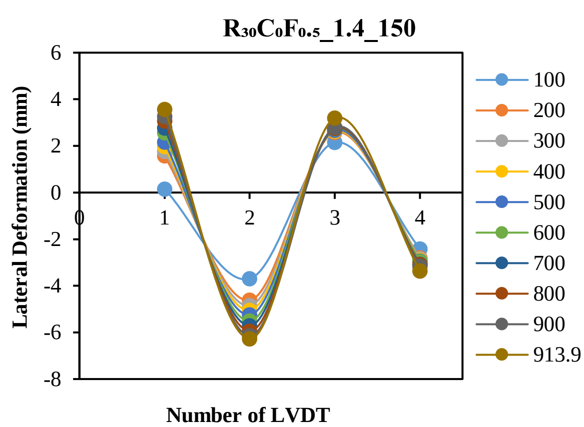

(a-6)

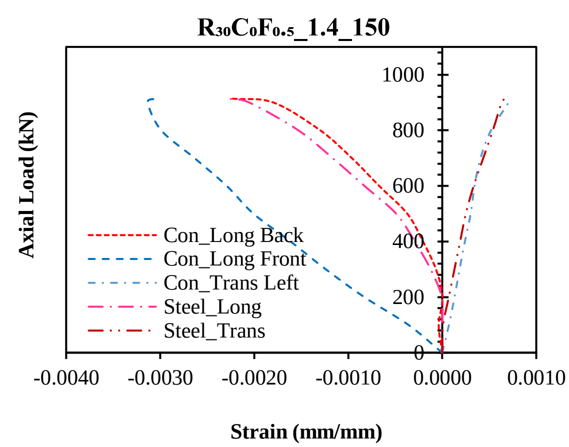

(b-6)

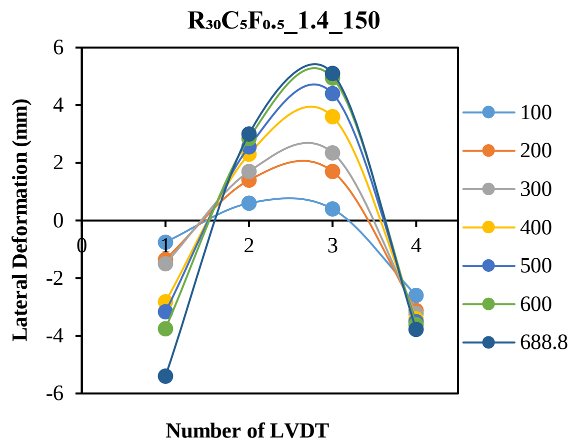

(a-7)

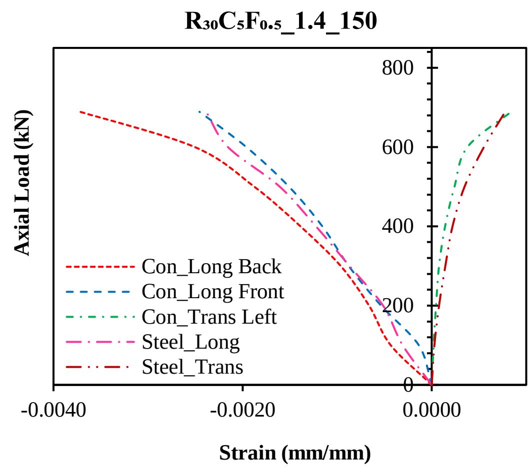

(b-7)

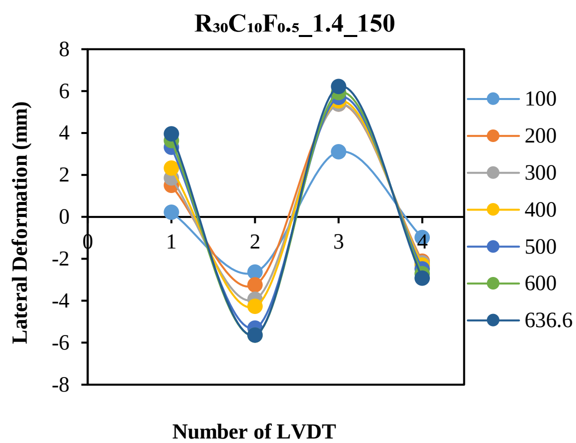

(a-8)

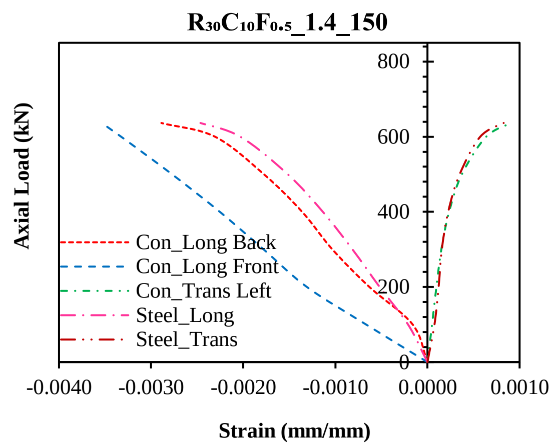

(b-8)

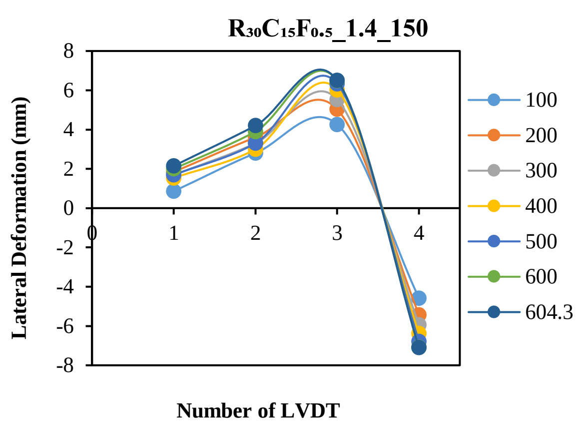

(a-9)

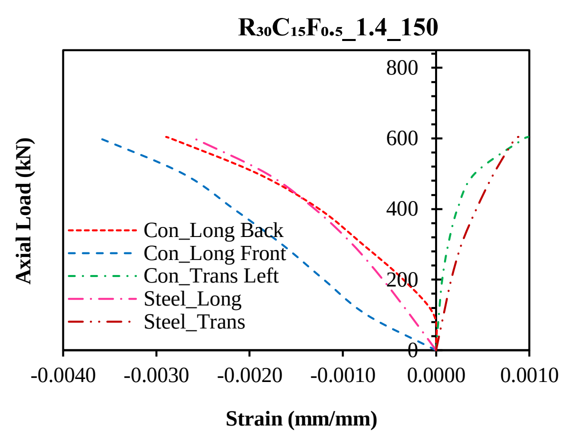

(b-9)

Figure B.2 Lateral deformations and strain value for different columns with ρ = 1.4% and 150 mm tie spacing: (a) Lateral deformation at the midpoint of the columns on different surfaces and (b) axial load vs strain curves.

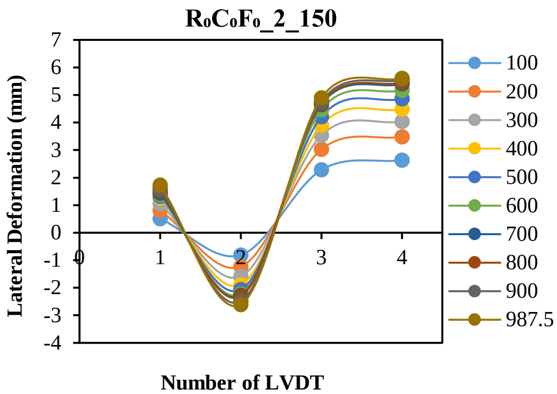

(a-1)

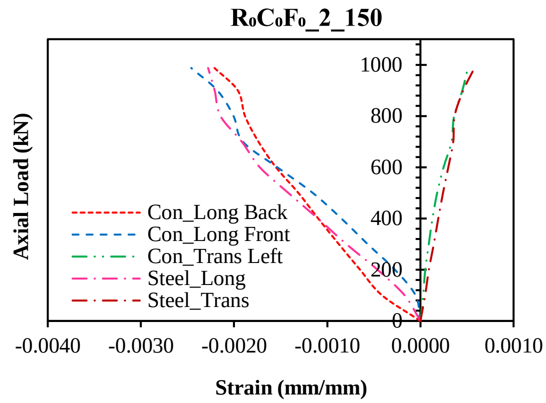

(b-1)

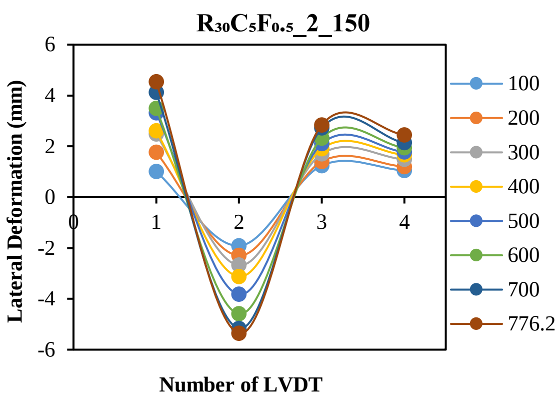

(a-2)

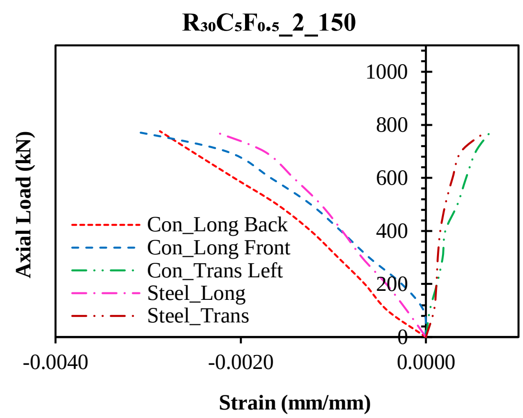

(b-2)

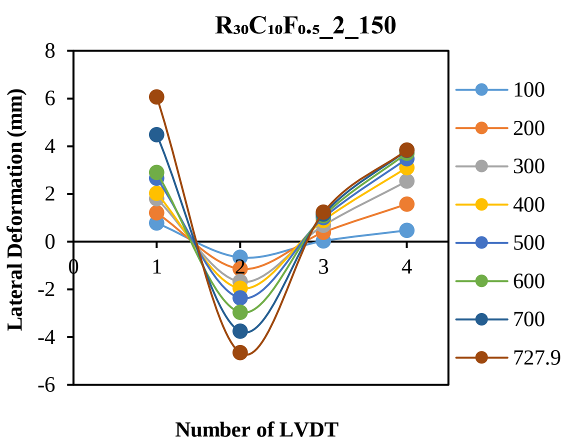

(a-3)

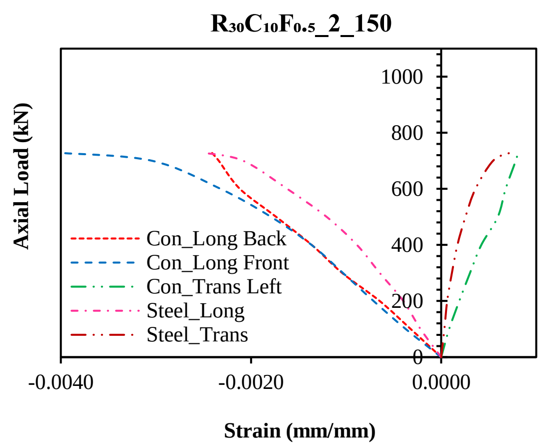

(b-3)

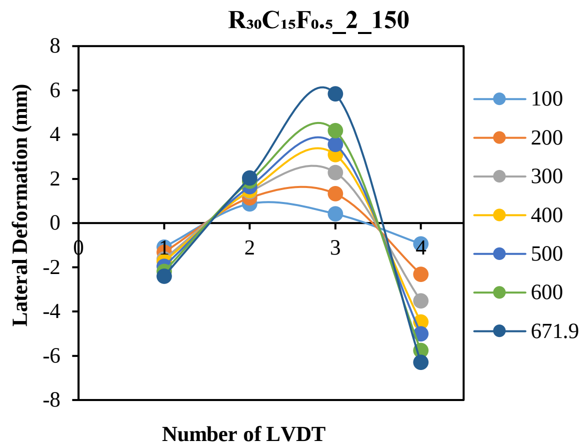

(a-4)

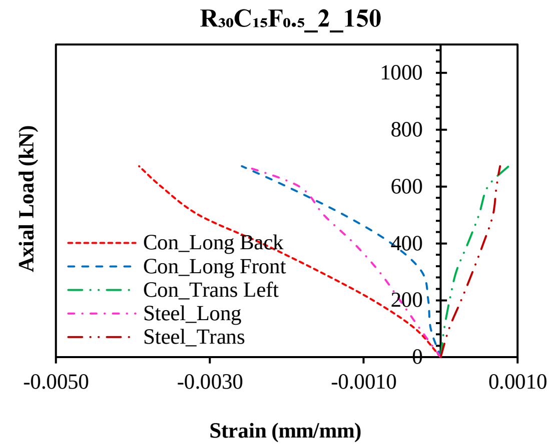

(b-4)

Figure B.3 Lateral deformations and strain value for different columns with ρ = 2.0% and 150 mm tie spacing: (a) Lateral deformation at the midpoint of the columns on different surfaces and (b) axial load vs strain curves.

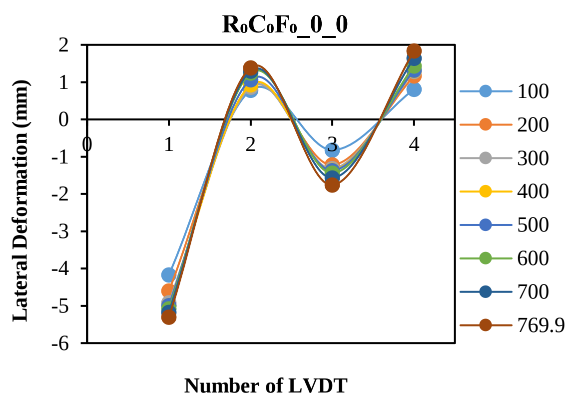

(a-1)

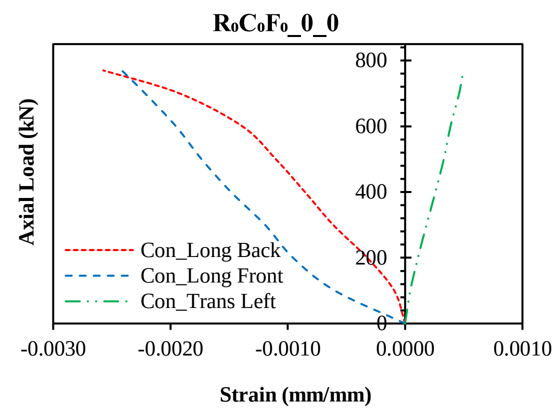

(b-1)

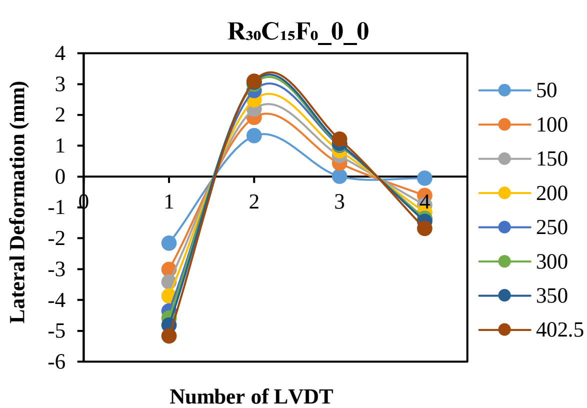

(a-2)

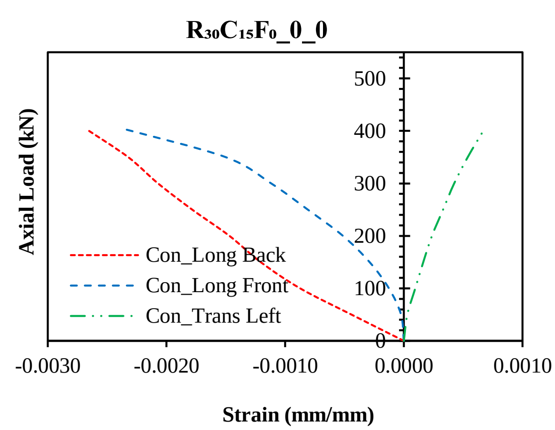

(b-2)

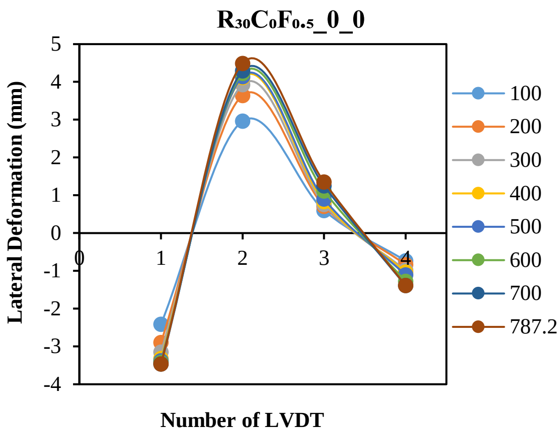

(a-3)

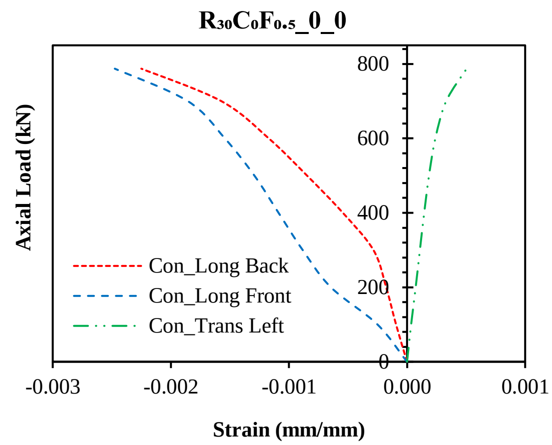

(b-3)

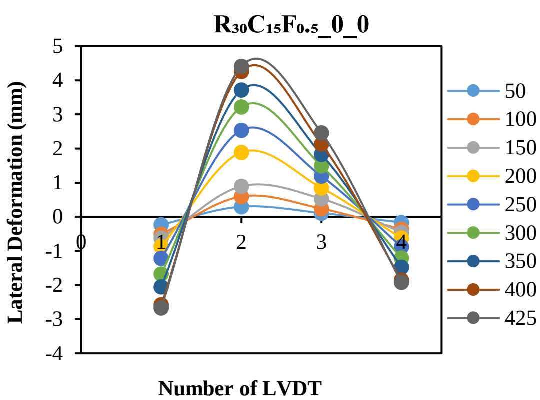

(a-4)

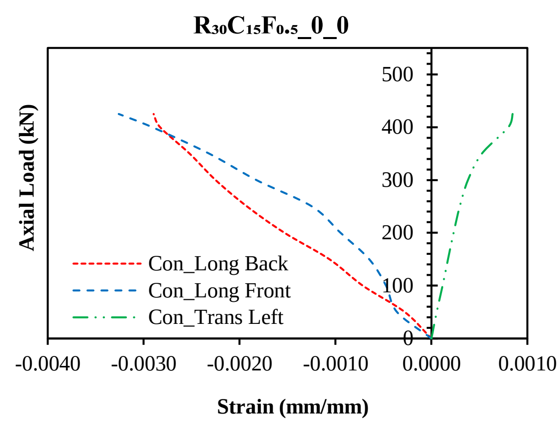

(b-4)

Figure B.4 Lateral deformations and strain value for different plain concrete columns: (a) Lateral deformation at the midpoint of the columns on different surfaces and (b) axial load vs strain curves.

Table B.1 Prediction of axial load carrying capacity of different RC columns.

Column Name	P_{peak} (kN)	P_{ACI} (kN)	P_{ACI}/P_{exp}	P_{CSA} (kN)	P_{CSA}/P_{exp}	P_{pro}/P_{exp}
$R_0C_0F_0$_1.4_75	971.7	1033.0	1.1	958.6	0.99	0.97
$R_{30}C_0F_0$_1.4_75	891.2	928.6	1.04	870.7	0.98	0.95
$R_{30}C_5F_0$_1.4_75	685.7	867.7	1.27	818.3	1.19	1.12
$R_{30}C_{10}F_0$_1.4_75	636.1	802.9	1.26	762.0	1.20	1.08
$R_{30}C_{15}F_0$_1.4_75	608.1	676.0	1.11	649.2	1.07	0.89
$R_{30}C_0F_{0.5}$_1.4_75	968.3	1053.7	1.09	975.9	1.01	0.92
$R_{30}C_5F_{0.5}$_1.4_75	707.2	966.4	1.37	902.7	1.28	1.12
$R_{30}C_{10}F_{0.5}$_1.4_75	652.1	867.2	1.33	818.0	1.25	1.04
$R_{30}C_{15}F_{0.5}$_1.4_75	626.4	814.2	1.30	771.9	1.23	0.96
$R_0C_0F_0$_1.4_150	902.0	1033.0	1.1	958.6	1.06	0.98
$R_{30}C_0F_0$_1.4_150	840.6	928.6	1.10	870.7	1.04	0.94
$R_{30}C_5F_0$_1.4_150	625.8	867.7	1.39	818.3	1.31	1.14
$R_{30}C_{10}F_0$_1.4_150	575.1	802.9	1.40	762.0	1.32	1.09
$R_{30}C_{15}F_0$_1.4_150	545.0	676.0	1.24	649.2	1.19	0.89
$R_{30}C_0F_{0.5}$_1.4_150	913.9	1053.7	1.15	975.9	1.07	0.93
$R_{30}C_5F_{0.5}$_1.4_150	688.8	966.4	1.40	902.7	1.31	1.09
$R_{30}C_{10}F_{0.5}$_1.4_150	636.6	867.2	1.36	818.0	1.28	1.00
$R_{30}C_{15}F_{0.5}$_1.4_150	604.3	814.2	1.35	771.9	1.28	0.93
$R_0C_0F_0$_2_150	987.5	1104.7	1.12	1030.9	1.04	0.99
$R_{30}C_5F_{0.5}$_2_150	776.1	1038.5	1.34	975.3	1.26	1.08
$R_{30}C_{10}F_{0.5}$_2_150	727.9	940.0	1.29	891.1	1.22	1.00
$R_{30}C_{15}F_{0.5}$_2_150	671.9	887.4	1.32	845.3	1.26	0.97

APPENDIX C

Table C.1 Summary of max acceleration and horizontal top displacement of columns.

Batch No		BN-1	BN-2	BN-3	BN-4	BN-5	BN-6	BN-7	BN-8	BN-9
Batch Name		$R_0C_0F_0$	$R_{30}C_0F_0$	$R_{30}C_5F_0$	$R_{30}C_{10}F_0$	$R_{30}C_{15}F_0$	$R_{30}C_0F_{0.5}$	$R_{30}C_5F_{0.5}$	$R_{30}C_{10}F_{0.5}$	$R_{30}C_{15}F_{0.5}$
Max Acceleration, $\ddot{x}$ (m/sec^2)	Exp_E = 1.54 N.m	0.309	0.189	0.324	0.337	0.342	0.210	0.347	0.357	0.654
	Exp_E = 2.13 N.m	0.309	0.200	0.358	0.356	0.415	0.296	0.361	0.430	0.728
	Exp_E = 2.83 N.m	0.314	0.230	0.397	0.427	0.464	0.349	0.405	0.530	0.729
Max Horizontal Disp. (mm)	Exp_E = 1.54 N.m	0.587	0.453	0.603	0.652	1.125	0.589	0.634	0.942	1.151
	Exp_E = 2.13 N.m	0.707	0.534	0.743	0.806	1.370	0.699	0.747	1.447	1.609
	Exp_E = 2.83 N.m	0.781	0.619	0.876	0.916	1.495	0.795	0.891	1.855	1.976